UNIVERSITÉ D'AVIGNON ET DES PAYS DE VAUCLUSE

Ecole Doctorale 536 « Agrosciences et Sciences»

THESE

Pour obtenir le grade de Docteur de l'Université d'Avignon et des pays de Vaucluse

---

Analyse expérimentale et modélisation de l'hétérogénéité de la qualité et de la maturité des mangues

---

Thibault NORDEY

Soutenue le 09 décembre 2014

Jury :

Mr Laurent Urban, professeur à l'université d'Avignon et des pays de Vaucluse (EA 4279), Avignon	Président
Mr Hervé Cochard, directeur de recherche INRA (UMR PIAF), Clermont Ferrand	Rapporteur
Mr Gerhard Buck-Sorlin, professeur à AgroCampus Ouest (IRSH, FruitQual), Angers	Rapporteur
Mr Jean Dauzat, chercheur CIRAD (UMR AMAP), Montpellier	Examinateur
Mr Philippe Vivin, directeur adjoint de recherche INRA (UMR EGFV), Bordeaux	Examinateur
Mr Michel Génard, directeur de recherche INRA (UR PSH), Avignon	Directeur de thèse

Co-encadrants : Mathieu Léchaudel (CIRAD, HortSys) et Jaques Joas (CIRAD, Qualisud)

cirad

UPR HortSys

INRA SCIENCE & IMPACT

UR PSH

Remerciements

Je tiens à remercier tout particulièrement Mathieu Léchaudel, mon encadrant à la Réunion, pour ses conseils avisés et la confiance qu'il m'a accordée. Merci pour sa patience et sa disponibilité qui m'ont permis d'avancer sereinement tout au long de ma thèse.

Je remercie Michel Génard, mon directeur de thèse, son recul et son expérience m'ont aidé à structurer et à approfondir mon raisonnement.

Merci à mon troisième encadrant, Jacques Joas, avec qui j'ai pu échanger sur la gestion du fruit en post récolte et ainsi considérer la qualité de manière intégrée.

Un grand merci au personnel de la station de Bassin Plat sans qui cette thèse ne se serait pas aussi bien passée. Merci à Elodie, expérimentant en même temps les tourments liés à la thèse, nos échanges nous ont permis de les appréhender plus facilement. Merci au personnel de la station de bassin plat et du laboratoire de la MRST : Doralice, Murielle, Marie D., Christian et Jérôme qui par leur sympathie et leur disponibilité ont permis que le travail de terrain et de laboratoire se passe pour le mieux. Je remercie les VSC, Marie R. et Pierre Emmanuel pour leur soutien et Juliette pour l'aide apportée pendant son stage. Merci à Frédéric à Jean Paul et Fabrice pour nos échanges, à Jean Pierre, voisin de l'entre, pour ses conseils en mécanique, à Philippe pour son enseignement de la langue créole, à André pour son soutien amical et à Gilles pour ses conseils sur la culture de la salade.

J'aimerais terminer ces remerciements en ayant une pensée pour mes proches en les remerciant pour leur présence malgré la distance. Enfin, merci à Amélie de m'avoir accompagné et soutenu pendant ces trois années.

Sommaire

Introduction

I - La maitrise de la qualité, un enjeu pour la commercialisation de la mangue.

Avec une production de l'ordre de 31.7 millions de tonnes en 2009 la mangue est le fruit tropical le plus produit à travers le monde (FAO, 2011a, FAO, 2011b). Cultivé dans plus de 90 pays, c'est un fruit dont les qualités organoleptiques sont communément appréciées. La valeur nutritive de la mangue est en outre intéressante du fait de sa richesse en sucres, en vitamines (A et C), en minéraux (calcium et potassium) et en antioxydant (β-carotène)(Tharanathan et al., 2006).

La mangue est de plus en plus consommée dans les pays du Nord. Les importations de mangue au niveau mondial, à 50% à destination de l'Union européenne et de l'Amérique du nord, ont été multipliées par plus de 1.8 fois entre 1999 et 2009 (FAO, 2011b).

Malgré la demande croissante des pays importateurs la majeure partie de la production de mangue est destinée à un marché local. En 2009, environ 1.2 millions de tonnes de mangues ont été exportées, soit moins de 4% de la production totale (FAO, 2011b, FAO, 2011a). L'exportation de la mangue représente une voie de développement économique intéressante pour les pays du Sud qui sont les principaux producteurs (Loeillet, 1994).

En plus d'être impactée par l'irrégularité de la production causée par les phénomènes d'alternance, les ravageurs et les maladies, la commercialisation de la mangue est freinée par la gestion difficile de la qualité des fruits (Sivakumar et al., 2011). D'importantes variations de maturité, de calibre et de qualité organoleptique sont effectivement observées à la récolte engendrant d'importantes pertes tout au long de la chaine de distribution (Sivakumar et al., 2011, Kitinoja et al., 2010)(Figure 1).

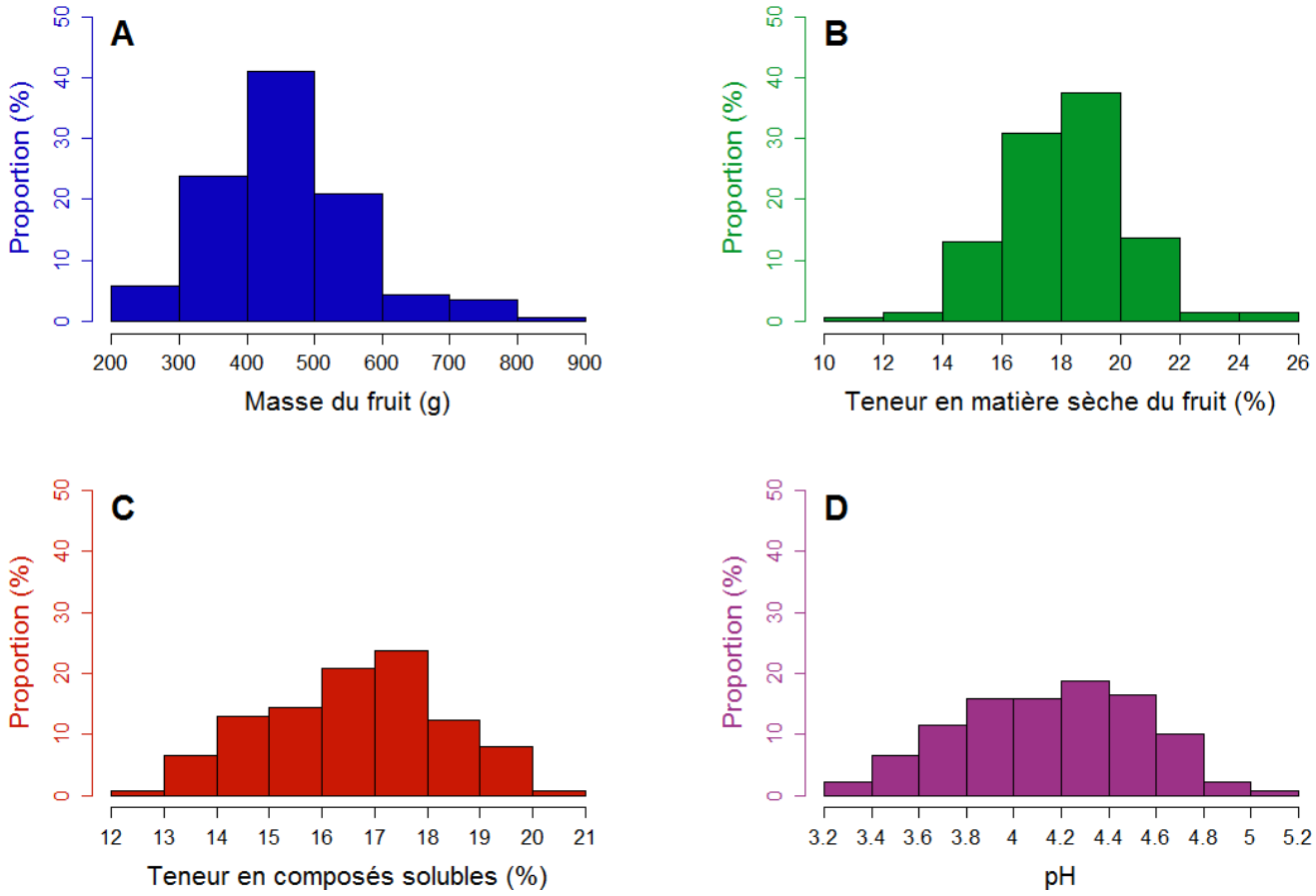

Figure 1 : Variabilité du poids des mangues (A), de leur teneur en matière sèche (B), de leur teneur en composés solubles (C) et de leur acidité (D) à la récolte.

II - La qualité de la mangue : de nombreux attributs qui varient au cours de la croissance et de la maturation du fruit.

La qualité est une notion qui varie selon que l'on se place du point de vue du producteur, du distributeur ou du consommateur. Le producteur définira la qualité en termes de productivité, calibre, précocité, et résistance aux maladies. Le distributeur lui, sera sensible à l'homogénéité et à la durée de conservation des produits. Enfin, du point de vue du consommateur la qualité se définit par les propriétés nutritionnelles et organoleptiques du produit. Les professionnels des filières fruitières accordent de plus en plus d'attention aux qualités organoleptiques et nutritionnelles des produits car les consommateurs y sont d'avantage sensibles, même si le prix reste un critère important dans leurs choix (Jaeger et al., 2011, Schreiner et al., 2013).

La qualité organoleptique regroupe un ensemble de caractéristiques qui sont à la fois externes, comme la forme, la taille et la couleur, et interne au fruit, comme la saveur sucrée et acide. La préférence des consommateurs n'étant pas uniforme et évoluant dans le temps, il n'existe pas de référentiel de qualité qui soit universel (Schreiner et al., 2013). Les distributeurs doivent identifier les variétés de mangue qui correspondent le mieux aux demandes des consommateurs ciblés. On observe effectivement d'importantes variations de calibre, d'acidité, de teneur en sucre, de texture, de saveur et de couleur entre les variétés de mangue (Figure 2). Cette variabilité s'explique par la diversité génétique du manguier induite par le grand nombre de zones tropicales et subtropicales où il a été introduit (Olano et al., 2005). Actuellement, les variétés les plus utilisées pour le marché international sont de type Floridien, comme Tommy Atkins, Irwin, Kent et Cogshall (Figure 2).

Figure 2 : Variétés de mangues floridiennes (A-D), thaïlandaise (E), et indiennes (F et G). Crédits photos : Frédéric Normand (A, B, C, D, E, et G) et Asit K. Ghosh (F).

Les mangues floridiennes se différencient des autres par leur forme ellipsoïdale, leur calibre important (350-750g), leur coloration rouge-violacée, et leur saveur sucrée et parfumée. Bien que présentant des qualités organoleptiques toutes aussi intéressantes, les variétés de type Asiatique ne répondent pas aux critères pour l'export vers les marchés du Nord.

C'est notamment le cas pour la mangue Alphonso, la variété la plus vendue en Inde (Schreiner et al., 2013, Litz, 2009, Tharanathan et al., 2006) (Figure 2) et la mangue José, la variété emblématique de la Réunion, qui malgré leur richesse en sucres et en arômes ne correspondent pas aux critères pour l'export du fait de leur coloration verte-jaune et leur petit calibre.

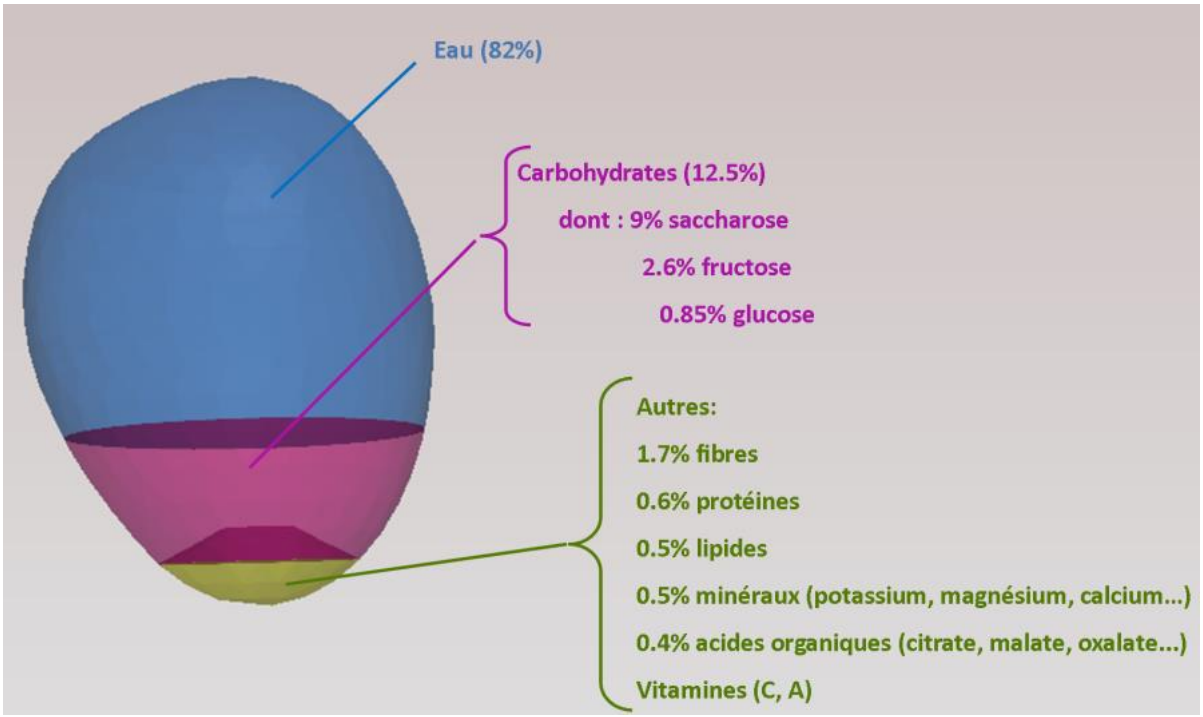

Figure 3: Composition d'une mangue mûre (Source : USDA/ARS, 2007).

La qualité de la mangue dépend de sa concentration en composés primaires (sucres, acides) et secondaires (pigments, vitamines et arômes) (Figure 3). Ces composés sont contenus dans la matière sèche du fruit et leur concentration varie en fonction de la matière fraiche du fruit du fait de l'effet de dilution (Génard et al., 2014). La matière fraiche et la matière sèche s'accumulent pendant la croissance du fruit sur l'arbre (Léchaudel et al., 2005a, Léchaudel et al., 2007). En conséquent, la qualité de la mangue varie en fonction de la date de récolte (Léchaudel and Joas, 2006, Joas et al., 2012). Une mangue cueillie précocement se conserve certes plus longtemps, mais au détriment de sa concentration en arômes et en matière sèche (Joas et al., 2012, Lebrun et al., 2008). La durée de conservation des fruits est liée à leur vitesse de mûrissement. Le mûrissement regroupe un ensemble de processus physiologiques irréversibles et inévitables qui transforment la composition du fruit. En quelques jours le fruit murît, il devient attractif et comestible, puis sa qualité se dégrade et il devient immangeable à cause de la sur maturation (Figure 4).

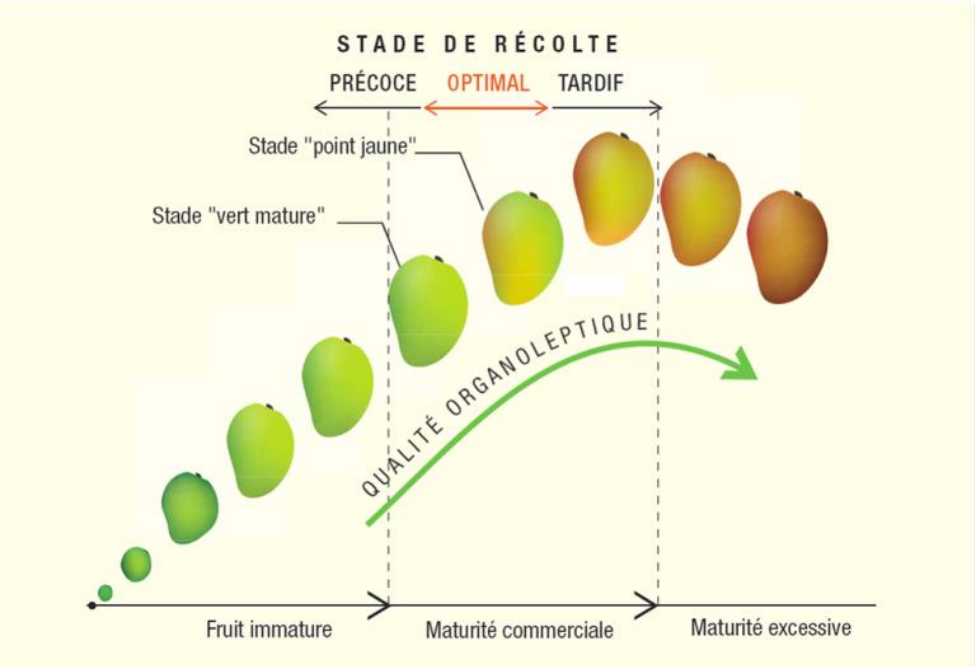

Figure 4 : Evolution de la qualité de la mangue en fonction de son stade de maturité, issue de Joas and Léchaudel (2009).

On distingue classiquement les fruits en deux groupes selon leur manière de mûrir. La mangue, l'avocat ou bien la banane sont des fruits climactériques, ils se distinguent des fruits non climactériques, comme le raisin, l'ananas ou l'orange par le fait que leur respiration augmente pendant la maturation et qu'ils produisent d'importante quantité d'éthylène (Biale, 1964, Burg and Burg, 1962).

Cette classification est cependant discutée car la quantité d'éthylène synthétisée et l'intensité de la crise respiratoire pendant le mûrissement varient considérablement selon les fruits climactériques (Burg and Burg, 1962). Par ailleurs, il a été montré que l'éthylène est également impliquée dans le mûrissement de certains fruits non climactériques (Paul et al., 2012).

La qualité du fruit mûr dépend de sa composition avant son mûrissement (Joas et al., 2012). On peut considérer que c'est pendant la croissance sur l'arbre que s'élabore le potentiel de qualité du fruit, par l'accumulation de matière sèche et de matière fraiche, et que c'est la transformation de ce potentiel lors du mûrissement qui définira sa qualité (Hewett, 2006).

III - Les facteurs influençant la qualité et le mûrissement de la mangue : synthèse bibliographique.

Comme indiqué précédemment, la qualité du fruit regroupe de nombreux attributs, tels que le calibre, la couleur, la saveur sucrée et acide. Ces attributs dépendent de l'accumulation de matière fraiche et de matière sèche pendant la croissance du fruit et de son stade de maturité. Plusieurs études ont montré que la masse fraiche, la masse sèche et la maturité de la mangue varient en fonction du lieu de production, des pratiques culturales et de la position du fruit au sein de l'arbre (Hofman et al., 1995, Joas et al., 2012, Simmons et al., 1998, Léchaudel et al., 2005a, Léchaudel et al., 2007). Les conditions de croissance du fruit impactent sa composition et sa maturité en modifiant les échanges d'énergie, de matière sèche et d'eau entre le fruit, l'arbre et le milieu extérieur (Génard et al., 2007). Il en est déduit que les conditions de croissance du fruit affectent sa qualité et sa maturité en faisant varier ses bilans énergétique, carboné et hydrique. Il est donc proposé dans cette synthèse bibliographique d'étudier comment les conditions de croissance affectent chacun de ces bilans.

A - Le bilan énergétique du fruit varie en fonction de son micro environnement.

Le fruit échange avec l'environnement extérieur de l'énergie par convection, rayonnement et vaporisation de l'eau (transpiration). L'intensité de ces échanges varie en fonction des variables climatiques (température de l'air, rayonnement, humidité relative, …) et des propriétés physiques et thermiques du fruit (conductance de la peau à l'eau, capacité calorifique, conductivité thermique, …). Une approche de modélisation a permis de simuler l'impact des échanges d'énergie entre le fruit et son environnement sur sa température (Saudreau et al., 2007, Saudreau et al., 2009). Ces études ont mis en avant l'importance des conditions climatiques sur la température du fruit. Il a par ailleurs été montré que l'hétérogénéité des conditions climatiques au sein de l'arbre induit d'importantes variations de température au sein du fruit et entre les fruits. Sur le manguier, il a été montré qu'un fruit à l'extérieur de la canopée recevait de 6 à 10 fois plus d'énergie lumineuse qu'un fruit positionné à l'intérieur de l'arbre (Léchaudel et al., 2012). Ces différences d'exposition

lumineuse au sein de l'arbre sont à l'origine des écarts de température entre les fruits à l'ombre et au soleil qui peuvent excéder 10°C à la surface des fruits. Des écarts de température supérieurs à 5°C ont également été mesurés entre les faces ensoleillée et ombragée d'une mangue (Léchaudel et al., 2012). Du fait de son implication dans la vitesse des réactions chimiques (loi d'Arrhenius), la température affecte de nombreux processus physiologiques dans le fruit, comme la respiration (Ravindra and Goswami, 2008), la croissance (Grossman and DeJong, 1994, Léchaudel et al., 2007) et le mûrissement (Yamada et al., 1994, Génard and Gouble, 2005). Aussi les variations de température au sein du fruit et entre les fruits, pourraient expliquer les différences de maturité et de qualité mesurées au sein des fruits (Biais et al., 2010, Moing et al., 2011, Sugiyama, 1999, Mitcham and McDonald, 1992) et entre les fruits dans l'arbre (Hofman et al., 1995, Bonora et al., 2013).

B - Le bilan hydrique du fruit est lié à son bilan carboné et énergétique.

Le bilan hydrique du fruit est égal à la différence entre les échanges (entrées ou sorties) d'eau entre la plante et le fruit par le xylème et le phloème, et les pertes en eau par transpiration. Le calibre des fruits à pulpe comme la mangue est intiment lié à leur bilan hydrique étant donné qu'ils sont principalement composés d'eau. Par ailleurs, les teneurs en composés primaires et secondaires du fruit sont également liées au bilan hydrique du fruit à cause des phénomènes de dilution (Génard et al., 2014). Les stress hydriques sur les arbres fruitiers, comme le manguier (Simmons et al., 1998), la pomme (Mills et al., 1996), ou la vigne (Castellarin et al., 2007) sont ainsi connus pour induire une diminution du calibre des fruits et une augmentation de leur teneur en solutés. La transpiration des organes végétaux est pilotée par le déficit de pression de vapeur (VPD) qui dépend de l'humidité relative, de la température de l'air et de celle du fruit. La relation entre la transpiration du fruit et sa température indique donc que le bilan hydrique du fruit dépend de son bilan énergétique.

La transpiration est également impliquée dans l'accumulation de minéraux dans le fruit (Marschner, 1995, Montanaro et al., 2010). Il a été montré pour plusieurs espèces, incluant la mangue (Simmons et al., 1998), l'avocat (Tingwa and Young, 1974) et la tomate (Park et al., 2005), que la durée de conservation des fruits varie en fonction de leur concentration en calcium. Des études ont suggéré que le calcium est impliqué dans le mûrissement du fruit à

travers son impact sur la synthèse d'éthylène (Tingwa and Young, 1974, Njoroge et al., 1998). Il a par ailleurs été rapporté que les désordres physiologiques liés à la sur-maturation interne sont moins fréquents dans les mangues avec une faible teneur en azote et une forte teneur en calcium (Young et al., 1965, Cracknell Torres et al., 2002, Burdon et al., 1991).

Le bilan hydrique de la mangue est lié à son bilan carboné (Léchaudel et al., 2005a). Il a ainsi été montré que lorsque la disponibilité carbonée du fruit est réduite, sa croissance en matière fraiche est diminuée. Des approches de modélisation ont permis de simuler la croissance en matière fraiche de la mangue (Léchaudel et al., 2007) et de la pêche (Fishman and Génard, 1998) en déterminant le bilan hydrique du fruit.

Par soucis de simplification, il a été estimé dans ces modèles que la température des fruits est égale à celle de l'air. Ces modèles ne tiennent donc pas compte des différences de température et de transpiration entre les fruits dans l'arbre. Hors, il peut être supposé que ces différences peuvent expliquer les variations de calibre rapportées entre les mangues selon leur position dans l'arbre (Hofman et al., 1995). Par ailleurs, ces modèles font l'hypothèse que la conductivité hydraulique des vaisseaux conducteurs de sève augmente proportionnellement avec la taille du fruit. Néanmoins, il a été rapporté que la conductivité hydraulique des vaisseaux du xylème diminue à la fin du développement du pigment (Trifilò et al., 2010), de la pomme (Dražeta et al., 2004), de la vigne (Tyerman et al., 2004) et du kiwi (Mazzeo et al., 2013). Cette diminution de conductivité hydraulique pourrait être à l'origine de la diminution des flux de xylème mesurée à la fin du développement de nombreux fruits comme la pomme (Lang and Ryan, 1994, Dražeta et al., 2004), le kiwi (Morandi et al., 2010) et la vigne (Greenspan et al., 1994). Il serait donc intéressant d'étudier les variations des flux de xylème pendant le développement de la mangue et leurs conséquences sur l'accumulation de matière fraiche.

C - Le bilan carboné de la mangue varie en fonction de la charge en fruits

Le bilan carboné du fruit est égal à la somme de carbone que le fruit produit par la photosynthèse et qu'il reçoit par le phloème moins la quantité de carbone qu'il consomme pour sa respiration. D'après les études réalisées sur la tomate, il semblerait que la quantité de carbone produite par l'activité photosynthétique du fruit soit négligeable en comparaison de celle qui est utilisée pour sa respiration et sa croissance (Lytovchenko et al., 2011, Carrara et al., 2001). On peut donc considérer que le bilan carboné du fruit est égal à

la différence entre la quantité de carbone qui entre dans le fruit par le phloème et celle qui est consommée par sa respiration. La respiration de la mangue varie en fonction de sa vitesse de croissance (Léchaudel et al., 2005a), son stade de maturité (Burg and Burg, 1962) et de la température (Ravindra and Goswami, 2008). Un modèle a été proposé par Léchaudel et al. (2005a) pour simuler la croissance en matière sèche de la mangue. Cette approche de modélisation a mis en évidence que les différences de charge en fruit causent d'importantes variations de croissance en matière sèche entre les mangues. Cependant ce modèle n'a pas étudié l'impact des différences de température et d'exposition lumineuse entre les fruits dans l'arbre sur leur croissance en matière sèche. L'hétérogénéité des conditions climatiques au sein de l'arbre cause vraisemblablement des différences d'accumulation de matière sèche entre les fruits du fait des variations de respiration et de disponibilité carbonée.

Il a par ailleurs été montré par une approche de modélisation sur la pêche que la synthèse d'éthylène est liée à la croissance en matière sèche du fruit (Génard and Bruchou, 1992). Ces résultats ont été confirmés sur la mangue, puisqu'il a été montré que des fruits avec un apport en carbone limité murissent plus tard (Léchaudel and Joas, 2006). Ces études indiquent donc que le bilan carboné de la mangue impacte à la fois sa qualité et sa maturation.

D - Conclusions de la synthèse bibliographique

L'hétérogénéité de la qualité des mangues à la récolte cause des pertes importantes tout au long de la chaine de distribution. La qualité de la mangue dépend de sa concentration en composés primaires (sucres, acides) et secondaires (pigments, vitamines, arômes). Ces composés sont contenus dans la matière sèche du fruit et leur concentration varie en fonction de la matière fraiche et du stade de maturité de la mangue. La croissance en matière fraiche et en matière sèche de la mangue ainsi que son stade maturité, varient en fonction de ses bilans énergétique, hydrique et carboné. De nombreux facteurs sont impliqués dans la variation de ces bilans, comme les conditions climatiques, la charge en fruits et la position du fruit dans l'arbre. Une approche de modélisation sur la pêche et sur la pomme a mis en évidence que les variations spatiales des conditions climatiques au sein de l'arbre cause des différences de température au sein du fruit et entre les fruits (Saudreau et al., 2007, Saudreau et al., 2009). Ces différences ont été confirmées sur la mangue

(Léchaudel et al., 2012). Etant donné l'effet de la température sur la croissance en matière fraiche et en matière sèche de la mangue et sur sa maturité, il est supposé que les variations des conditions climatiques au sein de l'arbre sont impliquées dans l'hétérogénéité de la qualité et de la maturité au sein des mangues et entre les mangues.

Des travaux de modélisation ont été proposés précédemment sur la mangue et la pêche pour simuler la croissance en matière fraiche et en matière sèche du fruit (Léchaudel et al., 2005a, Léchaudel et al., 2007) et son mûrissement au travers de sa production d'éthylène (Génard and Gouble, 2005). Cependant, ces approches ne permettent pas de prendre en compte l'effet des conditions climatiques sur la qualité et la maturité du fruit. Il est en effet estimé dans ces modèles que la température des fruits est égale à celle de l'air et ne varie pas en fonction de l'exposition lumineuse. Il est donc proposé d'intégrer à ces modèles les travaux de modélisation de la température des fruits proposé par Saudreau et al. (2007). Par ailleurs, les modèles de croissance en matière fraiche proposés jusqu'à présent ne tiennent pas compte de la diminution de la conductivité hydraulique des vaisseaux de xylème mesurée à la fin du développement de nombreux fruits. Il est donc proposé d'intégrer à ces modèles de nouvelles hypothèses basées sur les résultats d'analyses expérimentales. Le couplage de tous ces modèles issus de différentes disciplines, i.e. thermodynamique et écophysiologie, permettra d'avoir une vision globale des facteurs impliqués dans les processus liés à l'élaboration de la qualité du fruit et à sa maturation, à deux échelles, celle du fruit et celle de l'arbre.

E - Plan de travail

Cette thèse est organisée en deux parties. Une **première partie** s'intéresse à la variabilité de qualité et de maturité au sein de la mangue. Le **premier chapitre** de cette première partie est consacré à l'étude des variations de couleur de la peau de la mangue, un attribut important de la qualité du fruit. Cette étude met en évidence le lien complexe entre la couleur de la peau et sa teneur en pigments.

Le **deuxième chapitre** de cette partie est consacré à l'établissement d'un modèle thermodynamique pour simuler les gradients de température et de transpiration au sein d'une mangue en croissance. Il s'est intéressé aux facteurs physiques et thermiques du fruit et aux conditions climatiques à l'origine des variations spatiales et temporelles de la température et de la transpiration du fruit. Les résultats de cette étude ont été utilisés dans le **troisième chapitre** de cette partie pour déterminer si les différences de température au sein de la mangue sont liées à la variabilité de qualité et de maturité au sein du fruit.

La **seconde partie** de cette thèse s'intéresse à déterminer comment la variabilité des conditions de croissance des fruits est à l'origine des différences de qualité et de maturité entre les mangues.

Un **premier chapitre** est dédié à l'étude des facteurs pré et post-récolte qui impactent la crise climactérique et la synthèse d'éthylène des mangues. Cette étude introduit le **deuxième chapitre** portant sur le développement d'un modèle simulant la synthèse d'éthylène dans la mangue. Le **troisième chapitre** est consacré à l'étude des variations des flux de xylème au cours de la croissance de la mangue et à leurs causes. Les résultats de cette étude expérimentale ainsi que ceux sur la modélisation de la température et de la transpiration du fruit sont utilisés dans le **quatrième chapitre** consacré à la modélisation de la croissance en matière fraiche de la mangue. Le **cinquième** et dernier **chapitre** de cette thèse présente le couplage des modèles de température, croissance en matière fraiche et synthèse d'éthylène à un modèle de croissance en matière sèche. Le couplage de ces modèles permet d'étudier comment les conditions de croissance de la mangue affectent sa qualité et sa maturité.

Partie I : Hétérogénéité de la qualité et de la maturité au sein de la mangue

Cette partie est consacrée à l'étude de l'hétérogénéité de la qualité et de la maturité au sein de la mangue. Elle lie des approches expérimentales et de modélisation afin de mesurer les différences de qualité et de maturité au sein du fruit et de déterminer leurs sources de variations.

Un premier chapitre s'intéresse aux causes de l'hétérogénéité de la couleur de la peau de la mangue et aux différences de couleur entre les variétés. Il est proposé dans cette étude de mesurer la teneur en pigments de la peau, i.e. chlorophylles, caroténoïdes et anthocyanes et d'étudier la relation entre cette teneur et la couleur de la peau du fruit.

Le second chapitre de cette partie présente une approche de modélisation qui simule les variations spatiales et temporelles de la température et de la transpiration de la mangue. Ce modèle est utilisé pour déterminer l'impact des changements des propriétés physiques et thermiques de la mangue au cours de sa croissance sur sa température et sa transpiration. Cette approche de modélisation est également employée dans le troisième chapitre de cette partie qui vise à déterminer l'effet des différences de température au sein de la mangue sur sa qualité, i.e., couleur de la pulpe et de la peau, acidité et teneur en composés solubles, et sa maturité.

I - Non-destructive prediction of color and pigment contents in mango peel

Objectifs :

La couleur est un attribut important de la qualité du fruit. Celle-ci varie considérablement au sein de la mangue et entre les variétés de mangue. Pour déterminer d'où proviennent ces différences, il est proposé dans ce chapitre d'étudier les relations entre la couleur et la teneur en pigments de la peau. Pour se faire des modèles ont été établis pour prédire de manière non destructive les concentrations de la peau en anthocyanes, caroténoïdes et chlorophylles en utilisant des mesures de réflectance. Cette étude s'appuie sur plusieurs variétés de mangue qui présentent des colorations contrastées, i.e., Cogshall, Kent, Caro, Sensation, Tommy Atkins, Nam Doc Mai, Irwin et Heidi. Ce chapitre a fait l'objet d'une publication dans **Scientia Horticulurae** sous forme d'un article intitulé « *Non-destructive prediction of color and pigment contents in mango peel*».

Principaux résultats :

- Les modèles développés permettent de prédire correctement les teneurs en pigments de la peau.

- D'importantes différences de couleur et de teneur en pigment ont été mesurées au sein des variétés et entre les variétés.

- Les relations entre la couleur et la teneur en pigment de la peau sont complexes et dépendent de la variété.

Non-destructive prediction of color and pigment contents in mango peel

Thibault Nordey[1*], Jacques Joas[2], Fabrice Davrieux[2], Michel Génard[3] and Mathieu Léchaudel[1]

[1]CIRAD, UPR HORTSYS, F-97455 Saint-Pierre, La Réunion, France

[2]CIRAD, UMR QUALISUD, F-34398 Montpellier, France

[3]INRA, UR 1115, Plantes et Systèmes de Culture Horticoles, F-84000 Avignon, France

A - Abstract

The pigment content of mango peel is an important quality determinant due to its involvement in the nutritional value and coloration of the fruit. In addition, pigment content in the peel is related to the fruit maturity stage and has been suggested as a reliable harvest criterion. Measurements of pigment content by vis-spectrophotometry and chromatography methods are destructive, time-consuming and expensive. This study deals with the potential of reflectance measurements as a non-destructive method to assess pigment content and color in mango fruit peel. We also investigated the relationship between the pigment content of the peel and its color. Eight mango cultivars, i.e., Cogshall, Kent, Caro, Sensation, Tommy Atkins, Nam Doc Mai, Irwin and Heidi, were studied. Hue angle distribution was used to characterize and to compare cultivar colors. The peel contents in anthocyanin, carotenoids, chlorophyll a and chlorophyll b were predicted using Partial Least Square Regressions based on reflectance indexes and compared between cultivars. Our results showed that reflectance measurements can accurately ($R^2 \geq 0.91$, RMSE ≤ 5.74 $\mu g.gFW^{-1}$) predict the contents of the main pigment contained in the mango peel. Further studies are nevertheless required to increase PLSR robustness. Significant differences were found in the hue angle distribution and the predicted peel pigment content between the eight mango cultivars studied. All relationships between pigments and hue angle values were found to be cultivar-dependent. The highest correlations between hue angle values and pigment contents were found for anthocyanin content in red cultivars ($0.76 \geq R^2 \geq 0.58$), and chlorophyll content in green cultivars ($0.88 \geq R^2 \geq 0.62$). Results showed that reflectance measurements could be used to predict mango quality determinants such as the fruit maturity stage according to the peel chlorophyll content, the fruit coloration and the content of valuable components, i.e., anthocyanins and carotenoids.

B - Introduction

The chlorophyll content in mango peel was recently found to be a reliable indicator of the mango maturity stage (Lechaudel et al., 2010). In addition, anthocyanins and carotenoid pigments of mango fruit have been the object of increasing interest since they are known to provide health benefits due to their antioxydant activity(Ajila et al., 2010, Ajila et al., 2007a, Ajila et al., 2007b, Berardini et al., 2005). Spectrophotometric and HPLC measurements were used to measure pigment content in mango peel and revealed their variations between cultivars (Berardini et al., 2005, Ajila et al., 2007a, Ketsa et al., 1999) and fruit maturity stages (Ketsa et al., 1999, Medlicott et al., 1986). However, these methods are destructive, time-consuming and expensive. Non-destructive measurements of surface reflectance in the visible range have been suggested to predict the pigment content of leaves and apple skin (Merzlyak et al., 2003a, Mielke et al., 2012, Gitelson et al., 2001, Sims and Gamon, 2002, Zude, 2003). Such measurements could also be used to assess the content of the main pigments of mango fruit peel, i.e., chlorophyll a, chlorophyll b, carotenoids and anthocyanins (Medlicott et al., 1986). These pigments are involved in the photosynthesis activity and in the photo protection of the fruit (Merzlyak et al., 2002, Steyn et al., 2002) and determine the fruit color (Lancaster et al., 1997). Fruit color is an important factor for market acceptance (Nguyen H. et al., 2004, Vásquez-Caicedo et al., 2002, Litz, 2009) and could be used as a tool to describe mango cultivars (Ayala-Silva et al., 2005) or to predict mango maturity stages (Jha et al., 2007). Colorimetric coordinates can be deduced from reflectance measurements using color-matching functions (Vos, 1978). These functions make it possible to calculate the quantity of red, green and blue color of a reflectance spectrum in order to reproduce the sensitivity of the human eye (Abbott, 1999). Several authors found relationships between colorimetric measurements and pigment content in the skin (Iglesias et al., 2012, Lancaster et al., 1997, Steyn et al., 2004) or flesh tissues (Ornelas-Paz et al., 2008) (Vasquez-Caicedo et al., 2005, Sánchez et al., 2006) for various fruits and vegetables.

In this paper, reflectance measurements were used to evaluate the relationships between the color and the pigment content of mango peel. The study is based on eight mango cultivars in order to ensure a wide range of variation in fruit colors and pigment contents.

C - Materials and methods

1) **Fruits samples, measurements of reflectance spectra and color determination**

The study was carried out on 61, 60, 79, 60, 51, 51, 51, and 58 mangoes from cv. Cogshall, Kent, Caro, Sensation, Tommy Atkins, Nam Doc Mai, Irwin and Heidi, respectively. Fruits were grown during the 2012-2013 production season in the CIRAD orchard collection of Reunion Island (20°52' 48'' S, 55°31' 48" E), consisting of 7-years-old trees grafted on 'Maison Rouge' cultivars. Trees were well-irrigated, spaced 5 x 6 m, and approximately 3 m high. Fruits were randomly chosen on the tree in order to represent the variability of sun exposure conditions, and harvested at the optimal harvest stage for the local market, considering that fruits are at their prime during the next three to five days (Léchaudel and Joas, 2006). Just after the harvest, approximately four NIR spectra of fruit peel surface at random locations on each fruit were monitored from 350 to 2500 nm with the contact probe of a portable spectrometer (LABSPEC 2500, Analytical Spectral Devices, Inc., Boulder, CO, USA). For 33 supplementary samples representing the observed color variability observed within the studied cultivars, pigment concentrations in the peel were determinate after extraction by vis-spectrophotometry in order to develop predictive models based on reflectance spectra. NIR spectra were monitored on these skin samples prior to their destructive analysis to determine pigment content.

XYZ colorimetric coordinates of skin color were obtained from its reflectance spectra in the visible range (Colorimetry, 2004), where S(δ) is the spectral reflectance of the measured mango peel, $I(\delta)$ is the spectral irradiance of the illuminant, and $\overline{x(\delta)}$, $\overline{y(\delta)}$ and $\overline{z(\delta)}$ are the color-matching functions. The CIE standard illuminant, D65, was used in this paper (Xn = 0.9503, Yn = 1 and Zn=1.0891). The calculated XYZ color coordinates were then converted to CIELAB coordinates, and the hue angle value (H°) was calculated from a* and the b* coordinates using Equation 2.

$$\begin{cases} X = \frac{1}{N} \int_{380}^{700} I(\delta) \times \overline{x(\delta)} \times S(\delta) \times d\delta \\ Y = \frac{1}{N} \int_{380}^{700} I(\delta) \times \overline{y(\delta)} \times S(\delta) \times d\delta \\ Z = \frac{1}{N} \int_{380}^{700} I(\delta) \times \overline{z(\delta)} \times S(\delta) \times d\delta \end{cases}$$ *Equation 1*

where: $N = \int_{380}^{700} I(\delta) \times \overline{y(\delta)}$

$$h_{ab} = \arctan(\frac{b*}{a*})$$ *Equation 2*

2) **Determination of peel pigment concentration**

The photosynthetic pigments, chlorophylls *a* and *b*, as well as the total carotenoids (x + c), were extracted with 100% DiMethylSulfOxyde (DMSO). Approximately 5 cm² of mango peel samples were removed with a peeler on each fruit studied, and then immediately frozen in liquid nitrogen and stored in an ultra-freezer (−80°C) until chlorophyll and carotenoid extraction and quantification were performed. Approximately 0.5 g of the mango peel samples were extracted with 5 mL of DMSO after incubation in the dark, in a dry bath at 65°C for 5 h. Heated samples were removed from the dry bath and allowed to reach room temperature. The absorbance (A) of supernatants was then measured at 480, 649, and 665 nm with a VIS scanning spectrophotometer (Helios Epsilon, Thermo Fisher Scientific, USA). To calculate the chlorophyll *a* ($[C_a]$), chlorophyll *b* ($[C_b]$) and total carotenoid ($[C_{x+c}]$) content, the equations of Wellburn (1994) were used (Equation 3).

$$[C_a] = 12.47 \times (A_{665}) - 3.62 \times (A_{649})$$
$$[C_b] = 25.06 \times (A_{649}) - 6.5 \times (A_{665})$$
$$[C_{\mathrm{x+c}}] = (1000 \times (A_{480}) - 1.29 \times [C_a] - 53.78 \times [C_b]) / 220$$ *Equation 3*

Anthocyanin pigments were extracted according to the procedure described by Jing and Giusti (2007). Briefly, approximately 0.5 g of crushed mango peel was added to 4 ml of

deionized water. The sample was shaken in a dry bath at 50°C for 1 hour. The resulting extract was filtered through a Whatman No.1 filter paper under a vacuum using a Büchner funnel. Extraction with deionized water provides the highest yield in comparison to other extraction solvents (Jing and Giusti, 2007).

The monomeric anthocyanin content of the mango peel was measured using a spectrophotometric pH differential protocol (Lee et al., 2005). A VIS scanning spectrophotometer (Helios Epsilon, Thermo Fisher Scientific) was used to measure absorbance at 520 and 700 nm against a distilled water blank. Anthocyanin content was expressed as micrograms of cyanidin-3-glucoside equivalent per gram of fresh mango peel.

3) **Prediction of peel pigment content using reflectance spectra**

In order to non-destructively predict the peel contents in pigments using reflectance spectra, a model based on Partial Least Square Regression (PLS) was established. The tested preprocessing methods (first and second derivation) did not improve the models accuracy so no transformed spectral data ($\log(\frac{1}{Reflectance})$) were used to build models.

Model calibrations were performed from the destructive measurements of pigment content of the 33 epidermis samples. As proposed by several authors (Merzlyak et al., 2003a, Mielke et al., 2012, Gitelson et al., 2001, Sims and Gamon, 2002), the PLS regression was calculated from reflectance indexes based on optical pigment features. The number of latent variables for the PLSR model was obtained by using leave-one-out cross-validation to avoid over-fitting of the equation. The procedure provided by the PLS package (Mevik and Wehrens, 2007) developed in R software (RDC Team, 2012) and fully described by Cornillon (2010) was applied.

Model prediction error was evaluated using the Root Mean Square Error (RMSE) and the coefficient of determination (R^2) as indicators. Calculation of the RMSE is described in Equation 4, were y_t is the t^{th} observed or reference value, $\widehat{y_t}$ is the t^{th} simulated value, and n is the number of observed or simulated values.

$$\mathrm{RMSE} = \sqrt{\frac{\sum_{t=1}^{n}(y_t - \widehat{y_t})^2}{n}} \qquad \textit{Equation 4}$$

Models calibrated using the 33 peel samples were applied to the all reflectance measurements in order to predict the peel contents in pigments of cultivars studied.

Statistical analysis

All analyses and graphical renderings were performed with R software (RDC Team, 2012) implemented with Colorspace (Ihaka et al., 2008) and PLS packages (Mevik and Wehrens, 2007). The probability density function of the hue angle values was calculated for each cultivar using the density function of R software. The probability densities of the hue angle values were compared between cultivars according to the non-parametric test of Kolmogorov-Smirnov. Multiple comparisons between cultivars of the predicted pigment content averages were performed using the Tukey test performed with the HSD.test R function provided in the Agricolae package. For all statistical analysis, the nul hypothesis was rejected, i.e. absence of effect or difference, when the p-value was less or equal to the significance level of 0.05.

D - Results and discussion

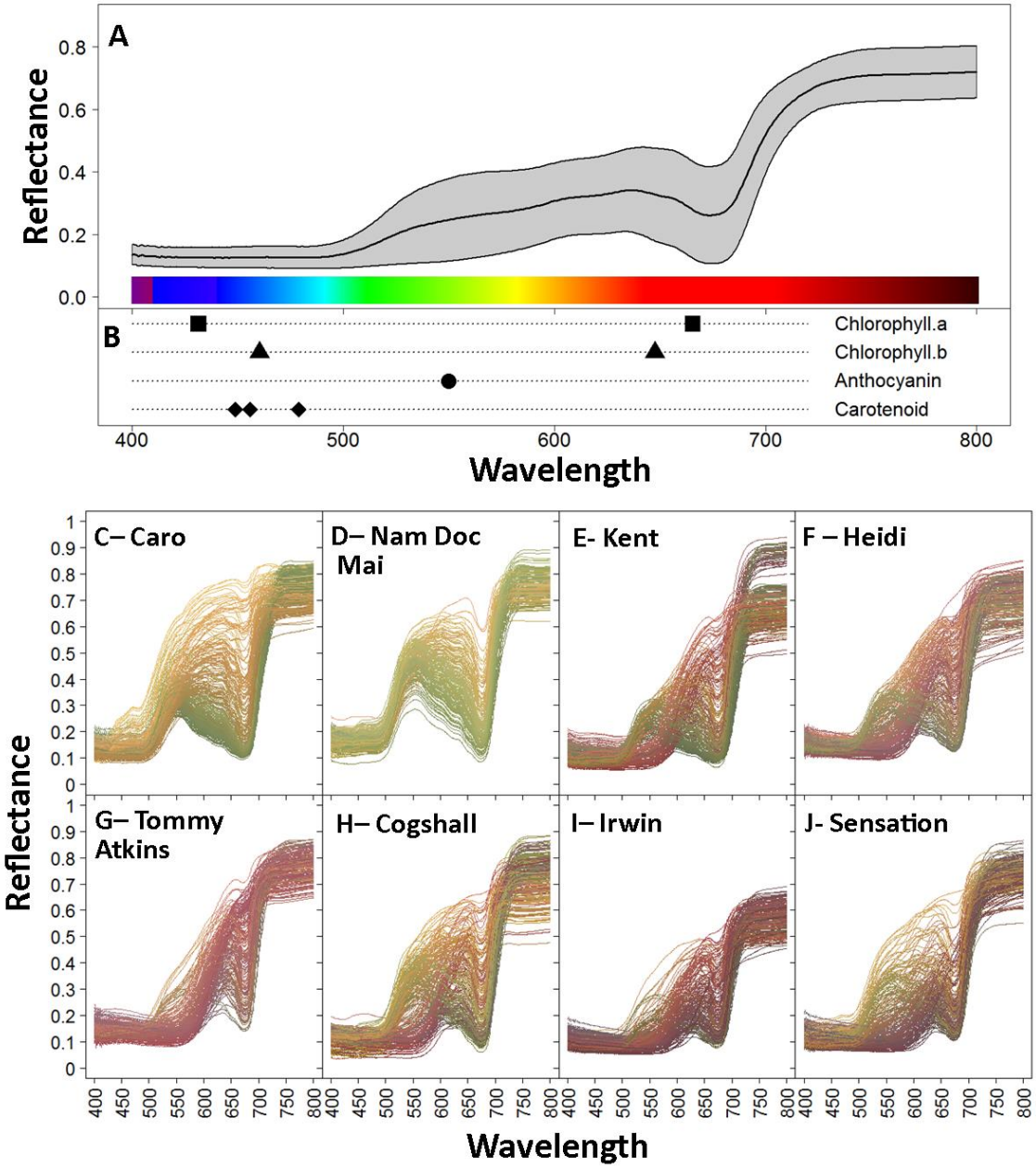

Figure 5: Peel reflectance average in the visible range (solid line) ± the standard deviation (dashed lines) calculated from all mango cultivars studied (A), completed by a diagram of the color of the visible spectra, and by a diagram of the maximal absorbance of pigments (B), i.e., chlorophyll a (431.5 and 665.6 nm), chlorophyll b (460.3 and 647.6 nm) (Wellburn A.R., 1994), anthocyanins (550 nm) (Merzlyak et al., 2003b), and carotenoids (479, 456 and 449 nm) (Wellburn A.R., 1994). C to J: peel reflectance measurements in the visible range according to the mango cultivars studied. The color of each curve corresponds to the color of the peel sample.

1) **Analysis of reflectance spectra**

The average spectra of peel cultivars in the visible region (Figure 5-A) had a pattern similar to those found in apple fruits (Merzlyak et al., 2003b) and leaves (Gitelson et al., 2002). The reflectance was more variable and higher in the red region (600 to 800 nm) and in the green region (500 to 600 nm) than in the blue region (400 and 500 nm) (Figure 5A). In fact, reflectance was found to fluctuate for all cultivars between 0.04 and 0.26 at 450 nm, between 0.04 to 0.63 at 550 nm, and between 0.06 and 0.77 at 673 nm (Figure 5C to Figure 5J). In the visible range, the reflectance of fruit peels fluctuates with the variation in the pigment contents (Merzlyak et al., 2003b). The increase in the reflectance in the red region (640 -700 nm) can be mainly linked to a decrease in the chlorophyll content (Figure 5A) that absorbs radiations in this region (Merzlyak et al., 2003b) (Figure 5B). However, since the chlorophyll pigment also absorbs radiations near 450 nm (Figure 5B), it was expected that the presumed chlorophyll variation suggested by the variation in the red region would also be observed in the blue region (Figure 5A and Figure 5B). Lack of a relationship between the variation in the blue and the red regions may be explained by the presence of carotenoid pigments that absorb radiations in the blue region, like chlorophyll (Wellburn A.R., 1994, Gitelson et al., 2002) (Figure 5B). Merzlyak and Solovchenko (2002) suggested that the carotenoid synthesis is induced when the chlorophyll degradation occurs during fruit senescence in order to provide protection to light-sensitive constituents of plant tissues from radiation in the blue part of the visible spectrum. The reflectance variation near 550 nm (Figure 5A) can be linked to the variation in anthocyanin absorption (Merzlyak et al., 2003b, Gitelson et al., 2001) (Figure 5B).

It can be observed in Figure 5C to Figure 5J that reflectance spectra varied between mango cultivars, suggesting different pigment contents, as previously discussed. Color and reflectance spectrum variations were found to be related in some cases. For example, yellow coloration was associated with a higher reflectance in the red region than in the green one for Caro mangoes (Figure 5C), suggesting a lower chlorophyll content. Furthermore, red curves were associated with a lower reflectance near 550 nm than green ones (Figure 5C to Figure 5J), which can be linked to higher anthocyanin content. However, it can be observed for all cultivars that the same color can result from variations in spectral

distribution, especially for Tommy mangoes (Figure 5G), which exhibited a quite homogenous red coloration despite various reflectance curves in the red region.

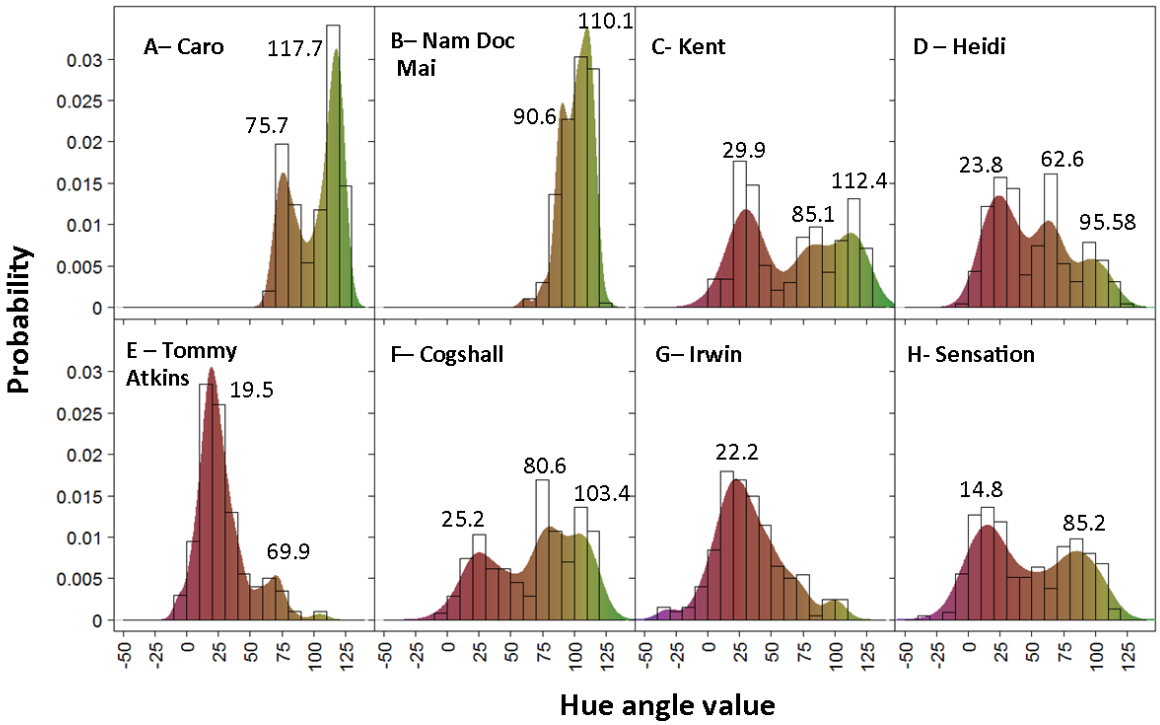

Figure 6: Hue angle probability function (colored curve) and histogram (bars) calculated for each cultivar. Values indicated next to the curve correspond to the hue angle value of the peaks.

2) **Peel color variations.**

A wide color variation was found between cultivars and within cultivars (Figure 6).

The commercial success of mango cultivars depends in part on their external coloration since most cultivars intended for the Southeast Asia market have green skins, whereas the ones intended for the northern market have a red coloration (Litz, 2009).

Among the eight cultivars studied, only Caro (Figure 6A) and Nam Doc Mai (Figure 6B) did not show a red coloration, i.e., hue angle ≤ 50°. Hue angle distribution differed considerably between cultivars (Figure 6) with regard to their ranges of variation and patterns. For example, hue angle values ranged from 60° (yellow skin) to 126° (green skin) for Nam Doc Mai mangoes (Figure 6B), compared to -30° (purple skin) to 116° (green skin) for Sensation mangoes (Figure 6H). The proportion of red coloration varied between cultivars (Figure 6),

and sorting cultivars according to their proportion of blush area (H° < 50°) in decreasing order resulted in the following ranking: Tommy Atkins, Irwin, Sensation, Heidi, Kent, Cogshall, Nam Doc Mai and Caro, with 85.5%, 77.6%, 55.1%, 51.1%, 44.3%, 33.7%, 0% and 0% of blush area, respectively. Multiple comparisons (Tukey test, $P < 0.05$) of the hue angle averages of cultivars indicated significant differences. However, no distinction was made between Caro and Nam Doc Mai, Cogshall and Kent, Heidi and Sensation, and Irwin and Tommy Atkins (data not shown). Ayala-Silva *et al.* (2005) had already observed the limit of the use of the hue angle averages for comparing colors between cultivars because few significant differences were found due to the large standard errors associated with each average value. Comparisons of the peel colors based on the distribution of the hue angle values (Figure 6) made it possible to significantly differentiate each cultivar from the others. These results suggested that the study of the hue angle distribution is an effective method for characterizing mango cultivar color since it takes their color heterogeneity into account (Figure 6).

3) **Measurements and non-destructive prediction of peel pigment content.**

Use of reflectance measurements to access pigment contents requires a calibration phase, but has the advantage of being non-destructive and convenient. For 33 samples, pigment concentrations in the peel were determinate after extraction by vis-spectrophotometry in order to develop predictive models based on reflectance spectra. Measurements varied from 1.97 to 99.29 $\mu g.gFW^{-1}$ for chlorophyll *a*, and between 1.81 and 58.7 $\mu g.gFW^{-1}$ for chlorophyll *b*, in accordance with Wang et al. (2008) who found that total chlorophyll contents fluctuated between 33.8 and 199.1 $\mu g.gFW^{-1}$ in the peel of Tainong mangoes. Carotenoid content in the fresh peel varied from 14.37 to 35.9 $\mu g.gFW^{-1}$, in line with the measurements of Ketsa *et al.* (1999) who found that the β –carotenoid content, i.e., the main carotenoid pigment in mango peel (Medlicott et al., 1986), for Nam Doc Mai and Tongdum mangoes varied between 5 and 25 $\mu g.gFW^{-1}$ of fresh peel. Concerning anthocyanin content in the peel, measurements varied between 0 and 100.6 $\mu g.gFW^{-1}$. Ajila *et al.* (2007) reported anthocyanin contents in the dry mango peel varying between 2030 and 5650 $\mu g.gDW^{-1}$, contrary to Berardini *et al.* (2005) who reported anthocyanin contents varying between 0.211 to 3.72 $\mu g.gDW^{-1}$ for several mango cultivars, and to Dorta et al.

(2012) who reported values fluctuating between 15 and 33 µg.gDW^{-1} for ripe Keitt mangoes. Differences between authors are probably related to the differences in extraction and measurement methods used.

Several authors (Gitelson et al., 2001, Merzlyak et al., 2003b, Mielke et al., 2012) estimated the pigment content in the peel using indexes related to the optical features of the different pigments in the visible range (Table 1).

Table 1: Reflectance indexes used to predict chlorophyll a, chlorophyll b, carotenoid, and anthocyanin content in mango peel, and NIR calibrations performances, with R², the determination coefficient, RMSE, the Root Mean Square Error and n the number of samples.

Pigment	Indexes	
Chlorophyll ***a***	$[Chl.a] \sim \frac{R_{800}}{R_{650}} + \cdots + \frac{R_{800}}{R_{700}}$	(R^2 =0.99, RMSE = 3.54, n = 33)
Chlorophyll ***b***	$[Ch.b] \sim \frac{R_{800}}{R_{645}} + \cdots + \frac{R_{800}}{R_{700}}$	(R^2 = 0.99, RMSE = 1.73, n = 33)
Total anthocyanins	$[Anthocyanin] \sim \frac{R_{700}}{R540} + \cdots + \frac{R_{700}}{R580}$	(R^2 = 0.98, RMSE = 5.74, n = 33)
Total carotenoids	$[Carotenoid] \sim \frac{R_{800}/R_{700}}{R_{400}} + \cdots + \frac{R_{800}/R_{700}}{R_{600}}$	(R^2 = 0.99, RMSE = 0.86, n = 33)

Various indexes are proposed in the literature. The ones used in this study were inspired by those found by Merzlyak et al. (2003). Since reflectance data are composed of many noisy and collinear variables, the use of PLS regression is recommended (Wold et al., 2001) and commonly used (Nicolaï et al., 2007). Moreover, multivariate analysis, such as PLS regression, of absorbance values was found to improve the prediction of pigment performed with linear regression (Zude-Sasse et al., 2002). The cross validation leave-one-out method used to determine the number of latent variables for the PLSR (Figure 7) made it possible to maximize the predictive ability of the model and to avoid model over-fitting (Cornillon, 2010). The average RMSE ratios of measured pigment contents were 6.8%, 5.9%, 10.3%, and 15.3%, for chlorophyll *a*, chlorophyll *b*, carotenoid and anthocyanin, respectively.

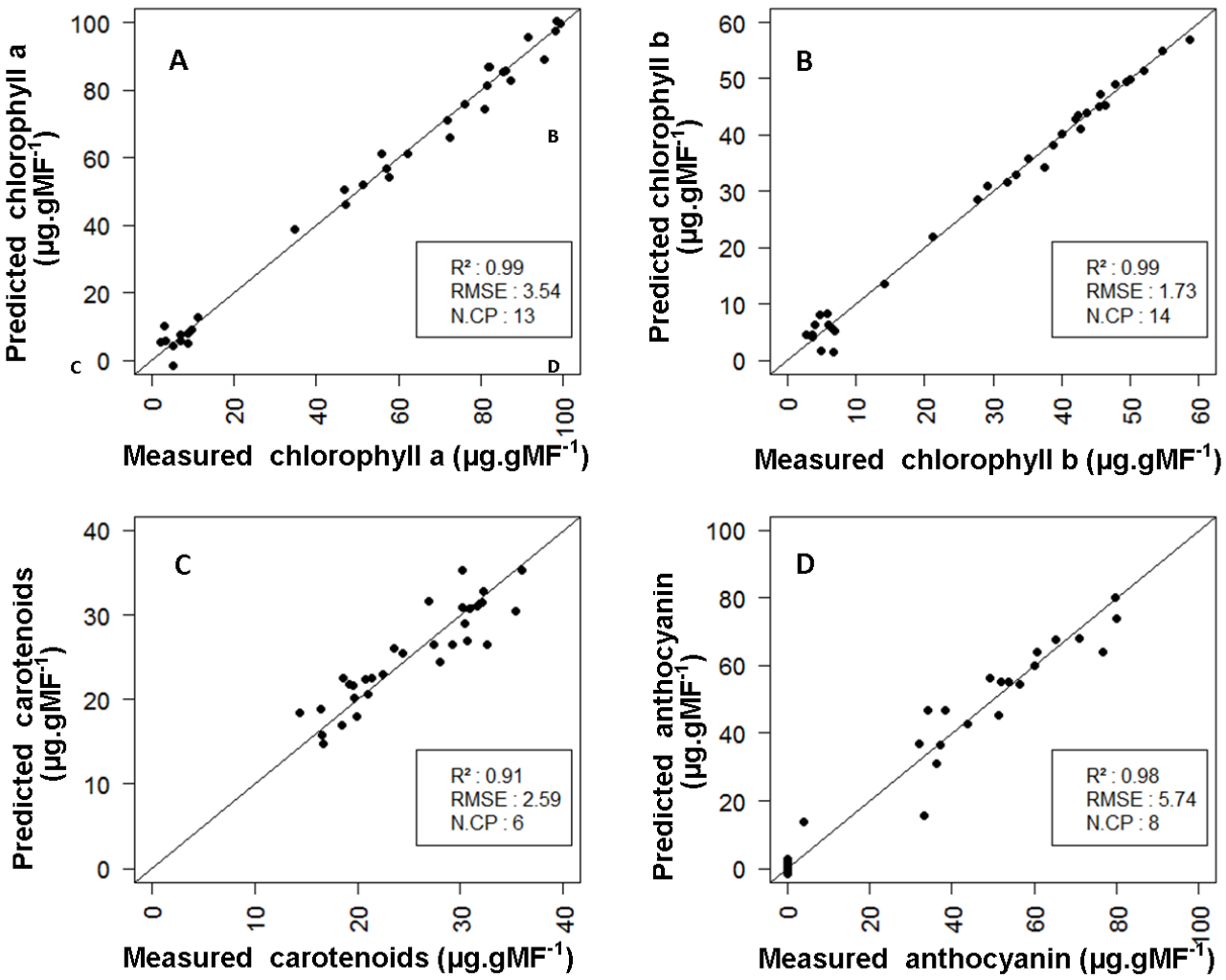

Figure 7: Adjustment of partial least square regression to non-destructively predict contents in the peel of chlorophyll a (A), chlorophyll b (B), carotenoids (C), and anthocyans (D), according to reflectance spectra, with R^2, values of the determination coefficient, RMSE, values of the root mean square error and N.CP, the number of latent variables selected.

Higher prediction errors were observed for anthocyanin pigment (Figure 7D) compared to the other pigments (Figure 7A, Figure 7B and Figure 7C). The assessment of pigment contents using peel spectral measurements assumes that the optical pigment features remain the same in the different cultivars and through different stages of fruit development (Merzlyak et al., 2003b). However, anthocyanin optical features are affected by several factors such as pH, temperature, light and the presence of enzymes, flavonoids and metallic ions (Castañeda-Ovando et al., 2009). These variations can explain the higher prediction error obtained for these pigments. Several anthocyanin measurements were close or equal to 0, inducing model predictions that were below zero (Figure 7D). Predictions below 0 were not considered in further analyses. To increase the robustness and the accuracy of the

model for further applications, the amount of calibrating data should be increased, especially in the range of pigment contents not covered by this study. Moreover, additional studies are required to determine whether or not the optical features of pigments vary between cultivars and/or with fruit maturity stages. Nevertheless, the accuracy of PLS regressions (R^2 > 0.91, RMSE < 5.75 µg.gFW^{-1}) (Figure 7) suggested the applicability of reflectance spectroscopy for assessing pigment contents in the peel of mango fruits.

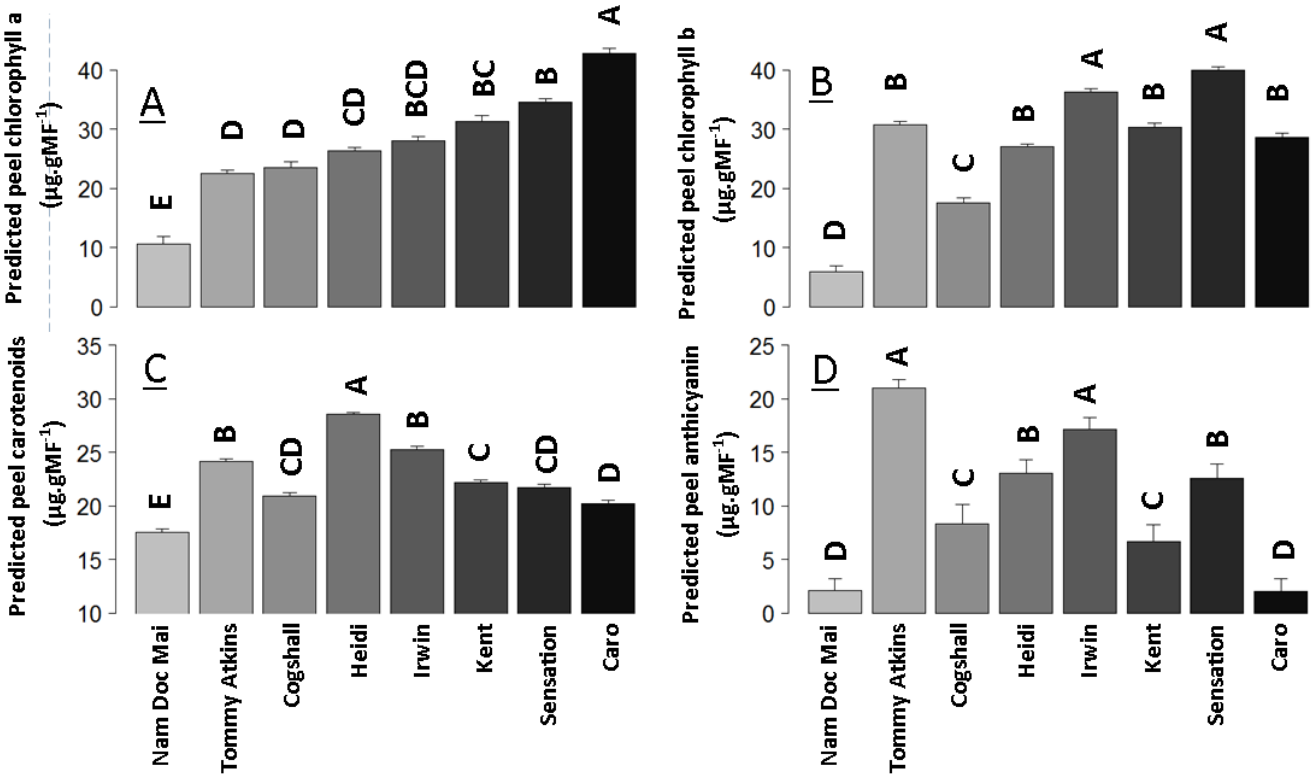

Figure 8: Comparison of the predicted pigment contents in mango peel between cultivars. (A) chlorophyll a; (B) chlorophyll b; (C) carotenoids; (D) anthocyanins. Bars represent the average ± standard deviation of the predicted pigment content. Different letters signify that the averages of the pigment content were different at P < 0.05 (according to Tukey's multiple comparison test).

The pigment content averages predicted varied between cultivars (Figure 8), in accordance with previous studies (Ornelas-Paz et al., 2008, Ajila et al., 2007a, Ketsa et al., 1999). The lowest average of chlorophyll *a* content was found for Nam Doc Mai mangoes (10.65 µg.gFW-1), and the highest one for Caro mangoes (42.76 µg.gFW-1) (Figure 8A). Nam Doc Mai cultivar also had the lowest chlorophyll *b* content (5.93 µg.gFW-1), and Sensation cultivar had the highest content (39.91 µg.gFW-1) (Figure 8B). The chlorophyll *a* to chlorophyll *b* ratio varied between cultivars and was higher than 1 for Caro, Cogshall, Kent and Nam Doc Mai, and lower than 1 for Heidi, Tommy Atkins, Irwin and Sensation (Figure 8A and Figure 8B). This ratio was found to decrease with the maturity stage for Tommy Atkins mangoes from 2.2 to 0.8 in a ripe fruit due to a faster degradation of chlorophyll *a* than chlorophyll *b* during fruit ripening (Medlicott et al., 1986). Since fruits from the cultivars studied were harvested at a similar maturity stage, it was deduced that the chlorophyll *a* to chlorophyll *b* ratio was cultivar-dependent. The average of predicted contents in anthocyanins varied between cultivars, from 2.03 $\mu g.gFW^{-1}$ for Caro mangoes, to 21.02 $\mu g.gFW^{-1}$ for Tommy Atkins mangoes. The presence of anthocyanin pigments was predicted in the peel of all cultivars (Figure 8D), even for green-yellow ones, i.e., Caro (Figure 6A) and Nam Doc Mai (Figure 6B), but in significantly lower quantities than in red cultivars. Anthocyanin pigments were previously found in the peel of green-yellow cultivars such as Badami (Alphonso) (Ajila et al., 2007b) and José (Berardini et al., 2005). Moreover, Wolfe et al. (2003) found trace amounts of anthocyanin pigment in the peel of Golden Delicious apples, which are characterized by a lack of red pigmentation. The predicted averages of anthocyanin content according to cultivars were related to their proportion of red skin. In fact, Tommy Atkins and Irwin cultivars showed the highest peel anthocyanin contents (Figure 8A) as well as the highest proportion of blushed area (Figure 6-F and Figure 6-G, respectively).

Significant differences were also found in the carotenoid contents between cultivars. The average content of carotenoid in the peel fluctuated from 17.56 $\mu g.gFW^{-1}$ for Nam Doc Mai mangoes to 28.59 $\mu g.gFW^{-1}$ for Heidi mangoes (Figure 8D). Carotenoid content variations between all fruits were smaller than the variations predicted for chlorophyll and anthocyanins, confirming the lower reflectance variation observed in the blue region compared to that of the green and blue region (Figure 5).

Chlorophyll content in the peel has been suggested to be a reliable indicator of maturity stage for several fruits such as mango (Lechaudel et al., 2010), papaya (Urbano Bron et al., 2004) and apple (Song et al., 1997). However, results suggest that chlorophyll content differed between mango cultivars for a similar maturity stage, in line with the observations of Ketsa et al. (1999). Consequently, further studies are required to establish specific cultivar relationships between peel pigment contents and fruit maturity stages. Development of non-destructive and convenient tools to assess maturity stage, such as reflectance measurements, would help to harvest fruits at an optimum compromise between shelf-life and quality.

4) **Correlation between color and pigment content**

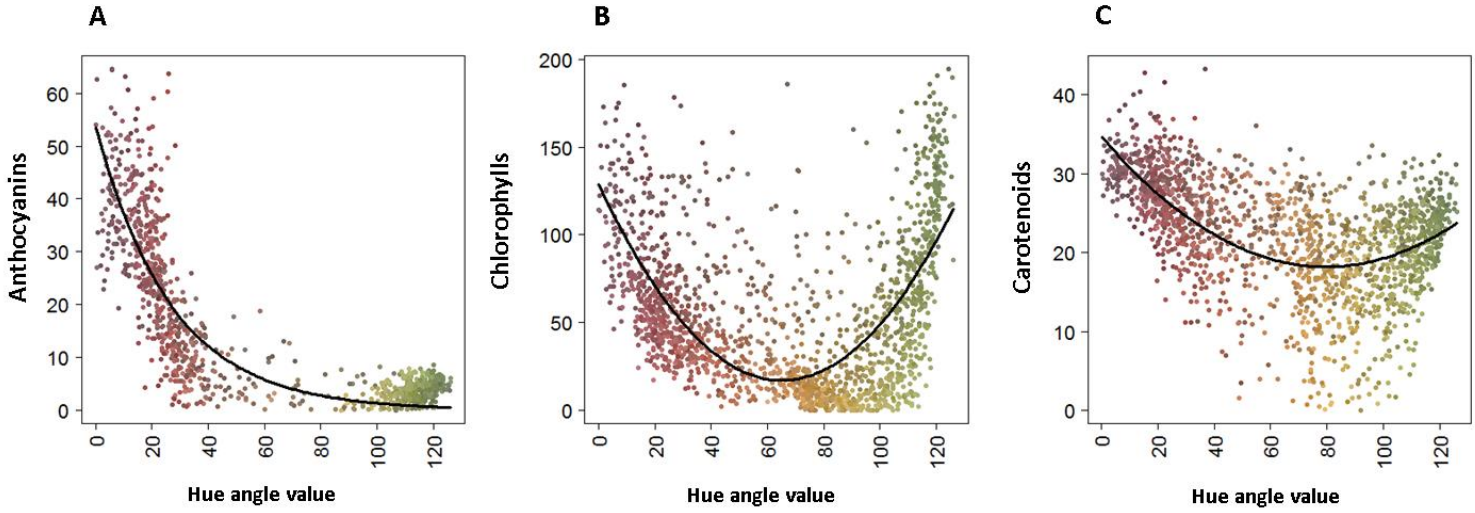

Figure 9: Predicted contents in mango peel of, anthocyanins (A), chlorophylls (B), and carotenoids (C) in µg.gFM-1 according to hue angle. Continuous lines represent the relationship established between hue angle and pigment content, regardless of the cultivar.

Table 2: Parameters and coefficients of determination of regressions between hue angle values (H, in degrees) anthocyanin, chlorophyll (a + b) and carotenoids, in mango peels for each cultivar studied and regardless of the cultivar.

	Anthocyanin $[Anthocyanin] = a \times e^{b \times H}$			Chlorophyll $[Chlorophyll] = a \times H^2 + b \times H + c$				Carotenoids $[Carotenoid] = a \times H^2 + b \times H + c$			
Cultivars	**a**	**b**	**R^2**	**a**	**b**	**c**	**R^2**	**a**	**b**	**c**	**R^2**
All	53.70	$-3.70\ 10^{-2}$	0.75	$2.60\ 10^{-2}$	-3.44	128.90	0.43	$2.66\ 10^{-3}$	-0.41	34.66	0.35
Cogshall	47.69	$-2.51\ 10^{-2}$	0.62	$2.39\ 10^{-2}$	-3.04	108.48	0.41	$2.55\ 10^{-3}$	-0.42	34.70	0.34
Kent	48.69	$-4.34\ 10^{-2}$	0.74	$3.26\ 10^{-2}$	-4.09	147.59	0.50	$4.16\ 10^{-3}$	-0.58	36.78	0.40
Heidi	60.96	$-3.78\ 10^{-2}$	0.76	$1.93\ 10^{-2}$	-2.29	101.62	0.34	$1.27\ 10^{-3}$	-0.21	34.79	0.44
Tommy	65.36	$-5.01\ 10^{-2}$	0.75	$2.84\ 10^{-2}$	-3.13	106.92	0.67	$3.74\ 10^{-3}$	-0.49	33.58	0.60
Caro	0.00	$6.22\ 10^{-2}$	0.38	$8.76\ 10^{-2}$	-14.44	600.62	0.88	$5.61\ 10^{-3}$	-0.94	55.91	0.25
Irwin	53.68	$-3.81\ 10^{-2}$	0.58	$1.90\ 10^{-2}$	-2.35	108.89	0.24	$2.22\ 10^{-3}$	-0.35	33.41	0.30
NDM	0.08	$3.49\ 10^{-2}$	0.22	$4.42\ 10^{-2}$	-7.54	320.85	0.62	$7.33\ 10^{-3}$	-1.29	72.14	0.15
Sensation	50.37	$-3.53\ 10^{-2}$	0.75	$2.05\ 10^{-2}$	-3.05	152.87	0.54	$2.02\ 10^{-3}$	-0.39	34.05	0.63

An exponential relationship (R^2 = 0.75) was found between the hue angle and the predicted anthocyanin contents in mango peel (Figure 9A and Table 2), in line with the results of Iglesias *et al.* (2012) and Steyn *et al.* (2004) for apple fruit. This relationship was found to be cultivar-dependent ($P < 10^{-12}$, data not shown) and led to medium to good predictions of anthocyanin content based on hue angle value (Table 2). Red epidermis color was related to higher anthocyanin content than that of yellow and green epidermises. The implication of anthocyanin pigments in red skin coloration was highlighted for several fruits such as apples (Iglesias et al., 2008), mangoes (Proctor and Creasy, 1969), and pears (Steyn et al., 2004). A wide variety of anthocyanins exists in nature. However, only three anthocyanins have been identified in mango peel: peonidin-3-galactoside (Proctor and Creasy, 1969), cyanidin 3-*O*-galactosidase and 7-*O*-methylcyanidin 3-*O*-*β*-D-galactopyranoside (Berardini et al., 2005).

Chlorophyll contents were found to be slightly related to hue angle values by a polynomial function (R^2 = 0.42)(Figure 9B, Table 2). This relationship was also cultivar-dependent ($P< 10^{-12}$, data not shown). Yellow skins had lower contents in chlorophyll than green and red ones. These results are supported by the studies of Medlicott *et al.* (1986) and Ketsa *et al.* (1999) who found that the appearance of yellow coloration was induced by a decrease in the chlorophyll content of the skin. The increase in the green coloration was associated with an increase in the chlorophyll content, in accordance with the measurements of León et al. (2007) for lettuce.

Carotenoid pigment contents were also slightly correlated ($R^2 < 0.64$) to the hue angle values by a polynomial function (Table 2 and Figure 9C), which was also cultivar-dependent ($P < 10^{-12}$, data not shown). Unexpectedly, epidermises with yellow coloration were not related to higher carotenoid contents, contrary to Medlicott *et al.* (1986) who showed that the development of yellow coloration was associated with an increase in carotenoids. This can be explained by the maturity stage of the fruits studied, which was supposed to be close to a ripe stage since these fruits were ripe in the next three to five days after the were harvested. Effectively, Solovchenko et al. (2005) indicated for apple fruit that chlorophyll and carotenoid pigments were simultaneously degraded at the beginning of ripening until a chlorophyll threshold content was reached, triggering the carotenoid synthesis. Consequently, further studies are needed to better understand the evolution of pigment content in the peel during maturation and their effects on fruit coloration.

These results suggested that there is no unique relationship between pigment content and peel color, as proposed by Lancaster *et al.* (1997). This can be explained by the fact that colorimetric measurements reduce the reflectance spectra in the visible range to three tristimulus values corresponding to the excitation levels of the three color receptors of the eye in order to reflect human color perception (Equation 1). Different reflectance spectra can then give the same tristimulus value and, as a result, the same color sensation, i.e., a metamerism phenomenon (Figure 5C to Figure 5J).

Furthermore, red peel color, previously associated with an increase in anthocyanin pigments due to high sun exposure, was also related to an increase in chlorophyll and carotenoid content (Figure 9B and Figure 9C). These results suggested that sun exposure also induces the accumulation of chlorophyll and carotenoid pigments. Paper-bagged mangoes were in fact found to have lower chlorophyll and carotenoid contents than non-bagged mangoes (Chonhenchob et al., 2011). These authors explained these results by the positive effect of light on chlorophyll and carotenoid synthesis. Other studies suggested that the pigment contents in the peel change in response to sun radiation in order to increase the photo protective capacity of the fruit (Merzlyak et al., 2002, Steyn et al., 2002). Future studies could use reflectance measurements to determine the effect of sun exposure on the peel pigment content of mango fruit.

II - Model-assisted analysis of spatial and temporal variations in fruit temperature and transpiration highlighting the role of fruit development

Objectifs :

Ce chapitre s'intéresse à l'impact des conditions climatiques et des propriétés physiques et thermiques du fruit sur sa température et sa transpiration. Un modèle thermodynamique a été développé pour prédire les variations spatiales et temporelles de la température et de la transpiration d'une mangue en croissance. Le modèle développé est utilisé dans les chapitres suivants pour déterminer l'impact des conditions climatiques sur la qualité et la maturité de la mangue. Ce chapitre a fait l'objet d'une publication dans **PLOS One** sous la forme d'un article intitulé « *Model-Assisted Analysis of Spatial and Temporal Variations in Fruit Temperature and Transpiration Highlighting the Role of Fruit Development* ».

Principaux résultats :

- Le modèle permet de prédire avec précision les variations spatiales et temporelles de la température de la mangue.
- Les mesures ont indiqué que les propriétés physiques et thermiques de la mangue changent pendant sa croissance.
- Les changements des propriétés physiques et thermiques de la mangue impactent les gradients de température au sein du fruit et sa transpiration mais n'ont pas d'incidence sur sa température moyenne.

Model-assisted analysis of spatial and temporal variations in fruit temperature and transpiration highlighting the role of fruit development

Thibault Nordey[1,*], Mathieu Léchaudel[1], Marc Saudreau[2], Jacques Joas[3] and Michel Génard[4]

[1]CIRAD, UPR HORTSYS, 97455 Saint-Pierre, La Réunion, France
[2] INRA, UMR 547 PIAF, BP 10448, 63000 Clermont-Ferrand, France
[3]CIRAD, UMR QUALISUD, 34398 Montpellier, France
[4]INRA, UR 1115, Plantes et Systèmes de Culture Horticoles, 84000 Avignon, France

A - Abstract

Fruit physiology is strongly affected by both fruit temperature and water losses through transpiration. Fruit temperature and its transpiration vary with environmental factors and fruit characteristics. In line with previous studies, measurements of physical and thermal fruit properties were found to significantly vary between fruit tissues and maturity stages. To study the impact of these variations on fruit temperature and transpiration, a modelling approach was used. A physical model was developed to predict the spatial and temporal variations of fruit temperature and transpiration according to the spatial and temporal variations of environmental factors and thermal and physical fruit properties. Model predictions compared well to temperature measurements on mango fruits, making it possible to accurately simulate the daily temperature variations of the sunny and shaded sides of fruits.

Model simulations indicated that fruit development induced an increase in both the temperature gradient within the fruit and fruit water losses, mainly due to fruit expansion. However, the evolution of fruit characteristics has only a very slight impact on the average temperature and the transpiration per surface unit. The importance of temperature and transpiration gradients highlighted in this study made it necessary to take spatial and temporal variations of environmental factors and fruit characteristics into account to model fruit physiology.

B - Introduction

Numerous physiological processes involved in fruit development depend on temperature. Temperature is implied in fruit growth (Grossman and DeJong, 1994, Léchaudel et al., 2007, Normand and Habib, 2001, Adams et al., 2001), fruit respiration (Fonseca et al., 2002, Mangaraj and Goswami, 2011, Ravindra and Goswami, 2008) and fruit ripening (Paull and Jung Chen, 2000). In addition, temperature has a major impact on fruit physiology through its effect on fruit water losses by transpiration (Montanaro et al., 2012, Leonardi et al., 2000a) due to its influence on the pressure vapour deficit (VPD) that drives the transpiration rate (Monteith and Unsworth, 1990). Water losses by transpiration are in fact responsible for fruit diurnal shrinkage (Léchaudel et al., 2007, Morandi et al., 2007), and affect both growth rate (Guichard et al., 2005, Leonardi et al., 2000b) and fruit quality (Leonardi et al., 2000b, Montanaro et al., 2006). Many studies have highlighted the impact of temperature on several fruit quality traits such as appearance, taste and size (Génard and Bruchou, 1992, Léchaudel and Joas, 2007, Hewett, 2006). The temperature of a fruit results from its heat budget, which is defined by energy exchanges caused by radiation, evaporation, convection, conduction and metabolic activity (Cellier et al., 1993). Different factors have an impact on the components of the fruit heat budget and can be broken down into environmental factors (solar radiation, air moisture, air temperature and wind), fruit thermal properties (heat capacity, density and conductivity), and fruit physical properties (skin permeability to water diffusion, peel reflectance and fruit volume)(Saudreau et al., 2007).

Modelling approaches based on physical processes made it possible to highlight the impact of variations in environmental factors on plant organ temperature, as shown on sunflower capitulum (Guilioni and Lhomme, 2006), maize ear (Khabba et al., 2001) and fruit (Saudreau et al., 2007). The model developed by Saudreau et al. (Saudreau et al., 2007) on peach and apple fruits revealed that the heterogeneity of environmental conditions at the fruit scale induced large temperature gradients within the fruit. However, until now, no model has focused on the effect of the variations of the fruit's physical and thermal properties induced by its development on the fruit temperature.

Many studies have shown that fruit properties involved in fruit temperature variation were modified by the fruit environment (Gautier et al., 2008, Léchaudel and Joas, 2007, Hewett, 2006, Léchaudel et al., 2012) and during its development (Gibert et al., 2010, Jordan et al.,

2000). Water content is known to be related to the three fruit thermal properties ,i.e., conductivity, heat capacity (Lewicki, 2004) and specific gravity (Jordan et al., 2000). However, it was reported that water content changes during fruit development (Fishman and Génard, 1998, Léchaudel et al., 2007) and depending on the fruit tissue (peel, pulp or stone) (Lechaudel et al., 2002). Furthermore, coloration of fruit skin is known to vary due to variations in the contents of peel pigments (Lancaster et al., 1997) as a result of fruit development and exposure to light (Kang et al., 2008). Since pigment contents affect fruit reflectance (Merzlyak et al., 2003b), changes in peel colour are assumed to be related to variations in fruit optical properties involved in radiation flux (Hetherington, 1997). Peel conductance to water, which regulates fruit transpiration, also varies with fruit development (Lescourret et al., 2001, Gibert et al., 2010) and sun exposure (Maguire et al., 1999, Léchaudel et al., 2012).

The aim of this study was therefore to determine how changes in thermal and physical properties during fruit development affect spatio-temporal variations of the fruit's temperature and its transpiration.

A tropical fruit, the mango (cv. "Cogshall"), was taken as reference since it is a large-size drupe that grows under high-temperature environments.

First, changes in fruit density, heat capacity, thermal conductivity and size, as well as peel reflectance and conductance to water, were measured during fruit development in contrasting sun exposure conditions. A model to predict spatial and temporal variations of fruit transpiration and temperature was then developed, taking the heterogeneity and the evolution of fruit thermal and physical properties within the fruit tissues and during their development into account. After evaluating the quality of model predictions, the model was used to assess the effect of a fruit's thermal and physical properties on its temperature and transpiration.

C - Materials and methods

1) **Model presentation**

The model presented simulates spatial and temporal variations of temperature and transpiration of a mango fruit during its development. Cogshall mango fruit and its stone were considered to have a triaxial ellipsoid shape defined by three distinct semi-axes: the León gth (H), the large diameter (W) and the small diameter (w) (Figure 10A).

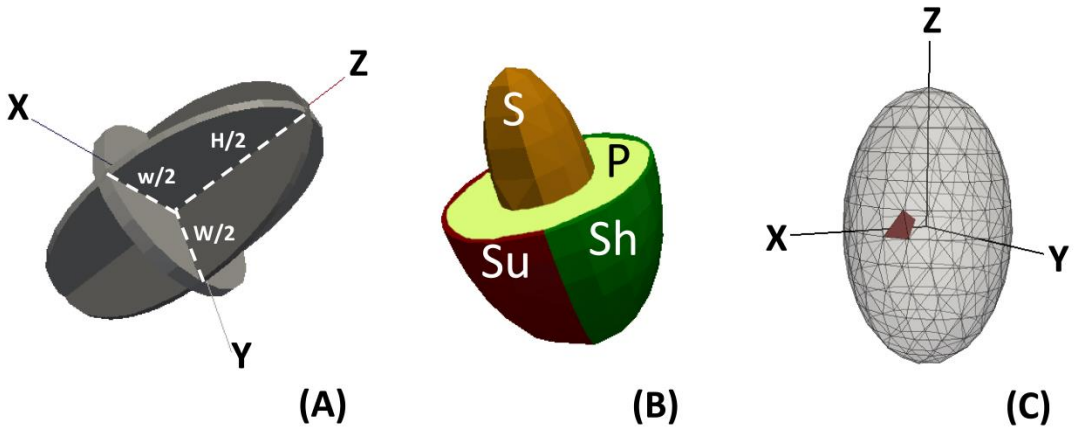

Figure 10: Schematic representation of the mango volume as an ellipsoid shape (A) defined by three distinct semi-axes, corresponding to its semi-length (H), semi-large diameter (W) and semi-small diameter (w); of the mango tissues (B), including three compartments, the stone (S), the pulp (P) and the peel, separated between the sunny (Su) and the shaded (Sh) sides; and of the fruit mesh and its sub-units (C).

The fruit was considered to be located at the exterior of the canopy, with a sunny side directly exposed to sun radiation and with a shaded side that received a fraction of the global radiation. The simulated mango fruit was considered to be composed of four different tissues: the pulp, the stone, and the shaded and sunny parts of the peel, characterised by different physical and thermal properties (Figure 10B).

The temperature of a system is linked to its heat budget and varies with the gain or loss of energy. On the basis of the first law of thermodynamics without any energy loss due to work, the relationship between temperature variation (ΔT, in Kelvin) and heat variation (ΔQ, in Joules) is shown in Equation 5, where Cp is the heat capacity (in $J.Kg^{-1}.K^{-1}$), V is the volume of the tissue (in m^3) and S_g is the specific gravity of the tissue ($Kg.m^{-3}$):

$$\Delta T = \frac{Sg \times V \times Cp}{\Delta Q}$$ *Equation 5*

In the case of a whole fruit in a tree, the heat budget (ΔQ) varies as a result of (i) energy exchanges at the fruit surface by radiation, transpiration, conduction and convection, and (ii) the energy source within the fruit due to chemical activities (Cellier et al., 1993). The heat released from metabolic activities within the fruit and the energy exchanged between the plant and the fruit were assumed to be low and were therefore not taken into account.

ΔQ was determined using Equation 6, where the heat rate as a function of radiation ($P_{Radiation}$), transpiration ($P_{Transpiration}$), convection ($P_{Convection}$) and conduction ($P_{Conduction}$) is expressed in Watts, and the time (Δt) is expressed in seconds:

$$\Delta Q = (P_{Radiation} + P_{Transpiration} + P_{Convection} + P_{Conduction}) \times \Delta t$$ *Equation 6*

Heat flux equations are taken from the spatio-temporal model of fruit temperature developed by Saudreau et al. (Saudreau et al., 2007) and are summarised in the following sections.

a) Radiation

The radiation heat rate ($P_{Radiation}$, W) received by a surface S (m^2) was determined using Equation 7, where A_{sw} and A_{lw} are the fruit surface reflectance coefficients for short-wave and long-wave radiations, respectively, $R_{lw} = \sigma T_a^4$ is the long-wave radiation component (TIR, in $W.m^{-2}$) calculated with the air temperature (T_a, K), R_{sw} is the short-wave radiation component (PAR and NIR, in $W.m^{-2}$) of the global radiation, T_s (K) is the fruit surface temperature, and σ is the Stefan–Boltzmann constant (= $5.67.10^{-8}$ J K^{-4} m^{-2} s^{-1}).

$$P_{Radiation} = [(1 - A_{sw}) R_{sw} + (1 - A_{lw})(R_{lw} - \sigma Ts^4)] \times S$$ *Equation 7*

b) Transpiration

The latent heat rate released by transpiration ($P_{Transpiration}$, W) through a surface S (m^2) was calculated using Equation 8, as proposed by Monteith and Unsworth (Monteith and Unsworth, 1990):

$$P_{Transpiration} = [Gw \times \varphi_{air} \times Cp_{air} \times \frac{\Delta \times (Ts - Td)}{\tau}] \times S$$ *Equation 8*

where Gw ($m.s^{-1}$) is the fruit surface conductance to water, φ_{air} ($Kg.m^{-3}$) is the air density estimated using equations established by Picard et al. (Picard et al., 2008), Cp_{air} is the air heat capacity considered as a constant = 1004 $J.Kg^{-1}.K^{-1}$, τ is the psychrometric constant (66.5 $Pa.K^{-1}$), Td (K) is the temperature at the dew point, and Δ is the rate of increase in saturation vapour pressure with the temperature at the dew point, deduced from the relationship established by Buck (Buck, 1981). The mass of water lost by transpiration (Kg) was deduced from the amount of energy (J) dissipated by transpiration by the whole fruit and the water enthalpy of vaporisation considered as a constant ($2.25x10^6$ $J.Kg^{-1}$).

c) Convection

The sensible heat rate by convection ($P_{Convection}$, W) through a surface S (m^2) was calculated using Equation 9. The value of the convective heat transfer coefficient (h, $W.m^{-2}.K^{-1}$) was calculated with relationships established for a spherical shape (Whitaker, 1972), since, to our knowledge, no relationship has yet been found for an ellipsoidal form. This hypothesis seems reasonable since drag forces are fairly similar in a vertical ellipsoid and in a sphere (Richter and Nikrityuk, 2012).

$$P_{Convection} = [h \times (T_s - T_a)] \times S \qquad \textit{Equation 9}$$

d) Conduction

The heat rate by conduction ($P_{Conduction}$, W) through a surface S (m^2) was modelled by Fourier's Law (Equation 10), where K is the thermal conductivity ($W.m^{-1}.K^{-1}$) and $\vec{\nabla}T|_s$ the temperature gradient ($K.m^{-1}$) normal to the surface S. In the model, $\vec{\nabla}T|_s$ is approximated by the ratio of the temperature difference (ΔTemperature) to the distance (Distance) between the two cells adjacent to the surface S.

$$P_{Conduction} = K \times S \times \vec{\nabla}T|_s \approx K \times S \times \frac{\Delta\,\text{Temperature}}{\text{Distance}} \qquad \textit{Equation 10}$$

2) **Numerical method**

a) Fruit mesh

Fruit volume was divided into sub-units by a regular mesh (Figure 10C). The increase in the number of sub-units increases the precision of the model predictions, but increases the calculation time as well. A mesh with more than 800 sub-units was considered to be a good compromise. The physical and thermal properties of sub-units were defined according to their position in the fruit and the tissue that they belonged to (Figure 10B).

b) Determining thermal conductivity

Since thermal conductivity was considered to vary within the fruit, calculation of K between two sub-units with different thermal properties was done using Equation 11, where K is the resulting conduction coefficient ($W.m^{-1}.K^{-1}$) between two sub-units separated by the sum of the distances from the centre of each unit to the interface of the two sub-units (e_1 and e_2, in m), and K_1 and K_2 are the thermal conductivity ($W.m^{-1}.K^{-1}$) of the two sub-units, respectively.

$$K = \frac{e_1 + e_2}{\frac{e_1}{K_1} + \frac{e_2}{K_2}} \qquad \textit{Equation 11}$$

The total heat flux by conduction received by a sub-unit of the fruit is equal to the sum of the conduction exchanges between all adjacent sub-units.

c) Equation resolution

The equation system was solved using the finite volume method with an explicit method for time integration. A Courant-Friedrichs-Lewy (CFL) condition (Courant et al., 1928) was therefore used to ensure the stability of the numerical integration, leading to a time step Δt that was smaller than the critical CFL number, defined as $\frac{\rho_{min} \times Cp_{min} \times \Delta x_{min}}{2 \times k_{max}}$ where Cp_{min} is the minimum heat capacity ($J.Kg^{-1}.K^{-1}$) of the sub-units, Δx_{min}(m) is the minimum distance between two sub-units, ρ_{min} is the minimum sub-unit density, and k_{max} is the maximum thermal conductivity of the sub-units.

3) **Fruit material, measurements and model parameterisation**

a) Fruit material

The study was carried out at the CIRAD Research Station located in St. Pierre (Reunion Island, 20° 52' 48'' S, 55° 31' 48'' E), with CIRAD's permission. It was conducted on 18-year-old (in 2008) mango trees, *Mangifera indica* L. cv. "Cogshall" grafted on "Maison rouge". Trees were well irrigated, spaced 5 x 6 m, and were approximately 3 m high. Measurements of surface temperature and of internal factors were taken on fruits of the 2006 and 2008 growing seasons, respectively. Four maturity stages were distinguished on the basis of the number of Days After full Bloom (DAB). The first stage, M1, corresponded to an immature green fruit with a size of approximately 6-8 cm, which corresponded to the end of cell division (DAB = 60). The second stage, M2, made reference to a green immature fruit in the cell expansion phase (DAB = 90). The following maturity stage, M3, described a green mature stage (DAB = 120). The last stage, M4, described mature fruits (DAB = 130).

b) Measurements of climatic variables and fruit surface temperatures.

Climatic data such as air temperature, global radiation, air humidity and wind speed were measured every minute and averaged and stored every hour on a data logger (Model 21 X, Campbell Scientific Ltd.; Logan, UT, USA) during the 2006 and the 2008 growing seasons. Direct and diffuse parts of global radiation were estimated using the model developed by Maxwell (Maxwell E.L., 1987). The sun's course was determined using the solar position algorithm (SPA) developed by Reda and Andreas (Reda and Andreas, 2004). The fraction of the global radiation received by the shaded side of a fruit located at the exterior of the canopy was equal to 20% of the global radiation, according to our measurements.

Fruit surface temperature measurements were carried out on three green immature, three green mature and three mature fruits during the 2006 growing season. These fruits corresponded to well-exposed fruits at the M2, M3 and M4 maturity stages, measuring approximately 115, 123 and 125 mm in length, 73, 78 and 80 mm in large diameter, 69, 73, and 75 mm in small diameter, and weighing approximately 269, 330 and 350 x 10^{-3} kg, respectively. Copper-constantan thermocouples (diameter: 0.2 mm) were attached to the fruit surface on the sunny and shaded sides. Measurements of fruit temperature surface were taken every minute and averaged and stored every hour on a data logger (Model 21 X,

Campbell Scientific Ltd.; Logan, UT, USA) over three (from 28th to 30th December 2006), eight (from 12th to 19th January 2007) and three days (from 22nd to 24th January 2007) for fruits at the M2, M3 and M4 maturity stages, respectively.

c) Measurements of physical properties

Three model parameters related to radiation must be known before simulations can be carried out: fruit surface reflectance to short-wave radiations (A_{sw}), fruit surface reflectance to long-wave radiations (A_{lw}), and the emissivity for long-wave radiations (ε). No data was available in the literature for mango peel emissivity, so it was considered to be equal to peach surface emissivity, ε = 0.94 (Saudreau et al., 2007). The A_{lw} value was deduced from the fruit surface emissivity using Kirchhoff's law: Alw = 1 - ε.

Fruit peel reflectance (A_{sw}) to short waves of solar irradiation was calculated using Equation 12, where the peel reflectance spectra was determined on 10 to 20 fruits for each fruit side and each maturity stage, from 350 nm to 2500 nm, every 1 nm, with a portable spectrometer (LABSPEC 2500, Analytical Spectral Devices, Inc.; Boulder, CO, USA), and the sun spectral irradiance values were taken from ASTM G173-03 standard tables established by the American Society for Testing and Materials (ASTM).

Equation 12

$$A_{sw} = \frac{\int_{300}^{2500} \text{Sun Spectral Irradiance}_{[300,2500]} \times \text{Peel Reflectance Spectra}_{[300,2500]}}{\int_{300}^{2500} \text{Sun Spectral Irradiance}_{[300,2500]}}$$

Fruit conductance (Gw, in m s^{-1}) was calculated for sunny and shaded fruit, on 6 to 20 fruits for each maturity stage, using the method detailed by Léchaudel et al. (Léchaudel et al., 2012).

The model simulates the increase in fruit size by considering a constant number of sub-units and by increasing each sub-unit's dimensions by a proportion of the fruit growth rate that has to be determined prior to the simulation. It was assumed that fruit proportions were constant during fruit development, so the fruit growth rate was determined on the basis of the increase in fruit height, calculated from the average of ten fruits measured weekly from the end of cell division (60 DAB) to total fruit maturity (130 DAB). Stone dimensions were deduced from fruit dimensions according to the following empirical relationships:

$H_{Stone} = 0.56 \times H_{Fruit}$ $(n = 109, R^2 = 0.65)$

$W_{Stone} = 0.56 \times W_{Fruit}$ $(n = 109, R^2 = 0.55)$

$w_{Stone} = 0.56 \times w_{Fruit}$ $(n = 109, R^2 = 0.53)$

where W_{stone} and w_{stone} are the large and small diameters of the stone, respectively.

Peel thickness was considered constant and equal to 1 mm for Cogshall mango.

d) Estimation of fruit thermal properties

Fruit thermal properties such as heat capacity (Cp, in $J.Kg^{-1}.K^{-1}$) and thermal conductivity (K, in $W.m^{-1}.K^{-1}$) vary according to water content. The relationship given by Valente and Nicolas (Valente and Nicolas, 1990) was used to estimate thermal conductivity (Equation 13). Concerning the heat capacity, the relationship given by Siebel (Siebel, 1982) was used (Equation 14).

$$K = 0.094 + 0.483 \times Water_{content} \qquad \textit{Equation 13}$$

$$Cp = (0.837 + 3.349 \times Water_{content}) \times 1000 \qquad \textit{Equation 14}$$

The water content of each compartment was deduced from equations taken from Léchaudel et al. (Lechaudel et al., 2002) and the fruit fresh mass was deduced from the growth measurements on the ten fruits. Since mesh resolution was higher than the peel thickness, sub-units located at the fruit surface were a mix of peel and pulp tissues. Thus, heat capacity and thermal conductivity of these sub-units were determined according to the relative proportion of pulp and peel.

The specific gravity of fruit and stone was measured on 8 to 12 fruits at each of the four maturity stages. Specific gravity was calculated using Archimedes' principle, by measuring the fruit fresh mass in the air and its upward force when the fruit was immersed in water with a basket hanging from a balance. The specific gravity (Sg, $Kg.m^{-3}$) is deduced as $S_g = \frac{m}{|m - r|} \times Sg_{Water}$, where m is the mass (kg) of the fruit or the stone, r is the upward force (kg), and Sg_{water} is the specific gravity of water in which the fruit is immersed, considered as a constant (Sg_{water} = 1000 $Kg.m^{-3}$). For the sake of simplicity, the specific gravity of peel and pulp were assumed to be equal and was deduced from the specific gravities of the fruit and stone.

e) Measurements of peel colour

XYZ coordinates of peel colour were calculated from the peel reflectance values (see section: Measurements of physical properties) and converted to CIELAB coordinates. Since they have been described as good colour descriptors of fruit (Ayala-Silva et al., 2005, Kang et al., 2008), hue angle (H°) and chroma (C) values were calculated from a and b coordinates (Equation 15 and Equation 16, respectively).

$$H° = \arctan(\frac{b}{a}) \qquad \textit{Equation 15}$$

$$C = \sqrt{a^2 + b^2} \qquad \textit{Equation 16}$$

4) **Simulations and post-processing**

Fruit temperature and transpiration were simulated from the phase of cell expansion, which begins after the period of cell division when the mango reaches approximately 6-8 cm in length (Léchaudel et al., 2005a), to ripening. Fruit internal factor changes according to the number of DAB were given as inputs into the model in order to simulate fruit temperature and transpiration during fruit development.

a) Model assessment

As proposed by Saudreau et al. (Saudreau et al., 2007), the ability of the model to simulate heat conduction within a material and to handle heat fluxes at boundary conditions was first tested by simulating a physical situation for which an analytical solution exists. The case of a spherical object of radius R = 4 x10^{-3} m, initially at a temperature T_0 = 16°C, immersed in an atmosphere at a constant temperature T_a = 20°C, was studied. The sphere was heated by a constant convective heat transfer coefficient h = 5 W.m^{-2}.K^{-1} and had a heat capacity of 3600 J.Kg^{-1} K^{-1} and a thermal diffusivity of 0.1 W.m^{-1}.K^{-1}. The expression of the analytical solution is detailed by Saudreau et al. (Saudreau et al., 2007).

Secondly, the model was assessed in a more realistic and complex situation by simulating the temperature dynamics over several days at three maturity stages of the fruit, i.e., M2, M3 and M4, during which temperature measurements were taken. For this case, input parameters and input climatic data were those relative to the measurement period.

b) Analysis of spatial and temporal variations of energy exchanges, temperature and transpiration.

Simulation outputs carried out on fruits throughout the day-night cycle from 12th January 2007 at the four studied maturity stages with climatic input data were analysed in detail. Variations of power (in $W.kg^{-1}$) by radiation, convection, transpiration and conduction at different locations within the fruit - at the fruit centre and at the surface of the shaded and the sunny sides - were compared. In addition, the variability of temperature and transpiration during the day-night cycle and within the fruit was examined for fruits at the M1 and M3 maturity stages with climatic input data from 12th January 2007.

c) Model analysis

A one-at-a-time sensitivity analysis was performed with the same input data as those used for testing the model assessment in order to identify the most influential parameter on temperature and transpiration. Conceptually, the simplest method for carrying out a sensitivity analysis is to repeatedly vary one parameter at a time while keeping the others fixed (Hamby, 1994). As proposed by Génard and Souty (Génard and Souty, 1996), the sensitivity of the minimum, the mean and the maximum value of temperature and transpiration simulated for the whole fruit to changes in parameter values (±20%) was studied using sensitivity coefficients. A sensitivity coefficient is equal to the ratio of the change in output (minimum, mean or maximum predicted temperature and transpiration value), to the change in the input parameter (0.4), while all other parameters remain constant (Hamby, 1994). This local sensitivity analysis provides information about the effect of small changes in the parameters on the model responses and does not provide information about the effect of simultaneous or large parameter changes.

A second analysis was performed to evaluate the impact of variations in thermal and physical fruit properties during fruit development on its temperature and its transpiration, taking their measured evolutions into account. Temperature and transpiration simulations were carried out with the climatic data of the 2008 growing season and with the measured evolution of fruit properties as input data. The impact of the evolution of the fruit properties during fruit development was determined by simulating temperature and transpiration, fixing one fruit property at a time to its initial value, corresponding to the M1 maturity stage. The effect on the evolution of all parameters on fruit temperature and

transpiration was studied by fixing all parameters at the values measured at the first maturity stage.

5) **Statistical analysis**

All analyses were performed with R software (RDC Team, 2012), implemented with the Colorspace (Ross Ihaka et al., 2012) and R.matlab (Bengtsson and Riedy, 2011) packages. For evaluating model accuracy, the Root Mean Square Error (RMSE) was calculated using Equation 17, where y_t is the t^{th} observed or reference value, $\hat{y}_t$ is the t^{th} simulated value, and n is the number of observed or simulated values. Multiple comparisions of measured fruit properties and peel colour descriptor averages were performed using the Tukey test. Graphical renderings were performed using Paraview software (Ahrens et al., 2005).

$$\mathrm{RMSE} = \sqrt{\frac{\sum_{t=1}^{n}(y_t - \hat{y}_t)^2}{n}}$$ *Equation 17*

D - Results

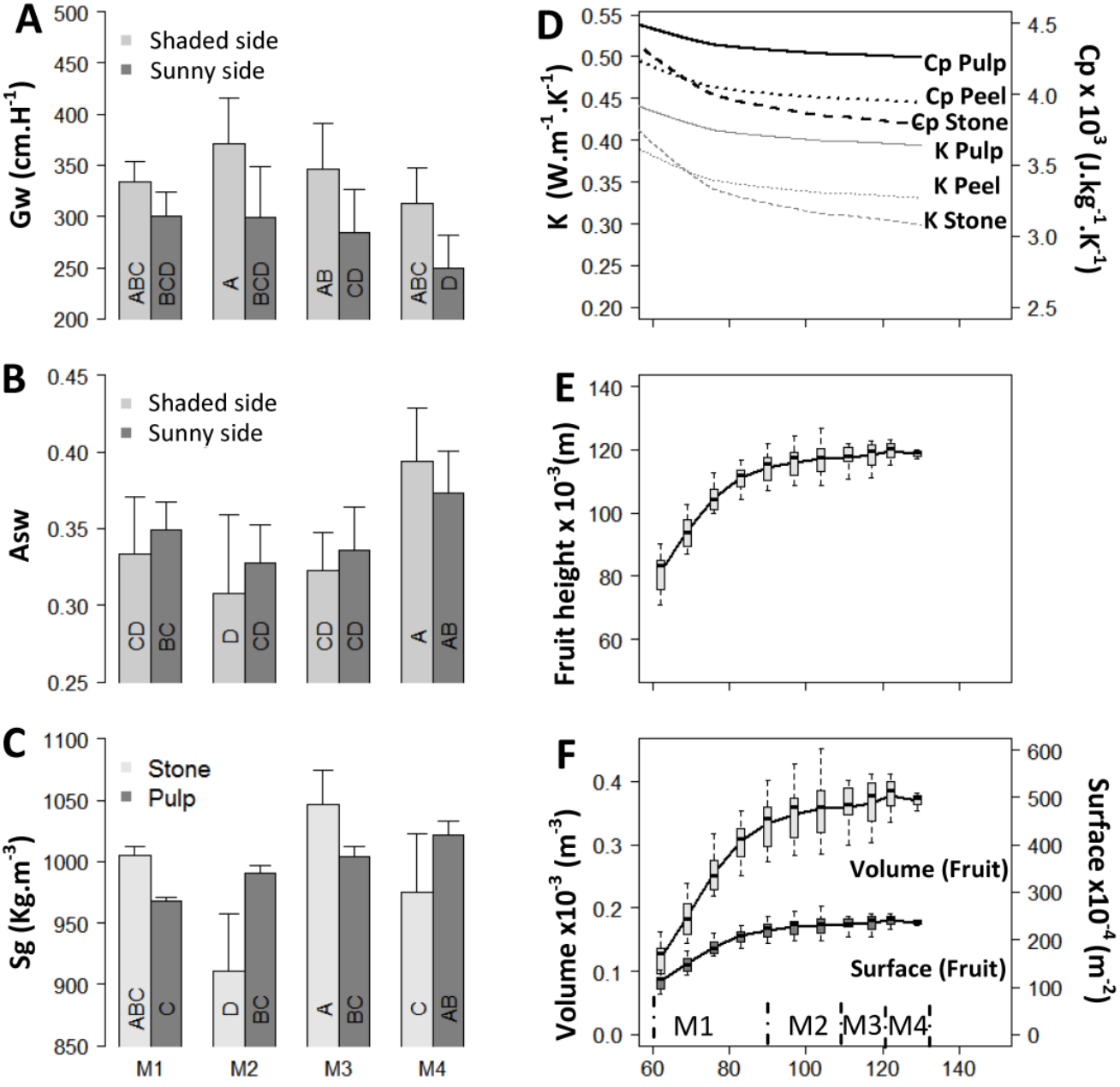

Figure 11: Thermal and physical parameters measured on mangoes, including peel conductance to water (A) and peel reflectance (B) according to four maturity stages and two sun exposures, the specific gravity of the stone and the pulp (C) according to four maturity stages, the heat capacity and the thermal conductivity of the stone, the pulp, and the peel (D), the fruit height (E) volume and surface (F) according to the number of days after full bloom. Different letters signify that the averages of the treatments are significantly different at P < 0. 05 (according to Tukey's multiple comparison test).

1) **Variations of the measured physical and thermal properties during fruit development**

For all tested maturity stages except for the first one, peel conductance to water of sunny fruit was significantly lower than that of shaded fruit (Figure 11A). The maximum difference was found at the M2 maturity stage where the peel conductance to water of the sunny side was 19.3% lower than the shaded one. Peel conductance to water decreased for both fruit sides from M2 to M4, even if no significant difference could be established.

Table 3: Effects of maturity stage and sun exposure on the hue angle, chroma and lightness of fruit peel. Different capital, lower and italic case letters signify that data are significantly different for the hue angle value, chroma and lightness, respectively, at P < 0.05 (according to Tukey's multiple comparison test).

		M1	M2	M3	M4
Shaded	Hue angle	116.61 (A)	122.64 (A)	122.24 (A)	94.70 (B)
side	Chroma	30.26 (bc)	33.19 (ab)	33.71 (ab)	37.86 (a)
	Lightness	52.8 (*b*)	49.73 (*b*)	51.03 (*b*)	67.5 (*a*)
Sunny	Hue angle	113.66 (A)	58.68 (C)	9.31 (D)	20.18 (D)
side	Chroma	30.08 (bc)	13.14 (d)	15.24 (d)	26.59 (c)
	Lightness	53.26 (*b*)	43.93 (*c*)	40.93 (*b*)	49.93 (*b*)

Hue angle (H°) and chroma (C) values of the peel of the sunny and shaded sides were found to be significantly different at all maturity stages except for the earliest one (Table 3). The shaded side remained green during fruit development, with hue angle values comprised between 116.6° and 122.7°, until the last development stage when the fruit was ripe. At this stage (M4), it turned yellow, with an H° value of 94.7° (Table 3). At the first stage of fruit development, the sunny side was green and turned red, as indicated by the H° values lower than 58.7°. Whereas colour varied significantly between fruit sides, no significant difference was found between the reflectance coefficients (A_{sw}) of the sunny and the shaded sides (Figure 11B). Changes in the A_{sw} values during fruit development were similar for both fruit sides, with a continuous rise from the M2 maturity stage to the M4 stage. Maximal increases in reflectance values were observed between the M2 and M4 maturity stages, reaching 27.8% and 13.8% for the shaded and the sunny fruit sides, respectively.

Significant differences were found between the specific gravities of stone and pulp, especially at the three maturity stages, M2, M3 and M4 (Figure 11C). The maximum difference was found at the M2 maturity stage where the specific gravity of the stone was 8.0% lower than that of the pulp. Specific gravities of stone and pulp significantly changed with fruit maturity stages, but their respective evolutions were different since the specific gravity of the pulp continuously increased, contrary to that of the stone, which was inconstant (Figure 11C). Maximal differences in stone density were observed between the M2 and M3 maturity stages since an increase of 14.8% was measured between these two maturity stages. For the specific gravity of the pulp, the greatest difference was measured between the first and the last maturity stages and represented an increase of 5.6%.

Specific gravity increased by 5.6% for the pulp and decreased by 2.9% for the stone from the first to the last maturity stages.

According to our estimation, based on Equation 13 and Equation 14, thermal properties such as heat capacity (Cp) and thermal conductivity (K) varied between the three fruit tissues - peel, pulp and stone - and decreased with fruit development (Figure 11D). During all fruit development stages for all fruit tissues, Cp and K decreased by less than 20%. Except for the first maturity stage, the Cp and K of the stone were lower than those of the peel, which were themselves lower than those of the pulp. The maximum difference was found at the M4 maturity stage where the Cp and K of the pulp were 15.31% and 16.13% higher than those of the stone, respectively. Fruit dimensions increased by 46.13% from the first maturity stage to the last one (Figure 11E), inducing an increase in the fruit volume and surface area (Figure 11F) of 208.31% and 112.61%, respectively.

2) **Model validation and spatial-temporal variations of temperature and transpiration**

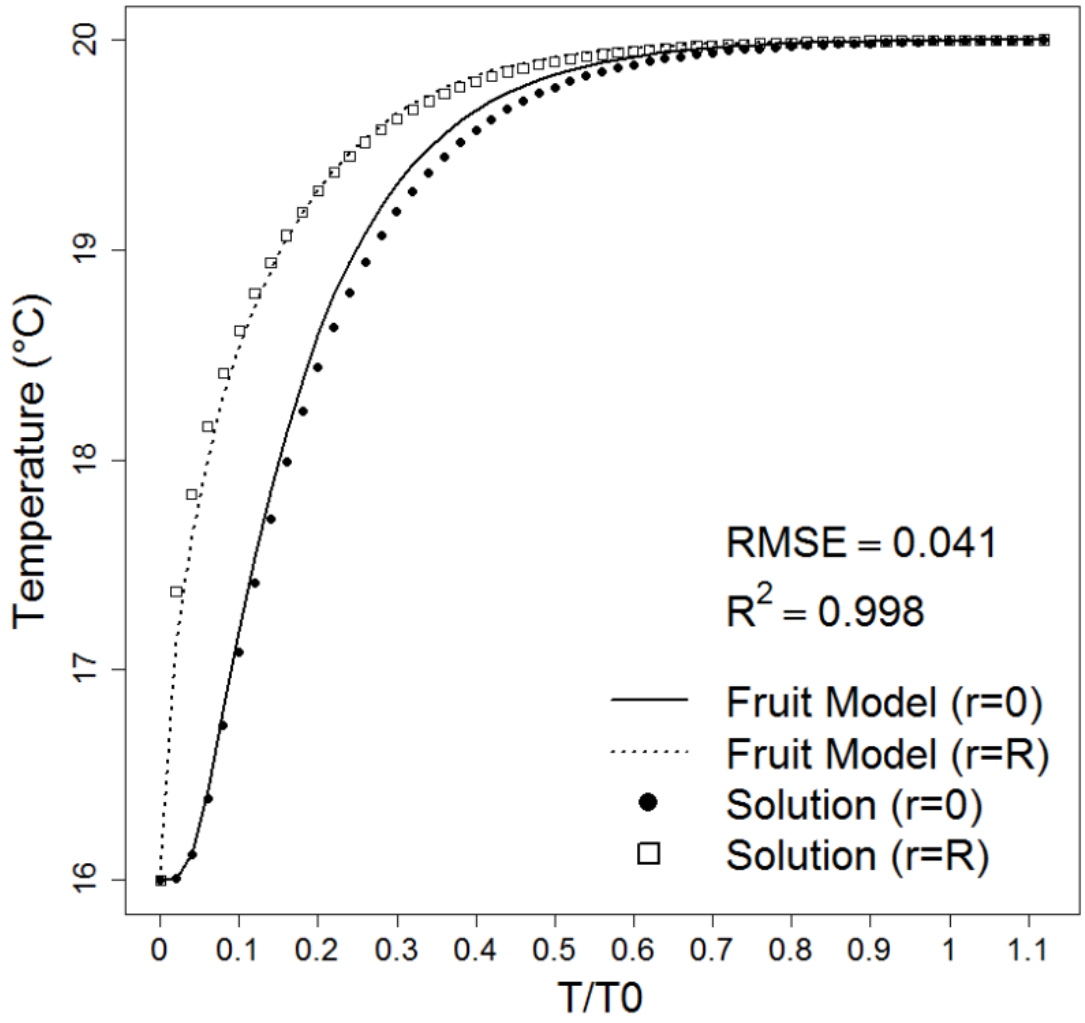

Figure 12: Temperature variations simulated by the model and determined by an analytical solution of a spherical object at an initial temperature of 16°C, immersed in an atmosphere at a constant temperature of 20°C, at the sphere surface, i.e., r=R, and at the sphere center, i.e., r=0, vs. time; expressed as the ratio of the time (T) to T0, the characteristic time at which the entire object reaches the air temperature.

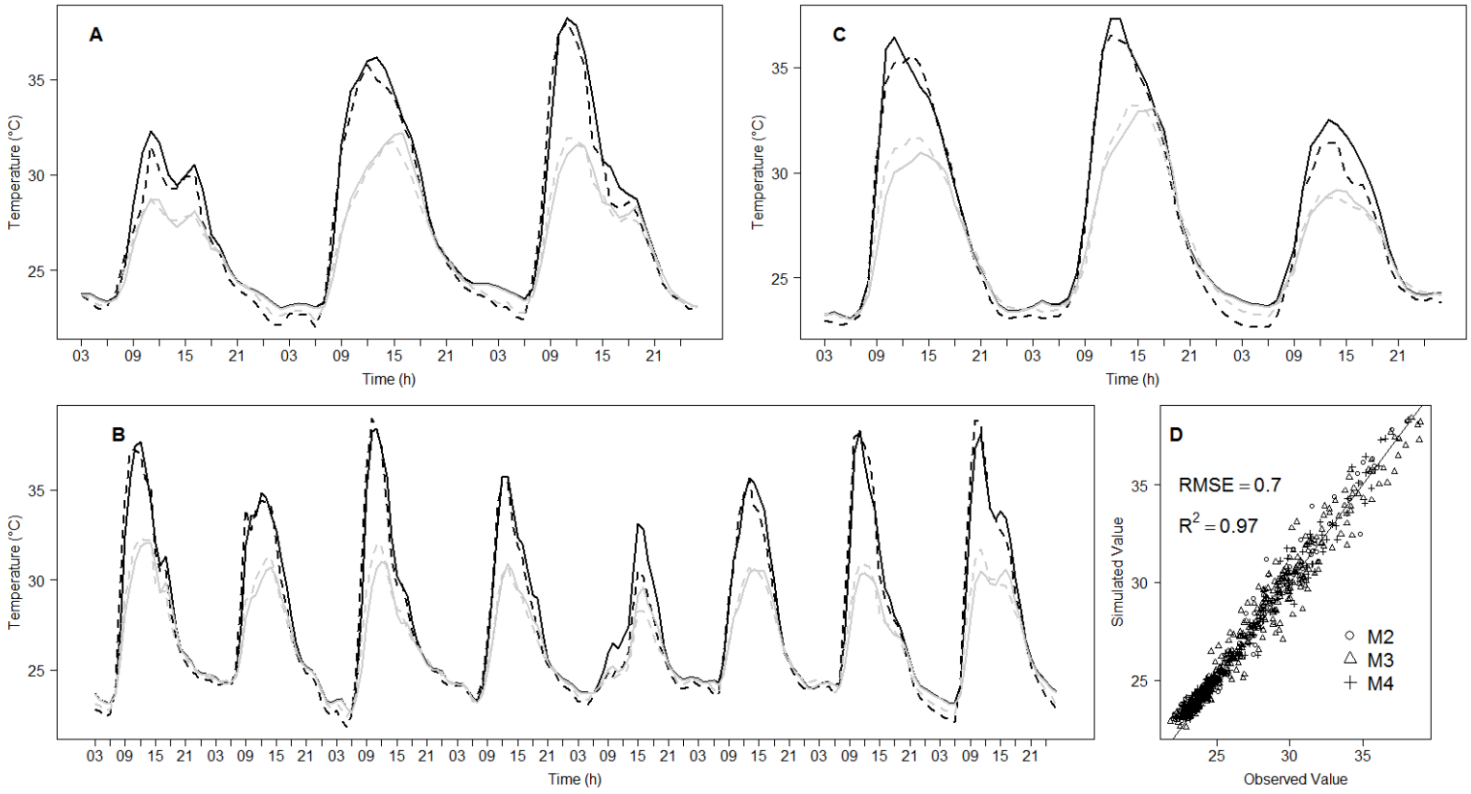

Figure 13: Changes in fruit surface temperatures for a period of 3, 8 and 3 days, measured (dashed line) and simulated (solid line) at the centre of the sunny side (black line) and at the centre of the shaded one (grey line) of a sunny fruit at the M2 (A), M3 (B), M4 (C) maturity stages, and comparison of these simulated data with those observed (D), with the curve y = x (continuous black line), the determinant coefficient, R², and Root Mean Square Error (RMSE), between observed and predicted values.

The temperatures predicted by the model for the case of a spherical object were close to analytical solutions (RMSE < 0.041, R^2 = 0.998; Figure 12) and proved that conduction and convection processes were well integrated into the model. Surface temperatures simulated by the model for the sunny and the shaded sides of a fruit were compared to the ones measured for a period of 3, 8 and 3 days for fruits at the M2, M3 and M4 maturity stages, respectively (Figure 13A to Figure 13C). The model was able to accurately predict spatial and temporal temperature variations of mango fruit, regardless of the maturity stage, as shown by the good agreement with the measurements (R^2 > 0.97 and RMSE = 0.7°C; Figure 13D).

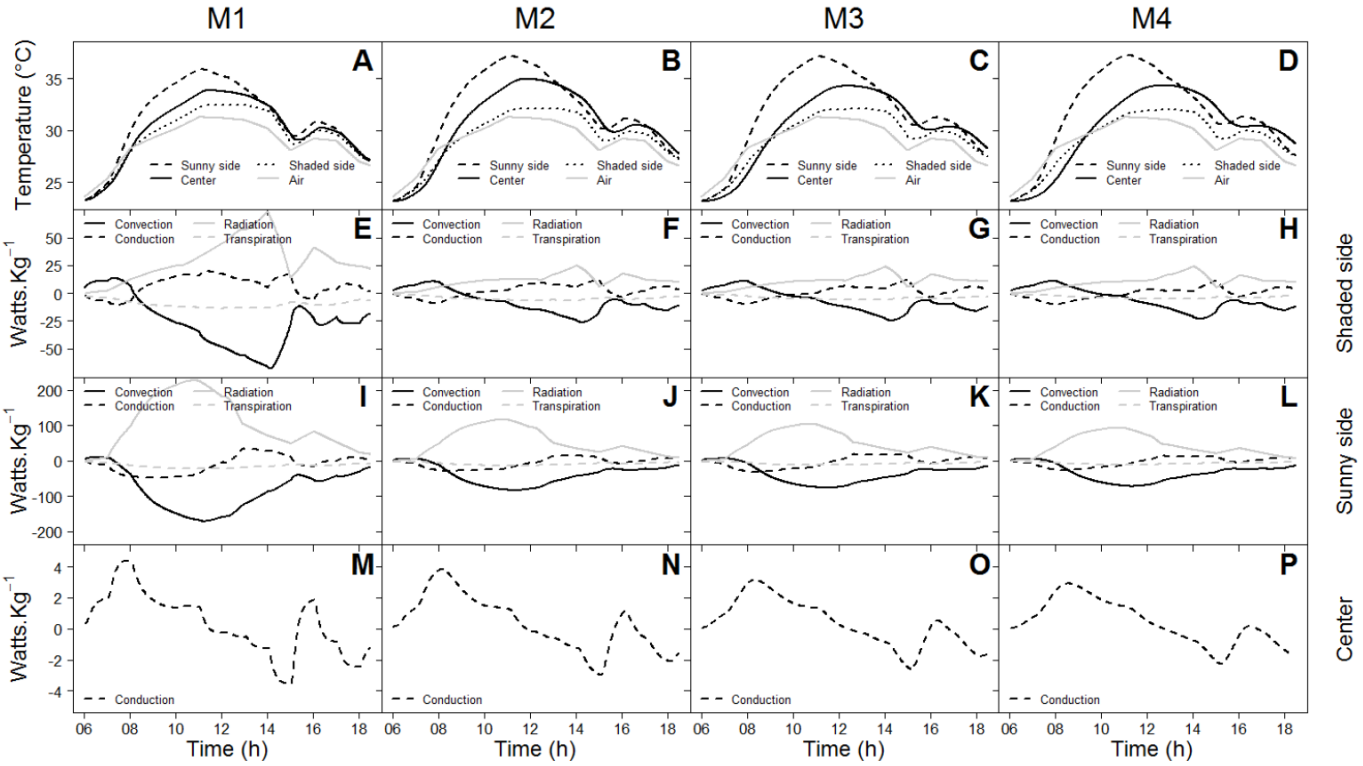

Figure 14 : Daily changes in air and fruit temperatures at different positions within the fruit - the sunny side, the centre and the shaded side - at M1 (A), M2 (B), M3 (C) and M4 (D) maturity stages, and variations of power per mass unit by convection, conduction, radiation and transpiration of sub-units on the shaded fruit surface (E to H), on the sunny fruit surface (I to L) and at the fruit centre (M to P) for fruit at the M1, M2, M3 and M4 maturity stages.

Figure 14 compares the daily changes in simulated temperatures of sub-units located on the fruit surfaces of the sunny and shaded sides, and at the fruit centre, as well as the various components of the heat budget of these three fruit sub-units over one day for all of the maturity stages studied. Differences in temperature between the sunny and the shaded sides of the fruit increased with fruit maturity stages (Figure 14A to Figure 14D). The highest powers per mass unit were simulated at the M1 maturity stage (Figure 14E to Figure 14H). Differences in power per mass unit between maturity stages were related to the variations of the physical and thermal fruit properties over time and to the more rapid increase in fruit volume than in fruit surface (see previous section). The major components of the energy balance of the fruit surface were the radiation and the convective rates (Figure 14E to Figure 14L). The transpiration flux had the lowest impact on the heat budget of elements on the fruit surface and was negligible in comparison to the other heat fluxes (Figure 14E to Figure 14L).

The influence of the radiation flux on fruit temperature was particularly evident around 3:00 pm when the low increase in radiation (Figure 14E to Figure 14L) induced an increase in temperature at the different fruit positions Figure 14A to Figure 14D)

Powers simulated were greater for the sunny side of the fruit (Figure 14I to Figure 14L) than the shaded one (Figure 14E to Figure 14H), regardless of the maturity stage. For example, radiation and the convective powers were more than three times higher for the sunny side than for the shaded one at midday, regardless of the maturity stage.

The analysis of the conductive rate in the fruit center indicated that during the first part of the day, the surface layers heat the underlying ones since the conductive heat is positive, whereas during the second part of the day, the underlying layers heat the surface layers since the conductive heat is negative (Figure 14M to Figure 14P).

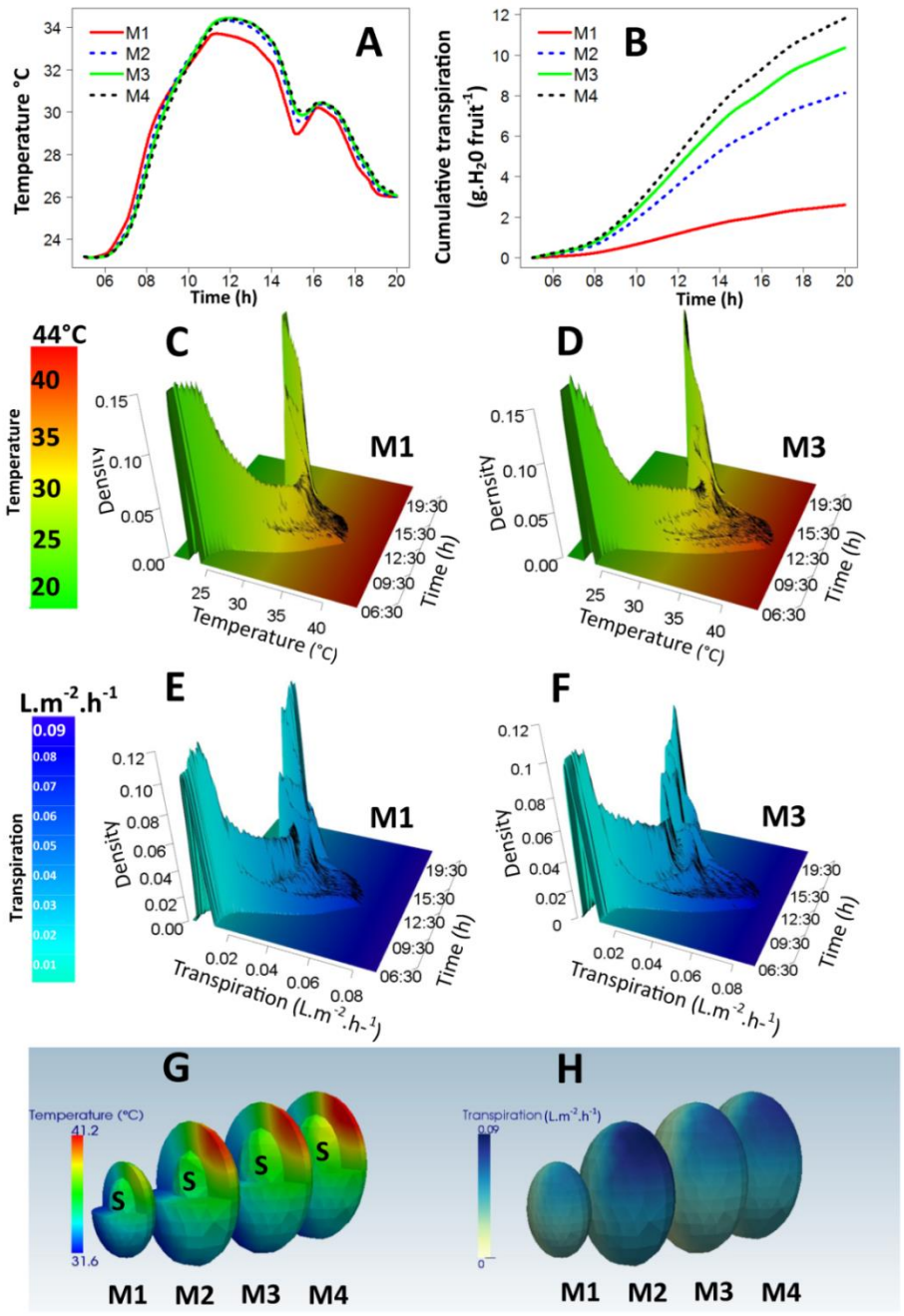

Figure 15: Effects of the maturity stage on the daily spatial and temporal variations of the temperature and the transpiration of fruit. The average daily evolution of temperatures (A) and cumulative water losses by transpiration (B) for fruits at the M1, M2, M3 and M4 maturity stages, and the probability distribution functions of the simulated temperatures (C and D) and the simulated transpiration rates (E and F) within the fruit at the M1 and M3 maturity stages, respectively, are represented. At a given time, the curve has a total area of one. The spatial distribution of temperatures (G) and water losses by transpiration (H) at 12:00 were obtained from simulations of a fruit at the four maturity stages, M1 to M4. S corresponded to the stone compartment.

Patterns of the diurnal changes in the average fruit temperature were quite similar, regardless of the maturity stage (Figure 15A). It was observed that the average fruit temperature of the smallest fruit, i.e., at the M1 maturity stage, increased and decreased faster than that of the large fruits, i.e., at the M2, M3 and M4 maturity stages. Daily water losses by transpiration increased with fruit maturity stages (Figure 15B). For fruit at the M4 maturity stage, the daily sum of water losses by transpiration reached 11.81 grams and represented more than 4.5 times that of a fruit at the M1 maturity stage.

The daily variability of the temperature (Figure 15C and Figure 15D) and transpiration (Figure 15E and Figure 15F) of fruits at the M1 and M3 stages were compared. Fruits at the M1 and M3 maturity stages were considered because they had contrasting sizes. Fruits start to grow at the M1 maturity stage, whereas they have almost reached their final size at the M3 maturity stage. The daily changes in the distributions of temperature and transpiration showed similar patterns for the two maturity stages. Temperature and transpiration were homogenous before the sun rose, and became more and more variable until the middle of the day (Figure 15C to Figure 15F). Then, as the sun went down, fruit temperature and transpiration tended to return to the homogenous state observed at the beginning of the day. Temperature and transpiration gradients were more pronounced for the oldest fruit since they increased faster in the morning and decreased more slowly in the afternoon (Figure 15C to Figure 15F). These gradients of temperature and transpiration were found to be approximately 9.5°C (Figure 15D) and 0.051 $L.m^{-2}.H^{-1}$ (Figure 15F) for the oldest fruit, compared to 6.8°C (Figure 15C) and 0.036 $L.m^{-2}.H^{-1}$ (Figure 15E) for the youngest one. These gradients are illustrated in Figure 15G and Figure 15H, which compare the spatial variability of temperature and transpiration at 12:00 pm of fruits at the M1, M2, M3 and M4 stages. Temperature gradients within fruits at the M2, M3 and M4 maturity stages were similar and higher than those within fruit at the M1 maturity stage. The highest transpiration gradient was simulated for fruit at the M2 maturity stage and can be related to the highest difference in peel conductance to water between sunny and the shaded fruit sides measured for this maturity stage (Figure 11A).

Table 4: Simple analysis of the sensitivity of simulated temperature and transpiration to parameter variations, based on the sensitivity coefficient of the maximum value. A value of 1 or -1 signifies that the variations of the parameters induce a proportional increase or decrease, respectively, of the maximum of simulated temperature or transpiration.

	$Centre_{T°max}$	$Sun_{T°max}$	$Shade_{T°max}$	$Sun_{Transpiration\ max}$	$Shade_{Transpiration\ max}$
Heat Capacity (Cp)	-6.4E-03	-1.3E-02	-9.9E-04	-3.3E-03	-3.8E-04
Reflectance (Asw)	-5.6E-02	-1.3E-01	-2.4E-02	-5.3E-02	-1.2E-02
Specific gravity	-6.4E-03	-1.3E-02	-9.9E-04	-3.3E-03	-3.8E-04
Skin permeability to water (Gw)	-2.2E-03	-2.3E-03	-2.4E-03	1.0E+00	1.0E+00
Thermal conductivity (K)	8.6E-04	-3.8E-02	1.4E-02	-1.1E-02	6.8E-03
Peel thickness	3.5E-05	1.4E-04	-1.4E-05	-8.3E-05	8.5E-05
Stone/Fruit ratio	2.2E-03	3.2E-02	-1.7E-02	1.0E-02	-8.2E-03
Fruit size	2.8E-02	6.2E-02	6.3E-03	1.4E-02	2.5E-03

a) Sensitivity analysis to fruit internal factors and impacts of their measured evolution on fruit temperature and transpiration

The effects of variations of thermal and physical fruit properties on fruit temperature and transpiration were studied for different positions within the fruit at the fruit centre and at the surface of the sunny and shaded fruit sides using the sensibility coefficients calculated with the average, maximum and minimum predicted values. For the sake of simplicity, only the results related to the maximum values are presented since they showed the highest sensitivity to parameter variations (Table 4). Predicted temperature and transpiration values were slightly affected by the parameter variations, with the exception of the impact of the G_w variation on transpiration. Temperature and transpiration of the sunny side were found to be more sensitive to parameter variations than those of the other positions within the fruit. Peel reflectance, A_{sw}, and fruit size were the model parameters that had the most impact on fruit temperature for all tested positions within the fruit. Skin permeability to water, G_w, and peel reflectance, to a lesser extent, were found to have the highest impact on fruit transpiration for both fruit sides.

Table 5 Effects of the variation of thermal and physical parameters during fruit development on fruit temperature, maximum transpiration per surface unit and total water losses by transpiration.

	Temperature mean (°C)	Temperature max (°C)	Temperature min (°C)	Transpiration max ($L.m^{-2}.H^{-1}$)	Total water losses (L)
Evolution of all parameters	24.20	41.38	17.00	$7.241\ 10^{-2}$	0.569
All parameters constant	24.18	39.27	16.99	$6.604\ 10^{-2}$	0.202
Constant fruit size	24.19	39.27	16.99	$6.607\ 10^{-2}$	0.191
Constant fruit conductance to water (Gw)	24.21	41.37	17.00	$7.360\ 10^{-2}$	0.547
Constant fruit reflectance (Asw)	24.18	41.00	17.04	$7.081\ 10^{-2}$	0.567
Constant thermal parameters (K, Cp, SG)	24.20	41.21	17.00	$7.161\ 10^{-2}$	0.569

Table 5 summarizes the effects of the evolution of physical and thermal parameters during a fruit's growth on its temperature and transpiration. The greatest effect of the evolution of fruit properties was found for the total water losses by transpiration since these losses were multiplied by more than 2.8 when taking parameter variations into account. Evolutions of fruit properties had minor effects on the minimum and the average of predicted temperatures, whereas the predicted maximum values of temperature and transpiration per surface unit somewhat increased. The impact of the evolution of a fruit's characteristics in terms of transpiration and temperature were mainly due to its increase in size. The evolution of the peel conductance to water did not sharply affect fruit transpiration. The reflectance evolution did not affect fruit temperatures.

E - Discussion

a) Model accuracy and gradient of transpiration and temperature within the fruit

The established model in this study is able to predict fruit temperature variations at both space and time scales, taking changes in physical and thermal parameters during fruit development and between fruit tissues into account. The discrepancy between the model predictions and the observed data was satisfactory and on the same order of magnitude of another fruit temperature model previously developed by Saudreau et al. (Saudreau et al., 2007). Confirming the previous study of Saudreau et al. (Saudreau et al., 2007), radiation and convection were the main heat fluxes driving fruit temperature. The fruit temperature surface area was found to differ from that of the air and to greatly vary during the day, as observed for many fruits such as apple (Saudreau et al., 2007, Saudreau et al., 2009), peach (Saudreau et al., 2007) and avocado (Woolf et al., 1999). The simulated gradient of temperature and transpiration within the fruit fluctuated during the course of the day and was non-negligible since it exceeded 9°C and 0.051 $L.m^{-2}.h^{-1}$, respectively. The large inner temperature gradient previously observed by Saudreau et al. (Saudreau et al., 2007) and the large transpiration gradient should be considered for modelling physiological processes. It was recently suggested that differences in light conditions between the two sides of a mango induce the differences in water and osmotic potentials observed between the sunny and shaded sides of the fruit (Léchaudel et al., 2012). Since temperature is known to affect enzymatic reaction speed, the temperature gradient is expected to induce differences in substrate and product concentrations within the fruit. Consequently, it would be interesting to determine whether or not the temperature gradient highlighted in this study is related to sugar variations within the fruit, in accordance with relationships established between the accumulation of temperature and sugar content for peach (Génard and Souty, 1996) and mango (Léchaudel et al., 2007). In addition, due to the impact of temperature on respiration rate (Mangaraj and Goswami, 2011, Ravindra and Goswami, 2008, Fonseca et al., 2002), temperature variations within the fruit are expected to affect the gas concentration gradients previously reported for several fruits such as apple (Verboven et al., 2008, Ho et al., 2010b) and pear (Ho et al., 2010a). Further studies are also required to study the impact of the transpiration gradient within the fruit highlighted in this study on mineral and water

content. Water losses by transpiration induce variations in mineral content, as shown for several fruits such as kiwi (Montanaro et al., 2006) and apricot (Montanaro et al., 2010), and affect water content, as shown for tomato (Leonardi et al., 2000b).

b) Effects of variations of thermal and physical fruit properties during fruit growth on temperature and transpiration.

None of the variations in fruit properties except those representing the increase in fruit size was found to have a high incidence on fruit temperature and transpiration. The absence of strong effects was due to the weak influence of fruit thermal and physical properties on fruit temperature and transpiration per surface unit, as revealed in the local sensitivity analysis, and to the fact that these properties changed very little during fruit development, as shown by their measurements. Although changes in fruit colour were observed during fruit development and according to the fruit side, peel reflectance was found to increase only slightly during the last maturity stage. The increase in peel reflectance during fruit ripening could be related to the degradation of chlorophyll pigments, which induces the appearance of yellow peel colour (Medlicott et al., 1986), as observed for the shaded side in the late development stage. Surprisingly, no difference in the peel reflectance values was found between the two fruit sides, although the sunny fruit side had a pink blush. A purple peel colour was effectively presumed to be related to a higher heat absorbing capacity than a green one (Hetherington, 1997). In fact, the accumulation of anthocyanin pigments is reported to be involved in peel blushing (Proctor and Creasy, 1969, Honda et al., 2002) in response to high irradiance (Steyn et al., 2009), and is probably responsible for decreasing peel reflectance. As observed by Ribero Da Luz (Ribeiro da Luz, 2006) for leaves, accumulation of wax on exposed tissues affects optical properties. Therefore, differences in wax accumulation between fruit sides due to sun exposure differences, as observed on grape (McDonald et al., 1993, Nordby and McDonald, 1995), could explain the absence of differences in reflectance values between the two fruit sides, even if their anthocyanin pigment contents were assumed to be different. Low variations in the peel conductance to water were found with the fruit maturity stages as well. The slight tendency of a decrease in the peel permeability to water with fruit development, regardless of the fruit side, could be explained by the assumed increase in the epicuticular wax per unit skin area (Bally, 1999, Vogg et al., 2004) and/or in the wound healing activity around cracks (Gibert et al., 2010,

Walter et al., 1990). The measured lower peel conductance to water of the sunny side compared to the shaded one would result from the presumably higher accumulation of wax on this side (McDonald et al., 1993, Nordby and McDonald, 1995). Finally, the decrease in the water content during fruit growth (Lechaudel et al., 2002) induced only a slight variation in thermal parameters, including heat capacity, thermal conductivity and specific gravity. Only the fruit size increase was found to extend the gradient of fruit temperature and transpiration, mainly due to the expansion in volume.

2) **Concluding remarks**

Significant variations in thermal and physical properties were measured between mango tissues at several mango maturity stages. To study the impact that mango development has on its temperature and transpiration, a physical model was developed. Model predictions have been satisfactorily compared to fruit temperature and have made it possible to accurately simulate the daily variations of temperature between fruit sides. Model outputs indicated that the average fruit temperature at the growing season scale was not affected by the evolution of the fruit's thermal and physical properties during its development. These results suggested that the calculation of an average temperature of a growing fruit, required, for example, for the calculation of the thermal time sum, can be achieved without taking the evolution of fruit properties into account. However, results indicated that changes in a fruit's properties during its development induced changes in the temperature and transpiration distribution within the fruit. Consequently, to represent the spatial and temporal variability of fruit temperature and transpiration of a growing fruit to model physiological processes such as growth, ripening and quality development, the variations in the fruit's properties during its development, and particularly its size, should be taken into account.

III - Spatial and temporal variations in mango colour, acidity, and sweetness in relation to temperature and ethylene gradients within the fruit

Objectifs :

Il est proposé dans ce chapitre d'étudier l'effet des gradients de température simulés dans la mangue sur sa qualité et sa maturité. Pour se faire, les variations de qualité, i.e., couleur de la peau et de la pulpe, acidité et teneur en composés solubles, et de maturité mesurées dans la mangue ont été confrontées aux gradients de degrés jours simulés à plusieurs stades de développement du fruit. Ce chapitre a fait l'objet d'une publication dans **Journal of Plant Physiologie** sous la forme d'un article intitulé « *Spatial and temporal variations of mango colour, acidity and sweetness in relation to temperature and ethylene gradients within the fruit* ».

Principaux résultats :

- D'importants gradients de qualité et de maturité ont été mesurés dans la mangue quel que soit le stade de développement.
- Les différences de qualité et de maturité mesurées à l'intérieur du fruit ne sont pas liées aux gradients de degrés jours simulés dans la mangue.
- Les différences de qualité au sein du fruit sont en partie liées aux variations de maturité mesurées dans la mangue.
- Les résultats suggèrent que d'autres gradients comme ceux en gaz, en eau et en acide abscissique sont également impliqués dans l'hétérogénéité de la qualité du fruit.

Spatial and temporal variations in mango colour, acidity,
and sweetness in relation to temperature and ethylene gradients within the fruit

Thibault Nordey[1*], Mathieu Léchaudel[1], Michel Génard[2] and Jacques Joas[3]

[1]CIRAD, UPR HORTSYS, 97455 Saint-Pierre, La Réunion, France
[2]INRA, UR 1115, Plantes et Systèmes de culture Horticoles, 84000 Avignon, France
[3]CIRAD, UMR QUALISUD, 34398 Montpellier, France

A - Abstract

Managing fruit quality is complex because many different attributes have to be taken into account, which are themselves subject to spatial and temporal variations. Heterogeneous fruit quality has been assumed to be partly related to temperature and maturity gradients within the fruit.

To test this assumption, we measured the spatial variability of certain mango fruit quality traits: colour of the peel and of the flesh, and sourness and sweetness, at different stages of fruit maturity using destructive methods as well as Vis-NIR reflectance. The spatial variability of mango quality traits was compared to internal variations in thermal time, simulated by a physical model, and to internal variations in maturity, using ethylene content as an indicator.

All the fruit quality indicators analysed showed significant spatial and temporal variations, regardless of the measurement method used. The heterogeneity of internal fruit quality traits was not correlated with the marked internal temperature gradient we modelled.

However, variations in ethylene content revealed a strong internal maturity gradient which was correlated with the spatial variations in measured mango quality traits. Nonetheless, alone, the internal maturity gradient did not explain the variability of fruit quality traits, suggesting that other factors, such as gas, abscisic acid and water gradients, are also involved.

B - Introduction

Management of fruit quality is essential because it defines fruit grade and, by extension, its commercial value. However, fruit quality is a complex notion because it involves numerous attributes including external appearance, taste, and nutritional value (Léchaudel and Joas, 2007, Abbott, 1999, Hewett, 2006). Fruit quality traits depend on concentrations of primary metabolites including sugars, organic acids, and amino acids, as well as secondary metabolites such as pigments, vitamins and aromas. The concentrations of these compounds vary during the course of fruit development (Léchaudel et al., 2007, Fishman and Génard, 1998, Gautier et al., 2008) and in different parts of the fruit tissues (Biais et al., 2010, Pedreschi et al., 2009, Moing et al., 2011). Several studies have focused on the determinants of temporal changes in fruit quality, but less information is available on the causes of the spatial variation in fruit quality.

Variations in sugar and acid contents in fruit are linked to thermal time, i.e. degree.days, as reported for several species including mango (Lechaudel et al., 2010), peach (Génard and Souty, 1996), and grapevine (Duchêne et al., 2012). It can thus be hypothesized that the marked temperature gradients caused by the heterogeneity of environmental factors at the fruit scale, measured (Léchaudel et al., 2012, Woolf et al., 1999) and modelled inside the fruit (Saudreau et al., 2007, Nordey et al., 2014c), could be involved in the spatial variability of fruit quality traits.

Variations in overall fruit quality during the fruit ripening process have been the focus of a number of studies. During this irreversible fruit development stage, fruit quality changes considerably, thereby rendering the fruit attractive to the consumer (Lelièvre et al., 1997, Bapat et al., 2010). Current knowledge emphasizes the involvement of abscisic acid and ethylene, two phytohormones known to be involved in ripening, in the regulation of the biochemical and physiological changes which occur during fruit ripening (McAtee et al., 2013). Several authors reported that ethylene content varies considerably within fruits (Hershkovitz et al., 2009, Mita et al., 1998, Fernández-Otero et al., 2006). It can thus be hypothesized that the spatial variation in the primary and secondary metabolites involved in quality traits could be partly explained by variations in the production and diffusion of phytohormones within the fruit, as suggested by Moing et al. (2011).

The aim of this study was to investigate to what extent the spatial variability of fruit quality traits is related to variations in ripening and to thermal time within the fruit. Mango fruit was chosen because quality management of this climacteric fruit is a major limit to its sale (Tharanathan et al., 2006). This study focuses on the quality traits responsible for the external appearance of the fruit, using peel colour as the indicator, sweetness, assessed by total soluble solids (TSS), sourness, measured by titratable acidity, and the carotenoid content of the flesh, deduced from the flesh colour. To facilitate measurement of titratable acidity and TSS content, a method was developed based on visible and near-infrared (Vis-NIR) reflectance. The spatial variability of mango quality traits was compared to variations in thermal time within the fruit during its development, simulated using a physical model (Nordey et al., 2014c), and to internal variations in maturity, using ethylene content as an indicator.

Our results advance our understanding of the processes involved in variations in quality traits within fruits and should help control fruit quality.

C - Materials and methods

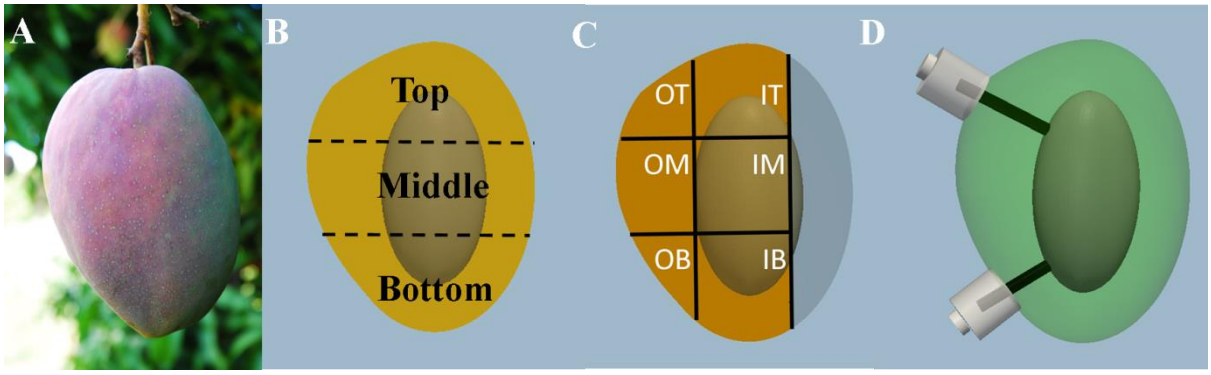

Figure 16: Mango fruit cv. Cogshall (A) and a schematic diagram to illustrate the method used for the compartmentalization of fruit for destructive (B) and Vis-NIR reflectance (C) measurements of TSS content, titratable acidity, and flesh colour, and for measurements of ethylene content in the seed (D), where OT: Outer Top, IT: Inner Top, OM: Outer Middle, IM: Inner Middle, OB: Outer Bottom, IB: Inner Bottom indicate the position of the measurement in the flesh.

a) Fruit samples

The study was carried out on mangoes of the Cogshall cultivar (Figure 16A). Fruits were grown during the 2012-2013 production season in the CIRAD orchard in Reunion Island (20°52' 48'' S, 55°31' 48" E), which is composed of 7-year-old trees grafted on a 'Maison Rouge' cultivar. The trees were well irrigated, spaced 5 x 6 m apart, and were approximately 3 m tall at the time of the study.

A first set of fruit was used to destructively analyse variability of peel colour, TSS content, titratable acidity, and the colour of the fruit flesh, in the bottom, middle, and top parts of the fruit, and between the shaded and sunny sides. Fifty-two fruits were harvested at four commercial maturity stages: green mature, turning, yellow point (YPS) (Léchaudel and Joas, 2006), and ripe, corresponding to 90, 110, 120, and 130 days after full bloom, respectively. Between 12 and 15 fruits were analysed for each maturity stage. Titratable acidity was only measured on fruits at the green mature and ripe stages, without taking exposure to sunlight into account.

A second set of 50 fruits was used to calibrate the partial least square (PLS) regressions required to predict TSS content and titratable acidity using Vis-NIR reflectance. Each fruit was randomly divided into three samples of flesh (Figure 16B). For each sample, reflectance spectra were monitored before destructive measurements of TSS content and titratable acidity.

A third set of fruit was used to analyse spatial variability of TSS contents, titratable acidity and flesh colour from the inner to the outer flesh, and from the bottom to the top of the fruit, measured by Vis-NIR reflectance (Figure 16C). A total of 33, 13, and 21 fruits were harvested at the green mature, turning and yellow point stages, respectively.

A fourth set of fruits was used to evaluate variability of ethylene from the bottom to the top of the fruit, and from the surface to the seed of the fruit. A total of 5, 5, 5 and 6 fruits were harvested at the green mature, turning, yellow point and ripe stages, respectively.

b) Sampling and analysis of mango quality traits

After harvesting the first set of fruits, the colour of the peel of each fruit was measured with a Minolta Chroma meter CR300 (Konica Minolta, Osaka, Japan). The CIELAB coordinates (L*, a*, b*) were measured on three areas of the fruit peel: the middle of the sunny side, the

middle of the shaded side, and the bottom of the fruit. As suggested by Ayala-Silva et al. (2005) and Kang et al. (2008), peel colour is described using the hue angle as the criterion (Equation 18).

$$h_{ab} = \arctan(\frac{b*}{a*}) \qquad \textit{Equation 18}$$

The fruits were then divided into two "sides" according to their exposure to sunlight. Each side was divided into three sections from the top to the bottom of the fruit in order to obtain three samples of equal length (Figure 1B). The colour of each flesh sample was measured with a Minolta Chroma meter CR300 (Konica Minolta, Osaka, Japan) and described using the hue angle criterion (Equation 18), as proposed by Vasquez-Caicedo et al. (2005). Flesh samples were then ground in a Grindomix blender (Retsch, Haan, Germany) to obtain fresh juice to measure TSS content using a refractometer ATC-1E (Atago, Tokyo, Japan) and titratable acidity. Titratable acidity, expressed as milli-equivalents of acid per 100 g fresh mass (Meq.100gFM^{-1}), was measured by colorimetric titration with phenolphthalein and 0.05 mol.L^{-1} NaOH solution.

Flesh samples from the second set of fruits used for model calibrations were prepared for analysis of their TSS content and titratable acidity in the same way as the first set of fruits.

c) Vis-NIR spectrophotometric measurements and partial least square regressions

For each sample of flesh from the second and the third sets of fruits, reflectance spectra were monitored from 350 to 2500 nm with a portable spectrometer (LABSPEC 2500, Analytical Spectral Devices, Inc., Boulder, CO, USA). Reflectance measurements in the second dataset were then used to calibrate the partial least square (PLS) regressions of TSS content and titratable acidity. To increase the accuracy of the predictions and the robustness of the model, the wavelengths used in PLS regressions were selected, as recommended by Andersen and Bro (2010) for reflectance data. Interval partial least square (IPLS) regressions associated with the stepwise method were performed to identify the best windows of wavelengths for the prediction of TSS content and of titratable acidity of the flesh. In addition, the number of latent variables in PLS regressions was selected to reduce the prediction error by cross validation using the leave-one-out method. The PLS package procedure (Mevik and Wehrens, 2007) developed in R software (RDC Team, 2012) and fully described by Cornillon (2010) was followed.

The model prediction error was evaluated using the root mean square error (RMSE) as an indicator. Calculation of the RMSE is described in Equation 4, where y_t is the t^{th} observed or reference value, $\hat{y}_t$ is the t^{th} simulated value, and n is the number of observed or simulated values. The root mean square error of the model (RMSEM) was calculated with the data used for model calibration, whereas the root mean square error of cross validation (RMSECV) was calculated with an independent set of data which was not used for model calibration.

Equation 19

$$\mathrm{RMSE} = \sqrt{\frac{\sum_{t=1}^{n}(y_t - \hat{y}_t)^2}{n}}$$

After the models were established, they were used to predict the TSS contents and the titratable acidity of flesh samples from the third dataset using their Vis-NIR reflectance measurements. Spectrophotometric measurements were made at the surface of the fruit flesh at six different positions to measure longitudinal and the transversal variability (Figure 1C).

d) Measurement of ethylene contents

Internal concentrations of ethylene were measured in the upper and lower parts of the seed and on the lower and upper surface of the fruit. A non-invasive method was used to measure ethylene content on the surface of the fruit. A gas collection apparatus was constructed using a small 30 cm^{-3} water glass. A hole was made in the bottom of the glass which was then closed with a septum to take the gas sample. The open side of the gas collection apparatus was fixed to the surface of the fruit with a ring of putty as a sealant to prevent leaks.

An invasive method was developed to measure the ethylene content of the seed. However, to reduce the stress caused by this invasive method, the different compartments of the fruit were not separated. A piece of flesh extending from the surface to the seed was removed using a corer measuring 6 mm in diameter. A glass tube with a similar diameter was then inserted until it touched the surface of the seed to prevent the diffusion of ethylene from the flesh into the gas collection apparatus placed on the fruit surface above the glass tube (Figure 16D). In addition, putty was wrapped around the glass tube at the fruit surface to limit ethylene diffusion due to wounding of the peel. The gas was collected with a syringe

three hours after the gas collection apparatus was attached to the fruit, to allow the concentration of gas in the apparatus to reach equilibrium with the concentration of gas in the fruit or in the seed at the time of measurement. The ethylene concentration was analysed by gas chromatography (HP 5890 Series II gas Chromatograph, Hewlett-Packard, Palo Alto, CA, USA).

e) Calculation of the thermal time in the fruit.

Spatial and temporal variations in thermal time, expressed in degree.days, in the fruit were simulated using the model previously developed by our team on mango (Nordey et al. (2014c). Briefly, this physical model simulates the spatial and temporal variations in temperature in the developing fruit by calculating energy fluxes between the fruit and its environment. Climatic data used as input by the model, such as air temperature, global radiation, air humidity and wind speed, were measured at one-minute intervals and averaged and stored every hour on a data logger (Model 21 X, Campbell Scientific Ltd, Logan, UT, USA) during the 2012-2013 growing season. Direct and diffuse global radiation were estimated using the model developed by Maxwell E.L. (1987). The sun's course was determined using the solar position algorithm (SPA) developed by Reda and Andreas (2004). The model also requires changes in the physical and thermal properties of the fruit during its development as input data. The fruit growth rate was determined on the basis of the increase in fruit height, calculated from the average of 10 fruits measured weekly from the end of cell division (60 DAB) to the fully ripe stage (130 DAB). Variations in the other fruit parameters - heat capacity, density, conductivity, skin permeability to water diffusion and peel reflectance - were taken from a previous study (Nordey et al., 2014c). Fruit temperature depends on its position within the tree (Saudreau et al., 2009). So to take this variability into account, fruits located on the east west, north and south side of the canopy were used. It was assumed that one side of each fruit was directly exposed to the sun (sunny side) and that the opposite side received 20% of the sunlight (shaded side), in line with the measurements made in the same previous study (Nordey et al., 2014c). Thermal time is expressed in degree.days (Bonhomme, 2000), calculated on the basis of a basal temperature considered equal to 16 °C, consistent with the results of (Léchaudel et al., 2005a).

f) Statistical analysis

Multiple comparisons were performed using Tukey's test to establish whether or not spatial and temporal variations in ethylene content and in fruit quality traits were significant.

Principal component analysis (PCA) was performed on the average of the quality traits predicted from reflectance, ethylene contents, and predicted thermal time, expressed in degree.days. Three positions in the fruit were considered for this analysis outside top (OT), inside middle (IM) and outside bottom (OB) at the four stages of maturity we studied, i.e. green mature, turning, yellow point, and ripe (Figure 16C). We assumed that ethylene content measured on the lower and upper parts of the fruit surface corresponded to the outside top and outside bottom positions (Figure 16C and Figure 16D). The average of the ethylene contents measured in the upper and lower parts of the seed was used for the inside middle position.

All statistical analyses were performed using the R software (RDC Team, 2012).

D - Results

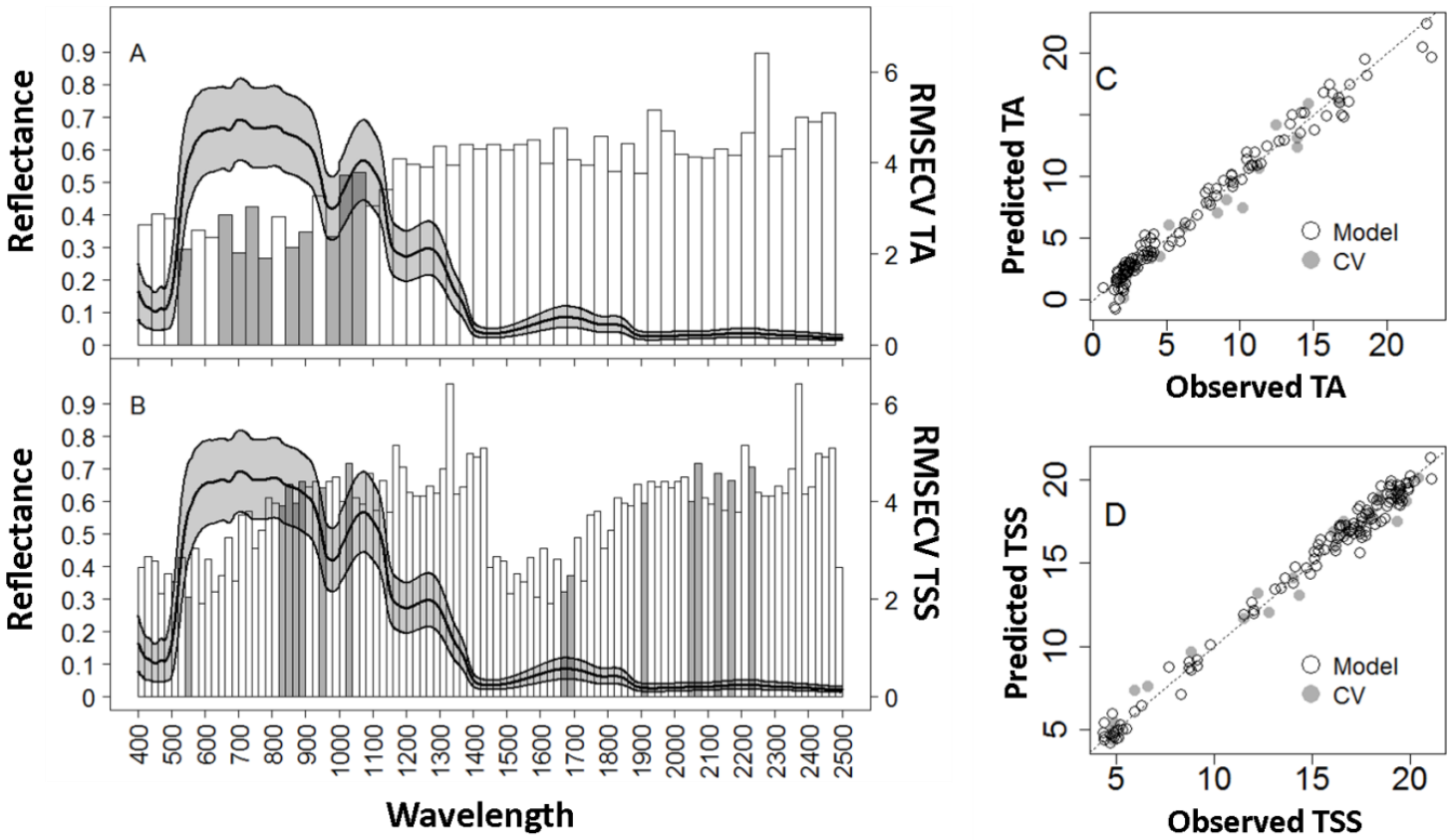

Figure 17: Variable selection and accuracy of Partial Least Square (PLS) regressions for predicting titratable acidity (TA, in Meq.100gMF-1) (A, C) and the total soluble solids (TSS, in °Brix) content (B, D) of the flesh of mango cv. Cogshall. Average (continuous lines) ± standard deviation (grey region) of reflectance spectra of mango flesh associated with the predictive value of the regions of the spectra (vertical bars), calculated by the root mean square error of cross validation (RMSECV) for titratable acidity (A) and TSS content (B), and with the selected regions used for PLS regressions (grey).

1) **Predictions of TSS content and titratable acidity in the flesh based on Vis-NIR reflectance**

Vis-NIR reflectance was used to predict the spatial variations in TSS content and titratable acidity of the fruit using PLS regressions. The highest reflectance of mango flesh was measured from 500 nm to 1400 nm (Figure 17A and Figure 17B). In the visible range, i.e., from 400 to 800 nm, the reflectance spectra of the mango flesh showed variations of approximately 480 and 680 nm, related to the absorption of carotenoid and chlorophyll pigments, respectively. The spectra in the NIR region were clearly dominated by the water spectrum with overtone bands of the O-H bonds at 740, 970, 1450 and 1940 nm. Interval partial least square regressions performed with wavelength windows of 20 and 30 nm gave

the best predictions of titratable acidity and TSS content of the flesh, respectively. Figure 17A and Figure 17B are graphic diagrams of the capacity of the reflectance spectrum regions to predict the TSS content and titratable acidity of the flesh.

The best wavelengths to predict titratable acidity were from 400 to 1100 nm (Figure 17A). Two regions of the spectra were best for the prediction of the TSS content of the flesh: one from 400 to 700 nm, and one from 1400 to 1800 nm (Figure 17B). The stepwise method selected window intervals in these two regions as well as in the regions from 820 to 1040 nm, and from 1900 to 2240 nm. The number of latent variables was 15 and 20 for the model of TSS content and acidity prediction, respectively.

The accuracy of the predictions of TSS content and titratable acidity was satisfactory since RMSEM were 0.56 and 0.74, and RMSECV were 0.88 and 1.03 for TSS content and the titratable acidity models, respectively (Figure 17C and Figure 17D). The models were tested for a wide range of TSS contents and titratable acidity and were shown to be suitable for predicting these quality traits in immature and mature fruits. These models can consequently be used to evaluate spatial variability of TSS content and titratable acidity from the inner to the outer flesh and from the bottom to the top of the mango fruit, at the stages of maturity desired.

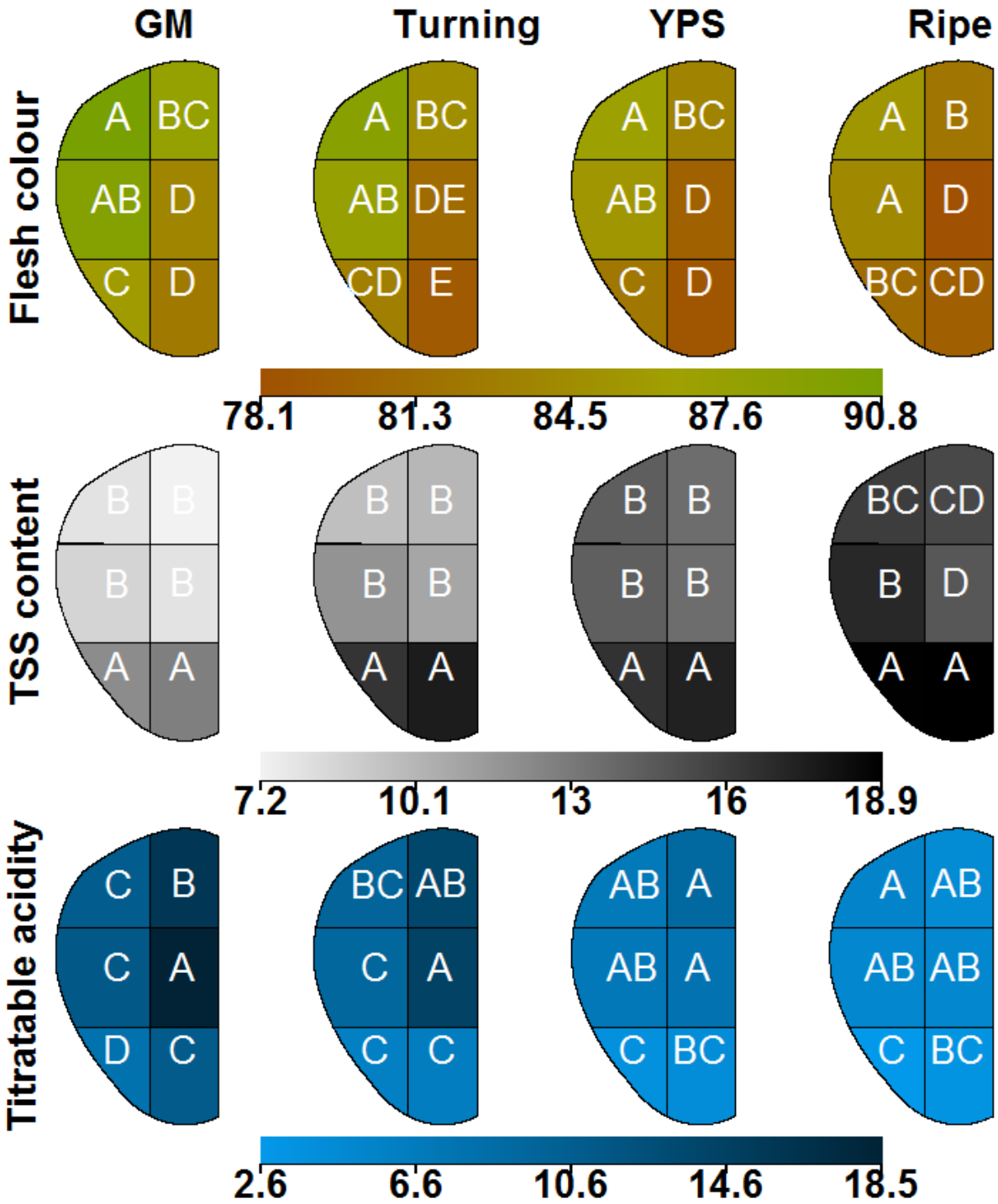

Figure 18: Spatial variations in total soluble solids (TSS content, in ° Brix), flesh colour, (expressed in hue angle value, °) and titratable acidity (TA, in milli-equivalents of acid per 100 g fresh mass) in the flesh of mango cv. Cogshall at the green mature (GM), turning, yellow point (YPS) and ripe maturity stages, measured by Vis-NIR reflectance. Different capital letters mean that data differ significantly at $P < 0.05$ (according to Tukey's multiple comparison test) between different positions in the fruit flesh.

Table 6: Effect of the stage of maturity and fruit side on measurements of the colour of the peel, expressed by the hue angle values (in °). Values are means ± standard deviations. Different capital and lower case letters mean that data differ significantly between fruit sides and fruit maturity stages, respectively, at P < 0.05 (according to Tukey's multiple comparison test).

	Green Mature	Turning	Yellow point	Ripe
Fruit bottom	**123.6** ±2.3 (A)(a)	**122.1** ±2.7 (A)(a)	**96.3** ±6.5 (A)(b)	**82.6** ±7.9 (A)(c)
Shaded side	**120.1** ±3.6 (A)(a)	**120,9** ±4.3 (A)(ab)	**110.3** ±2.5 (B)(b)	**83.4** ±6.2 (A)(c)
Sunny side	**34.9** ±20.5 (B)(a)	**15.7** ±10.4 (B)(b)	**21.9** ±17.4 (C)(ab)	**20.8** ±9.7 (B)(ab)

Table 7: Effect of the maturity stage and fruit side exposure on the measured longitudinal variations in total soluble content (TSS, in °Brix) and the hue angle values of the flesh colour (in °) inside the fruit. Values are means ± standard deviations. Different capital and lower case letters mean that data differ significantly for the TSS content and the hue angle values, between flesh position in the fruit and fruit maturity stages, respectively, at P < 0.05 (according to Tukey's multiple comparison test).

Fruit Side	Position inside the fruit		Green Mature	Turning	Yellow point	Ripe
Shaded	Bottom	TSS content	**11.5** ±1.64 (A)(d)	**14.9** ±1.5 (A)(c)	**16.7** ±1.8 (A)(b)	**19.3** ±1.2 (A)(a)
		Hue angle	**91.3** ± 3.1 (AB)(a)	**88.2** ± 4.4 (C)(ab)	**88.1** ± 3.3 (BC)(ab)	**86.9** ± 1.5 (BC)(b)
	Middle	TSS content	**10.0** ±1.2 (A)(d)	**12.6** ±1.0 (B)(c)	**14.5** ±1.1 (B)(b)	**17.4** ±1.1 (B)(a)
		Hue angle	**91.8** ± 2.6 (AB)(a)	**89.8** ± 3.02 (ABC)(ab)	**88.5** ± 3.5 (BC)(b)	**88.7** ± 2.2 (AB)(b)
	Top	TSS content	**9.7** ±1.8 (A)(d)	**11.7** ±1.1 (B)(c)	**14.4** ±1.0 (B)(b)	**17.6** ±1.0 (B)(a)
		Hue angle	**94.3** ± 2.5 (A)(a)	**93.3** ± 1.6 (A)(a)	**92.0** ± 2.4 (A)(ab)	**90.4** ± 2.7 (A)(b)
Sunny	Bottom	TSS content	**11.8** ±2.1 (A)(c)	**15.5** ±1.7 (A)(b)	**17.1** ±1.4 (A)(b)	**19.3** ±1.3 (A)(a)
		Hue angle	**90.1** ± 4.8 (B)(a)	**87.3** ± 4.3 (C)(ab)	**87.8** ± 3.1 (C)(ab)	**85.5** ± 1.7 (C)(b)
	Middle	TSS content	**10.1** ±1.8 (A)(d)	**12.7** ±1.0 (B)(c)	**15.1** ±0.8 (B)(b)	**17.8** ±0.9 (B)(a)
		Hue angle	**90.8** ± 2.6 (B)(a)	**88.9** ± 2.6 (BC)(ab)	**88.2** ± 3.4 (BC)(ab)	**87.1** ± 2.0 (BC)(b)
	Top	TSS content	**10.4** ±2.0 (A)(d)	**12.5** ±1.8 (B)(c)	**14.5** ±1.4 (B)(b)	**17.4** ±1.4 (B)(a)
		Hue angle	**93.4** ± 1.9 (AB)(a)	**92.2** ± 2.5 (AB)(ab)	**91.4** ± 2.2 (AB)(ab)	**90.5** ± 1.6 (A)(b)

Table 8: Effect of the maturity stage on the measured longitudinal variations in titratable acidity (in Meq.gFM^{-1}) within the fruit. Values are means ± standard deviations. Different capital and lower case letters mean that data differ significantly at P < 0.05 (according to Tukey's multiple comparison test) between the position in the fruit flesh and the stage of fruit maturity, respectively.

	Green Mature	Ripe
Bottom	**18.9** ±8.3 (A)(a)	**6.3** ±1.2 (B)(b)
Middle	**25.8** ±6.5 (A)(a)	**9.0** ±1.0 (A)(b)
Top	**26.8** ±7.4 (A)(a)	**10.3** ±0.7 (A)(b)

a) Measurements of spatial and temporal variations in fruit quality traits

For all of the fruit quality determinants studied - flesh and peel colour, titratable acidity, TSS content - varied significantly within the fruit and with the stage of maturity, regardless of the measurement method used(Table 6, Table 7, Table 8 and Figure 18). Peel colour changed significantly depending on the stage of maturity, regardless of the position of the fruit, i.e., shaded, sunny or bottom side (Table 6). Differences in peel colour were observed between the two sides of the fruit at the same stage of maturity. The hue angle of the peel on the sunny side varied between 15 and 35°, corresponding to red colours, whereas the hue angle of the peel on the shaded and the bottom sides ranged between 82 and 124°, which corresponds to yellow/orange to green. At the yellow point stage, the colour differed significantly between the bottom and the shaded sides (Table 6). In fact, loss of green colour was measured earlier on the bottom side of the fruit.

Spatial and temporal variations in the colour of the flesh were also observed (Table 7, Figure 18). The hue angle values of the flesh decreased in all parts of the fruit with increasing fruit maturity, from green-yellow to orange. The lowest hue angle values were measured in the flesh located in the lower part of the centre of the fruit, regardless of the fruit maturity stage (Figure 18). However, no significant difference was found in the colour of the flesh between the shaded and the sunny sides (Table 7). Destructive and Vis-NIR spectrophotometric measurements showed that fruit sugar contents varied depending on the stage of maturity and on the position within the fruit (Table 7 and Figure 18).

However, as previously mentioned for flesh colour, no significant difference in the destructive TSS content measurement was found between the sunny and the shaded sides

of the fruit (Table 7). Destructive measurements showed that TSS content was significantly higher in the lower part of the fruit at all stages of maturity except at the first stage, i.e., the green mature stage (Table 7). This higher but non-significant content differed statistically from Vis-NIR reflectance measurements due to the larger number of measurements (Figure 18).No significant variations were found in predicted TSS content between the inner and the outer flesh, excepted in ripe fruits (Figure 18).

Destructive measurements showed that titratable acidity decreased with advancing fruit maturity and varied depending on the position in the fruit (Table 8). In ripe fruits, the flesh located in the lower part was significantly less acidic than the flesh in the middle and the upper parts of the fruit (Table 8). Vis-NIR reflectance supported the hypothesis that titratable acidity decreased with advancing fruit maturity and confirmed the existence of a gradient of titratable acidity from the lower to the upper part of the fruit. Spectrophotometric measurements revealed that the lower part of the fruit was significantly less acidic than the middle and the upper parts of the fruit, regardless of the stage of maturity of the fruit (Figure 18). This method of measurement enabled us to establish a gradient of acidity at the green mature and turning stages (Figure 18), since the inner part was found to be more acidic than the outer part of the fruit.

Spectrophotometric measurements revealed the highest gradients in TSS content, titratable acidity, and flesh colour in green mature and turning fruits, which then decreased with fruit ripening (Figure 18).

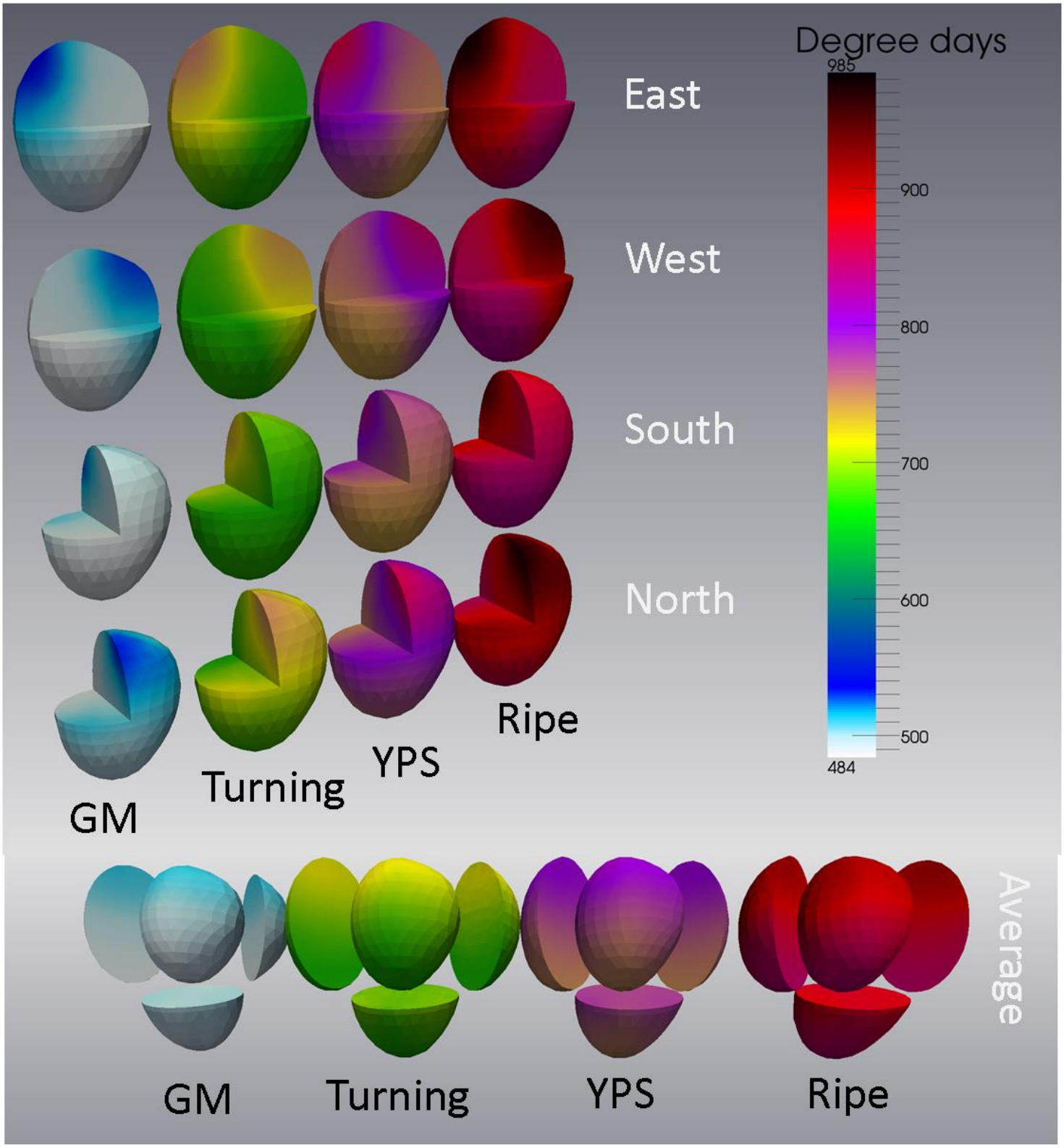

Figure 19 : Simulation of thermal time, expressed in degree days (°C.days), in mango fruits growing in the east, west, south and north parts of the canopy, and the average of these four simulations at the green mature (GM), turning, yellow point (YPS) and ripe stages.

b) The thermal time gradient and measurements of ethylene variations in mango fruits and relationship with fruit quality

Temperature modelling of a growing mango fruit revealed spatial and temporal variations in thermal time in fruits located in the east, west, north and south part of the canopy (Figure 19). The position of the fruit in the tree affected fruit temperature, as evidenced by the fact that fruits located in the north part of the canopy accumulated more degree days than the other fruits.

Irrespective of the position of the fruit and their stage of maturity, a large gradient of degree days was simulated within the fruit from the lower part of the shaded side of the fruit to the upper part of the sunny side of the fruit. The gradient of degree.days simulated in the fruit located in the east part of the canopy was 52, 103, 128 and 151 degree.days at the green mature, turning, YPS, and ripe stages, respectively.

Although model outputs revealed marked differences in temperature between the sunny and the shaded side of the fruit, no significant difference in TSS content or the colour of the flesh were established between the different sides of the fruit (Table 7).

Figure 19 simulated average thermal time gradients for fruits located in the north, south, west and east parts of the canopy. This simulation revealed that there is usually a temperature gradient from the bottom to the top of the fruit. The temperature gradient between the two fruit sides observed irrespective of the position of the fruit in the canopy, disappeared when the temperature gradients were averaged.

Regardless of the method of measurement used, the above-mentioned results showed that the lower part of the fruit had a higher TSS content, was more intensely coloured and less acidic, than the upper part of the fruit. This led us to deduce that the gradients of flesh quality traits from the bottom to the top of the fruit were the opposite of the simulated average temperature gradient.

Table 9: Effect of the maturity stage on the measured longitudinal and transversal variability of ethylene contents (in ppm). Values are the mean of measurement ± standard deviation. Different capital and small letters mean data differ significantly at P < 0.05 (according to Tukey's multiple comparison test) between the position inside the fruit and the stage of maturity, respectively.

		Green mature	Turning	YPS	Ripe
Stone	**Bottom**	0.401 ±0.171 (A)(a)	0.315 ±0.187 (A)(a)	0.292 ±0.098 (AB)(a)	0.289 ±0.207 (A)(a)
	Top	0.449 ±0.115 (A)(a)	0.322 ±0.161 (A)(a)	0.271 ±0.082 (AB)(a)	0.309 ±0.166 (A)(a)
Surface	**Bottom**	0.020 ±0.02 (B)(b)	0.102 ±0.042 (B)(b)	0.334 ±0.054 (A)(a)	0.284 ±0.171 (A)(a)
	Top	0.018 ±0.02 (B)(b)	0.075 ±0.047 (B)(b)	0.146 ±0.011 (B)(ab)	0.291 ±0.173 (A)(a)

Spatial and temporal variations in ethylene content were also measured (Table 9). The ethylene content measured at the surface of the fruit was found to significantly increase with advancing maturity, unlike in the seed, whose ethylene content remained constant. Significantly higher ethylene content was measured close to the seed than at the surface in fruits at the turning and green mature stages, whereas no difference in ethylene content was found between the bottom and the top of the fruit (Table 9). At the following maturity stage, YPS, significantly higher ethylene content was measured on the bottom than at the top of the fruit. At the final fruit maturity stage, no significant variation in ethylene content was measured between positions in the fruit.

These results showed that the maturity gradient, highlighted by the variation in ethylene content, did not match the simulated temperature gradient inside the fruit. TSS contents, acidity and flesh and peel colour gradients from the bottom to the top of the fruit were consistent with the measured gradient of maturity. Variations in ethylene content between the inner part and outer part of the fruit were in agreement with the change in flesh colour but did not explain the variation in TSS content and acidity. Our results thus show that spatial variation in fruit quality traits can only be partly attributed to the maturity variation within the fruit.

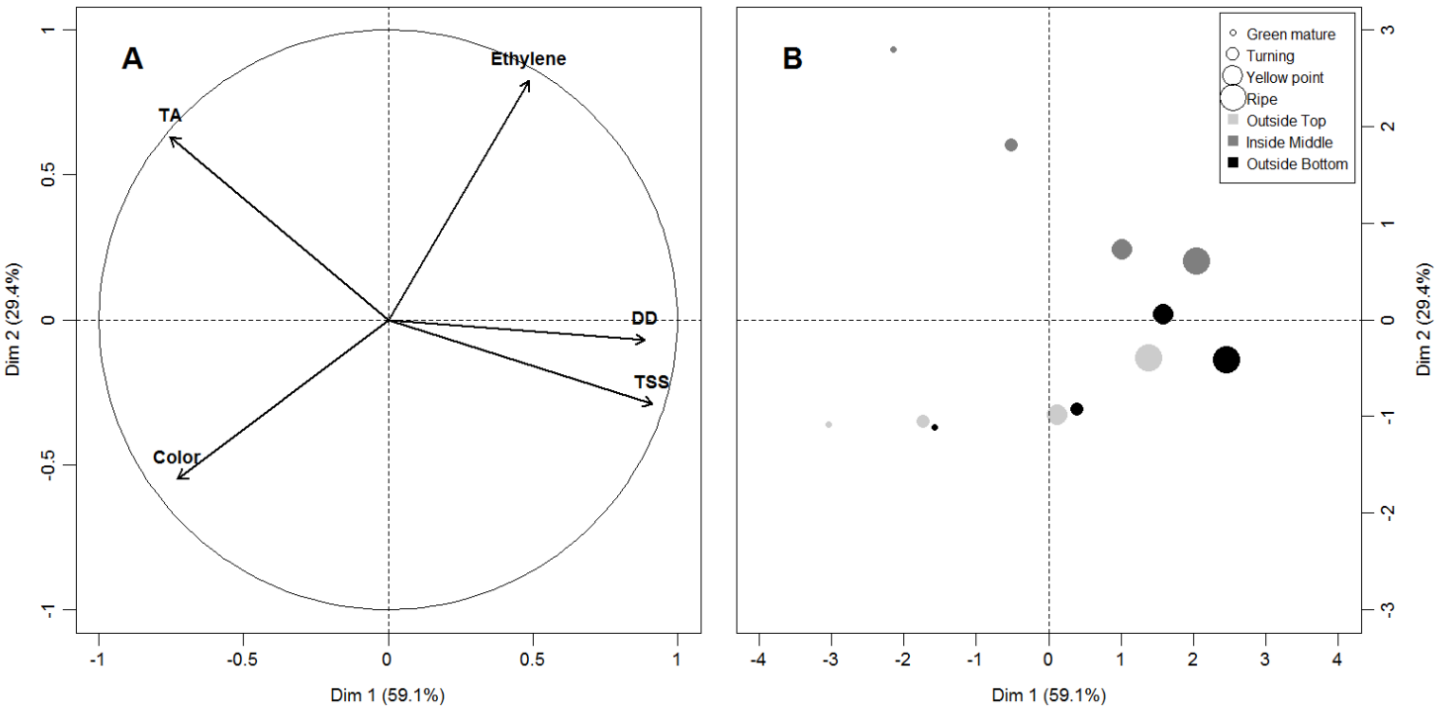

Figure 20: Principal component analysis of relationships between the spatial and temporal variations in fruit quality traits, thermal time, and ethylene content. Vectors (A), DD, TSS, TA, Colour, and Ethylene, represent thermal time, expressed in degree.days, total soluble solids content, titratable acidity, the hue angle of the flesh colour, and ethylene content, respectively. The size and colour of the dots (B) are related to the fruit maturity stage and to the position in the fruit, respectively.

We performed principal component analysis (PCA) for an overview of the relations between fruit quality traits, thermal time, and ethylene contents. About 88% of observed variability was explained by the first two components (Figure 20). Total soluble solids content (TSS), thermal time from full bloom, expressed in degree.days (DD), titratable acidity (TA), flesh colour (Colour), and ethylene content (Ethylene), contributed respectively 28%, 26%, 19%, 17%, and 8% to the first component of the PCA (PC1), (Figure 20A). The variable ethylene contributed 46% to the second component of the PCA (PC2) and the variables TA and colour also contributed but to a lesser extent TA (27%) and Colour (20%). The graph of the variables (Figure 20A) shows that TA and TSS were more correlated with DD, R= -0.66 and R=0.74, respectively, than with ethylene, R = 0.14 and R = 0.22, respectively, in contrast to Colour which was more related to Ethylene (R=-0.7) than to DD (R=-0.5).

Unlike TA and Colour, TSS and DD were positively correlated with PC1. Figure 20B shows that the maturity stages of the fruit were separated on PC1, with the green mature stage on the left and the ripe stage on the right. This confirmed previous results showing a decrease

in the hue angle of the flesh colour and in TA with advancing fruit maturity in contrast to TSS content, which increased.

Ethylene was positively correlated with PC2 (Figure 20A) which separates points corresponding to the “Inside Middle” to the “Outside Bottom” and “Outside Top” parts of the fruit at the green mature and turnings stages. This was due to the fact that higher ethylene contents were measured near the fruit seed at these particular stages.

E - Discussion

The aim of the present study was to determine the impact of temporal and spatial temperature and maturity gradients on variations in mango fruit quality.

In line with the results of previous studies on mango (Joas et al., 2012, Litz, 2009), our results showed that quality traits change considerably during fruit ripening. From the green mature to the ripe stage, sugar content increased, the colour of the flesh turned to orange, the peel lost its green colour, and acidity decreased.

Loss of the green colour of the peel, which is a sign of fruit ripening in many mango cultivars, has been only observed since the yellow point stage, despite the fact that the flesh quality traits of mango, i.e., flesh colour, sweetness and sourness had changed since the green mature stage. We therefore deduced that the loss of green peel colour occurred long after the beginning of the internal fruit maturation processes which cause changes in flesh quality. This is in agreement with several authors who considered that skin colour is not an adequate maturity index for mango since the fruit is already soft when the colour of the skin changes (Sivakumar et al., 2011, Litz, 2009).

Results of principal component analysis (Figure 20A and Figure 20B) revealed that differences in the fruit quality traits between the different fruit maturity stages were more highly correlated with variations in the thermal time than with variations in ethylene content. In addition to temporal variations, all the quality traits measured in this study varied depending on the position in the fruit, regardless of the stage of maturity of the fruit. The flesh quality trait gradients reached maximum in green mature and turning fruits and thereafter decreased as the fruit ripened.

The lower part of the fruit was found to have higher TSS content, lower acidity, a more pronounced orange flesh colour, and the green colour of the peel disappeared faster than in

the rest of the fruit. Longitudinal acidity and TSS gradients were highlighted by both destructive measurements and Vis-NIR reflectance. This confirms the robustness of the PLS models established in this study, based on reflectance spectra to predict TSS content and titratable acidity. Vis-NIR reflectance measurements made it possible to demonstrate variations in quality traits from the inner to the outer part of the fruit flesh. Regardless of the stage of fruit maturity, the inner flesh of the mango was found to have a more pronounced orange colour, which could be due to higher β-carotene content (Vasquez-Caicedo et al., 2005), the major carotenoid in mango flesh (Godoy and Rodriguez-Amaya, 1989). This result is in accordance with results of the study by Lester (2008), who reported an increase in β-carotene content from the surface to the centre of the melon mesocarp. Our results showed that the inner flesh of mango was significantly more acid at the green mature and turning maturity stages. This is in line with the accumulation of organic acids in the centre of the fruit reported by Pedreschi et al. (2009) in pear, and by Biais et al. (2010) in melon. We measured higher TSS contents in the outer part of the flesh of ripe fruit, in line with measurements made by Cieslak et al. (2013) in nectarine. However, the TSS gradient we observed is the opposite to the gradient measured by Sugiyama (1999) and Lester (2008) in melon.

A modelling approach was used to simulate spatial and temporal variations in fruit temperature (Figure 19). For the sake of simplicity, the model we previously developed (Nordey et al. (2014c) did not take the heat released by metabolic activities into account. However, it is well known that some plants are able to increase their temperature via a mitochondrial respiratory pathway that is distinct from the cytochrome chain and involves a cyanide–resistant alternative oxidase (AOX) (Wagner et al., 2008). In climacteric fruit, like mango and tomato, it has been reported that the cytochrome chain component played an important role in the climacteric burst in respiration, whereas AOX played a role in post climacteric processes (Almeida et al., 2002, Considine et al., 2001). Consequently, it can be assumed that the marked increase in respiration observed during ripening of mango does not influence temperature distribution inside the fruit.

Surprisingly, no differences were found in the TSS content and flesh colour between the sunny and the shaded side of the fruit, even though major differences in temperature were simulated. Furthermore, the colour, acidity, and TSS gradients of the flesh were the

opposite of the average temperature gradient simulated. These unexpected results were confirmed by the results of the principal component analysis (Figure 20). This analysis revealed that thermal time was not correlated with PC2 which was related to the spatial variability within the fruit. Our results thus provide several pieces of evidence that the spatial variation in flesh quality traits measured in this study cannot be attributed to variations in temperature inside the fruit.

However, the difference in exposure to sunlight was responsible for variations in the colour of the mango peel since the sunny side of the peel was redder than the shaded and the bottom parts of the fruit. This variation may be related to the accumulation of anthocyanin pigments, which are responsible for the red colour of the peel(Nordey et al., 2014a, Proctor and Creasy, 1969), and is triggered in response to high sun exposure (Steyn et al., 2002).

The lower acidity, higher TSS content, more pronounced orange colour of the flesh and the earlier appearance of the yellow peel colour in the lower part of the fruit matched the longitudinal maturity gradient revealed by the ethylene measurements. This result was also confirmed by principal component analysis (Figure 20), showing that ethylene content was the main variable contributing to the PC2. This latter separated individuals according to the three different positions they occupied along the longitudinal section of the fruit.

Higher ethylene content was measured close to the seed than at the surface of the fruits before and at the beginning of mango ripening, i.e. at green mature and turning stages. At the following maturity stage, YPS, the ethylene content of the fruit surface increased and tended to reach the same ethylene content as that measured in the tissues close to the seed, thereby reducing variations in ethylene content within the fruit. However, the increase in ethylene content was more rapid in the lower part of the fruit than in the upper, leading to a longitudinal ethylene gradient within the fruit. The difference in the rate of increase could be explained by more rapid diffusion of ethylene from the seed to the surface in the lower part of the fruit due to a shorter distance between the surface and the seed.

The ethylene measurements in this study suggest that the induction of the autocatalytic synthesis of ethylene (Génard and Gouble, 2005) first began near the seed tissues. Involvement of the seed coat or the seed in the ethylene crisis has already been suggested for several fruits including avocado (Hershkovitz et al., 2010, Hershkovitz et al., 2011) and

tomato (Zhang et al., 2009). In our study, the higher ethylene content in the centre of the fruit showed that the ripening process started near the seed. This result is in accordance with (Mitcham and McDonald, 1992), who reported that Tommy Atkins and Keitt mangoes ripened from the inside to the outside.

It is interesting to note that the longitudinal gradient in mango quality traits appeared prior to the longitudinal ethylene gradient. In fact, variations between the lower and the upper parts of the fruit in the traits describing flesh quality were measured regardless of the maturity stage of the fruit, whereas the difference in ethylene content was only observed at the yellow point maturity stage. This could be explained by a recent study by Zaharah et al. (2013) on mango, who suggested that abscisic acid was involved in the onset of the ripening, and that ethylene was only involved in later ripening stages.

We hypothesized that the inner flesh would be less acidic than the outer flesh because of the maturity gradient, but our measurements revealed the opposite. It has been reported elsewhere that the acidity gradient in fruit can be attributed to internal factors other than ethylene content. Pedreschi et al. (2009) in pear and Biais et al. (2010) in melon suggested that the variation in organic acid content from the periphery to the centre of the fruit depends on the oxygen gradients, which can lead to hypoxia in the centre of the fruit. In mango, a positive relationship has been observed between the internal CO_2 content and acidity (Baldwin et al., 1999, Carrillo-Lopez et al., 2000).

The maturity gradient we highlighted did not explain the TSS gradient measured between the inner and the outer flesh in ripe fruits. In nectarine, similar sugar and TSS gradients have been explained by the transport of water within the fruit, which is driven by the transpiration flux and the distribution of vascular bundles (Cieslak et al., 2013).

Further studies on measurements or on modelling approaches of supplementary internal factors variations such as gas (CO_2, O_2), water contents, or hormonal balances (Verboven et al., 2008, Ho et al., 2010a, Fanta et al., 2013), are required to better explain the spatial variation in quality traits in the mango fruit.

Partie II: Hétérogénéité de la qualité et de la maturité entre les mangues.

Cette partie s'intéresse à l'effet des conditions de croissance de la mangue sur sa qualité et sa maturité. Elle vise plus particulièrement à déterminer comment la variabilité des conditions de croissance au sein de l'arbre est impliquée dans les différences de calibre, de teneur en matière et de maturité des mangues à la récolte.

Un premier chapitre est dédié à l'étude des facteurs pré et post-récolte qui font varier la crise climactérique et la synthèse d'éthylène de la mangue pendant son mûrissement. Cette approche expérimentale introduit le second chapitre de cette partie qui présente l'adaptation du modèle proposé par Génard and Gouble (2005) pour simuler la synthèse d'éthylène dans la mangue. Cette approche de modélisation est utilisée pour comprendre comment les conditions de croissance et le détachement de la mangue de l'arbre affectent sa synthèse d'éthylène. Ce modèle sera également utilisé dans les chapitres suivants pour simuler l'effet des conditions de croissance de la mangue sur son mûrissement.

Le troisième chapitre est consacré à l'étude des variations des flux de xylème pendant la croissance de la mangue et à ses causes. Les résultats de cette approche expérimentale sont utilisés dans le chapitre suivant qui simule la croissance en matière fraiche des mangues en fonction de leurs conditions de croissance. Ce chapitre s'appuie sur l'adaptation du modèle de Léchaudel et al. (2007) qui simule la croissance en matière fraiche de la mangue et sur le modèle présenté précédemment (Partie I Chapitre II) qui simule l'impact des conditions climatiques sur la température et la transpiration du fruit. Le modèle présenté dans ce quatrième chapitre est ensuite couplé au modèle de synthèse d'éthylène présenté précédemment et au modèle de croissance en matière sèche de la mangue proposé par Léchaudel et al. (2005a) afin d'étudier l'effet des conditions de croissance du fruit sur son calibre, sa teneur en matière sèche et son mûrissement.

I - Factors affecting ethylene and carbon dioxide concentrations during ripening: incidence on final dry matter, total soluble solids content and acidity of mango fruit.

Objectifs :

Ce chapitre vise à étudier l'impact de facteurs pré et post-récolte sur la respiration et la synthèse d'éthylène de la mangue pendant son mûrissement ainsi que leurs effets sur sa composition, i.e. teneur en matière sèche, teneur en composés solubles et acidité. La résistance de la peau à la diffusion des gaz a également été mesurée afin de déterminer son implication dans la crise climactérique et la synthèse d'éthylène. Les résultats de cette étude seront utilisés dans le chapitre suivant qui s'intéresse à modéliser la synthèse d'éthylène dans la mangue. Il est prévu de soumettre cette étude au journal **Postharvest Biology and Technologie** avant la fin de l'année 2014.

Principaux résultats :

- La crise respiratoire, la synthèse d'éthylène et la composition de la mangue varient en fonction des conditions de croissance et de conservation.

- La résistance de la peau à la diffusion des gaz augmente considérablement après la récolte du fruit.

- Les mangues récoltées précocement synthétisent de grande quantité d'éthylène.

Factors affecting ethylene and carbon dioxide concentrations during ripening: incidence on final dry matter, total soluble solids content and acidity of mango fruit.

Thibault Nordey[1*], Mathieu Léchaudel[1], Michel Génard[2] and Jacques Joas[3]

[1]CIRAD, UPR HORTSYS, 97455 Saint-Pierre, La Réunion, France
[2]INRA, UR 1115, Plantes et Systèmes de Culture Horticoles, 84000 Avignon, France
[3]CIRAD, UMR QUALISUD, 34398 Montpellier, France

A - Introduction

Fruit ripening is an unavoidable and irreversible physiological process during which the overall fruit quality radically changes. In just a few days, fruit quality increases until it reaches its optimum and then declines until the fruit becomes inedible due to over-ripening. Stakeholders within the supply chain have to manage fruit ripening in order to provide the best fruit quality to consumers. For climacteric fruits such as bananas, mangoes and avocados, this is a real challenge because they are perishables that cause considerable economic losses (Joas et al., 2012, Lechaudel et al., 2010).

Ripening of climacteric fruits is associated with pronounced changes in fruit gas composition caused by a concomitant rise in respiration and ethylene production (Burg and Burg, 1962). The impact of fruit gas changes on ripening processes has been the focus of numerous studies. The increase in ethylene production initiates a cascade of events that lead to many interactive signaling and metabolic pathways responsible for ripening progress in climacteric fruits (Paul et al., 2012, Bapat et al., 2010), although studies on cantaloupe melon (Pech et al., 2008) and tomato (Jeffery et al., 1984) suggest that some ripening processes such as the accumulation of sugar and the degradation of organic acids are not regulated by ethylene. The involvement of the respiration rise in the ripening process is unclear. Several studies report the absence of or a reduced rise in respiration when fruits are ripened on the tree, despite a pronounced peak in ethylene production (Shellie and Saltveit, 1993, Bower et al., 2002, Saltveit, 1993). This result has been interpreted as evidence that the rise in respiration is not required for ripening (Lelièvre et al., 1997, Bower et al., 2002).

It was previously reported that several factors may induce variations in the respiratory crisis and in ethylene production, including the environment encountered by the fruit during its development (Joas et al., 2012, Bower et al., 2002), the fruit physiological age at harvest (Song and Bangerth, 1996), fruit detachment from the tree (Shellie and Saltveit, 1993, Bower et al., 2002, Saltveit, 1993) and storage conditions (Eaks, 1978, Finger et al., 1995).

Until now, it was assumed that changes in fruit gas composition have been assumed to result from changes in ethylenic and/or respiratory metabolisms. However, these changes may also be attributed to variations in fruit skin resistance to gas diffusion. This would be consistent with the numerous studies stating that report that fruit surface features such as the presence of cracks and the thickness of the cuticle and the hypodermis vary during fruit development and as a function of growing conditions (Gibert et al., 2005, Milad and Shackel, 1992, Paul et al., 2007).

For climacteric fruits, changes in fruit gas concentration cannot be separated from the ripening process. This study therefore presents an overview of pre- and post-harvest factors that lead to variations in the respiratory crisis and ethylene production, and attempts to determine their impacts on fruit composition, i.e., dry matter, total soluble solids content and acidity. Mango fruit was chosen because quality management of this fruit is a major limit to its sale (Tharanathan et al., 2006).

The first part of this study focuses on factors involved in variations in fruit gas content. In order to take an integrated approach to the factors involved in both climacteric respiration and ethylene production, we considered the impact of (i) growing conditions such as the fruit position in the canopy and the fruit carbon supply; (ii) fruit detachment from the tree, including the maturity stage at harvest; and (iii) storage conditions after harvest, i.e., relative humidity and temperature. Changes in skin resistance to gas diffusion during fruit growth and storage were measured in order to determine their involvement in fruit gas content changes. The second part of this study was dedicated to measuring and to discussing changes in fruit composition, i.e., dry matter, total soluble solids content and acidity, related to changes in fruit gas content.

B - Material and methods

1) **Fruit sampling**

The study was carried out on mangoes of the Cogshall cultivar. Fruits were grown during the 2009-2010, 2010-2011 and 2011-2012 growing seasons in the CIRAD orchard collection of Reunion Island (20°52' 48'' S, 55°31' 48" E), composed of 19-year-old trees in 2009, grafted on the 'Maison Rouge' cultivar. Trees were well irrigated, spaced 5 x 6 m apart, and were approximately 3 m high. Full flowering corresponds to the date when more than 50% of the panicles of all the trees were open. This was observed on August 18, September 1, and September 5, for the 2009-2010, 2010-2011 and 2011-2012 growth seasons, respectively.

To estimate the impact of storage temperature on the climacteric respiration of detached fruit, fruits were divided into three batches of four fruits harvested at 106 Days after Full Bloom (DAB) during the 2009-2010 growing season. The respiration rates of fruits from the first batch that were left to ripen under normal storage conditions, i.e., 20°C and 90% relative humidity, were measured daily in the morning. Fruits from the second and third batches were initially stored at 7°C and 12°C, respectively, with 90% relative humidity for 20 days, and then left to ripen under normal storage conditions, i.e., 20°C and 90% relative humidity. The respiration rates of fruits from the second and third batches were measured daily while they were stored under normal storage conditions.

To test the impact of the harvest on fruit gas concentration, non-destructive measurements of internal concentrations in ethylene (C_2H_4) and carbon dioxide (CO_2) were made on five attached fruits at 100 DAB during the 2010-2011 growing season. These fruits were then detached and their internal carbon dioxide and ethylene concentrations were measured 6 hours after they were harvested and the following days.

During the last growing season, i.e., 2011-2012, to differentiate between three growing conditions - sunny and shaded fruit with normal carbon supply and sunny fruit with low carbon supply - branches inside or outside the canopy were girdled by removing a 10-15-mm-wide band of bark and sometimes defruited and defoliated at 60 DAB to establish a fixed leaf-to-fruit ratio of either 25 leaves or 100 leaves per fruit. The 100 leaf-to-fruit ratio (L/F) corresponded to the non-limiting condition of carbohydrate supply for fruit growth (Léchaudel et al., 2005b). During this growing season, nondestructive measurements of skin

resistance to CO_2, oxygen (O_2) and C_2H_4 diffusion were made at 63, 78, 92, 113 and 125 DAB for five to six sunny attached fruits with a normal carbon supply (100 L/F).

To test whether there was skin resistance to gas diffusion changes after the harvest, four to six sunny fruits with a normal and low carbon supply were harvested at 113 DAB and left to ripen under normal storage conditions, i.e., 20°C and 90% relative humidity. The skin resistance of these fruits was measured at the green stage, two days after they were harvested, and at the ripe stage, seven days after they were harvested.

In addition, the respiration rate and the internal content in CO_2 of six other sunny fruits with normal carbon supply, harvested at 113 DAB and left to ripen under normal storage conditions, were measured daily.

At each measurement date of the skin resistance to gas diffusion of attached fruits, i.e., 63, 78, 92, 113 and 125 DAB, nine to 11 sunny fruits that were grown with a normal carbon supply were harvested and left to ripen under normal storage conditions. The respiration rates of these harvested fruits were measured daily. Ethylene concentrations were measured in these fruits one day after they were harvested, the day when the maximal respiration rate value was assessed, and two days later.

To test the impact of the fruit water losses on the climacteric respiration of mango, the respiration rates of four sunny fruits that were grown with a normal carbon supply, harvested at 92 DAB and placed in a dry atmosphere, i.e., 50% relative humidity at 20°C, were measured.

Finally, to determine changes in the gas concentration of fruits attached to the tree during their development, internal concentrations in CO_2, O_2 and C_2H_4 were nondestructively measured on four to six attached fruits undergoing the different tested growing conditions between 60 and 165 DAB.

For each harvest, regardless of the growing season, fruit quality measurements were performed on four to ten fruits just after harvest, and on four to ten other fruits at the ripe stage.

2) **Measurements of fruit gas content and emission**

Internal concentrations of CO_2, O_2 and C_2H_4 were non-destructively measured with a gas collection apparatus made with a small 30-mL water glass. A hole was made at the bottom of the glass and then closed with a septum to take the gas sample. The open side of the gas collection apparatus was held in place on the fruit surface with a ring of putty as a sealant to prevent leaks, 24 h before a gas sample was taken, so that the gas concentration in the apparatus was in equilibrium with the internal concentration of gas within the fruit at the time of measurement. Gas samples were taken by inserting a needle in the gas collection apparatus through the septum. The other extremity of the needle was inserted into a glass Venoject blood-collecting tube (Terumo Corp.; Tokyo, Japan) in which a vacuum existed. When the vacuum was broken, gas in the collector migrated to the Venoject blood-collecting tube. The Venoject tube and then the needle were removed after 2 min to equalize the pressure in the gas collection apparatus and the Venoject tube. For each gas sample measurement, fruit surface temperature was accessed using a contact thermometer. Concentrations of CO_2, O_2 and C_2H_4 inside the Venoject tube were measured by gas chromatography. An Agilent M200 apparatus (SRA, Marcy l'Etoile, France) was used to assess CO_2 and O_2 concentrations, whereas an HP 5890 Series II gas chromatograph (Hewlett-Packard, Palo Alto, CA, USA) was used for C_2H_4.

Respiration rates of detached fruits (expressed in mmol of CO_2 kg^{-1} h^{-1}) were measured daily using a closed system method. On each measuring day, fruits from each treatment were placed in individual 3-L airtight jars at 20°C. Carbon dioxide and oxygen changes inside airtight containers were measured every 20 min for 1 h by gas chromatography with an Agilent M200 apparatus (SRA, Marcy l'Etoile, France).

3) **Measurements of fruit quality, fruit carbon losses and fruit transpiration.**

Fruit quality traits were measured just after the harvest and at the ripe stage. To ensure that ripe fruits had the same physiological age for analysis, respiratory metabolism and climacteric rise were used as indicators. In line with Joas et al. (2012), it was assumed that 'Cogshall' mangoes were ripe 3 days after their respiration rates had reached their highest values. The fruit flesh was subsampled, weighed, and then dried at 75°C for 48 h. The corresponding dry weights were recorded to calculate total flesh dry weight.

The remainder of the flesh was homogenized using a Grindomix blender (Retsch, Haan, Germany), and then used to determine the Total Soluble Solids content (TSS, in °Brix) using a refractometer ATC-1E (Atago, Tokyo, Japan), and the Titratable Acidity (TA, milliequivalents of acid per 100 g of fresh matter) by titration with a 0.1N NaOH solution up to a pH 8.1 end point using an automated titrimeter (Schott, Mainz, Germany).

Fruit water losses during storage (expressed as gH_20 gMF^{-1} day^{-1}) were estimated by measuring changes in fruit fresh mass on the days following the harvest. The quantity of fruit carbon losses by respiration, expressed by mass unit (gC gMF^{-1}), from the harvest until fruits were ripe, was deduced from fruit respiration rate measurements.

4) **Estimation of fruit skin resistance to gas diffusion**

C_2H_4, O_2 and CO_2 diffusion from inside the fruits to the gas sample apparatuses sealed at their surfaces was measured to determine skin resistance of attached fruits to gas diffusion.

According to Fick's first law, diffusion of "x" gas (D_x, in mol s^{-1}) in a gas sample apparatus sealed at the fruit surface depends on the difference in gas concentrations between the inside of the fruit ($[X]_{Fruit}$, in mol m^3) and the gas sample apparatus ($[X]_{Apparatus}$, in mol m^3), the skin resistance to gas diffusion (R_x, in s m^{-1}) and the exchange surface between the fruit and the gas sample apparatus (A, in m²).

$$D_x = \frac{A}{R_x}\left([X]_{Fruit} - [X]_{Appartus}\right) \qquad \textit{Equation 20}$$

The internal gas concentration of a fruit attached to the tree is assumed to change due to daily fruit temperature variations (Nordey et al., 2014c, Ravindra and Goswami, 2008). The impact of temperature change, from T_0 (in °C) to T (in °C), on the fruit respiratory rate, RR (either in mmol CO_2 h^{-1} or in mmol O_2 h^{-1}), is commonly estimated using the Q_{10} concept (Léchaudel et al., 2005a, Ravindra and Goswami, 2008) as:

$$RR = RR_0\, Q_{10}^{\frac{T-T0}{10}} \qquad \textit{Equation 21}$$

where RR is the fruit respiratory rate at temperature T, and RR_0 is the fruit respiratory rate at temperature T_0. Q_{10} values of 1.61 and 1.67 were used for O_2 and CO_2, respectively, in line with the measurements of Ravindra and Goswami (2008).

Since temperature is assumed to affect fruit concentrations in CO_2 and O_2 rather than skin resistance to gas diffusion, it was assumed that the diffusion of CO_2 (D_{CO2}, in mol s^{-1}) and O_2

(D_{O2}, in mol s^{-1}) could be expressed as in Equation 22 and Equation 23. Details of the calculations are presented in Appendix 1.

$$D_{(CO_2)} = \frac{A}{R_{CO_2}} \times \left([CO_2]_{Fruit}\, Q_{10}^{\frac{T1-T0}{10}} - [CO_2]_{Appartus} \right) \quad \textit{Equation 22}$$

$$D_{(O_2)} = \frac{A}{R_{O_2}} \times \left([O_2]_{Air}(1 - Q_{10}^{\frac{T-T0}{10}}) + [O_2]^0_{fruit}\, Q_{10}^{\frac{T-T0}{10}} - [O_2] \right) \quad \textit{Equation 23}$$

To our knowledge, there is no equivalent of the Q_{10} concept for C_2H_4 production. For the sake of simplicity, the impact of temperature on fruit C_2H_4 concentration was not considered for the estimation of skin resistance to C_2H_4 diffusion. It was therefore assumed that diffusion of C_2H_4 from the fruit to the gas sample apparatus is described as:

$$D_{(C_2H_4)} = \frac{A}{R_{C_2H_4}} \times ([C_2H_4]_{Fruit} - [C_2H_4]) \quad \textit{Equation 24}$$

Nonlinear regression was used to determine the resistance values of the skin to CO_2, O_2 and C_2H_4 diffusion, which made it possible to describe changes in gas concentration measured in the gas sample apparatus using Equation 22, Equation 23 and Equation 24.

5) **Statistical analyses**

All statistical analyses were performed with R software (RDC Team, 2012), implemented with the agricolae package (De Mendiburu, 2012). Analysis of variance and multiple pairwise comparisons were performed to assess the effect of the maturity stage at harvest on the dry matter, the TSS content, the TA, the transpiration rate and carbon losses during ripening, for each stage of fruit sampling, i.e., at harvest and at the ripe stage. Analysis of variance was also performed to establish whether the dry matter content, the TSS content and the TA significantly changed during the fruit climacteric crisis for each maturity stage at harvest.

A pairwise comparison with a variance analysis was performed to compare resistances to gas diffusion estimated at different times of the fruit development using nonlinear regression. A Bonferonni correction was used on the p.value, expressed as:

$P.value = \frac{0.05}{number\ of\ comparisons}$ to counteract the problem of multiple comparisons.

C - Results

1) **Changes in the skin resistance to gas diffusion during fruit development and ripening**

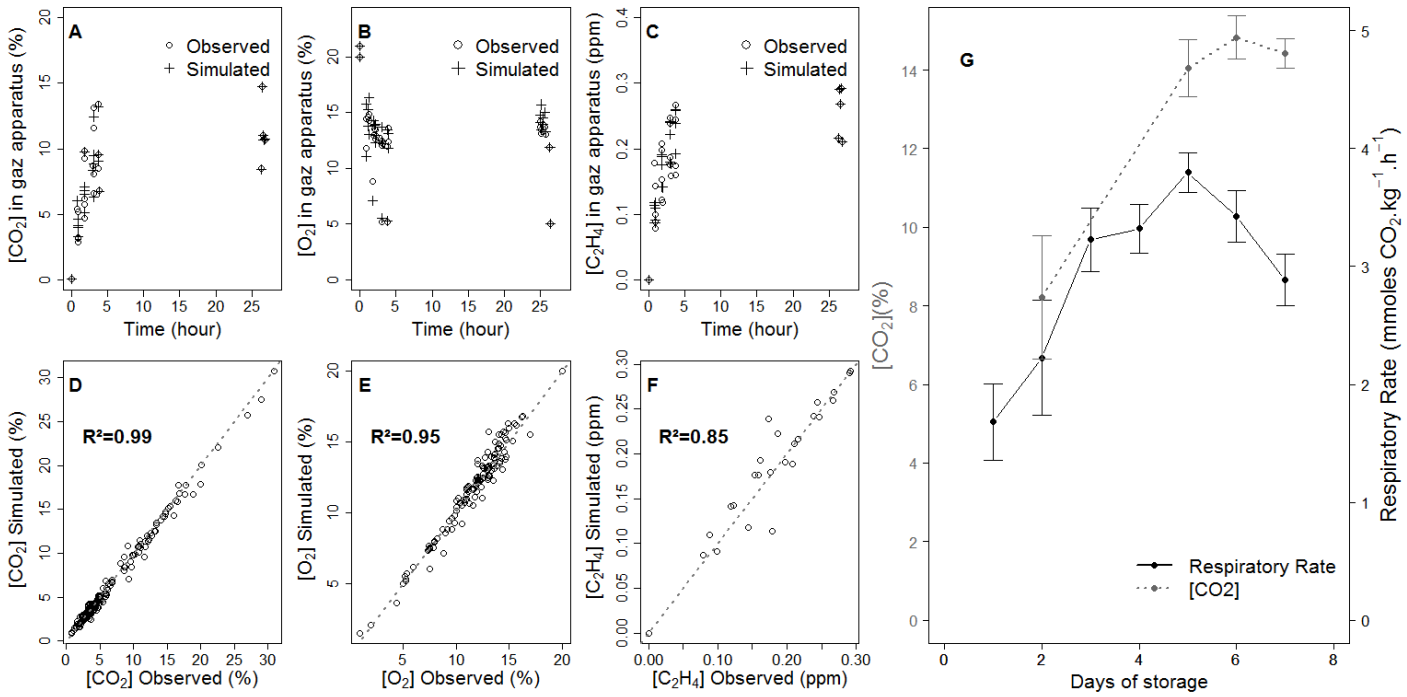

Figure 21: Observed (circle) and simulated (cross) concentrations in CO_2 (A), O_2 (B) and C_2H_4 (C) of gas sample apparatuses sealed at the surfaces of attached fruits at 113 DAB; simulated vs. measured concentrations in CO_2 (D), O_2 (E) and C_2H_4 (F) of gas sample apparatuses for all measurement dates; and measured variations in CO_2 concentration and in the respiration rate of sunny fruits with 100 leaves per fruit harvested at 113 DAB and stored under normal conditions (G). Vertical bars represent the standard deviations of measurements.

Table 10: Variations in skin resistance to CO_2 (RCO_2, in s m^{-1}) and O_2 (RO_2, in s m^{-1}) diffusion estimated with nonlinear regressions ± standard deviations, of sunny fruits attached to the tree at 78, 93, 113 and 125 days after full bloom (DAB), and of sunny fruits harvested at 113 DAB with normal and low carbon supply, i.e., 100 and 25 leaves per fruit (L/F), at the green stage and at the ripe stage.

Attached/Harvested	Maturity	L/F	RCO_2	RO_2
Attached	78 DAB	100	$1.23\ 10^5 \pm 6.16\ 10^3$ (a)	$6.5\ 10^4 \pm 3.82E\ 10^3$ (a)
Attached	93 DAB	100	$1.11\ 10^5 \pm 3.20\ 10^3$ (a)	$6.04\ 10^4 \pm 6.01\ 10^3$ (a)
Attached	113 DAB	100	$1.25\ 10^5 \pm 6.77\ 10^3$ (a)	$4.36\ 10^4 \pm 5.99\ 10^3$ (a)
Attached	125 DAB	100	$1.16\ 10^5 \pm 4.37\ 10^3$ (a)	$7.16\ 10^4 \pm 2.56\ 10^3$ (a)
Harvested	Green mature	100	$3.05\ 10^5 \pm 3.31\ 10^3$ (b)	
Harvested	Green mature	25	$3.13\ 10^5 \pm 3.31\ 10^3$ (b)	
Harvested	Ripe	100	$3.76\ 10^5 \pm 5.43\ 10^3$ (c)	$2.74\ 10^5 \pm 3.00\ 10^3$ (b)
Harvested	Ripe	25	$5.14\ 10^5 \pm 1.09\ 10^4$ (d)	$3\ 24\ 10^5 \pm 7.52\ 10^3$ (b)

Skin resistances to gas diffusion of attached and detached fruit at different times during fruit development and for different fruit load treatments are presented in Table 10. Estimated values made it possible to accurately simulate temporal changes in CO_2, O_2 and C_2H_4 concentrations in the gas sample apparatuses (Figure 21A to Figure 21F). The good adjustment between simulations and measurements (Figure 21D to Figure 21F) indicated that skin resistances to gas diffusion were well estimated. Differences in CO_2, O_2 and C_2H_4 concentrations were measured between mangoes at a similar maturity stage (Figure 21A to Figure 21C). It was assumed that these differences were related to temperature variations between mangoes. Measurements revealed that fruit surface temperatures fluctuated between 22°C and 44°C (data not shown). It was also observed that simulations for C_2H_4 were less well adjusted to measurements than simulations for CO_2 and O_2 (Figure 21D to Figure 21F). This may be due to the fact that the impact of temperature on C_2H_4 concentration in fruit was not considered, to the contrary of the impact of temperature on CO_2 and O_2 concentrations in fruit.

Skin resistance to CO_2 diffusion was higher than that estimated for O_2, regardless of the maturity stage (Table 10). Skin resistance to C_2H_4 diffusion estimated on attached fruit at 125 DAB was equal to $1.32\ 10^5 \pm 8.30\ 10^3$ s m^{-1}. Skin resistance to CO_2 and O_2 diffusion did not significantly change during fruit development on the tree but significantly increased after the harvest and during fruit storage (Table 10). Measurements revealed that the skin resistance to CO_2 diffusion increased from $1.25\ 10^5$ to $3.05\ 10^5$ s m^{-1} two days after mangoes

were harvested at 113 DAB, and reached 3.76 10^5 s m^{-1} after fruits were left to ripen for five days (Table 10). This result is illustrated in Figure 21G. This figure also shows that the decline in fruit CO_2 emissions measured five days after harvest was not related to a proportional decline in fruit CO_2 concentrations. On the basis of these measurements, it was possible to deduce that the skin resistance to CO_2 diffusion increased from 3.81 to 5.01 s m^{-1} during fruit storage. These results confirmed that the values of skin resistance to CO_2 diffusion previously estimated (Table 10) were within the correct range of magnitude.

Measurements presented in Table 10 indicated that the skin resistance to CO_2 diffusion measured in ripe detached fruits was higher for the 100 L/F treatment than for the 25 L/F treatment. Nevertheless, this difference was not measured for green mature detached fruits. In addition, no difference in skin resistance to O_2 diffusion was established between detached mangoes from different fruit load treatments.

2) Effects of pre- and post-harvest factors on fruit gas concentration.

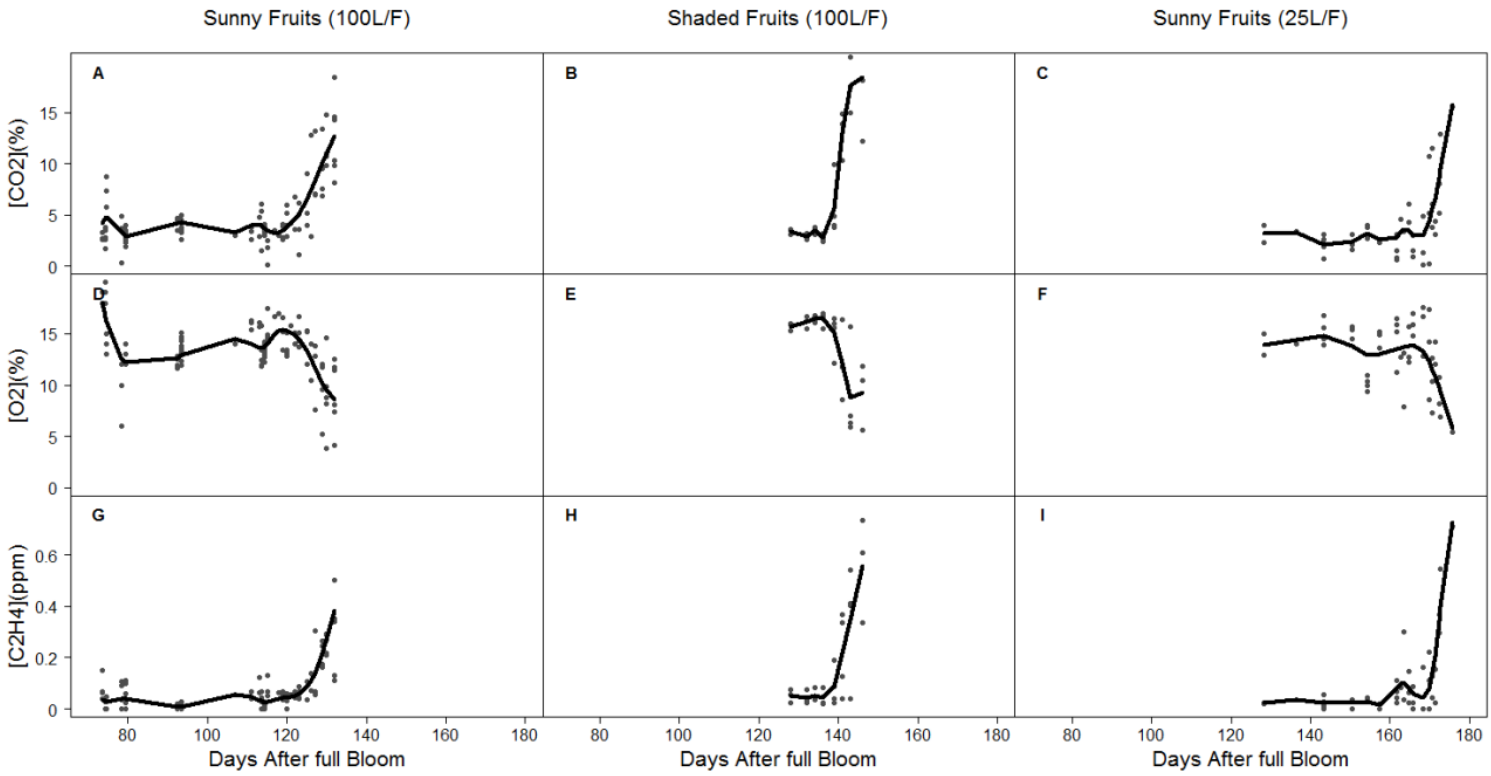

Figure 22: Seasonal variations of CO_2 (A, B and C), O_2 (D, E and F) and C_2H_4 (G, H and I) concentrations of sunny fruits with 100 leaves per fruit (L/F), shaded fruits with 100 L/F and sunny fruits with 25 L/F. Growing conditions are indicated on the graphs.

Concentrations in CO_2 and C_2H_4 of mangoes attached to the tree increased at the end of the growing season, in contrast with O_2 concentration that decreased, regardless of the growing conditions (Figure 22). Large variations in fruit gas concentrations were measured on the same measurement date and for the same growing conditions. These variations were assumed to be caused by temperature and maturity differences between fruits. The increase in ethylene concentration first began in sunny fruits, then in shaded fruits and, finally, in sunny fruits with a low carbon supply.

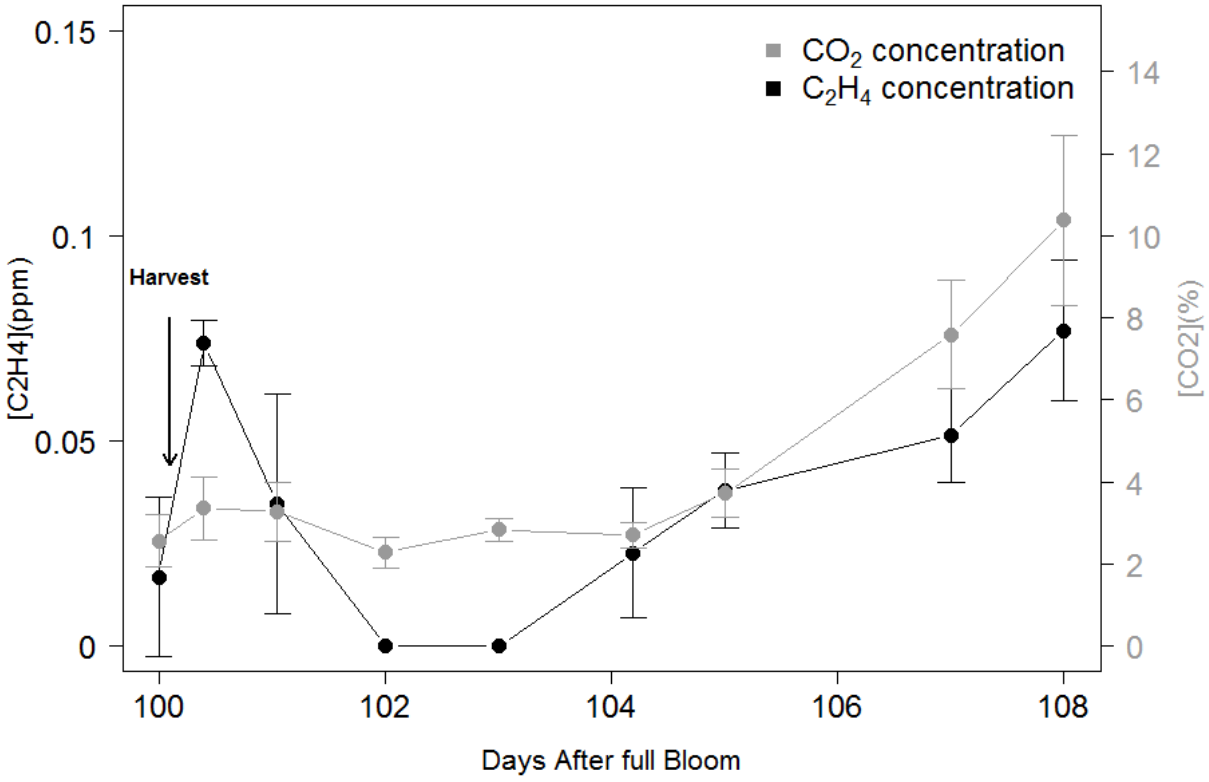

Figure 23: Changes in CO_2 (gray line, in %) and C_2H_4 (black line, in ppm) concentrations measured in fruits harvested 100 days after full bloom. Each value is the mean and vertical bars represent the standard deviations of measurements.

To study the impact of mango detachment from the tree on its gas concentration, CO_2 and C_2H_4 concentrations of mangoes were measured before and after fruits were picked at 100 DAB (Figure 23). A transitional increase in C_2H_4 and CO_2 concentrations was measured in the hours following the harvest. Two days after the harvest, no C_2H_4 was measured in fruits and CO_2 concentrations were similar to the ones measured before mangoes were harvested. The climacteric respiration and the increase in C_2H_4 concentration began approximately four days after the harvest.

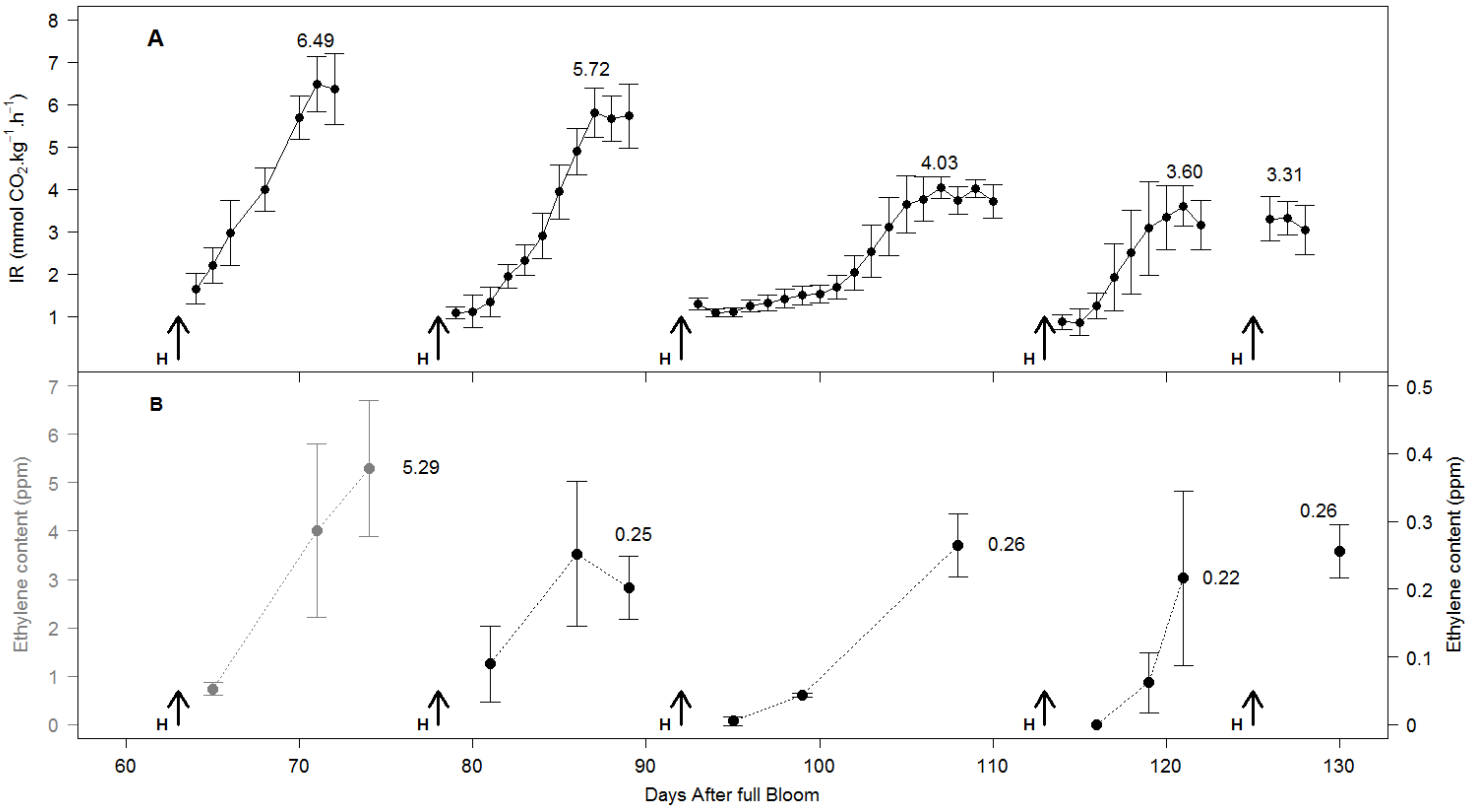

Figure 24: Changes in respiratory rates (A) and C_2H_4 concentration of harvested fruits at 63, 78, 92, 113 and 125 days after full bloom. Arrows represent harvest dates. Each value is the mean and vertical bars represent the standard deviations of measurements. Ethylene measurements of fruits harvested at 63 DAB are presented in gray and are plotted according to the left vertical axis. The ethylene measurements of fruits harvested later are presented in black and plotted according to the right vertical axis.

Changes in fruit CO_2 emission and fruit C_2H_4 concentration were measured in sunny fruits after they were harvested at 63, 78, 92, 113 and 125 DAB (Figure 24). Results showed that fruit detachment promoted changes in fruit gas concentration, regardless of the harvest date. The pre-climacteric phase varied between 0 and 8 days, depending on the harvest date. No pre-climacteric period was measured in fruits harvested at 63 and 78 DAB since their respiration rates and their ethylene concentrations increased just after the harvest. The pre-climacteric period of fruits harvested at 92 and 113 DAB was approximately 8 and 2 days, respectively (Figure 24A). For the last harvest, i.e., at 125 DAB, no pre-climacteric period was observed since ethylene concentration and respiratory rates had increased prior to the time that fruits were picked. The intensity of the climacteric crisis and of the autocatalytic ethylene production considerably changed between harvests.

The highest respiration rates measured during the storage of fruits harvested at 63, 78, 92, 113 and 125 DAB were 6.48, 5.59, 4.03, 3.6 and 3.31 mmol CO_2 Kg^{-1} h^{-1}, respectively. Ethylene concentration of fruits harvested at 63 DAB reached 5.29 ppm in an average of two days after the maximal respiration rate value was assessed (Figure 24B). This was 20 times higher than the ethylene concentrations measured in fruits from the following harvests at the same stage of the respiratory crisis.

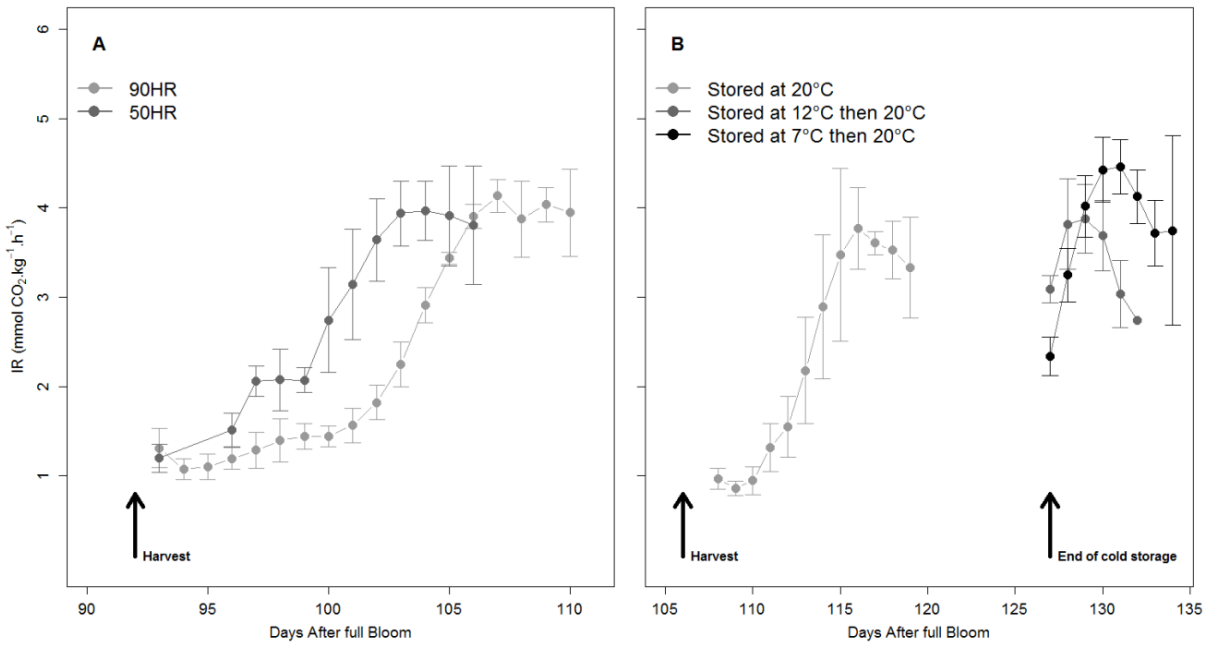

Figure 25: Changes in respiratory rates of fruits harvested at 92 days after full bloom and stored at 20°C and 90% or 50% relative humidity (RH) (A), and of fruits harvested at 106 days after full bloom and stored either at 20°C, 12°C and 7°C (B). Each value is the mean and vertical bars represent the standard deviations of measurements. Storage conditions are indicated on graphs. Arrows represent harvest dates and the date of the end of cold storage.

Storage conditions also had an impact on gas concentration in detached fruits. The pre-climacteric period of fruits stored in a dry atmosphere was shorter than that of mangoes stored under normal conditions of relative humidity (Figure 25A). Reduction of the storage temperature from 20°C to 12°C or 7°C increased the time of the pre-climacteric phase from 3 to 21 days (Figure 25B). The intensity of the climacteric respiration of fruits stored at 7°C was slightly higher than that of fruits stored at 20°C and 12°C (Figure 25B).

3) **Changes in fruit composition during ripening in relation to harvest dates and post-harvest treatments.**

Table 11: Variations in fruit dry matter, total soluble solids content and titratable acidity at harvest and at the ripe stage according to harvest dates and storage conditions.

Year	Harvest (DAB)	Treatment	Shelf life (days)	Harvest mass (10^{-3} Kg)	% Dry matter		°Brix		Titratable Acidity (Meq.gMF-1)		Carbon losses ($gC.gMF^{-1}$)	Water losses ($gH2O.gMF^{-1}.day^{-1}$)
					Harvest	Ripe	Harvest	Ripe	Harvest	Ripe		
2011	63	Stored 90% RH, 20°C	11 (cd)	66.9 (f)	11.5 (d)	9.7 *(d)* *	9.15 (d)	9.2 *(e)*	50.8 (a)	13.9 *(ab)* ***	1.05 (b)	1.6E-02 (b)
2011	78	Stored 90% RH, 20°C	11 (cd)	174.3 (ef)	13.1 (cd)	10.0 *(d)* ***	9.9 (d)	9.3 *(e)*	53.1 (a)	17.8 *(a)* ***	1.03 (b)	1.1E-02 (c)
2011	92	Stored 90% RH, 20°C	15.5 (b)	337.1 (bcd)	14.6 (c)	11.6 *(cd)* ***	11.4 (c)	10.6 *(e)*	52.5 (a)	5.182 *(cd)* ***	1.07 (ab)	8.2E-03 (cd)
2011		Stored 50% RH, 20°C	12.5 (c)			12.8 *(cd)* ***		11.44 *(de)*		12.8 *(ab)* ***	0.84 (c)	2.2E-02 (a)
2009	107	Stored 90% RH, 20°C	12.25 (c)	387.9 (b)	14.0 (c)	13.6 *(bcd)*	6.9 (e)	13.8 *(d)* ***	32.7 (c)	3.6 *(d)* ***		
2009		Stored 90% RH, 12°C	24.6 (a)			13.9 *(bcd)*		13.8 *(d)* ***		3.2 *(d)* ***		
2009		Stored 90% RH, 7°C	26 (a)			10.6 *(cd)*		13.1 *(d)* ***		3.2 *(d)* ***		
2011	113	Stored 90% RH, 20°C	9.0 (d)	366.8 (bc)	18.5 (ab)	17.8 *(ab)*	13.9 (b)	16.26 *(bc)* ***	42.7 (b)	5.43 *(cd)* ***	0.63 (d)	5.2E-03 (e)
2011	125	Stored 90% RH, 20°C	2.7 (e)	564.4 (a)	20.6 (a)	20.4 *(a)*	16.1 (a)	18.8 *(a)***	22.4 (d)	5.68 *(cd)* ***	0.28 (e)	6.8E-03 (de)

Table 11 presents measurements of fruit composition at harvest and at the ripe stage for different harvest dates and storages conditions. Fruit fresh mass increased from 66.9 g to 564 g between the first and the last harvest. Fruit composition at harvest considerably changed during the growing season. The pulp dry matter content increased from 11.5 to 20.6%, the TSS content increased from 9.15 to 16.1 °Brix, and the Titratable Acidity (TA) decreased from 50.8 to 22.4 Meq gMF^{-1}. Measurements indicated that the amounts of carbon and water lost by mangoes when they ripening changed between harvest dates and storage conditions. Fruit water losses decreased from 1.6 10^{-2} to 6.8 10^{-3} gH_2O $gMF^{-1}day^{-1}$ between the first and the last harvest. Fruits stored in a dry atmosphere, i.e., at 50% RH, lost 2.6 times as much water as fruits stored under normal conditions, i.e., at 90% RH (Table 11). The amount of carbon lost by respiration during fruit ripening was related to the length and the intensity of the climacteric crisis. Fruits harvested at 63 and 78 DAB lost more carbon per mass unit than fruits harvested at 113 DAB due to the fact that their climacteric respiration was higher (Figure 24A). Fruits harvested at 92 DAB and stored under dry conditions lost less carbon than fruits harvested at the same date and stored at 90% RH in normal conditions because their climacteric crisis was shorter. The dry matter content of fruits harvested at 63, 78 and 92 DAB significantly decreased after the climacteric crisis, contrary to fruits harvested later (Table 11). It was also observed that the TSS content of

early harvested fruits did not change after the climacteric crisis, whereas the ones of late harvested mangoes increased. However, measurements revealed that the TA significantly decreased after the climacteric crisis in all of the mangoes (Table 11).

D - Discussion

1) **Impact of pre- and post-harvest factors on ethylene concentration and climacteric respiration**

The first goal of this study was to establish how pre- and post-harvest factors lead to variations in the fruit climacteric crisis and ethylene concentration. Results indicated that C_2H_4 and CO_2 concentrations increased in the last stages of attached fruit development, regardless of the growing conditions. These results are consistent with the previous studies of Andrews (1995) on tomato and Hadfield et al. (1995) on melon, which reported that attached fruits undergo an increase in C_2H_4 production and the climacteric respiratory during ripening. However, they contradict studies on purple passion fruit (Shiomi et al., 1996), tomato (Saltveit, 1993) and melon (Bower et al., 2002), which reported the absence or the reduction of the climacteric respiratory rate during the ripening of attached fruit.

Gas concentration in mangoes changed with fruit load and sun exposure treatments. This result was in line with the previous study of Génard and Gouble (2005) on peach that reported that C_2H_4 production depends on temperature and on the increase in fruit dry mass. As previously reported on purple passion fruit (Shiomi et al., 1996) and on apple (Lin and Walsh, 2008), detachment of mango speeds up fruit ripening. Measurements of C_2H_4 and CO_2 concentrations just after the harvest indicated that fruit detachment triggered a transitional increase in fruit respiration and in C_2H_4 production. This was consistent with previous studies that reported that higher respiration rates and C_2H_4 contents are measured in plant tissues in response to wounding (Morgan and Drew, 1997, Fonseca et al., 2002). Wounding of figs is therefore used to induce C_2H_4 stress and to promote fruit ripening (Saltveit, 1999). A delay of several days was observed between the C_2H_4 burst and the autocatalytic C_2H_4 production. This is consistent with the study of Agar et al. (1999), indicating that the delay between exogenous treatment with C_2H_4 and the increase in C_2H_4 content in pears may be several days. Further studies should examine how fruit detachment affects the biosynthetic pathway of C_2H_4.

Our results indicated that changes in fruit gas concentration in detached fruit depends on the harvest date, in line with a previous study on apple (Song and Bangerth, 1996). Higher respiratory rates and higher ethylene concentrations were measured in early harvested fruits, i.e., at 63 and 78 DAB. These results contradict the results of Song and Bangerth (1996) who reported that early harvested apples had reduced respiration rates and ethylene production, but they were in line with those of Mercado-Silva et al. (1998) who showed that guavas harvested early in the season produced more ethylene.

In line with previous studies (Eaks, 1978, Paull, 1999), a decrease in storage temperature was found to delay the climacteric crisis in detached fruit. This result was consistent with our measurements on attached fruits, showing that the increase in CO_2 and C_2H_4 concentrations began earlier in warmer fruits, i.e., sunny fruits (Léchaudel et al., 2012). Our results indicated that changes in fruit gas concentration were also modulated by relative humidity during storage. This was consistent with previous studies on banana (Finger et al., 1995) and avocado (Adato and Gazit, 1974) that reported that the onset of the climacteric crisis was related to fruit water losses by transpiration. As suggested by Barry and Giovannoni (2007), it can be hypothesized that the cessation of water input to the fruit induced by its detachment may trigger changes in fruit gas concentration. This would explain the faster ripening of detached fruit. This assumption is moreover supported by the study of Nakano et al. (2003) who reported that C_2H_4 synthesis in persimmon fruit tissues is modulated by water loss. The effect of water loss on C_2H_4 synthesis would explain the higher C_2H_4 concentration measured in small fruits harvested at 63 DAB that had lost more water per mass unit during storage (Figure 24, Table 11).

Our results provide evidence that changes in fruit gas concentration are not explained by changes in respiratory and ethylenic metabolism alone since changes in fruit resistance to gas diffusion were measured. In line with a previous study on banana (Banks, 1985), our results showed that skin resistance to CO_2 diffusion increases after harvest. This may be related to changes in wax composition, as reported for apple during storage (Veraverbeke et al., 2001), and/or to fruit withering after harvest that reduces fruit porosity. Changes in skin resistance to gas diffusion affect fruit gas concentration (Génard and Gouble, 2005). Consequently, the increase in skin resistance to gas diffusion measured in mangoes after harvest may therefore be involved in the faster ripening of detached fruit.

2) **Effect of gas content on changes in fruit composition**

The second goal of this work was to establish the impact of gas concentration changes on fruit composition. Mango composition at harvest and at the ripe stage was found to vary with the maturity stage at harvest and storage conditions. In line with a previous study on mango (Joas et al., 2012), results indicated that late harvested fruits had higher dry matter contents, higher Total Soluble Solid contents (TSS), and were less acidic. In contrast to late harvested fruits, no change in the TSS content was observed in early harvested fruits after ripening. This result suggested that soluble sugar synthesis did not or only partially occurred during the climacteric period of early harvested fruits. This result confirmed current knowledge that there is a developmental point where the fruit acquires the ability to ripen (McAtee et al., 2013). Results suggested that a fruit's capacity to ripen is not related to its ability to synthesize ethylene alone since higher C_2H_4 concentrations were measured in early harvest fruits. This is in line with current knowledge that physiological processes linked to fruit ripening are also regulated by abscisic acid (McAtee et al., 2013, Pech et al., 2008). Contrary to the TSS content, the TA was found to decline after the climacteric crisis in all mangoes, regardless of the maturity stage. Since organic acids are a substrate of fruit respiration (Etienne et al., 2002, Lobit et al., 2003), it can be hypothesized that the climacteric crisis is involved in the decline in the TA during mango ripening. This would explain the higher respiration rates measured in early harvested fruit that exhibited higher titratable acidity. The involvement of organic acid in climacteric respiration has not yet been clearly established; consequently, further studies are required to validate this assumption.

II - Growing conditions and fruit detachment impacts on ethylene production: a modeling approach.

Objectifs :

L'analyse expérimentale présentée dans le chapitre précédent a mis en évidence que la synthèse d'éthylène dans la mangue varie en fonction des conditions de croissance et est impactée par le détachement du fruit de l'arbre. Il est proposé dans ce chapitre d'utiliser une approche de modélisation pour étudier de quelle manière ces facteurs sont impliqués dans la production d'éthylène dans la mangue. Pour se faire, le modèle proposé par Génard and Gouble (2005) a été adapté à la mangue et couplé au modèle simulant l'impact des conditions climatiques sur la température du fruit (Partie I chapitre II). Le modèle présenté dans cette étude sera par la suite utilisé dans le chapitre IV de cette partie pour simuler le mûrissement de la mangue.

Principaux résultats :

- Le modèle développé permet de simuler les différences de concentration d'éthylène mesurées entre les mangues selon leur condition de croissance.

- Les différences de concentration d'éthylène entre les mangues dans l'arbre s'expliquent en grande partie par les différences d'accumulation de matière sèche et dans une moindre mesure par les différences de température.

- L'augmentation de la résistance de la peau à la diffusion des gaz explique en partie le mûrissement plus rapide des fruits détachés.

- De prochaines études sont nécessaires pour mieux simuler la synthèse autocatalytique de l'éthylène et l'impact du bilan hydrique du fruit sur cette dernière.

Growing conditions and fruit detachment impacts on ethylene production: a modeling approach

A - Introduction

Substantial changes in fruit quality are observed during ripening. In few days, fruit quality increases until reaching its optimum and then declines until the fruit becomes inedible due to senescence. It is so essential for fruit suppliers to manage fruit ripening in order to provide the best fruit quality to consumers. Differences in quality and post-harvest behaviour of fruits are explained partly by variations in maturity stage at harvest (Joas et al., 2012, Lebrun et al., 2008, Urbano Bron et al., 2004). A part of these variations Joas et al. (2012)is believed to be related to fruit position in the tree. Mangoes (Hofman et al., 1995) and peaches (Bonora et al., 2013) on the top of the canopy ripe faster than the ones located under the canopy. Faster ripening of well exposed fruits may be caused by higher temperatures. Several studies on mango (Léchaudel et al., 2012), apple (Saudreau et al., 2011), and avocado (Woolf et al., 1999) have indeed reported large differences in temperatures between fruits according to their positions in the tree. Studies of Léchaudel and Joas (2006) on mango and Souty et al. (1999) on peach indicate that differences in maturity between fruits may be also related to differences in fruit carbon supplies.

Ripening is accelerated by fruit detachment from the tree. In a previous study (chapter *I - I.I -)* it has been suggested that the faster ripening of detached mangoes may be caused by the cessation of water influx to the fruit, the increase in skin resistance to gas diffusion measured after the harvest, and the burst of ethylene production caused by fruit detachment. Ethylene is a phytohormone which is considered to have a major role in ripening process of climacteric fruits such as mango, tomato, banana and melon (Bapat et al., 2010), although some ripening processes such as sugar accumulation and organic acids degradation have been reported to be ethylene independent (Pech et al., 2008, Jeffery et al., 1984). It is assumed that ripening differences between mangoes may be caused by variations in ethylene production of fruits. The ethylene pathway is well known (Adams and Yang, 1977) and it has been modelled by Génard and Gouble (2005) to simulate ethylene emission of peach. It is proposed to couple this model adapted to mango to the one we

developed in previous study (Nordey et al., 2014c) that simulate the spatial and temporal variations of mango fruit temperature during its development within the canopy.

First, the goodness of model simulations was tested on contrasted fruit growing conditions such as sun exposures and carbon supplies. Then in a second time the developed model was used to establish causes of ripening variations observed between attached and detached fruits.

B - Material and methods

1) **Model presentation**

a) Governing Equations

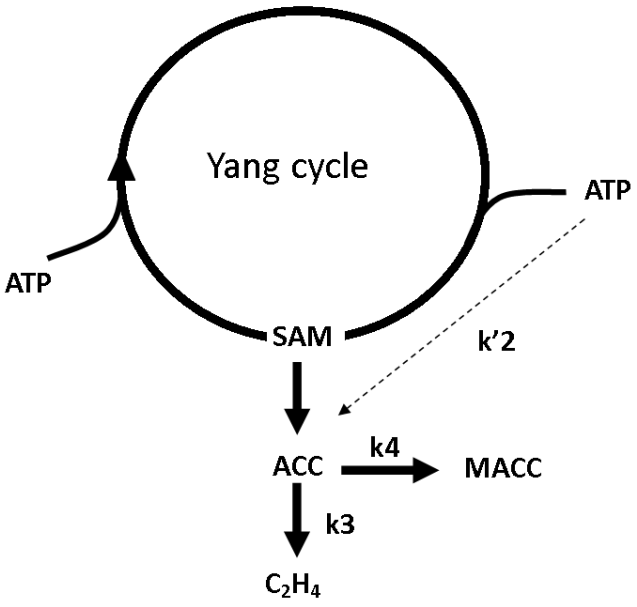

Figure 26: Schematic representation of the Yang cycle and SAM-C2H4 pathway adapted from Génard and Gouble (2005). The metabolites considered are ATP, SAM, MACC and C_2H_4. Chains of reaction are represented as simple reactions. The ki are rate constants of the reactions.

Synthesis of ethylene (C_2H_4) in mango fruit was simulated by adapting the model proposed by Génard and Gouble (2005) on peach. This model is based on chemical reactions of the Yang cycle and the S-adenosylmethionine (SAM) pathway (Figure 26). As shown by Figure 26, variations in the C_2H_4 concentration (in mol m^{-3}) depend on the balance between - its synthesis, regulated by the activity of the 1-aminocyclopropane-1-carboxylic acid (ACC)

oxidase (k_3, in h^{-1}) and by the ACC concentration, - its diffusion to the external atmosphere ($F_{C_2H_4}$, in mol h^{-1}) and - its dilution caused by changes in fruit water volume ($\frac{dV}{dt}$, in m^3 h^{-1}):

$$\frac{d[C_2H_4]}{dt} = k_3 \times [ACC] - \frac{F_{C_2H_4}}{V} - \frac{[C_2H_4]}{V}\frac{dV}{dt} \quad \textit{Equation 25}$$

The diffusion of C_2H_4 from the fruit inside to the external atmosphere is described in the model by Fick's first law for flat surface. Considering that the C_2H_4 concentration in the ambient atmosphere is nil, C_2H_4 diffusion is calculated using Equation 26, where $\rho_{C_2H_4}$ (m h^{-1}) is the apparent skin conductance to C_2H_4 diffusion and A is the skin area (m^2).

$$F_{C_2H_4} = \rho_{C_2H_4} \times A \times [C_2H_4] \quad \textit{Equation 26}$$

The ACC concentration (mol m^{-3}) depends on the quantity of ACC per fruit and on the dilution by fruit water. The variation in the quantity of ACC in the fruit is function of the balance between - its synthesis, depending on the concentration in SAM and on the activity of ACC synthase, - its degradation in C_2H_4, regulated by the activity of the ACC oxidase and - its conjugation with malonate to form malonyl-ACC (MACC) catalysed by the ACC N-malonyltransferase (k_4, in h^{-1}). Assuming the Yang cycle at steady state, the rate of synthesis of ACC from SAM is proportional to the concentration in ATP. As proposed by Génard and Gouble (2005) it is considered that ACC synthesis depends on the ATP concentration and on the activity of ACC synthase (k'_2, in h^{-1}):

$$\frac{d[ACC]}{dt} = k'_2[ATP] - k_3[ACC] - k_4[ACC] - \frac{[ACC]}{V} - \frac{[ACC]}{V}\frac{dV}{dt} \quad \textit{Equation 27}$$

The variation in MACC concentration depends on the conjugation of ACC, related to the activity of k_4, and on the dilution of MACC by fruit water:

$$\frac{d[MACC]}{dt} = k_4[ACC] - \frac{[MACC]}{V}\frac{dV}{dt} \quad \textit{Equation 28}$$

The ATP concentration in the fruit results from the balance between ATP production during the respiration process and consumption for energy requiring processes with a rate constant λ (h^{-1}), and from dilution due to fruit growth. One mole of CO_2 produced by respiration (re_{CO2}, in mol h^{-1}) is assumed to be coupled to the production of 5 moles of ATP (Cannell and Thornley, 2000). It is therefore assumed that the ATP concentration can be approximated as:

$$[ATP] = \frac{5re_{CO_2}}{\lambda V + \frac{dV}{dt}}$$ *Equation 29*

Equation 29 means that the ATP concentration depends on the fruit respiration, i.e. re_{CO2}, which was determined considering the respiration of growth and maintenance. The effect of temperature on the maintenance respiration was estimated using the Q_{10} concept. The fruit respiration in terms of CO_2 production (mol h^{-1}) is then calculated as:

$$re_{CO_2} = q_g \frac{dM_{dry}}{dt} + q_m M_{dry} Q_{10}^{\frac{T-20}{10}}$$ *Equation 30*

Where M_{dry} (g) is the fruit dry mass, q_g (mol g^{-1}) the growth respiration coefficient, q_m (mol g^{-1} h^{-1}) is the maintenance respiration coefficient at 20°C, Q_{10} is the temperature ratio of maintenance respiration, and T (°C) is the fruit temperature. The fruit temperature was obtained from the physical model developed by Nordey et al. (2014c) on mango. This model simulates spatial and temporal variation of fruit temperature by calculating energy exchanges by convection, radiation and transpiration between the fruit and its environment. The respired oxygen is calculated from the CO_2 produced by respiration using the respiratory quotient (RQ) concept:

$$re_{O_2} = \frac{re_{CO_2}}{RQ}$$ *Equation 31*

The oxygen (O_2) and carbon dioxide (CO_2) concentrations were calculated assuming they are under steady state conditions, i.e. respiration rates for O_2 (re_{O2}) and CO_2 (re_{CO2}) are equal to the fluxes of these gases through the skin to the external atmosphere. The gas diffusion to the external atmosphere can be described by Fick's first law:

$$[CO_2] = CO_2^{Air} + \frac{R_{CO_2} \times re_{CO_2}}{A}$$

$$[O_2] = O_2^{Air} + \frac{R_{O_2} \times re_{O_2}}{A}$$ *Equation 32*

Where R_{CO2} (h m^{-1}) and R_{O2} (h m^{-1}) are resistances to diffusion of CO_2 and O_2, respectively. The air CO_2 and O_2 concentrations (in mol m^{-3}) were calculated from the percentages of CO_2 and O_2 in the air using the ideal-gas equation.

b) Enzyme regulations

In lines with Génard and Gouble (2005), it has been considered that the activity of ACC N-malonyltransferase, i.e. k_4, was invariant although k_4 is developmentally regulated (Arshad

and Frankenberger Jr, 2002). Both ACCs and ACCo are encoded by multigene families and are regulated by several regulating factors, including C_2H_4 (Lelièvre et al., 1997). The effect of C_2H_4 on the activity of ACCs and ACCo was considered to be proportional to its concentration, for the sake of simplicity. Activity of ACCo is also regulated by the content in oxygen since it is a cosubstrate and inhibited by carbon dioxide (Rothan and Nicolas, 1994). To describe the effect of oxygen and carbon dioxyde on the activity of ACCo a generalized form of the Michaelis-Menten equation was used.

$$k_2' = ks\sqrt{[C_2H_4]}$$

$$k_3 = ko\frac{[O_2]}{(K_{O2} + [O_2])(1 + \frac{[CO_2]}{KCO_2}} \times \sqrt{[C_2H_4]} \qquad \textit{Equation 33}$$

c) Input data and initial conditions

Climatic data used as input by the model, such as air temperature, global radiation, air humidity and wind speed, were measured at one-minute intervals and averaged and stored every hour on a data logger (Model 21 X, Campbell Scientific Ltd, Logan, UT, USA) during the 2011-2012 growing season. Direct and diffuse global radiations were estimated by using the model developed by Maxwell E.L. (1987). The sun's course was determined using the solar position algorithm (SPA) developed by Reda and Andreas (2004). The model also requires changes in the physical and thermal properties and in the growth rate of the fruit during its development as input data which were taken from our previous study (Nordey et al., 2014c). Fruit temperature depends on its position within the tree (Saudreau et al., 2009). So to take this variability into account, temperature of fruits located on the east west, north and south sides of the canopy were simulated, and an average of these temperatures was considered. It was assumed that one side of each fruit was directly exposed to the sun (sunny side) and that the opposite side received 20% of the sunlight (shaded side), in line with the measurements made in the same previous study (Nordey et al., 2014c).

In lines with the model proposed by Génard and Gouble (2005) initial values of 5 10^{-4}, 10^{-5} and 10^{-6} mol m^{-3} were chosen for the internal concentrations of MACC, ACC and C_2H_4, respectively.

d) Model parameterization and validation

Parameters used in model simulating ethylene production are summarized in Table 12. Values of ACCo and ACCs parameters were determined by model calibration using nonlinear regression whereas the others model parameters where taken from the initial model (Génard and Gouble, 2005) and from literature on mango. The model was calibrated and validated on mango cv. "Cogshall". Measurements of changes in C_2H_4 concentration during the growth period of sunny fruits with a non-restrictive carbon supply, i.e. 100 leaves by fruit (L/F) (Léchaudel and Joas, 2006), were used to calibrate the model. The model validation was achieved by comparing ethylene concentrations measured in shaded fruit with 100 L/F and sunny fruit with 25 L/F to model simulations.

Table 12: Parameters of the ethylene model.

Parameters	Abbreviation	Value model on peach (Génard and Gouble, 2005)	Present study	References
Growth respiration coefficient	q_g	0.025 ($mol.g^{-1}$)	0.04 ($mol.g^{-1}$)	(Léchaudel et al., 2005a)
Maintenance respiration coefficient	q_m	12 10^{-5} ($mol.g^{-1}.h^{-1}$)	7.8 10^{-5} ($mol.g^{-1}.h^{-1}$)	(Léchaudel et al., 2005a)
Temperature ratio of maintenance coefficient	Q_{10}	2	1.61	(Ravindra and Goswami, 2008)
Respiratory quotient	RQ	0.834	0.834	(Génard and Gouble, 2005)
ATP parameter	λ	500 (h^{-1})	500 (h^{-1})	(Génard and Gouble, 2005)
MACC parameter	k_4	0.001 (h^{-1})	0.001 (h^{-1})	Model calibration
ACCs parameter	k_s	0.778 (h^{-1})	5.8 10^{-3} (h^{-1})	Model calibration
ACCo parameter	k_o	0.268 (h^{-1})	9.15 10^{-3} (h^{-1})	Model calibration
Michaelis constant involved in effect of O_2 on ACCo	k_{O2}	0.55 (mol m^{-3})	0.55 (mol m^{-3})	(Génard and Gouble, 2005)
Michaelis constant involved in effect of CO_2 on ACCo	k_{CO2}	3.37 (mol m^{-3})	3.37 (mol m^{-3})	(Génard and Gouble, 2005)
Skin resistance to diffusion of O_2	R_{O2}	120 (h m^{-1})	9.9 10^2 (h m^{-1})	Part II chapter I
Skin resistance to diffusion of CO_2	R_{CO2}	80 (h m^{-1})	1.9 10^3 (h m^{-1})	Part II chapter I
Skin permeability to C_2H_4 diffusion	ρC_2H_4	2.10^{-3} (m h^{-1})	4.5 10^{-4} (m h^{-1})	Part II chapter I

2) **Model simulations to evaluate the impact of fruit detachment on C_2H_4 production**

Model has been used to establish whether - the cessation of water and carbon incomes to the fruit, - the increase in skin resistance to gas diffusion and -the burst of ethylene production caused by fruit detachment are involved in changes in C_2H_4 production. These three processes were considered and model simulations were compared to ethylene measurements on fruits harvested at different dates, i.e. at 63, 78, 92, 113 and 125 days after full bloom (DAB). In the first model simulation, the cessation of water and carbon incomes to the fruit caused by the fruit harvest were considered in the model. Then, in the second simulation the increase in skin resistance to gas diffusion after the harvest was considered in addition to previous factors. The increase in skin resistance to CO_2 diffusion after the harvest was estimated from our previous study on mango (Part II chapter I). It has been assumed that skin resistances to C_2H_4 and O_2 diffusion increased by 2.8 times after the harvest as measured for CO_2 in this study. In the last simulation, the tree processes, i.e. cessation of carbon and water incomes, increase in skin resistance to gas diffusion and the ethylene burst after the harvest, were considered in the model. The ethylene burst after the harvest was simulated by increasing the fruit ethylene content to 3.1 10^{-6} mol m^{-3} during 12 hours , in lines with our precedent study (Part II chapter I).

3) **Plant material and experimental design**

Measurements were achieved during the 2011-2012 production season on 20-year-old mango trees grafted on a 'Maison Rouge' cultivar in the CIRAD orchard in Reunion Island (20°52' 48'' S, 55°31' 48" E). The trees were well irrigated, spaced 5 x 6 m apart, and were approximately 3 m tall at the time of the study. Two treatments of sun exposure were considered, sunny and shaded fruits, as well as two treatments of fruit load, 25 and 100 leaves to fruit ratio (L/F). Thus, three growing conditions were tested: sunny fruit with 100 L/F, shaded fruit with 100 L/F and sunny fruit with 25 L/F. Sunny fruits were chosen outside of the canopy contrary to shaded fruit which were chosen under the canopy. Leaf to fruit ratio treatments were established by girdling branches and sometimes defruiting and defoliating. Branches were girdled by removing a 10-15 mm wide strip of bark. Fruit enlargement in dry mass and in fresh mass was determined on the basis of the increase in fruit height using empirical relationships established by Léchaudel et al. (2007).

At 63, 78, 92, 113 and 125 DAB, sunny fruits with 100 L/F were harvested and let to ripen in normal storage condition, i.e. 20°C and 90% of air moisture. Ethylene concentrations in these fruits were measured one day after they were harvested, the day when the maximal respiration rate value was assessed and two days after.

4) **Gas measurements**

Fruit internal concentrations in CO_2, O_2 and C_2H_4 were measured on attached fruits to the tree non-destructively with a gas collection apparatus made with a small water glass of 30 mL, as presented by Nordey et al. (2014b). A hole has been made at the bottom of the glass and then closed with a septum to take the gas sample. The open side of the gas collection apparatus was held in place on the fruit surface with a ring of putty as a sealant to prevent leaks, 24h before a gas sample was taken, so that the gas concentration in the apparatus was in equilibrium with the internal concentration of gas within the fruit at the time of measurement. Gas samples were taken by inserting a needle in the gas collection apparatus through the septum. The other extremity of the needle was inserted into a glass Venoject blood-collecting tube (Terumo Corp., Tokyo, Japan) in which there was a vacuum. The vacuum being broken, gas in the collector migrated to the Venoject blood-collecting tube. After 2 min, to equalize pressures in the gas collection apparatus and the Venoject tube, the needle and the Venoject tube were removed. Carbon dioxide, oxygen and ethylene concentrations inside the Venoject tube were measured by gas chromatography.

C - Results

1) **Changes in fruit fresh mass and temperature according to growing conditions.**

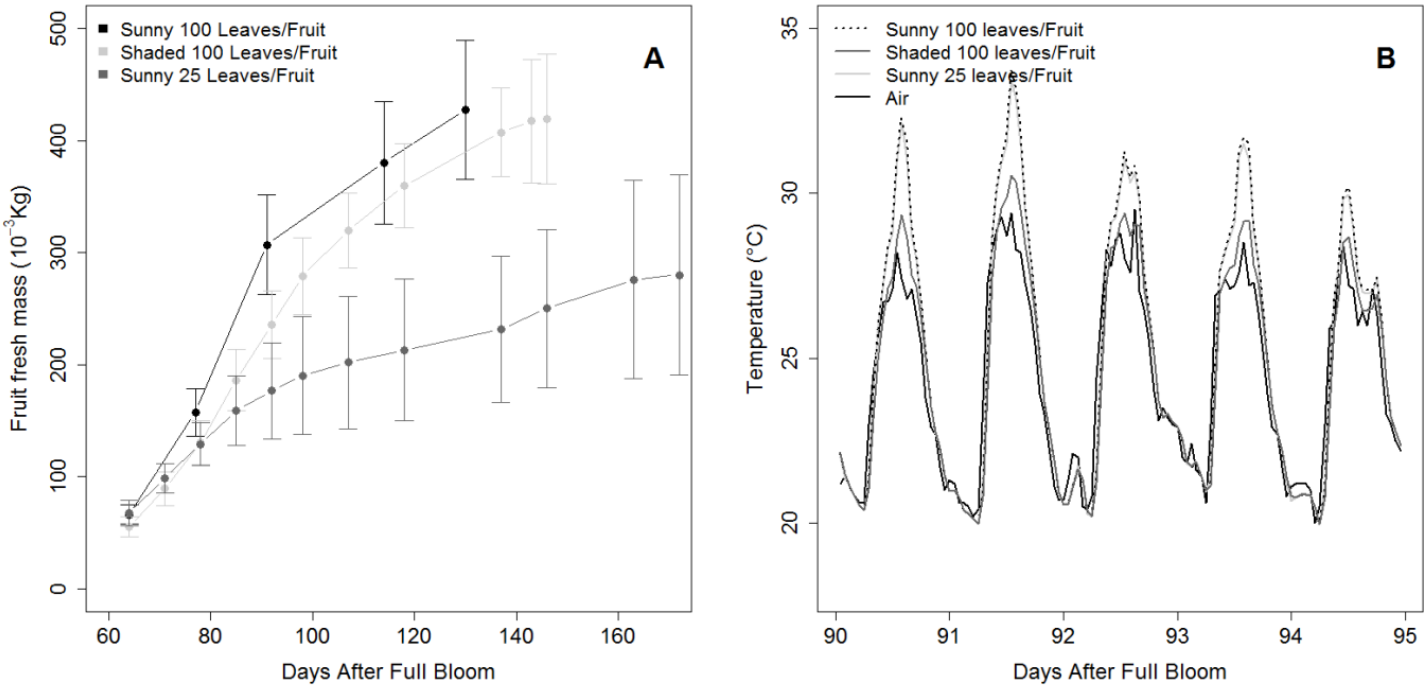

Figure 27: Seasonal variations in mango fruit fresh mass (A) and temperature simulated (B) according to growing conditions. Vertical bars represent standard deviation of measurements. Growing conditions are indicated on the graphs.

Reduction of the fruit carbon supply affects fruit fresh mass enlargement (Figure 27A). Sunny fruits with 25 L/F reached in average 280 g at the end of the growing season against 419 g for shaded fruits with 100 L/F and 427 g for sunny fruits with 100 L/F. Although slight differences in the final fresh masses were measured between sunny and shaded fruits it was noticed that sunny fruits growth faster (Figure 27A). Air temperature was lower than the fruit temperature average during daytime, whatever growing conditions. Simulations indicated that sunny fruits were warmer than shaded ones during daytime but no temperature difference was simulated at night time (Figure 27B). The maximal difference in average temperature simulated between sunny and shaded fruits through the growth season was 8°C. However, the temperature average of sunny fruits through the growing period was only 0.6°C higher than the one of shaded fruits. Temperature average simulated for sunny fruits with 25 L/F was similar to one simulated for sunny fruits with 100 L/F.

2) **Model adjustments and simulations of the impact of growing conditions**

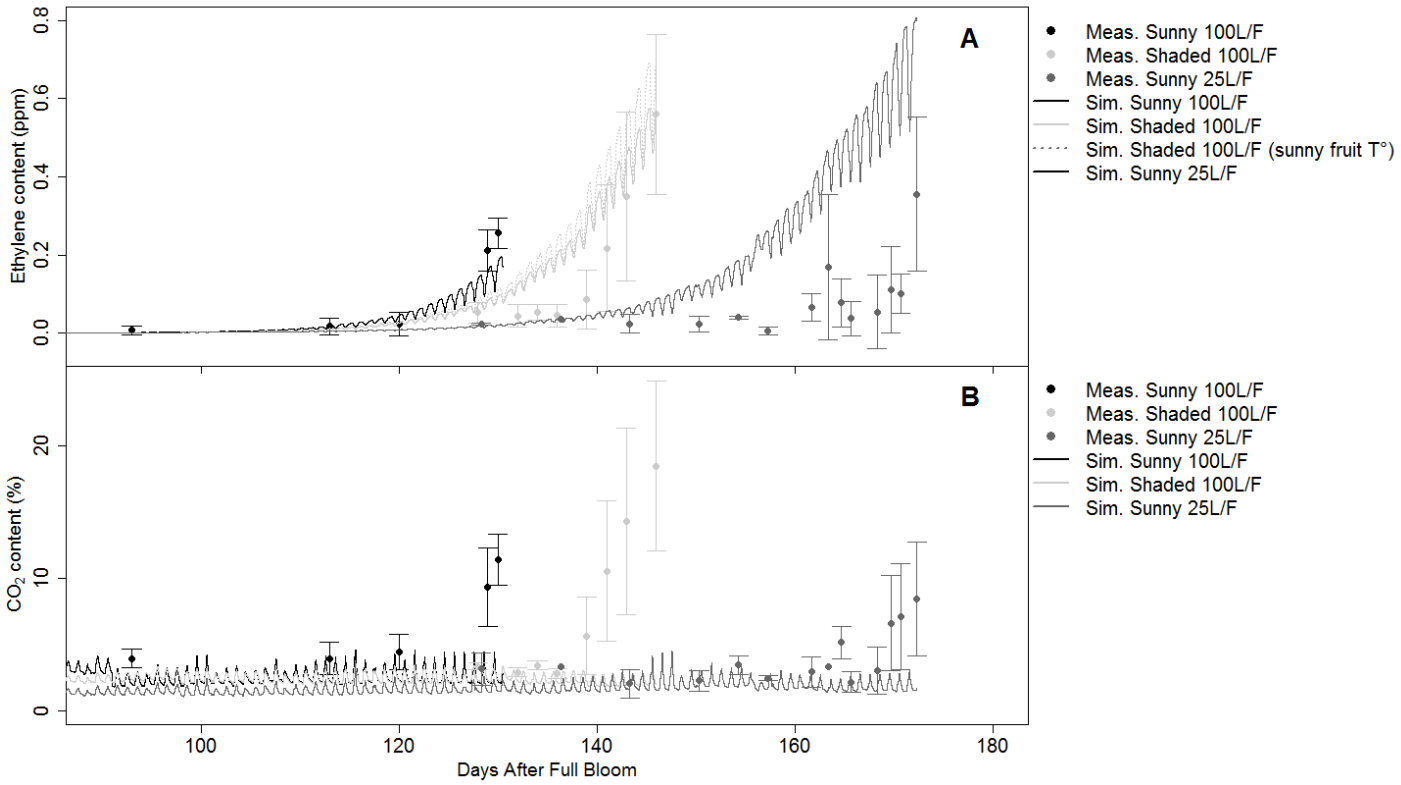

Figure 28: Observed (points) and simulated (lines) C_2H_4 (A) and CO_2 (B) concentrations in fruits according to growing conditions. Vertical bars represent standard deviation of measurements. Dotted grey line represents the C_2H_4 concentration simulated considering the growth rate of a shaded fruit and the temperature of a sunny one.

Figure 28 compares C_2H_4 and CO_2 concentrations simulated in mangoes for the different growing conditions to measurements. The model simulated quite well changes in C_2H_4 concentrations of sunny fruit with 100 L/F. However, cross validation indicated that model did not succeed to reproduce correctly the increase in C_2H_4 concentration measured in shaded fruits and sunny fruits with 25 L/F (Figure 28A). In lines with measurements the model simulated that C_2H_4 concentration increase firstly in sunny fruits, secondly in shaded ones and then in sunny ones 25 L/F. This indicated that model was able to simulate the impact of growing conditions on ethylene synthesis.

To establish whether differences in C_2H_4 concentration measured between shaded and sunny fruit were caused by differences in temperature; the ethylene production of a fruit with the growth rate of a shaded fruit and the temperature of a sunny fruit, was simulated (Figure 28A). Results of this simulation were slightly different to those obtained for a shaded

fruit (Figure 28A). This indicated that differences in ethylene concentrations measured between shaded and sunny fruits were caused by differences in fruit growth rate rather than differences in temperature.

Figure 28B indicates that the model simulated correctly CO_2 concentrations in mangoes during the pre-climacteric phase, whatever growing conditions. Model succeeds to simulate higher CO_2 concentrations measured in sunny fruits. However, the large increase in CO_2 concentration measured during the climacteric phase was not simulated by the model, whatever the growing conditions.

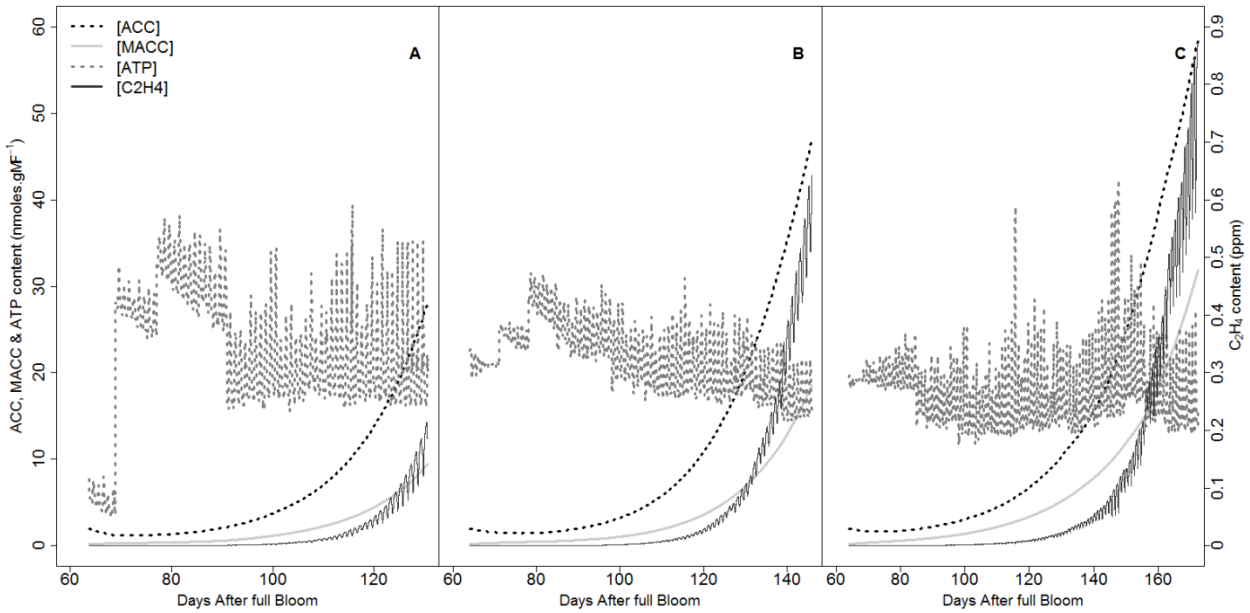

Figure 29: Seasonal variations of ATP, ACC, MACC and C2H4 concentrations, in sunny fruits with 100 leaves by fruit (A), in shaded fruit with 100 leaves by fruit (B) and in sunny fruit with 25 leaves by fruit (C), simulated by the model.

Figure 29 shows changes in ACC, MACC, ATP and C_2H_4 concentrations simulated in sunny fruits with 100 L/F (Figure 29A), in shaded ones with 100 L/F (Figure 29B) and in sunny ones with 25 L/F (Figure 29C). Changes in ATP concentration were related to the daily and seasonal variations of fruit respiration simulated (Figure 28B). Lower ATP concentrations were simulated for sunny fruits with low carbon supply, i.e. 25 L/F. A progressive increase in ACC, MACC and C_2H_4 concentrations were simulated during the season, regardless of growing conditions. The large increase in C_2H_4 concentration simulated at the end of fruit development was preceded by a large increase in the concentration of ACC, whatever growing conditions.

3) **Effect of fruit detachment on ethylene production**

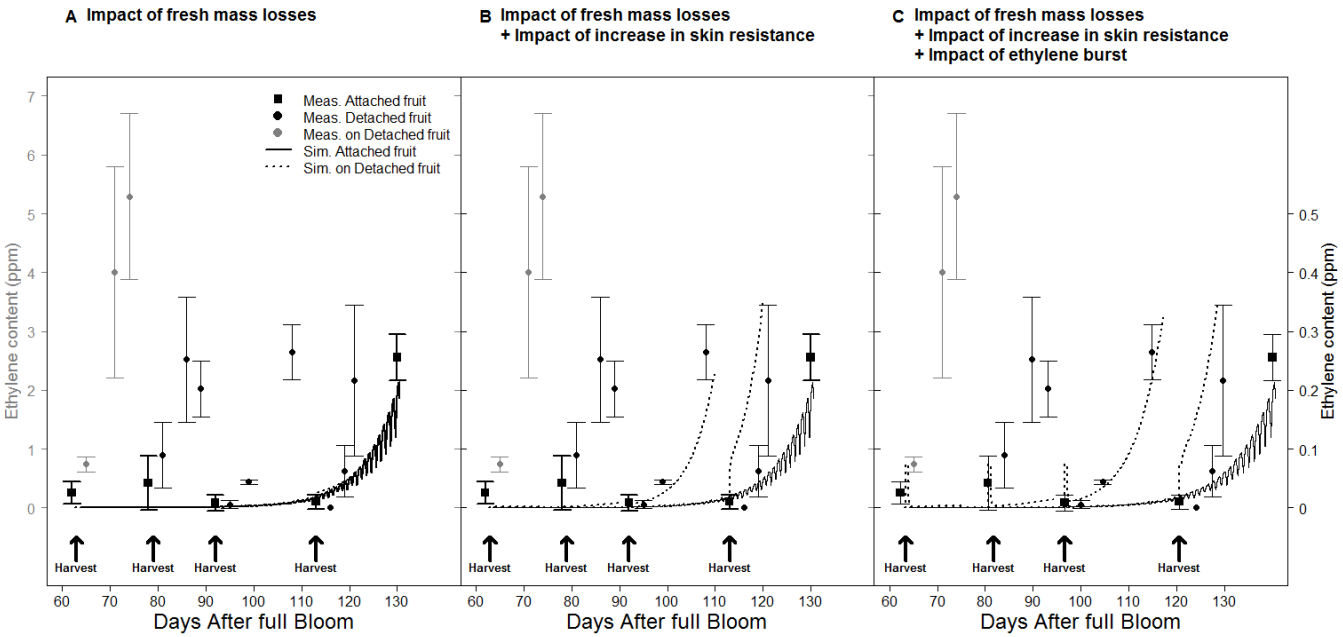

Figure 30: Observed (points) and simulated (lines) C2H4 concentrations in fruits harvested at 63, 78, 92, 113 and 125 days after full bloom by taking changes in fruit water losses into account (A), by taking changes in fruit water losses and the increase in skin resistance to gas diffusion into account (B) and by taking changes in fruit water losses, the increase in skin resistance to gas diffusion and the ethylene burst caused by fruit detachment into account (C). Vertical bars represent standard deviation of measurements.

Figure 30 presents changes in C_2H_4 concentration measured in fruit harvested at 63, 79, 92 and 113 days after full bloom. Results indicated that fruit detachment promoted the increase in C_2H_4 concentration, regardless of harvest date. Time before the autocatalytique C_2H_4 production varied between harvest dates. It was noticed that ethylene concentration in fruit harvested early in the season (grey color) was more than twenty time higher than the one measured in late harvested fruits (black color).

The model was used to determine how fruit detachment and maturity stage at harvest impact ethylene synthesis. It was hypothesized that fruit harvest impacts ethylene synthesis by, decreasing fruit water volume, increasing skin resistance to gas diffusion, and causing a burst of ethylene.

In the first case the model simulated ethylene concentrations in fruits harvested at 63, 78, 92 and 113 DAB, by taking the decrease in fruit volume due to water losses into account (Figure 30A). No difference in ethylene concentration was simulated by the model between

attached and detached mangoes. This indicated that fruit volume decrease was not involved in the faster ethylene production of detached fruit. In the second case, the model simulated ethylene concentration of detached fruits taking the decrease in fruit volume into account as well as the increase in skin resistance to gas diffusion (Figure 30 B). In this situation, model simulates an increase in the ethylene concentration of fruits days following their harvest, in lines with measurements. However, the increase in ethylene content measured in early harvested fruits was not simulated by the model (Figure 30 B). In the last situation (Figure 30 C), the model simulated ethylene content of detached fruits, taking the decrease in fruit fresh mass, the increase in skin resistance to gas diffusion and the ethylene burst caused by fruit detachment into account. Model simulations indicated that the ethylene burst caused by fruit detachment accelerated the autocatalytique ethylene production in harvested fruits. However, the model did not succeed to simulate the increase in ethylene concentration measured in early harvested fruit regardless of tested assumptions.

D - Discussion

1) **Model use, limit and improvement**

It has been assumed that differences in ripening between fruits within the tree (Bonora et al., 2013, Hofman et al., 1995) and between attached and detached fruits come from changes in ethylene concentrations. To determine how fruit detachment and growing conditions affect ethylene production in mango, the model we previously developed in order to simulate fruit temperature (Nordey et al., 2014c) has been coupled to the model ETHY (Génard and Gouble, 2005) that modelled ethylene pathway in fruit.

In lines with measurements, simulations showed that ethylene concentration increased first in sunny fruits, then in shaded fruits and lastly in sunny fruits with a restrictive carbon supply. These results indicate that model is able to simulate qualitatively the impact of growing conditions on ethylene synthesis in mango. Nevertheless, the model did not reproduce quantitatively the ethylene production kinetic in fruits grown in limiting conditions. The increase in ethylene concentration simulated by the model was not as sudden as the one measured. This suggests that the developed model did not simulate correctly the autocatalytic effect of ethylene on its own biosynthetic pathways (Bapat et al., 2010). In lines with measurements of previous studies (Léchaudel and Joas, 2006, Tovar et

al., 2001, Joas et al., 2012, Wang and Camp, 2000), the model simulated the accumulation of the ethylene precursor, i.e. ACC, during mango fruit development (Léchaudel and Joas, 2006, Tovar et al., 2001, Joas et al., 2012, Wang and Camp, 2000). Comparison of concentrations of compounds of the ethylene biosynthetic pathways, i.e. ACC and MACC, simulated by the model to those reported in the literature is not obvious due to the large differences between authors. It was reported that ACC concentration of unstressed mango during ripening fluctuate either, between 0 and 25 nmoles gFM^{-1}(Tovar et al., 2001), 1.2 10^{-3} and 1.4 10^{-3} nmoles gFM^{-1} (Joas et al., 2012), or between 5 10^{-2} and 4.5 10^{-1} nmoles gFM^{-1} (Léchaudel and Joas, 2006) or between 5 10^{-3} and 8 10^{-2} nmoles gFM^{-1} (Wang et al., 2009); whereas MACC content was reported to vary between 3.9 10^{-3} and 4.1 10^{-3} nmoles gFM^{-1} (Joas et al., 2012) and between 2 10^{-1} and 1 nmoles gFM^{-1} (Léchaudel and Joas, 2006). The large differences between authors may be attributed to different assay protocols.

Model simulated that the ACC concentration increase by 1.6 times during the last week of mango development contrary to Léchaudel and Joas (2006) measurements that showed that it increase by 4 time. It can be then supposed that the model misestimates the ethylene production due to the misestimation of the ACC concentration. This may come from inaccurate estimations of the activity of the ACC synthase or/and of the ATP content. The model analysis proposed by Génard and Gouble (2005) showed that ethylene synthesis is greatly sensitive to ATP concentration that vary with fruit respiration. Figure 28B indicates that the model did not simulate the large increase in fruit respiration rate measured. It can be so supposed that the model accuracy could be improved by simulating the fruit climacteric respiration. However, this hypothesis would require further studies since there is a debate in the literature concerning the effect of the respiratory climacteric on the ATP supply (Perotti et al., 2014). The plant mitochondrial electron transport chain contains a cyanide and antimycin-resistant alternative oxidase (AOX) that catalyses the reduction of oxygen to water without realizing H^+ in the cytosol, dissipating therefore the redox potential energy instead to promote ATP synthesis as in the cytochrome pathway respiration (Almeida et al., 2002, Perotti et al., 2014). In mango and tomato fruit, it has been reported that the cytochrome chain component plays a main role in the climacteric burst of respiration and AOX takes parts in post climacteric process (Almeida et al., 2002, Considine et al., 2001). Studies on apple report conversely results since climacteric burst was

associated with an enhanced capacity of the alternative path-enzyme but not of the cytochrome pathway (Duque and Arrabaça, 1999).

ATP concentrations may also vary during the fruit development and ripening due to changes in process requiring energy activity which has been considered as constant in the model. Consequently, further works should measure variations in the ATP concentration during fruit development and ripening in order to estimate whether the autocatalytic ethylene production is caused by the increase in ATP concentration.

2) **Growing conditions and fruit detachment impacts on ethylene synthesis**

In the second part of this work, the developed model has been used to study how growing conditions and fruit detachment impact ethylene concentration. Simulations indicated that differences in ethylene concentrations between sunny and shaded fruits and between fruit load treatments were explained by differences in fruit growth rate rather than differences in fruit temperature. This comes from the fact that slight differences in fruit temperature average were simulated between growing conditions. These results confirm those of Saudreau et al. (2009) on apple, showing slight differences in temperature average between fruits in the tree and our previous results (Nordey et al., 2014c) indicating that temperature average did not change with fruit size.

One of assumptions we tested through the model was that the ethylene production in detached fruits is increased by the decrease in fruit volume. Our simulations indicated that the decline in volume of detached fruits did not increase the ethylene production. This indicated that the impact of water losses on mango ripening is not related to the decrease in fruit volume. Study of Nakano et al. (2003) on persimmon fruit indicated that water losses active the transcription of a gene encoding for ACC synthase (DK-ACS2) and thereby modulate ethylene production. Further studies should determine how fruit water losses impact the activity of enzymes involved in the ethylene biosynthetic pathway in order to better simulate their impact on mango ripening.

Our results showed that the increase in the skin resistance to gas diffusion after harvest increased the ethylene concentration of late harvested fruits. These results support suggestion of Paul et al. (2012) that changes in the skin resistance to gas diffusion contribute to fruit ripening.

Further investigations are required to confirm this assumption since it is has been assumed that the increase in skin resistance to C_2H_4 and O_2 diffusion after harvest was proportional to the one measured for CO_2 in a previous study (Chapter I.I -).

The developed model indicated that ethylene burst at the harvest increased ethylene concentration of late harvested fruits. These results indicated that the injury applied to fruits by harvest is involved in the faster ripening of detached fruits.

No one of the assumptions we tested has explained the ethylene production in early harvested fruits. This indicated that the regulation of ethylene synthesis in early harvested fruits is different to the one of late harvested fruits. This would explain differences in ethylene concentration measured between harvests. Thus, further studies are required to understand how the ethylene biosynthetic pathway is regulated at the beginning of fruit growth.

III - Decline in xylem flow to mango fruit at the end of its development is related to apparition of embolism in fruit pedicel.

Objectifs :

L'approche expérimentale proposée dans ce chapitre vise à mesurer les variations des entrées d'eau dans le fruit par le xylème et les changements de conductivité hydraulique des vaisseaux du xylème pendant le développement de la mangue. Cette étude s'intéresse plus particulièrement à l'impact de l'embolie sur la conductivité hydraulique des vaisseaux du xylème dans le pédoncule. Les résultats de cette étude sont utilisés dans le chapitre IV de cette partie pour simuler la croissance en matière fraiche de la mangue. Il est prévu de soumettre cette étude dans le journal **Functional Plant Physiology** avant la fin de l'année 2014.

Principaux résultats :

- Les flux de xylème diminuent à la fin du développement de la mangue.

- La conductivité hydraulique des vaisseaux du xylème diminue à la fin du développement de la mangue du fait de l'apparition d'embolie.

- La diminution du potentiel hydrique de la mangue à la fin de son développement augmente le gradient de potentiel hydrique entre la mangue et la tige.

- L'embolisation des vaisseaux du xylème est liée au potentiel hydrique du fruit.

Decline in xylem flow to mango fruit at the end of its development is related to apparition of embolism in fruit pedicel.

Thibault Nordey[1*], Mathieu Léchaudel[1] and Michel Génard[2]

[1]CIRAD, UPR HORTSYS, 97455 Saint-Pierre, La Réunion, France

[2]INRA, UR 1115, Plantes et Systèmes de Culture Horticoles, 84000 Avignon, France

A - Abstract

The decline in xylem flow during the late growth stage in most fruits may be due either to a decrease in the water potential gradient between the stem bearing the fruit and the fruit tissues and/or to a decrease in the hydraulic conductivity of xylem vessels. In this study, we analyzed changes in xylem flows to the mango fruit during its development to identify the sources of variation by measuring changes in the water potential gradient and in the hydraulic properties of the fruit pedicel. The variations in xylem and transpiration flows were estimated at several stages of mango fruit development from daily changes in fresh mass of detached and girdled fruits. The water potential gradient was estimated by monitoring the diurnal water potential in the stem and fruit. The hydraulic properties of the fruit pedicel were estimated using a flow meter.

Results indicated that xylem flow increased in the early stages of fruit development and decreased in the late stage. Variations in xylem flow were related to the decrease in the hydraulic conductivity of xylem vessels but not to a decrease in the water potential gradient. Hydraulic conductivity of the fruit pedicel decreased during late growth due to embolism caused by a decrease in the fruit water potential.

Xylem impairment in the late stage of growth was assumed to be caused by a decrease in the hydraulic conductivity of the pedicel xylem network due to apparition of embolism. Further studies should establish whether hydraulic conductivity of other parts of the xylem hydraulic network between the fruit and the stem than pedicel change during the growth season.

B - Introduction

Increase in fruit fresh mass results in a balance between the supply or backflow of water through vascular tissues and the water losses by transpiration. In many fruits, including tomato (Ho et al., 1987), kiwifruit (Morandi et al., 2010), apple (Lang and Ryan, 1994, Dražeta et al., 2004), and grape (Greenspan et al., 1994), the amount of water flowing to the fruit via the xylem decreases in late growth stages thus affecting fruit growth (Morandi et al., 2010) and fruit mineral composition (Dražeta et al., 2004, Dichio et al., 2002, Montanaro et al., 2010).

In several species, including kiwifruit, apple and hot pepper, the decline in the flow of xylem at the end of fruit growth was attributed to a decrease in the hydraulic conductivity of the xylem vessels (Mazzeo et al., 2013, Morandi et al., 2010, Trifilò et al., 2010, Dražeta et al., 2004). However, the causes of these changes remained unclear. It was first suggested that xylem vessels became physically disrupted during fruit ripening (Dražeta et al., 2004, Findlay et al., 1987, Lang and Ryan, 1994) but this hypothesis was challenged by more recent studies (Bondada et al., 2005, Chatelet et al., 2008, Clearwater et al., 2012). Resistance to the movement of water from the stem to the fruit involves a series of resistances including in the pedicel, in the receptacle and in the fruit (Van Ieperen et al., 2003, Mazzeo et al., 2013). In hot pepper, Trifilò et al. (2010) suggested that xylem embolism in the fruit pedicel was the cause of the decrease in hydraulic conductivity. This hypothesis warrants further investigations since it is consistent with numerous studies on other plant organs, including roots, branches or petioles that showed the impact of embolism on the hydraulic conductivity of xylem vessels (Damour, 2008, Meinzer and McCulloh, 2013, Sperry and Ikeda, 1997). In their study Trifilò et al. (2010) deduced embolism in the fruit pedicel from the difference between the hydraulic conductivity obtained with different measurement methods. Direct assessment of embolism was thus needed to confirm its impact on the decrease in hydraulic conductivity of xylem.

Furthermore, changes in the xylem flow could also be caused by the variation in the water potential gradient, the driving force of water movement (Measham et al., 2014, Léchaudel and Joas, 2007, Fishman and Génard, 1998). In grapevine, although the hydraulic conductivity of xylem was found to decrease, the decrease in xylem flow was attributed to the decrease in the water potential gradient driving flow at the end of growth (Choat et al.,

2009, Bondada et al., 2005, Keller et al., 2006). The reasons given for the decline in xylem flow in grapevine may be specific to this species, since the water potential of several fruits, including mango (Léchaudel et al., 2012), apple (Mills et al., 1996), tomato (Hossain and Nonami, 2010) and hot pepper (Trifilò et al., 2010), has been reported to decrease in the final stages of fruit development, suggesting that the water potential gradient tends to increase with fruit age. On the other hand, studies on grapevine underlined the need to consider changes in the water potential gradient and in the hydraulic conductivity of xylem when investigating the causes of variations in xylem flow.

In this study, we measured changes in xylem flow during fruit development and identified their cause by measuring changes in two potential sources of variation, the water potential gradient and hydraulic conductivity. Mango was used as model since its water potential has been reported to decrease significantly during fruit development (Léchaudel et al., 2012) and few studies on xylem have been conducted in this species. In agreement with Trifilò et al. (2010), we hypothesized that embolism in xylem vessels causes the decrease in the hydraulic conductivity. During the late growth stage, the mango fruit pedicel becomes dry and its color changes from yellow to dark brown (Mendoza and Wills, 1984). These changes in the appearance of the mango fruit pedicel suggest changes in its hydraulic properties, and we consequently focused measurements of embolism and of hydraulic conductivity on the fruit pedicel.

C - Material and methods

1) **Fruit material**

All measurements were made on the fruit and pedicel of Mangifera indica L. cv. “Cogshall”, a Floridian commercial cultivar, grafted on cv. “Maison rouge”. The study was carried out at the CIRAD Research Station in Saint Pierre (Reunion Island, 20° 52’ 48’’ S, 55° 31’ 48’’ E) on 22-year-old (in 2012) mango trees. Trees were approximately 3 m in height, spaced 5 x 6 m apart, and well irrigated.

The diameter of the fruit pedicel, the hydraulic proprieties of the xylem vessels in the fruit pedicel and fruit fresh mass, were measured on 10 to 17 fruits at 40, 60, 90, 105, 120 and 135 days after full bloom (DAB). Fruit water potential was measured on three to eight fruits at 42, 59, 66, 80, 92, 97, 101, 106, 119, 130 and 135 DAB. Stem water potential was

measured at 45, 80, 97, 101, 119 and 130 DAB, with three to eight repetitions. Transpiration and xylem flows were measured at 50, 65, 70, 90, 94, 105, 115, 125 and 135 DAB on two and three to six fruits, respectively.

2) **Measurements of fruit and stem water potential**

The covered leaf technique was used to estimate xylem water potential of the stem (Turner, 1981). Mango leaves were covered with plastic bags wrapped in aluminium foil the day before measurements were made to avoid water losses due to transpiration. By blocking leaf transpiration, it was assumed that the leaf water potential was in equilibrium with that of the stem xylem at the point of leaf insertion. The water potential (Ψ, in MPa) is equal to the difference between turgor pressure (P, in MPa) and osmotic pressure (π, in MPa). Since the solute concentration in the xylem sap is almost null, it was assumed that its osmotic pressure was also null. Consequently, the pressure potential measured on enclosed leaves with a pressure chamber was assume to correspond to the water potential.

To measure fruit water potential, just after harvest, two discs of fruit flesh about 2.5 cm in diameter were removed from each side of the fruit and placed in a WP4 psychrometer (Decagon Devices, Pullman, WA, USA). Stem and fruit water potential were measured at 8 am excepted at 80, 101 and 119 DAB where stem and fruit water potentials were measured from 5 to 10 pm.

3) **Measurements of xylem and transpiration flows**

Xylem and transpiration flows were estimated using the subtractive method of Lang and Thorpe (1989) in grapevine and subsequently used in apple (Lang, 1990, Morandi et al., 2011), peach (Huguet et al., 1997) tomato (Guichard et al., 2005) and kiwifruit (Morandi et al., 2010). This method deduces xylem and transpiration flows by comparing changes in the fresh mass of detached and girdled fruits. It was thus assumed that: (i) xylem fluxes are not affected by girdling and (ii) the transpiration rate is not affected by fruit detachment. Fishman et al. (2001) reported that this method can lead to systematic overestimation of the calculated xylem flow. However, these errors appeared to be limited to a specific period of the day.

Changes in the diameter of several fruits of equal volume were recorded hourly with a linear variable differential transformer (LVDT) mounted on an INVAR frame (Li et al., 1989) and

connected to a data logger (Model 21 X, Campbell Scientific Ltd). The variation in fruit fresh mass (dMfruit, in Kg) with time (dt, in h) was deduced from the variation in fruit diameter ($dD_{fruit,}$ in mm) with time using the following empirical relationship:

$$\frac{dM_{fruit}}{dt} = 8.10^{-4} \times (\frac{dD_{fruit}}{dt})^{3.054}$$ N = 511, R^2 = 0.99 *Equation 34*

A set of fruits was removed from the tree and hung close to the fruits we used to deduce the xylem flows to estimate water losses by transpiration (Tf, Kg h^{-1}). We thus assumed that the changes in masses of the detached fruit ($dM_{fruit(detached)}$, Kg) with time (dt, in h) in were only related to the transpiration flows (Tf, Kg h^{-1}):

$$\frac{dM_{fruit(detached)}}{dt} = -Tf$$ *Equation 35*

The stems of the second set of fruits were girdled to stop the phloem translocation. For these fruits, it was assumed that changes in fruit mass ($dM_{fruit(girdled)}$, Kg) with time (dt, in h) were the sum of the xylem (Ix, in Kg h^{-1}) and transpiration flows:

$$\frac{dM_{fruit(girdled)}}{dt} = I_x - Tf$$ *Equation 36*

The xylem flow was computed from Equation 35 and Equation 36.

$$\frac{dM_{fruit(girdled)}}{dt} - \frac{dM_{fruit(detached)}}{dt} = I_x$$ *Equation 37*

4) **Measurements of the hydraulic properties of xylem vessels in the fruit pedicel**

The XYL'EM apparatus (Embolism Meter, INRA Licensed Instrumentec, France) was used to measure the hydraulic properties of xylem vessels in the fruit pedicel, following the method of Sangsing et al. (2004). The fruit pedicels were cut into sections approximately 5 cm long under water to prevent air entering the vessels and the sections were connected to a XYL'EM apparatus. The pedicel sections were wrapped with Teflon tape to prevent leaks and their extremity was gently debarked with a scalpel to avoid latex exudation that could block the xylem vessel. The initial conductivity (Ki, mmol m s^{-1} MPa^{-1}) of each pedicel was measured with a hydrostatic pressure gradient of 3 kPa using deionized water. The pedicel

sections were then perfused at a pressure of 0.175 MPa for 5 min to remove air bubbles from the xylem vessels. The hydraulic conductivity of the pedicel sections was measured again and flushes were repeated until maximum conductivity (Km, mmol m s^{-1} MPa^{-1}) was reached. The percentage loss of hydraulic conductivity (PLC) was calculated from:

$$PLC = \frac{K_m - K_i}{K_m} \times 100$$ *Equation 38*

5) **Statistical analysis**

Variance analyses and multiple comparisons between means of the measurements at the different fruit development stages were performed using the Tukey test to check whether or not fruit fresh mass, fruit and stem water potential, pedicel diameter, xylem flow, xylem hydraulic conductivity, and xylem embolism underwent significant changes during the growth period.

D - Results

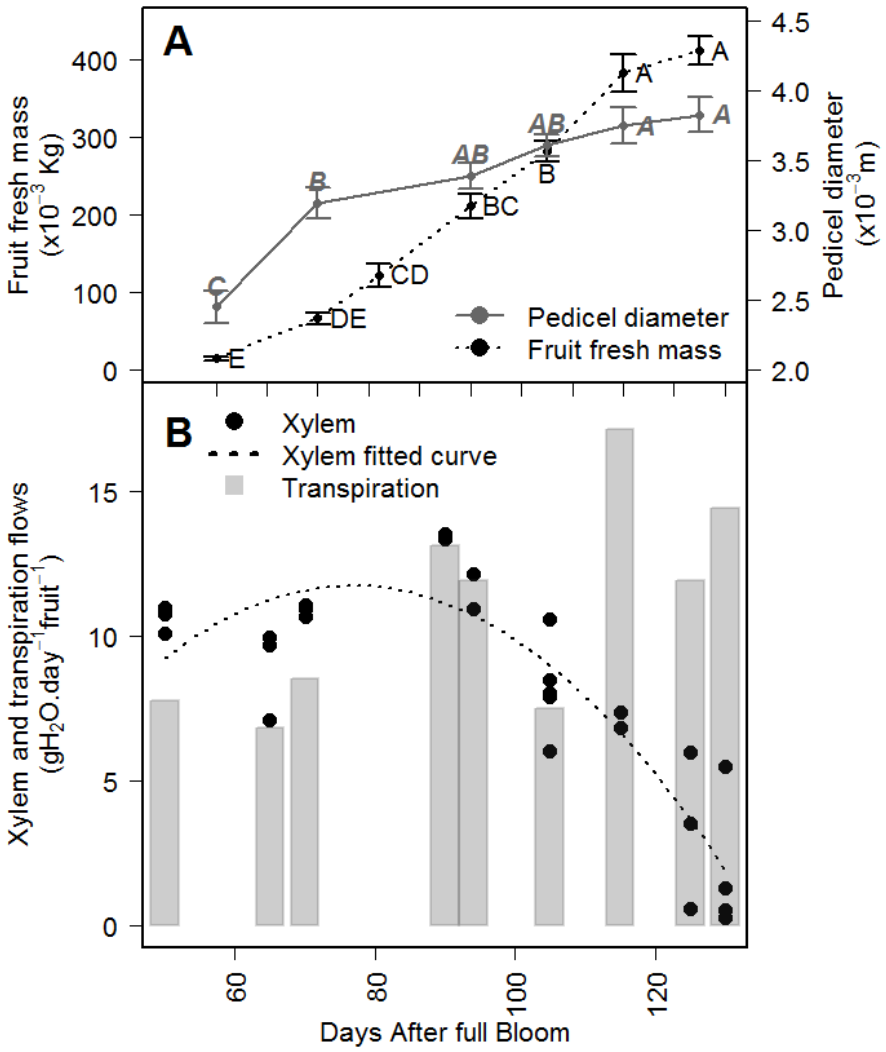

Figure 31: Seasonal variation in fruit fresh mass, pedicel diameter (A), fruit transpiration, and xylem flow to the fruit (B). Different letters indicate significant differences at P<0.05 according to Tukey's multiple comparison test.

1) **Fruit mass and changes in transpiration and xylem flows**

Mango fruit growth followed a simple sigmoid pattern (Figure 31A). After the period of cell division, at 60 DAB, fruit growth was almost linear until 120 DAB when it decreased. In contrast, growth of the mango pedicel was curvilinear. After a rapid increase from 40 to 60 DAB, the diameter of the fruit pedicel remained almost constant until harvest (Figure 31A). A weak relationship was found between fruit fresh mass and pedicel diameter (R^2= 0.62). A second order polynomial function was fitted to the xylem flow measurements (R^2 = 0.78) revealing an increase in flow from 10.6 to 13.4 gH_2O day^{-1} $fruit^{-1}$ between 50 and 90 DAB

followed by a continuous decrease to reach 1.91 $gH_2O\ day^{-1}\ fruit^{-1}$ at 130 DAB. Transpiration flows also varied considerably between 6.83 and 17.12 $g\ day^{-1}\ fruit^{-1}$ (Figure 31B), and tended to increase during the course of fruit development. Changes in transpiration flows could be partly due to variations in the environmental conditions on the day measurements were made and to the increase in the surface area of the fruit during growth.

2) **Changes in the water potential gradient during mango development**

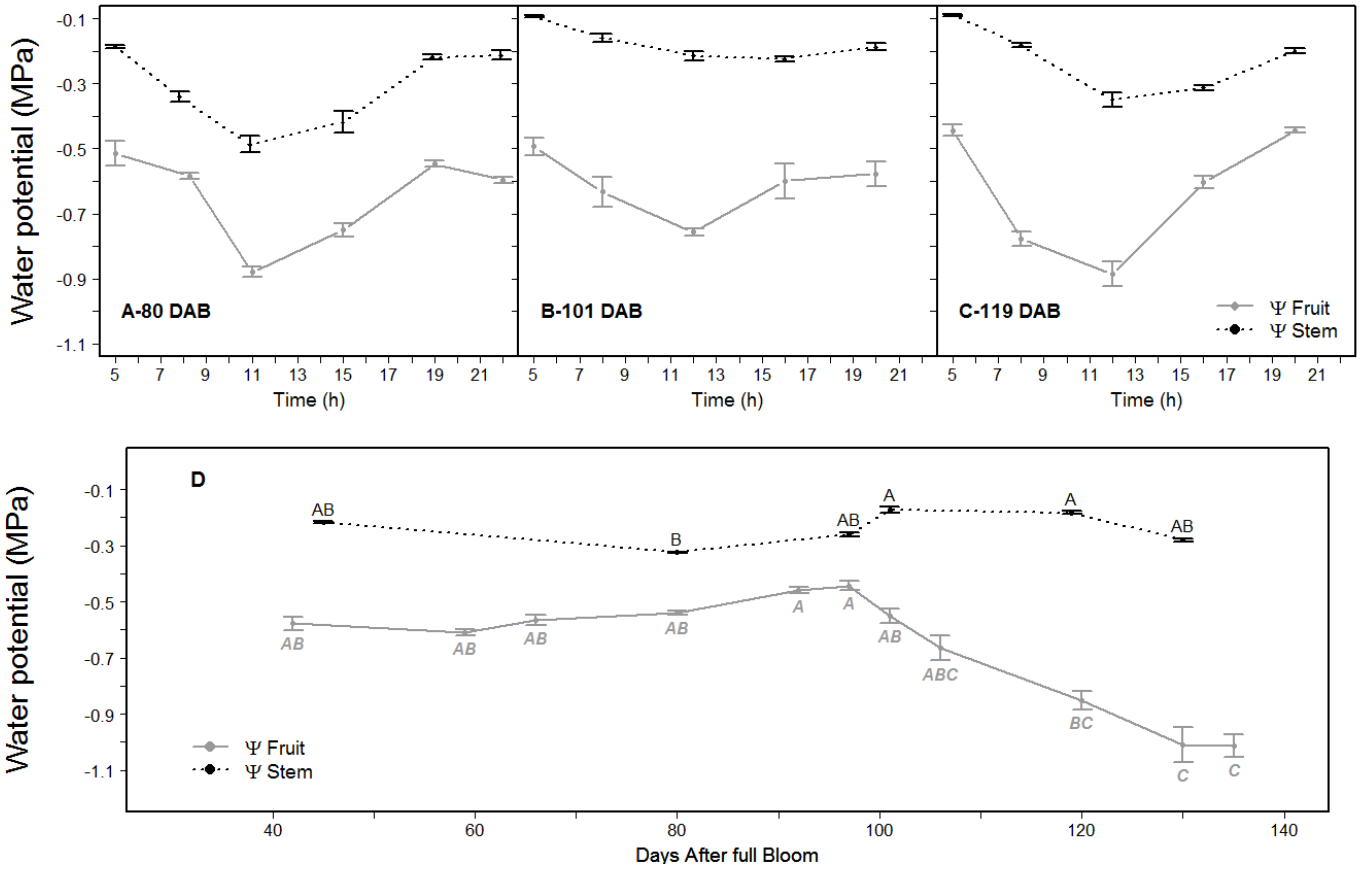

Figure 32: Daily variations, at 80, 101 and 119 DAB (A, B, C) and seasonal variation in the water potential of the fruit and the stem (D) measured at 8 am. Different letters indicate significant differences at P<0.05 according to Tukey's multiple comparison test.

Daily variations in the water potential of the fruit and stem were measured at 80, 101 and 119 DAB (Figure 32A to Figure 32C). Regardless of the measurement day, water potential of the fruit and the stem decreased considerably in the first half of the day and increased in the second half of the day to reach the values measured at the beginning of the day. Our measurements showed that the water potential gradient was always in favor of the fruit and remained relatively constant over the course of the day.

To study changes in the water potential gradient during growth, the water potential of the stem and the fruit was measured at 8 am at different dates between 40 and 135 DAB (Figure 32D). Between 42 and 97 DAB, fruit water potential increased from -0.57 to -0.44 MPa, although the difference was not significant. From 97 DAB on, fruit water potential decreased significantly to reach -1.02 MPa in the final stage of fruit development. The water potential of the stem was always higher (less negative) than that of the fruit and varied between -0.32 to -0.17 MPa during growth. Measurements indicated that water potential gradient was in favor to the fruit throughout growth (Figure 32E) and increased in the end of the growing season. This indicated that changes in the water potential gradient were not linked to changes in the xylem flows reported above.

3) **Changes in hydraulic conductivity during mango development**

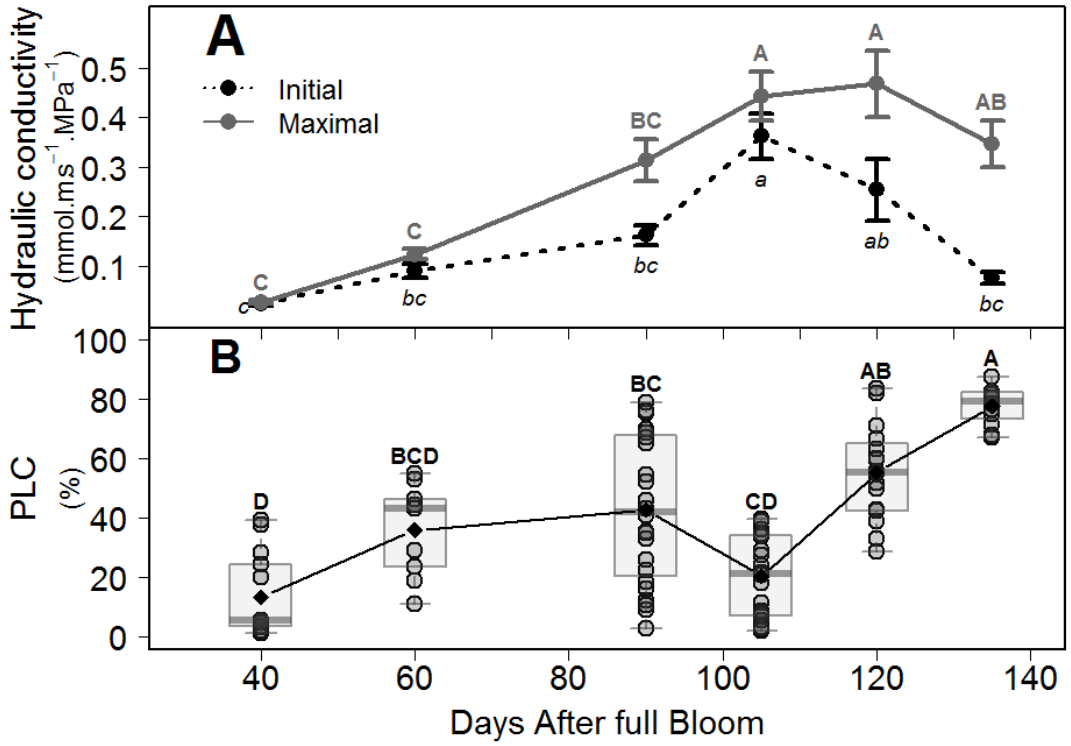

Figure 33: Changes in the initial and the maximum hydraulic conductivity (A) and in the percentage loss of hydraulic conductivity (PLC) due to embolism (B) during the growth period. Different letters indicate significant differences at P<0.05 according to Tukey's multiple comparison test.

Figure 33A shows changes in initial and maximum hydraulic conductivity in the xylem vessels of the mango fruit pedicel during growth. Initial hydraulic conductivity measured in pedicel vessels with embolism increased significantly from 40 to 105 DAB and then decreased significantly until the final stage of fruit development. Likewise, maximum hydraulic conductivity measured in pedicel vessels without embolism increased significantly from 40 to 105 DAB, but no significant decrease in maximum conductivity was measured from 105 to 135 DAB. A poor correlation (R^2 = 0.34) was found between the pedicel diameter and maximum hydraulic conductivity. The difference between the initial and maximum hydraulic conductivity enabled us to calculate the percentage loss of conductivity of xylem vessels due to embolism (Figure 33B).

Results showed that embolism of the xylem vessels in the fruit pedicel increased significantly during growth (Figure 33B). The average percentage loss of conductivity due to embolism increased from 13% at 40 DAB to 78% in ripe fruits at 135 DAB. Our results

showed that the decrease in hydraulic conductivity of xylem vessels in the fruit pedicel at the end of fruit development was due to xylem embolism. Embolism measurements varied significantly during early growth stages, especially around 90 DAB. At this stage, xylem vessels in the fruit pedicel exhibited had either a low or a high level of embolism: at 90 DAB, 61% of the fruit pedicels showed less than 45% loss of conductivity due to embolism, whereas the remaining fruit pedicels showed more than 67% loss of conductivity due to embolism.

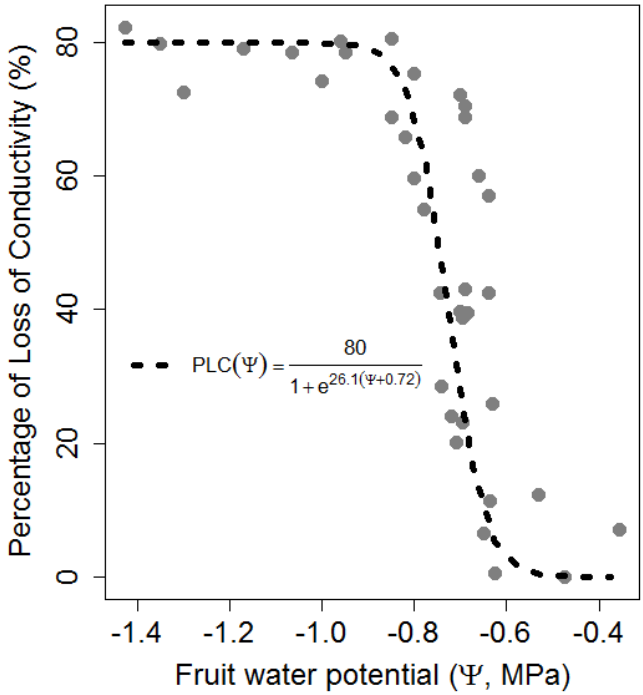

Figure 34: Percentage of loss of hydraulic conductivity as a function of fruit water potential. Dotted lines represent the nonlinear relationship established between the fruit water potential and the loss of hydraulic conductivity.

Plotting values of percent losses of conductivity versus the fruit water potential measured at the time of conductivity measurements revealed an increase in embolism in the fruit pedicel with a decrease in fruit water potential (Figure 34).

The loss of conductivity in the fruit pedicel was linked to fruit water potential by a decreasing logistic relationship. These results support the hypothesis that hydraulic conductivity of xylem vessels in the mango fruit pedicel decreases significantly during growth due to xylem embolism linked to the decrease in the fruit water potential.

E - Discussion

The aim of this study was to establish whether variations in xylem flow are due to changes in the water potential gradient between the fruit and the stem and/or to changes in hydraulic conductivity. Results indicated that the flow of xylem to the mango fruit increased up to 100 DAB and then decreased until the end of fruit development in line with results reported in other fruits (Ho et al., 1987, Morandi et al., 2010, Dražeta et al., 2004). Results showed that the changes in xylem flow were not related to changes in the water potential gradient which, in contrast to xylem flow, decreased until 100 DAB and then increased until the end of growth. The decrease in fruit water potential at end of fruit development may be related to the accumulation of soluble solids (Léchaudel et al., 2012) and to the increase in water losses by transpiration measured in this study, in line with Nordey et al. (2014c).

These results contradict those obtained in studies on grapevine stating that the decline in xylem flow at the end of growth was due to the decrease in the water potential gradient between the fruit and the stem (Bondada et al., 2005, Keller et al., 2006, Choat et al., 2009). In grapevine, the decrease in the water potential gradient was explained by changes in the fruit water balance caused by an increase in the water supply by the phloem which "hydraulically buffered" the fruit, and by a decrease in the fruit transpiration rate (Bondada et al., 2005, Keller et al., 2006, Choat et al., 2009). The reasons given for the decline in xylem flux in grapevine may be specific to this species, since the water potential of several fruits, including apple (Mills et al., 1996), tomato (Hossain and Nonami, 2010) and hot pepper (Trifilò et al., 2010), was reported to decrease in the last stages of development, suggesting that the water potential gradient increases with fruit age as observed in mango in the present study. In addition, water relations in the grape berry differ from those of other fruits since the water potential gradient was estimated not to favor the fruit throughout the day, causing continuous fruit water losses due to backflow (Choat et al., 2009, Tyerman et al., 2004). Backflow has been measured in other fruits including kiwi and mango, but only during a limited period in the morning (Higuchi and Sakuratani, 2006, Clearwater et al., 2009). Unlike Higuchi and Sakuratani (2006), the present study did not provide any evidence for backflow in mango since the water potential gradient was always in favor of the fruit.

Measurements of fruit water potential have been performed with a psychrometer, in lines with previous study of (Léchaudel et al., 2012) on mango. This destructive method requires collecting a fresh sample of fruit pulp. Consequently, since tissues excision can cause release of solutes in the intercellular space, this method may underestimated fruit water potential (give more negative values). However, even if fruits water potential may be slightly underestimated, our measurements gave evidences that the decrease in xylem flow was not related with a decrease in water potential gradients. Our results suggested thus that changes in xylem flows were caused by changes in xylem hydraulic conductivity. In agreement with Trifilò et al. (2010), our initial hypothesis was that changes in hydraulic conductivity of the xylem vascular network may be caused by changes in the hydraulic properties of the fruit pedicel due to xylem embolism. Like xylem flow, hydraulic conductivity of the fruit pedicel increased until 100 DAB and then decreased until the end of fruit development in agreement with studies in other fruits (Dražeta et al., 2004, Trifilò et al., 2010, Van Ieperen et al., 2003). The poor relationship between the pedicel diameter and its hydraulic conductivity ($R^2 = 0.34$) could be explained by the study of Lang and Ryan (1994) in apple in which the increase in xylem tissue was reported to be due to the proliferation of non-conducting and structural components. In agreement with these authors, we believe that the diameter of the pedicel is not an accurate indicator of the capacity of the pedicel to transport water to the fruit. An analysis of histological section of the fruit pedicel will be required to establish whether the variation in the hydraulic conductivity of the fruit pedicel is due to differences in the number of vessels and/or in vessel diameter. Our measurements suggest that the decrease in the hydraulic conductivity of the fruit pedicel in late development stages is due to xylem embolism, in line with suggestions by Trifilò et al. (2010) in hot pepper fruit. In our study, embolism caused a loss of almost 80% conductivity in the xylem vessels of the fruit pedicel of ripe fruit. To our knowledge, this is the first study to report measurements of xylem embolism in the fruit pedicel and its effect on hydraulic proprieties.

Since no significant decrease in maximum hydraulic conductivity was measured, our results suggest that the increase in the hydraulic conductivity of the fruit pedicel measured during the late fruit development stage was not linked to a physical disruption. This result is consistent with results of studies on hot pepper, grapevine and kiwi (Trifilò et al., 2010,

Choat et al., 2009, Keller et al., 2006, Bondada et al., 2005, Clearwater et al., 2012, Mazzeo et al., 2013), who reported that xylem remains functional during fruit ripening. Embolism was also measured in the pedicel of some fruit in the early stages of fruit development, i.e., from 40 to 90 DAB (Figure 3). It was hypothesized that the early occurrence of embolism in the pedicel of immature fruit could be the cause of premature fruit drop (Singh et al., 2010). The relationship between premature fruit drop and xylem embolism warrants further investigation.

Our study provided evidence that the drop in fruit water potential led to xylem embolism and decrease the hydraulic conductivity of the fruit pedicel. This is consistent with results of previous studies on petiole or branch segments in which xylem embolism was seen to increase with a drop in xylem water potential (Tyree and Sperry, 1988, Meinzer and McCulloh, 2013).

Our measurements have focused on changes in hydraulic conductivity in fruit pedicel, assuming that this part of the xylem network between the stem and the fruit was the main source of variations of hydraulic conductance. However, studies on kiwifruit (Mazzeo et al., 2013) and tomato (Van Ieperen et al., 2003) highlighted important changes in hydraulic conductivity in fruit receptacle at the end of the growing season. Consequently, further works should measure variations in hydraulic conductivity of mango fruit receptacle. In addition, since the enlargement and the mineral composition of fruit depend on xylem flow (Dražeta et al., 2004) (Dichio et al., 2002) (Montanaro et al., 2010) (Morandi et al., 2010), it would be interesting to investigate the impact of variations in the hydraulic conductivity of xylem vessels on the composition and the growth rate of mango fruit.

IV - La variation des conditions climatiques au sein de l'arbre et l'embolisation des vaisseaux conducteurs de sève expliquent en parties les différences de calibre entre les mangues : une approche de modélisation.

Objectifs :

Il est proposé dans ce chapitre d'étudier l'effet des conditions de croissance sur l'accumulation de matière fraiche de la mangue. Cette étude s'appuie sur le modèle développé par Léchaudel et al. (2007) qui simule la croissance en matière fraiche de la mangue et sur le modèle qui simule la température et la transpiration du fruit en fonction des conditions climatiques (Partie I chapitre II). Ce modèle intègre les résultats du chapitre précédent (Partie II chapitre III) concernant les changements de conductivité hydraulique des vaisseaux du xylème pendant la croissance de la mangue. Le modèle présenté dans ce chapitre est utilisé dans le chapitre suivant (Partie II chapitre V) pour simuler la croissance en matière fraiche de la mangue.

Principaux résultats :

- Le modèle proposé permet de simuler correctement l'impact des conditions de croissance sur l'accumulation de matière fraiche de la mangue.
- Les simulations indiquent que l'embolisation des vaisseaux conducteurs de sève est à l'origine du ralentissement de croissance de la mangue.
- La croissance en matière fraiche du fruit est fortement liée à sa croissance en matière sèche.
- Les différences de transpiration entre les fruits dans l'arbre expliquent en partie les différences de croissance en matière fraiche mesurées.

La variation des conditions climatiques au sein de l'arbre et l'embolisation des vaisseaux conducteurs de sève expliquent en parties les différences de calibre entre les mangues : une approche de modélisation.

A - Introduction

Pour être commercialisés les fruits doivent correspondre à des standards de qualité. Le calibre est un des premiers critères d'évaluation de la qualité du fruit et celui-ci varie considérablement à la récolte. Des études précédentes sur la mangue (Uthaibutra et al., 1998, Hofman et al., 1995), la pêche (Luchsinger et al., 2001), et le kiwi (Smith et al., 1994) ont montré que les variations de calibre peuvent être en partie attribuées à la différence de position des fruit dans l'arbre. Le calibre des fruits à pulpe, comme la mangue ou la pêche, est fortement lié à leur croissance en matière fraiche, étant donné que ces fruits sont principalement composés d'eau. L'accumulation d'eau dans le fruit dépend des entrées d'eau par le xylème et le phloème et des pertes en eau par transpiration. Plusieurs études sur la mangue (Léchaudel et al., 2012, Nordey et al., 2014c), la pomme (Saudreau et al., 2007) et l'avocat (Woolf et al., 1999) ont montré que la température et la transpiration des fruits varient selon leur position dans l'arbre à cause des différences de climat. Il est supposé que ces variations expliquent en partie les différences de calibre à la récolte.

Par ailleurs, il est connu que la croissance des organes de la plante est influencée par la conductivité hydraulique des vaisseaux du xylème (Raimondo et al., 2009, Hubbard et al., 1999). Des études sur la mangue (Partie II chapitre III), le pigment (Trifilò et al., 2010), la pomme (Dražeta et al., 2004) et le kiwi (Mazzeo et al., 2013) ont montré que la conductivité hydraulique du xylème diminue à la fin du développement du fruit. Cette diminution a été attribuée à l'embolisation des vaisseaux du xylème chez la mangue (Partie II chapitre III) et le pigment (Trifilò et al., 2010). La présence d'embolie a également été mesurée dans les vaisseaux du xylème de nombreux organes de la plante comme les racines, les branches ou les pétioles (Damour, 2008, Meinzer and McCulloh, 2013, Sperry and Ikeda, 1997). Il peut donc être supposé que les variations de calibre entre les fruits peuvent également s'expliquer par des différences de conductivité hydraulique due à l'embolisation des vaisseaux conducteurs de sève.

Cette étude vise à déterminer si les différences de climat au sein de l'arbre et de conductivité hydraulique entre les fruits sont impliquées dans les variations de calibre observées entre les mangues à la récolte. Nous proposons pour cela, de coupler le modèle proposé par Léchaudel et al. (2007) pour simuler la croissance en matière fraiche de la mangue au modèle que nous avons présenté précédemment (Partie I chapitre II) qui simule l'effet des conditions climatiques sur la température et la transpiration de la mangue. Il est par ailleurs proposé d'introduire dans cette approche de modélisation les résultats de notre étude précédente (Partie II chapitre III) sur l'impact de l'embolie sur la conductivité hydraulique des vaisseaux du xylème.

La qualité du nouveau modèle sera évaluée, puis une analyse par simulation permettra de mettre en évidence comment l'embolie et les conditions climatiques modifient les relations hydriques du fruit et induisent des différences de calibre entre les mangues.

B - Matériel et méthodes

1) **Présentation du modèle température.**

Un modèle thermodynamique a été développé pour simuler les variations spatiales et temporelles de la température et de la transpiration de la mangue (Nordey et al., 2014c). Ce modèle simule la température et la transpiration du fruit en déterminant les échanges d'énergie entre le fruit et son environnement. Pour ce faire, le fruit est divisé en une multitude de sous-unités de forme tétraédrique. Les températures des sous unités à la surface du fruit sont déterminées en quantifiant leurs échanges par convection, transpiration et rayonnement, avec l'environnement extérieur, et par conduction avec les autres sous unités. Les températures des sous unités à l'intérieur du fruit sont quant à elles déterminées en calculant les échanges par conduction avec les sous unités voisines.

2) **Présentation du modèle de croissance en matière fraiche.**

La croissance en matière fraiche des mangues est simulée sur la base du modèle proposé par Léchaudel et al. (2007). Comme dans le modèle initial, il est considéré que la croissance en matière fraiche du fruit est soit plastique (irréversible), soit élastique (réversible). Les variations de la masse d'eau du fruit ($\frac{dw}{dt}$, g h^{-1}) sont calculées en soustrayant les pertes en

eau par transpiration (Tf, g h^{-1}) aux apports d'eau par le xylème et le phloème (U, en g h^{-1}) (Equation 39).

$$\frac{dw}{dt} = U - Tf \qquad \textit{Equation 39}$$

Les pertes en eau par transpiration sont calculées grâce au modèle thermodynamique présenté précédemment. En accord avec le modèle initial (Léchaudel et al., 2007), la quantité d'eau qui entre dans le fruit est calculée comme le produit de la conductivité hydraulique globale (C, g MPa^{-1} h^{-1}) et de la différence de potentiel hydrique entre la tige (Ψ_{Tige}, en MPa) et le fruit (Ψ_{Fruit}, MPa) (Equation 40).

$$U = C \times (\Psi_{Tige} - \Psi_{Fruit}) \qquad \textit{Equation 40}$$

Dans le modèle initial, il a été estimé que la conductivité hydraulique est proportionnelle à la masse du fruit et qu'elle n'était pas impactée par la présence d'embolie. Hors, dans une étude précédente (Partie II chapitre III), nous avons montré que la conductivité hydraulique des vaisseaux du xylème du pédicelle augmente au cours de la croissance de la mangue jusqu'à un certain seuil, puis diminue à cause de l'apparition d'embolie. Par soucis de simplification, il a été considéré que la conductivité hydraulique globale (du xylème et du phloème) varie également en fonction de la présence d'embolie. Il a ainsi été estimé que la conductivité hydraulique est liée par une fonction logistique à la croissance en matière sèche du fruit et qu'elle diminue à cause de l'embolisation des vaisseaux conducteurs de sève (Percent Loss of hydraulic Conductivity, PLC en %) :

$$C = (c_1 + \frac{c_2}{1 + c_3 exp^{-c_4 \times MS_{Fruit}}}) \times PLC \qquad \text{Equation 41}$$

L'apparition d'embolie est fonction de la tension hydrostatique dans les vaisseaux du xylème. Celle-ci augmente avec la diminution du potentiel hydrique des organes de la plante. La relation établie dans la partie II chapitre III entre le potentiel hydrique du fruit et la perte de conductivité hydraulique des vaisseaux du xylème due à la présence d'embolie a été utilisée :

$$PLC = \frac{80}{1 + \exp^{26 \times (\Psi_{Fruit} + 0.72)}} \qquad \text{Equation 42}$$

La variation journalière du potentiel hydrique de la tige (Ψ_{Tige}) est déterminée en fonction de la température de l'air, de l'humidité relative, et du rayonnement global, d'après la relation empirique proposée par Léchaudel et al. (2007). Le potentiel hydrique du fruit (Ψ_{Fruit}) est calculé en soustrayant la pression osmotique du fruit (π_f, MPa) à la pression de turgescence (P_f, MPa):

$$\Psi_{Fruit} = P_f - \pi_f \qquad \textit{Equation 43}$$

La pression osmotique dans le fruit est calculée grâce à l'Equation 45, où R est la constante universelle des gaz parfait (R = 8.31 Pa cm^{-3} K^{-1} mol^{-1}), T est la température absolue (K), n_s est le nombre de moles de solutés osmotiquement actifs et w (cm^3) est le volume total d'eau dans la pulpe.

$$\pi_f = \frac{RTn_s}{w} \qquad \text{Equation 44}$$

Le nombre de moles de solutés osmotiquement actifs (sucres, acides organiques, minéraux, et acides aminés) est exprimé individuellement dans le modèle, sauf pour les acides aminés qui sont considérés comme un même groupe (Equation 45).

$$n_s = \sum_j n_j + n_{aa} \qquad \text{Equation 45}$$

Dans l'Equation 45, n_j représente le nombre de moles du soluté *j* dans la pulpe de la mangue et n_{aa} représente le nombre de moles totales d'acides aminés. Le nombre de moles des composés osmotiquement actifs est calculé grâce à l'Equation 46, où $prop_j$ (sans dimension) représente la proportion de masse du composé osmotiquement actif *j* dans la masse sèche (DM, g) et MMj (en g mol^{-1}) est la masse molaire de ce composé.

$$n_j = \frac{prop_j \times DM}{MM_j} \qquad \text{Equation 46}$$

La proportion de chaque composé osmotiquement actif dans la masse sèche du fruit est calculée avec des relations empiriques basées sur la somme de degrés jours depuis la floraison, la masse sèche du fruit, et leurs interactions.

La pression de turgescence correspond à la pression exercée par la vacuole sur la paroi cellulaire. Elle est fonction du volume d'eau dans les cellules, de la pression seuil de la croissance plastique (Y, MPa), de l'élasticité des parois cellulaires (ε, MPa), et de leur extensibilité (Φ, MPa^{-1} h^{-1}) :

$$\begin{cases} \frac{dP_f}{dt} = \frac{\varepsilon}{V}[U + P - Tf - \emptyset V(P_f - Y)] & if(P_f \geq Y) \\ \frac{dP_f}{dt} = \frac{\varepsilon}{V}[U + P - Tf] & if(P_f < Y) \end{cases}$$ Equation 47

Comme dans le modèle initial, il a été estimé que la pression seuil de la croissance plastique, i.e., Y, varie en fonction du volume du fruit (V_t, cm^3) et de h (Mpa cm^{-3}):

$$Y = h\, V_t$$ Equation 48

Il a également été estimé comme dans le modèle initial que l'extensibilité cellulaire, i.e., Φ, diminue au cours de la croissance du fruit :

$$\begin{cases} \emptyset = \emptyset_{max} \\ \emptyset = \emptyset_{max}\, \tau^{(dd - dd_{ini})} \end{cases}$$ Equation 49

Où dd (°C j) est le nombre de degrés jours depuis la floraison, dd_{ini} (°C j) est la somme de degré jour à partir de laquelle l'extensibilité cellulaire diminue et τ ($°C^{-1}\ j^{-1}$) est le taux de décroissance de l'extensibilité cellulaire.

3) **Données d'entrée du modèle.**

Les données climatiques utilisées pour le fonctionnement du modèle qui simule la température et la transpiration du fruit, comme la température de l'air, l'humidité relative, la vitesse du vent, et le rayonnement global, sont mesurées toutes les minutes, moyennées et enregistrées toutes les heures dans une centrale d'acquisition (Model 21 X, Campbell Scientific Ltd, Logan, UT, USA) pendant la saison de croissance. Les rayonnements direct et diffus sont déduits du rayonnement global en utilisant le modèle développé par Maxwell E.L. (1987). La course du soleil a été déterminée en utilisant l'algorithme de la position du soleil (SPA) développé par Reda and Andreas (2004). Le modèle requière également les propriétés physiques et thermiques du fruit comme données d'entrée. Celles-ci ont été extraites de notre étude précédente (Nordey et al., 2014c). Il a été estimé qu'une partie du fruit était directement exposée au soleil et que la face opposée a reçu 20% du rayonnement, en accord avec les mesures de notre étude précédente. La croissance des fruits en matière sèche a été déterminée en mesurant l'augmentation du diamètre des fruits et en utilisant les relations empiriques déterminées par Léchaudel et al. (2007).

4) **Détermination des relations empiriques du modèle**

Léchaudel et al. (2007) ont proposé des relations empiriques pour estimer la composition de la pulpe en fonction de la matière sèche du fruit et du nombre de degrés jours depuis la floraison. Les paramètres de ces relations empiriques ont été déterminés en fonction des degrés jours calculés avec la température de l'air. Contrairement à Léchaudel et al. (2007), il est estimé que la température du fruit est différente de celle de l'air. En conséquent les paramètres des relations empiriques doivent être estimés en fonction des degrés jour calculés avec la température du fruit. Pour tenir compte des variations de température au sein de l'arbre, la moyenne des températures simulées pour des fruits positionnés à l'est, à l'ouest, au nord et au sud de la canopée a été considérée.

5) **Mesures de la croissance en matière fraiche des fruits**

La croissance des mangues en matière fraiche a été mesurée de manière destructive pendant la saison de croissance 2000-2001 pour 5 traitements de charge en fruits : 10, 25, 50, 100 et 150 feuilles par fruit (L/F) et pendant la saison de croissance 2001-2002 pour un traitement de 100 L/F.

La contraction journalière d'un fruit du traitement 100 L/F a été mesurée pendant 7 jours successifs en décembre 2001, en utilisant un capteur de déplacement LVDT (Linear Variable Differential Transformer) connecté à une centrale d'acquisition (Model 21 X, Campbell Scientific Ltd, Logan, UT, USA).

6) **Calibration et paramétrisation du modèle.**

Les valeurs des paramètres d'extensibilité, i.e., Φ, et d'élasticité cellulaire, i.e., ε, ont été extraites de l'étude de Léchaudel et al. (2007). Les valeurs des paramètres liés à la décroissance de l'extensibilité cellulaire, i.e., τ et DD_{ini}, à la conductivité hydraulique, i.e., c_1, c_2, c_3 et c_4, et à la pression seuil, h, ont été estimées en calibrant le modèle avec les données de croissance en matière fraiche mesurées pendant la saison 2000-2001 pour le traitement 100 L/F en utilisant une régression non linéaire (nls). La croissance en matière fraiche a été mesurée sur des fruits à l'extérieur de la canopée mais on ne connait pas leur position dans l'arbre. Pour tenir compte des variations de température au sein de l'arbre, la moyenne des

températures simulées pour des fruits positionnés à l'est, à l'ouest, au nord et au sud de la canopée a été considérée.

C - Résultats

Table 13: Relations empiriques utilisées dans le modèle pour déterminer la proportion d'acide organiques, de sucres et de minéraux dans la matière sèche de la pulpe en fonction du nombre de degrés jours depuis la floraison (DDJ, °C j) et de la masse sèche de la pulpe (MS, g).

Solutés (g gMS^{-1})	Relations empiriques	R^2
Malate	$5.9 \times 10^{-2} + DDJ \times -4.69 \times 10^{-5} + MS \times -2.22 \times 10^{-3} + MS \times DDJ \times 2.19 \times 10^{-6}$	**0.59**
Citrate	$-6.66 \times 10^{-3} + DDJ^2 \times -4.833 \times 10^{-7} + DDJ \times 5.75 \times 10^{-4} + MS \times (-6.56) \times 10^{-4}$	**0.65**
Pyruvate	$-1.55 \times 10^{-3} + DDJ^2 \times -6.88 \times 10^{-9} + DDJ \times 1.057 \times 10^{-5} + MS \times -1.52 \times 10^{-5}$	**0.42**
Oxalate	$4.83 \times 10^{-3} + DDJ \times -4.25 \times 10^{-6} + \frac{1}{MS} \times -9.53 \times 10^{-3} + \frac{DDJ}{MS} \times 3.25 \times 10^{-5}$	**0.64**
K^+	$1.25 \times 10^{-2} + DDJ^2 \times 9.08 \times 10^{-9} + DDJ \times -1.36 \times 10^{-5} + \frac{1}{MS} \times 8.18 \times 10^{-3}$	**0.50**
Mg^{2+}	$7.07 \times 10^{-5} + \frac{1}{DDJ} \times 3.38 \times 10^{-1} + \log(MS) \times 7.85 \times 10^{-5} + \frac{\log(MS)}{DDJ} \times -8.35 \times 10^{-2}$	**0.78**
Ca^{2+}	$1.27 \times 10^{-3} + DDJ \times -8.56 \times 10^{-7} + \frac{1}{MS} \times -1.4 \times 10^{-3} + \frac{DDJ}{MS} \times 6.97 \times 10^{-6}$	**0.64**
NH_4^+	$-5.56 \times 10^{-4} + DDJ^2 \times -2.62 \times 10^{-9} + DDJ \times 3.72 \times 10^{-6} + MS \times -3.62 \times 10^{-6}$	**0.40**
Na^+	$4.08 \times 10^{-5} + DDJ^2 \times -2.90 \times 10^{-10} + DDJ \times 4.38 \times 10^{-7} + MS \times -4.99 \times 10^{-6} + MS \times DDJ \times 3.87 \times 10^{-9}$	**0.13**
Glucose	$7.61 \times 10^{-2} + DDJ \times -5.85 \times 10^{-5} + MS \times -1.061 \times 10^{-3} + MS \times DDJ \times 1.063 \times 10^{-6}$	**0.48**
Fructose	$5.11 \times 10^{-2} + DDJ \times 9.85 \times 10^{-5} + MS \times -9.17 \times 10^{-4} + MS \times DDJ \times -1.91 \times 10^{-7}$	**0.43**
Saccharose	$-6.18 \times 10^{-3} + DDJ \times 2.00 \times 10^{-4} + MS \times -7.032 \times 10^{-3} + DDJ \times MS \times 8.71 \times 10^{-6}$	**0.68**
Amidon	$-4.58 \times 10^{-1} + DDJ^2 \times -9.67 \times 10^{-7} + DDJ \times 1.69 \times 10^{-3} + MS \times 7.56 \times 10^{-3} + MS \times DDJ \times -8.91 \times 10^{-6}$	**0.52**

1) **Paramètrisation du modèle.**

Les relations empiriques reliant la composition de la pulpe, à la teneur en matière sèche du fruit, et au nombre de degrés jours depuis la floraison, sont présentées dans la Table 13.
La calibration du modèle a permis d'estimer les valeurs des paramètres de la pression seuil de la croissance plastique (Y, Equation 48), de la conductivité hydraulique (c_1, c_2, c_3 et c_4, Equation 41), et de la diminution de l'extensibilité cellulaire (τ et DD_{ini}, Equation 49). Les valeurs de ces paramètres, ainsi que celles des autres paramètres utilisés dans le modèle, sont présentées dans la Table 14.

Table 14: Paramètres du modèle.

Paramètres	Désignation	Valeurs	Références
ε (MPa)	*Elasticité des parois cellulaires*	15.32	(Léchaudel et al., 2007)
Φ_{max} (MPa^{-1} h^{-1})	*Extensibilité des parois cellulaires*	1.725 10^{-2}	(Léchaudel et al., 2007)
τ (°C^{-1} jour^{-1})	*Taux de décroissance de l'extensibilité des parois cellulaire*	/	Calibration du modèle
DD_{ini} (°C jour)	*Nombre de degrés jours à partir duquel l'extensibilité des parois cellulaires diminue*	/	Calibration du modèle
c_1 (g MPa^{-1} h^{-1})	*Paramètre de la conductivité hydraulique*	3.4	Calibration du modèle
c_2 (g MPa^{-1} h^{-1})	*Paramètre de la conductivité hydraulique*	2.65	Calibration du modèle
c_3	*Paramètre de la conductivité hydraulique*	70	Calibration du modèle
c_4 (gMS^{-1})	*Paramètre de la conductivité hydraulique*	0.05	Calibration du modèle
h (MPa cm^{-3})	*Paramètre de la Pression seuil de la croissance plastique*	/	
Y (MPa)	*Pression seuil de la croissance plastique*	0.29	Calibration du modèle

La calibration du modèle a indiqué que contrairement au modèle initial, la variation de la pression seuil de la croissance plastique (Y) et l'extensibilité des parois cellulaires (Φ) au cours de la croissance du fruit diminue la qualité prédictive du modèle. Il a donc été estimé que les paramètres Y et Φ sont constants.

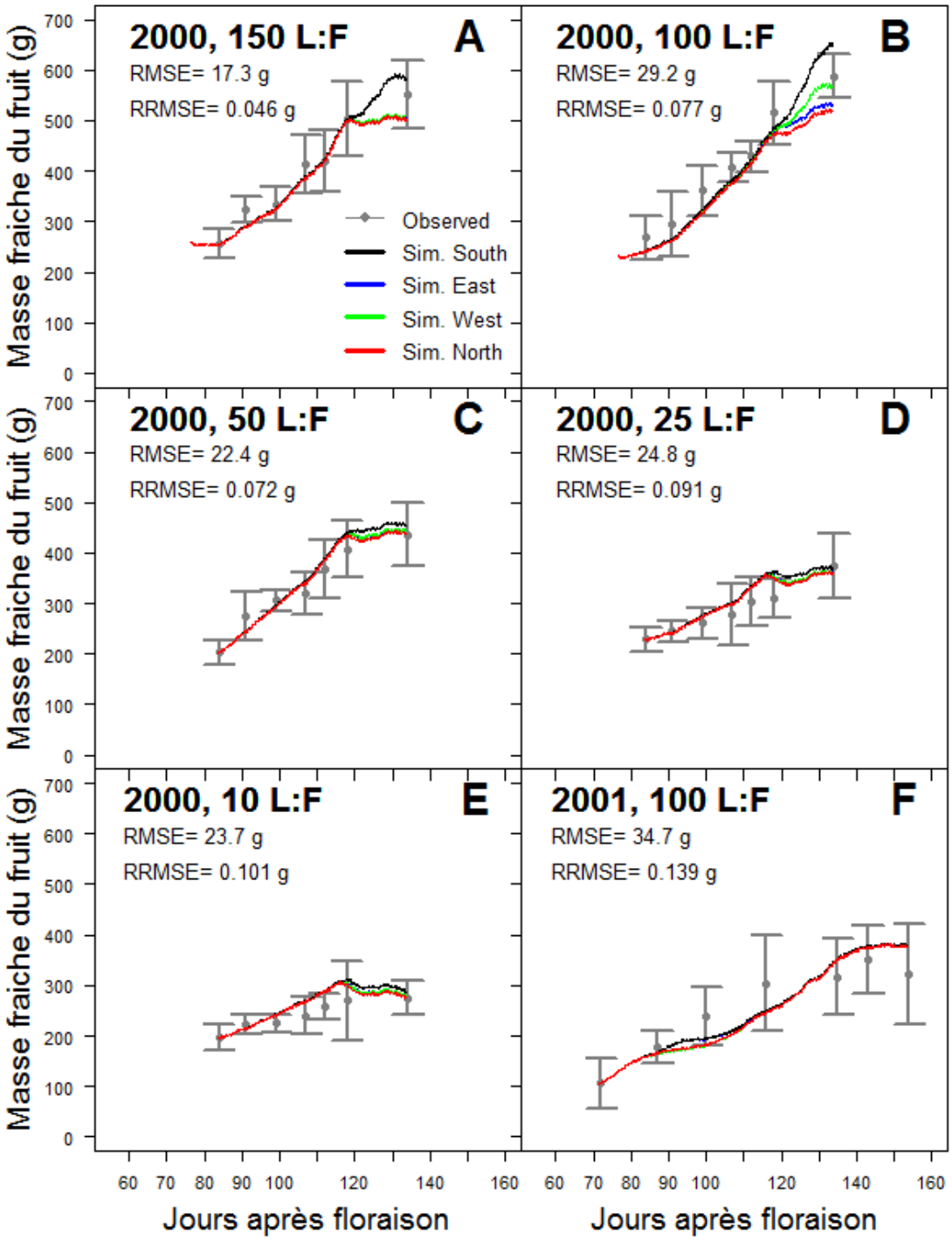

Figure 35: Les variations saisonnières simulées (ligne) et observées (points) de la matière fraiche des mangues, en fonction du nombre de feuilles par fruit (L:F), i.e. 10, 25, 50, 100 et 150 L:F, et de la position du fruit dans l'arbre, i.e. au nord, au sud, à l'est et l'ouest, pour la saison de croissance 2000-2001 (A à E) et 2001-2002 (F). La saison de croissance, le nombre de feuilles par fruit, la position du fruit dans l'arbre, le root mean square error (RMSE) et le relative root mean square error (RRMSE) sont indiqués sur les graphiques.

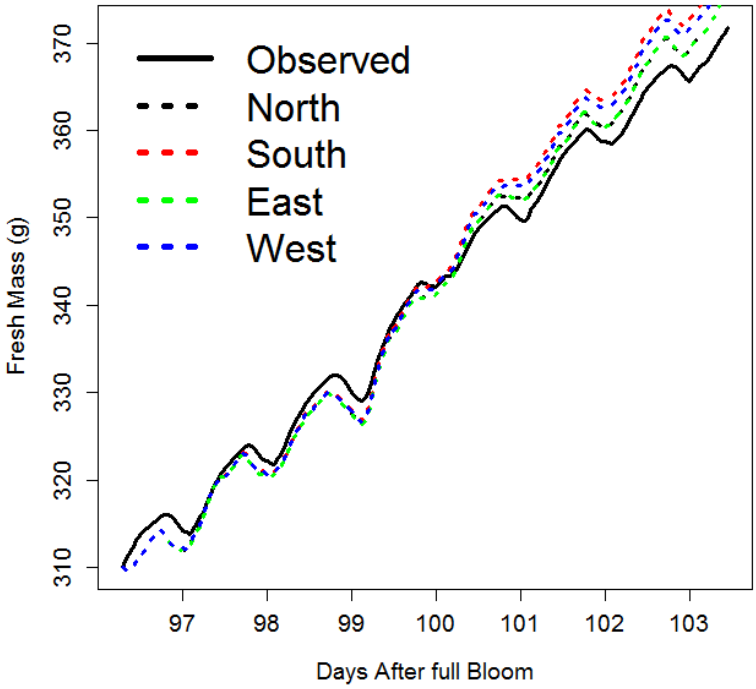

Figure 36: La variation horaire observée (ligne continue) et simulée (tirets) de la masse d'un fruit exposé au soleil sans contrainte carboné entre 96 et 104 jours après la floraison pendant la saison de croissance 2001-2002. Les positions des fruits dans l'arbre, i.e. au nord, au sud, à l'est, et à l'ouest, simulées sont indiquées sur le graphique.

2) **Validation du modèle.**

L'ajustement du modèle a été testé pour différentes charges en fruits (Figure 35A à Figure 35E). Les résultats indiquent que le modèle simule correctement la croissance en matière fraiche des fruits, quelle que soit la charge en fruits et la saison de production. Les différences de croissance en matière fraiche observées entre les traitements de charge en fruits, sont correctement simulées par le modèle proposé (Figure 35). L'ajustement du modèle en validation croisée est satisfaisant (RRME < 12%) (Figure 35A, 1C à 1F) et comparable à celui obtenu avec les données de calibration (Figure 35B). Le modèle simule des différences de croissance en matière fraiche entre les mangues selon leur position dans l'arbre. Le calibre des fruits les plus exposés au soleil, i.e. au nord de l'arbre, à la fin de la saison de croissance est inférieur à celui des fruits les moins exposés, i.e. au sud de l'arbre. La Figure 36 indique que le modèle simule également bien les contractions journalières du fruit qui ont été mesurées. Ces résultats montrent que le modèle proposé est correctement ajusté et qu'il décrit convenablement les processus impliqués dans la croissance en matière fraiche du fruit.

3) **Simulations des variables intermédiaires impliquées dans le bilan hydrique du fruit**

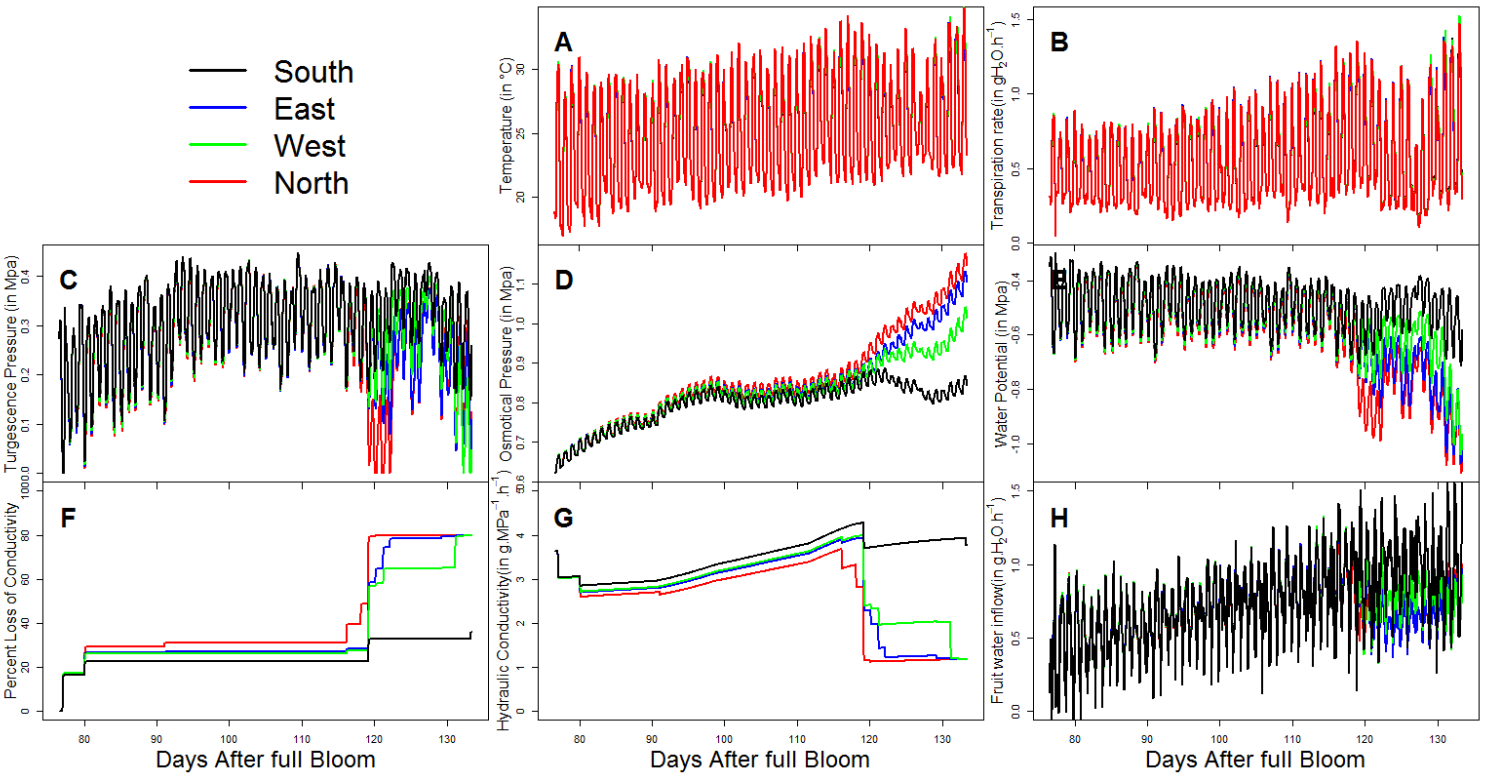

Figure 37: Les variations saisonnières de température (A), de transpiration (B), de pression de turgescence (C), de pression osmotique (D), de potentiel hydrique (E), de perte de conductivité hydraulique des vaisseaux conducteurs de sève (F), de conductivité hydraulique des vaisseaux conducteurs de sève (G) et des flux d'eau entrant dans le fruit (H) simulées pour des fruits ensoleillés sans contrainte carbonée, i.e., 100 feuilles par fruit, positionnés au nord, au sud, à l'est et à l'ouest de la canopée pendant la saison de croissance 2000-2001. Les positions des fruits dans l'arbre sont indiquées sur les graphiques.

La Figure 37 présente les variations simulées des variables impliquées dans le bilan hydrique des fruits du traitement 100 L/F pendant la saison de croissance 2000-2001. Quelle que soit la position du fruit dans l'arbre, d'importantes variations journalières de température et de transpiration ont été simulées par le modèle (Figure 37A et Figure 37B). Il a été simulé que les pertes en eau par transpiration augmentent au cours du développement du fruit quelle que soit sa position dans l'arbre (Figure 37B). Les résultats indiquent que la température et la transpiration des mangues varient selon leur position dans l'arbre (Figure 37A et Figure 37B). Les pertes en eau par transpiration simulées sur la période étudiée, i.e. de 77 à 133

DAB, pour les fruits positionnés au nord, à l'est, à l'ouest, et au sud, sont égales à 755, 750, 749 et 741 $gH_2O\ fruit^{-1}$, respectivement.

Les simulations du modèle ont indiqué que la pression osmotique de la mangue augmente au cours de son développement, quelle que soit sa position dans l'arbre (Figure 37D). Cette augmentation s'explique en partie par le fait que la concentration en solutés dans la pulpe augmente avec les degrés jours (Table 13). Les différences de potentiel osmotique simulées par le modèle s'expliquent donc en partie par les variations de température entre les fruits dans l'arbre (Figure 37D). Etant donné que la concentration en solutés dans la pulpe varie également en fonction de la masse d'eau du fruit (Equation 44), il en est déduit que les différences de transpiration simulées entre les fruits (Figure 37B) sont également à l'origine des variations du potentiel osmotique.

Des différences de pression de turgescence ont également été simulées en fonction de la position des fruits (Figure 37C). Ces variations s'expliquent par le fait que la pression de turgescence varie en fonction du potentiel osmotique et de la transpiration du fruit (Equation 47). L'augmentation de la pression osmotique, associée à la diminution de la pression de turgescence, est à l'origine de la diminution du potentiel hydrique du fruit simulée à la fin de la saison de croissance (Equation 43).

Il a été montré que la diminution du potentiel hydrique varie selon la position des fruits dans l'arbre (Figure 37E) et entraine l'apparition plus ou moins rapide d'embolie dans les vaisseaux conducteurs de sève (Figure 37F). Il a ainsi été simulé que les vaisseaux conducteurs de sève des fruits les plus exposés au soleil, i.e. au nord, s'embolisent plus rapidement (Figure 37F). En conséquent la conductivité hydraulique (Figure 37G) et les flux d'eau entrant dans le fruit (Figure 37H) diminuent à des vitesses différentes selon la position des fruits dans l'arbre. La diminution des flux d'eau entrant dans le fruit après 120 DAB (Figure 37H) est liée au ralentissement de croissance des mangues simulé et mesuré (Figure 375).

D - Discussion

Le modèle thermodynamique que nous avons développé précédemment (Nordey et al., 2014c) a été couplé au modèle de croissance en matière fraiche proposé par Léchaudel et al. (2007) afin d'étudier l'impact des variations climatiques au sein de l'arbre sur la croissance de la mangue. Les résultats que nous avions rapportés précédemment (Partie II chapitre III) concernant les changements de conductivité hydraulique du xylème au cours de la croissance de la mangue ont été pris en compte dans cette approche de modélisation.

L'ajustement du modèle proposé dans cette étude est satisfaisant et comparable à celui obtenu par Léchaudel et al. (2007). Il permet de simuler avec précision les contractions journalières de la mangue et les différences de croissance en matière fraiche mesurées entre les traitements de charge en fruits. En accord avec les études précédemment réalisées sur la mangue (Hofman et al., 1995, Uthaibutra et al., 1998), il a été simulé que les fruits les plus exposés, i.e. au nord, ont un calibre inférieur. Ces différences ont été attribuées aux variations de température et de transpiration simulées par le modèle entre les mangues dans l'arbre. Les variations de calibre simulées entre mangues selon leur position étaient plus marquées pour les traitements de faible charge en fruits, i.e. 100 et 150 L/F. Ceci peut s'expliquer par le fait que les différences de transpiration simulées entre les fruits selon leur position dans l'arbre augmentent avec le volume du fruit.

Les simulations ont indiqué que la conductivité hydraulique des vaisseaux conducteurs de sève, après avoir augmenté pendant la croissance du fruit, diminue au cours des derniers stades de son développement entrainant le déclin des flux d'eau entrant dans la mangue et le ralentissement de sa croissance. Ces simulations sont cohérentes avec les résultats de notre étude précédente qui montrent que la conductivité hydraulique du xylème et les flux de xylème entrant dans le fruit diminuent à la fin de la saison de croissance de la mangue (Partie II chapitre III). Dans le modèle proposé, la diminution de la conductivité hydraulique est liée à l'apparition d'embolie causée par le déclin du potentiel hydrique du fruit. Ces simulations sont en accord avec la diminution du potentiel hydrique du fruit et l'apparition d'embolie dans les vaisseaux du xylème mesurées dans les derniers stades de développement de la mangue (Partie II chapitre III) (Léchaudel et al., 2012) et du pigment (Trifilò et al., 2010).

En ajoutant au modèle proposé par Léchaudel et al. (2007) l'effet de l'embolie sur la conductivité hydraulique des vaisseaux conducteurs de sève, les paramètres utilisés pour simuler l'arrêt de croissance du fruit, i.e. DD_{ini} et τ, se sont avérés inutiles. Il avait été estimé dans le modèle initial, que la valeur de DD_{ini} varie selon la saison de production. La suppression de ce paramètre permet de ne pas devoir re-calibrer le modèle pour chaque saison de croissance. Il s'est par ailleurs avéré que l'augmentation de la pression seuil de la croissance plastique, i.e., Y, avec le volume du fruit diminue la qualité prédictive du modèle. En lien avec l'étude de Green et al. (1971), il a été estimé dans le modèle initial de Léchaudel et al. (2007) que Y augmente avec le volume du fruit. Hors, il a été montré que Y diminue en fonction du potentiel osmotique (Frensch and Hsiao, 1995). Etant donné que le potentiel osmotique du fruit augmente au cours de sa croissance, il est difficile de prédire comment varie Y. En conséquent par soucis de simplification il a été estimé que Y ne varie pas.

L'approche de modélisation proposée dans cette étude apporte donc des évidences théoriques de l'impact de l'embolie et des conditions climatiques sur la croissance du fruit en matière fraiche. Le modèle présenté n'a permis d'expliquer qu'une part des variations de croissance en matière fraiche observée entre les mangues. Ceci suggère que d'autres facteurs que ceux pris en compte dans le modèle sont impliqués dans les différences de calibre entre les mangues. Dans le modèle proposé, il a été considéré que la disponibilité carbonée des fruits ne variait pas selon leur position dans l'arbre. Hors, les différences climatiques au sein de l'arbre sont susceptibles de faire varier la disponibilité carbonée des fruits. Il serait donc intéressant dans une prochaine étude d'inclure au modèle présentement proposé l'effet des conditions climatiques sur la croissance en matière sèche du fruit.

V - Analyse des sources de variabilité du calibre, de la teneur en matière sèche et de la date de récolte des mangues : une approche de modélisation.

Objectifs :

Les chapitres précédents ont montré l'importance de la disponibilité carbonée de la mangue sur sa croissance en matière fraiche (Partie II chapitre IV) et son mûrissement (Partie II chapitre II). Pour simuler simultanément la croissance en matière fraiche et sèche de la mangue ainsi que son mûrissement, il est proposé dans ce dernier chapitre de coupler au modèle de croissance en matière sèche de la mangue proposé par Léchaudel et al. (2005a) l'ensemble des modèles présentés dans ce travail de thèse. Cette approche s'appuie sur le modèle de transpiration et de température présenté dans la partie I chapitre II, le modèle de synthèse d'éthylène présenté dans la partie II chapitre II, et le modèle de croissance en matière fraiche présenté dans la partie II chapitre IV. Le couplage de ces modèles permet d'avoir une vision globale des facteurs impliqués dans l'élaboration de la qualité de la mangue et dans son mûrissement.

Principaux résultats :

- Le calibre, la teneur en matière sèche et la date de récolte des mangues varient selon les conditions de croissance du fruit.

- La charge en fruits a un impact important sur le calibre, la teneur en matière sèche et la date de récolte des mangues.

- Les différences de floraison au sein de l'arbre et de masse sèche du fruit à la fin de la division cellulaire sont impliquées dans les variations du calibre, de la teneur en matière sèche, et de la date de récolte des mangues.

Analyse des sources de variabilité du calibre, de la teneur en matière sèche et de la date de récolte des mangues : une approche de modélisation.

A - Introduction

L'hétérogénéité de la qualité des mangues cause des pertes importantes tout au long de la chaine de distribution. La qualité du fruit regroupe un ensemble d'attributs comme le calibre, la saveur sucrée et acide, et la couleur qui varient avec les concentrations en composés primaires (sucres, acides) et secondaires (pigments, vitamines, et arômes) dans la mangue. Ces composés sont contenus dans la matière sèche et leur concentration varient avec la matière fraiche du fruit (Génard et al., 2014) et au cours du mûrissement (Litz, 2009, Joas et al., 2012). Il en est déduit que la croissance en matière sèche et fraiche du fruit ainsi que son mûrissement sont des processus déterminants de sa qualité.

Les études précédentes ont montré que les différences de climat et de charge en fruits au sein de l'arbre sont impliquées dans les différences de croissance en matière fraiche (Partie II chapitre IV) et sèche (Léchaudel et al., 2005b) et de maturité (Partie II chapitre II) entre les mangues. Ces différences peuvent être attribuées également aux décalages temporels entre les floraisons au sein du manguier (Dambreville et al., 2013). Léchaudel and Joas (2007) rapportent que les différences de masse sèche entre les mangues à la fin de la phase de division cellulaire expliquent en partie les différences de croissance des fruits.

Ces études indiquent que les processus liés à la croissance du fruit et à son mûrissement varient en fonction de nombreux facteurs. Une approche de modélisation a été développée pour étudier comment les conditions de croissance, i.e. conditions climatiques, charge en fruits, date de floraison, masse sèche du fruit à la fin de la division cellulaire, sont impliquées dans la croissance de la mangue et dans son mûrissement. Cette approche s'appuie sur le couplage des modèles présentés précédemment au modèle de croissance en matière sèche proposé par Léchaudel et al. (2005a).

Dans un premier temps, le modèle proposé par Léchaudel et al. (2005a) devra être calibré afin de prendre en compte l'impact de la température du fruit sur sa croissance en matière sèche. Puis la qualité du nouveau modèle sera évaluée et une analyse par simulation permettra de mettre en évidence comment les conditions de croissance sont à l'origine des différences de croissance et de maturité entres les mangues.

B - Matériels et méthodes

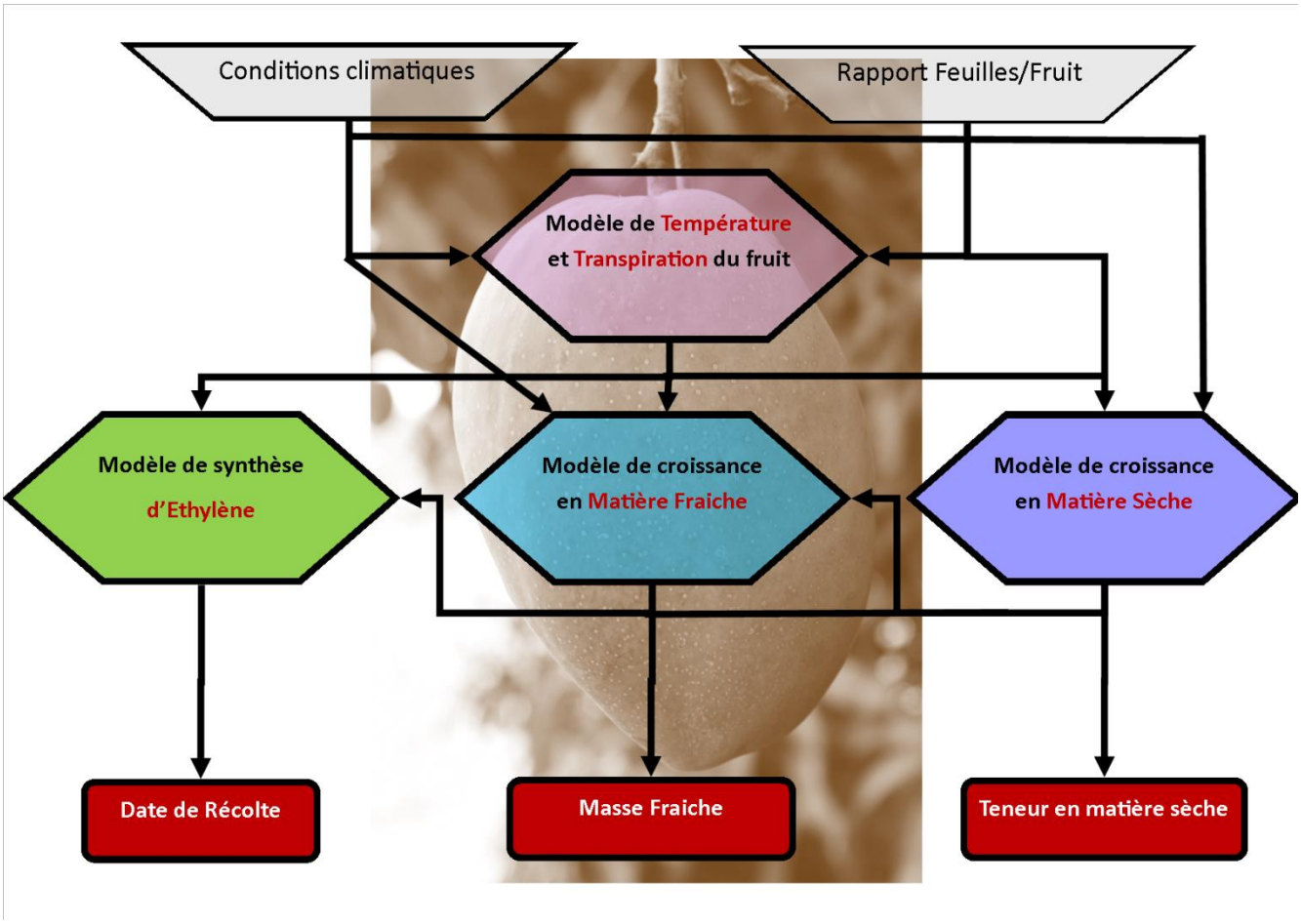

Figure 38: Représentation schématique du couplage des modèles (i) de transpiration et de température, (ii) de synthèse d'éthylène, (iii) de croissance en matière fraiche et (iv) de croissance en matière sèche de la mangue.

1) **Présentation du modèle**

Le modèle proposé dans cette étude est composé de quatre sous modules (Figure 38). Le premier module permet de simuler l'impact des conditions climatiques sur la température et la transpiration du fruit. Il s'appuie sur le modèle physique proposé par Nordey et al. (2014c) qui simule les variations spatiales et temporelles de la température de la mangue selon sa position dans l'arbre. Le second module permet de simuler la croissance en matière fraiche du fruit. Ce dernier repose sur le modèle présenté précédemment dans la partie II chapitre IV. L'évolution de la maturité de la mangue au cours de la saison est simulée grâce à un troisième module. Celui-ci s'appuie sur le modèle présenté dans la partie II chapitre II qui simule les variations saisonnières de la concentration en éthylène de la mangue, utilisée

comme un indicateur de la maturité du fruit. Enfin, le dernier module permet de simuler la croissance en matière sèche de la mangue en s'appuyant sur le modèle proposé par Léchaudel et al. (2005a). Ce modèle simule la croissance en matière sèche du fruit en décrivant les relations sources-puits à l'échelle du rameau. Il décrit un système basé sur trois composantes : le fruit, les feuilles et le rameau. La répartition des carbohydrates au sein de ce système satisfait dans l'ordre (1) les besoins de maintenance du système, (2) les besoins de croissance des organes reproducteurs, i.e. les fruits, (3) et enfin les besoins liés à l'accumulation de réserves dans les feuilles et dans le rameau.

a) Assimilation du carbone par les feuilles

Dans le modèle proposé par Léchaudel et al. (2005a), il est considéré que l'activité photosynthétique des feuilles est liée par une fonction asymptotique à la demande des fruits (D_{fruit}, gC m^{-2} $jour^{-1}$) quand elles sont saturées en lumière (P_{max}, µmol CO_2 m^{-2} s^{-1}):

$$P_{max} = \frac{p_1 D_{fruit} p_2}{p_1 D_{fruit} + p_2} \quad (if\ P_{max} < P^*_{max}) \qquad \textit{Equation 50}$$

$$P_{max} = P^*_{max} \qquad (if\ P_{max} \geq P^*_{max})$$

Où p_1 (µmol CO_2 m^{-2} s^{-1} gC^{-1}) et p_2 (µmol CO_2 m^{-2} s^{-1}) sont des paramètres et P^*_{max} (µmol CO_2 m^{-2} s^{-1}) est le potentiel photosynthétique des feuilles avec une saturation en lumière.

La photosynthèse par unité de surface foliaire (P_1, µmol CO_2 m^{-2} s^{-1}) est calculée par :

$$P_1 = (P_{\max} + p_3)\left[1 - \exp\left(\frac{-p_4\, PPF}{P_{\max} + p_3}\right)\right] - p_3 \qquad \textit{Equation 51}$$

Où PPF est le flux de photons photosynthétiquement actifs (µmol m^{-2} s^{-1}) et où p_3 (CO_2 m^{-2} s^{-1}) et p_4 sont des paramètres. PPF est estimé en fonction de la moyenne horaire du rayonnement global (RG, W m^{-2}) :

$$PPF = RG\ k_1\ k_2 \qquad \textit{Equation 52}$$

Où k_1=0.5 est la fraction du rayonnement global qui est photosynthétiquement actif et k_2 = 4.6 µmol W^{-1} s^{-1} est le coefficient de conversion de W m^{-2} en µmol m^{-2} s^{-1}. La photosynthèse des feuilles ombragées est calculée en fonction du rayonnement reçu par celles-ci (PPF_{shaded}, µmol m^{-2} s^{-1}) qui est déterminé par la relation empirique proposée par Léchaudel et al. (2005a).

$$PPF_{shaded} = 0.0529\ PPF \qquad \textit{Equation 53}$$

La quantité de carbone fixée par jour par la photosynthèse des feuilles (C_1, gC jour^{-1}) est égale à la somme de la photosynthèse horaire des feuilles ombragées et ensoleillées :

$$C_1 = \left(\sum_h P_1^{Ensoleillé} \; LA_{Ensoleillé} + \sum_h P_1^{Ombragé} \; LA_{Ombragé} \right) k \qquad \textit{Equation 54}$$

Où $LA_{Ensoleillé}$ et $LA_{Ombragé}$ sont les surfaces foliaires (m²), au soleil et à l'ombre, respectivement, et k = 0.0432 est le coefficient de conversion de la photosynthèse foliaire de µmol CO_2 s^{-1} en gC h^{-1}. La surface foliaire du rameau a été calculée en fonction du nombre de feuilles portées par celui-ci (n_{leaves}) en utilisant la relation empirique proposée par Léchaudel et al. (2005a) :

$$LA = 0.0051 \; (n_{leaves})^{0.937} \qquad \textit{Equation 55}$$

b) Demande du fruit

Dans le modèle proposé par Léchaudel et al. (2005a), il est estimé que la croissance des tiges et des feuilles est nulle pendant le développement du fruit. La demande journalière en carbone du fruit pour sa croissance (D_{fruit}, gC jour) est estimée par la relation suivante :

$$D_{fruit} = \frac{\Delta DM_f^{pot}}{\Delta dd} \frac{\Delta dd}{\Delta t} \left(c_{fruit} + GRC_{fruit} \right) \qquad \textit{Equation 56}$$

Où ΔDM_f^{pot} (g dd^{-1}) est l'accroissement potentiel en matière sèche du fruit par degré jour (Δdd, °C jour), c_{fruit} (gC g^{-1}) est la concentration du fruit en carbone et GRC_{fruit} (gC g^{-1}) est le coefficient de respiration de croissance du fruit. Contrairement au modèle initial proposé par Léchaudel et al. (2005a), les degrés jours sont calculés, non pas en fonction de la température de l'air, mais en fonction de la température moyenne du fruit simulée.

La croissance potentielle du fruit en matière sèche correspond à celle mesurée lorsque le fruit est placé dans des conditions non restrictives pour sa croissance en matière sèche. Il est considéré que la croissance en matière sèche de la mangue n'est pas limitée avec une charge en fruits inférieure ou égale à 100 feuilles par fruit (Léchaudel and Joas, 2006).

L'accroissement potentiel en matière sèche du fruit par degré jour, i.e. $\frac{\Delta DM_f^{pot}}{\Delta dd}$, est calculé à partir, du taux de croissance du fruit en matière sèche (RGR_f^{ini} , dd^{-1}), de la masse sèche du fruit (DM_f, g) et de la masse sèche du fruit à la fin de son développement (DM_f^{max}, g) :

$$\frac{\Delta DM_f^{pot}}{\Delta dd} = RGR_f^{ini}\, DM_f \left(1 - \frac{DM_f}{DM_f^{max}}\right) \quad \textit{Equation 57}$$

Dans le modèle proposé par Léchaudel et al. (2005a), DM_f^{max} est calculé en fonction de la masse sèche du fruit à la fin de la division cellulaire (DM_f^{ini}, g) et de deux paramètres, a et b.

$$DM_f^{max} = a\left(DM_f^{ini}\right)^b \quad \textit{Equation 58}$$

En lien avec le modèle initial proposé par Léchaudel et al. (2005a), il a été estimé que la division cellulaire se termine 350°C jours après la pleine floraison.

c) Respiration de maintenance

L'effet de la température sur la respiration de maintenance de l'organe *i* (R_i^{maint} , gC jour^{-1}) a été pris en compte grâce au concept du Q_{10}. R_i^{maint} , exprimée en gC jour^{-1}, a été déduite de la respiration de maintenance calculée à l'échelle horaire (MR_i, en gC h^{-1}) :

$$MR_i = MRR_i\, (Q_{10}^i)^{\frac{\theta_i - \theta_{ref}}{10}}\, DM_i \quad \textit{Equation 59}$$

Où MRR_i est la respiration de maintenance (gC g^{-1} h^{-1}) d'un organe *i* à la température de référence θ_{ref} (°C), Q_{10}^i est la valeur de Q_{10} pour l'organe *i*, θ_i est la température moyenne horaire de l'organe *i* (°C) et DM_i (g) est la masse sèche de l'organe. La température moyenne du fruit a été estimée grâce au modèle proposée par Nordey et al. (2014c), tandis qu'il a été considéré que les températures moyennes des feuilles et du rameau sont égales à celle de l'air.

d) Mobilisation des réserves

Si la quantité de carbohydrates produits par la photosynthèse est inférieure à celle requise pour la maintenance et la croissance du système, les réserves contenues dans les feuilles (R_l, gC jour^{-1}) sont mobilisées. Si la mobilisation des réserves contenues dans les feuilles ne suffit pas à satisfaire la demande, les réserves de la tige sont alors mobilisées (R_s, gC jour^{-1}) :

$$R_l = r_4\, n_{leaves} M_L c_L$$
$$R_s = r_5\, M_s c_s \quad \textit{Equation 60}$$

Où r_4 et r_5 représentent les fractions mobilisables des réserves des feuilles et de la tige, respectivement, n_{leaves} représente le nombre de feuille, M_l (gMS) et M_s (gMS) représentent

les masses sèches d'une feuille et de la tige, respectivement, et c_l (gC gMS^{-1}) et c_s (gC gMS^{-1}) représentent les teneurs en carbone de la feuille et de la tige, respectivement.

2) **Données d'entrée et valeurs initiales du modèle**

Les données climatiques utilisées pour le fonctionnement du modèle simulant la température et la transpiration du fruit, i.e., la température de l'air, l'humidité relative, la vitesse du vent, et le rayonnement global, sont mesurées toutes les minutes, moyennées et enregistrées toutes les heures dans une centrale d'acquisition (Model 21 X, Campbell Scientific Ltd, Logan, UT, USA) pendant toute la saison de croissance. Les rayonnements direct et diffus sont déduits du rayonnement global en utilisant le modèle développé par Maxwell E.L. (1987). La course du soleil a été déterminée en utilisant l'algorithme de la position du soleil (SPA) développé par Reda and Andreas (2004). Le modèle requière également les propriétés physiques et thermiques du fruit comme données d'entrée. Celles-ci ont été extraites de notre étude précédente (Nordey et al., 2014c). Pour les fruits au-dessus de la canopée il a été estimé qu'une partie du fruit était directement exposée au soleil et que la face opposée a reçu 20% du rayonnement, en accord avec les mesures de notre étude précédente. Pour les fruits sous la canopée il a été estimé qu'ils recevaient 20% du rayonnement global, comme les feuilles du rameaux qui les portent.

La masse sèche du fruit à la fin de la division cellulaire (DM_f^{ini}, g) est déterminée en mesurant le diamètre des fruits à 350°C jours après la pleine floraison (D_{ini}, mm) et en utilisant la relation empirique proposée par Léchaudel et al. (2007) :

$$DM_f^{ini} = 0.8191\ e^{0.051 D_{ini}} \qquad \textit{Equation 61}$$

3) **Paramétrisation et calibration du modèle.**

Les valeurs des paramètres des modèles simulant la croissance en matière fraiche et la synthèse d'éthylène de la mangue ont été extraites de nos études précédentes (Partie I chapitre II et Partie II chapitres II et IV). Les valeurs des paramètres du modèle de croissance en matière sèche ont été extraites de l'étude de Léchaudel et al. (2005a)(Table 15) sauf pour les paramètres RGR_f^{ini} , a et b qui ont été calibrés. Dans le modèle proposé dans cette étude il est considéré que la température du fruit est différente de celle de l'air et varie au sein de

l'arbre. Il a donc été nécessaire de calibrer les paramètres de la croissance potentielle du fruit en matière sèche (Equation 57) en fonction des degrés jour depuis la pleine floraison calculés à partir de la température du fruit simulée. La température du fruit dépend de sa position dans l'arbre (Saudreau et al., 2009). Pour tenir compte de ces variations, la moyenne des températures simulées pour des fruits positionnés au nord, au sud, à l'est, et à l'ouest de la canopée a été considérée.

Les paramètres de la croissance potentielle du fruit en matière sèche ont été estimés en minimisant le critère suivant:

$$\sum_{j} \frac{1}{N_j} \sum_{i} (DM_{ij}^{c} - DM_{ij})^2 \qquad \textit{Equation 62}$$

Où Nj est le nombre de fruits à la date *j*, DM_{ij}^{c} est la masse sèche du fruit *i* calculée à la date *j* grâce à l'Equation 57 et à l'Equation 58 et DM_{ij} est la masse sèche du fruit *i* mesurée à la date *j* sur des rameaux ayant une surface foliaire par fruit importante, i.e. 100 et 150 feuilles par fruit (L/F).

Table 15 : Paramètres du modèle de croissance en matière sèche de la mangue issus de Léchaudel et al. (2005a)

Paramètres	Signification	Valeur
P^*_{max}	Potentiel photosynthétique des feuilles avec une saturation en lumière	15.0 µmol CO_2 m^{-2} s^{-1}
p_1	Paramètre pour calculer le potentiel photosynthétique des feuilles	3.85 µmol CO_2 m^{-2} s^{-1} gC^{-1}
p_2	Paramètre pour calculer le potentiel photosynthétique des feuilles	33.23 µmol CO_2 m^{-2} s^{-1}
p_3	Paramètre pour calculer l'activité photosynthétique des feuilles	0.483 µmol CO_2 m^{-2} s^{-1}
p_4	Paramètre pour calculer l'activité photosynthétique des feuilles	0.034
c_{fruit}	Concentration en carbone du fruit	0.4239 gC g^{-1}
GRC_{fruit}	Coefficient de respiration de croissance du fruit	0.04 gC g^{-1}
T_b	Température de base	16°C
Q_{10}^{fruit}	Coefficient de température de la respiration de maintenance du fruit	1.90
Q_{10}^{tige}	Coefficient de température de la respiration de maintenance de la tige	1.96
$Q_{10}^{feuilles}$	Coefficient de température de la respiration de maintenance des feuilles	2.11
MRR_{fruit}	Respiration de maintenance du fruit	1.15 10^{-3} gC g^{-1} h^{-1}
MRR_{tige}	Respiration de maintenance de la tige	8.58 10^{-3} gC g^{-1} h^{-1}
$MRR_{feuille}$	Respiration de maintenance des feuilles	1.56 10^{-4} gC g^{-1} h^{-1}
r_4	Fraction mobilisables des réserves des feuilles	0.0162
r_5	Fraction mobilisables des réserves de la tige	0.0164
M_L	Masse sèche d'une feuille	0.8 g
M_s	Masse sèche de la tige	59.6 g
c_l	Teneur en carbone des feuilles	0.1 gC gMS^{-1}
c_s	Teneur en carbone de la tige	0.8 gC gMS^{-1}

4) **Simulations**

Pour tester l'ajustement du modèle, les croissances en matière fraiche et en matière sèche de fruits ensoleillés positionnés au nord, au sud, à l'est, et à l'ouest de la canopée avec des charges en fruits de 10, 25, 50, 100 et 150 L/F ont été simulées et comparées aux données mesurées.

Le modèle a ensuite été utilisé pour étudier l'impact des conditions de croissance sur le calibre, la teneur en matière sèche et la date de récolte des mangues. Pour se faire, la croissance en matière fraiche, la croissance en matière sèche et la concentration en éthylène des mangues ont été simulées pour différentes charges en fruits, i.e., 10, 25, 50, 100, et 150 L/F, différentes positions dans la canopée, i.e., au nord, au sud, à l'est, à l'ouest de la canopée, et sous la canopée, différentes dates de floraison, i.e., ± 15 jours, et différentes masses sèches de fruit à la fin de la division cellulaire, i.e., ± 25%.

Les mangues de la variété Cogshall sont communément récoltées pour la commercialisation à un stade de maturité appelé « point-jaune », facilement reconnaissable par la coloration jaune qui apparait à l'extrémité du fruit (Léchaudel and Joas, 2006). A ce stade de maturité, la concentration en éthylène du fruit est de l'ordre de 0.3 ppm (Nordey et al., 2014b). Il a donc été estimé dans les simulations que les mangues sont récoltées quand leur concentration en éthylène atteint 0.3 ppm.

5) **Données mesurées**

Les données de croissance utilisées sont celles présentées par Léchaudel et al. (2005a). Les mesures ont été effectuées pendant la saison de croissance 2000-2001 sur des manguiers de 11 ans situés à l'île de la Réunion (en 2000) de la variété « Cogshall » greffés sur la variété « Maison Rouge ». La croissance des fruits en matière fraiche et en matière sèche a été mesurée de manière destructive pendant la saison de production 2000-2001 pour 5 traitements de charge en fruits : 10, 25, 50, 100 et 150 feuilles par fruit. Ces traitements ont été réalisés en annelant et en défoliant les branches et en retirant si besoin des fruits.

C - Résultats

1) **Simulation de la croissance en matière fraiche et en matière sèche de la mangue et de sa concentration en éthylène.**

La calibration du modèle de croissance en matière sèche a permis d'estimer que les paramètres a, b et RGR_f^{ini} valent 82.78, 0.11 et 0.0108 dd^{-1}, respectivement. Les mesures ont indiqué que la masse sèche des mangue à la fin de la division cellulaire était égale à 15.26, 16.20, 18.5, 18.77 et 25.26 g pour les traitements de charge en fruits de 10, 25, 50, 100 et 150 L/F.

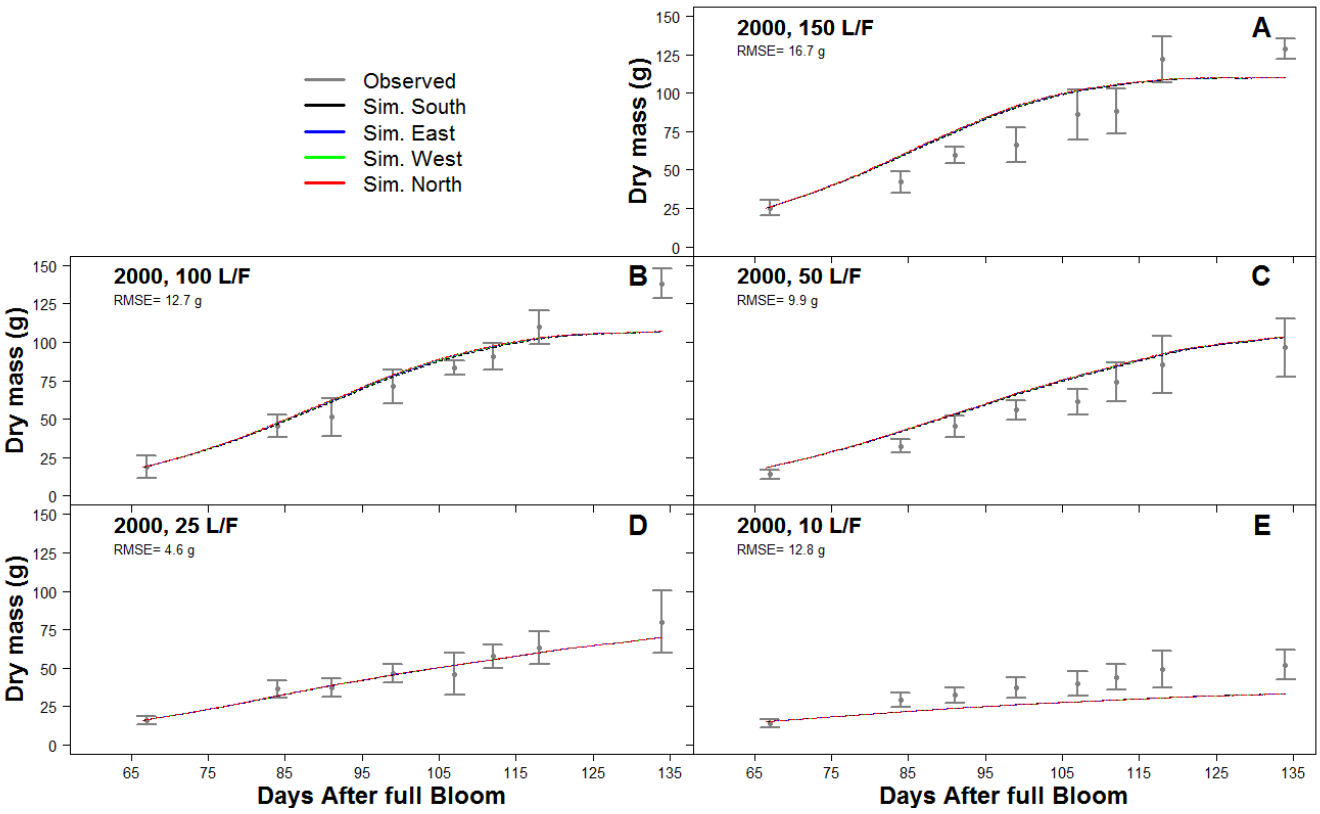

Figure 39: Les variations saisonnières simulées (ligne) et observées (points) de la matière sèche des fruits, en fonction du nombre de feuilles par fruit (L:F), i.e. 10, 25, 50, 100 et 150 L:F, et de la position du fruit dans l'arbre, i.e. au nord, au sud, à l'est et à l'ouest, pour la saison de croissance 2000-2001. Le nombre de feuilles par fruit, la position du fruit dans l'arbre, le root mean square error (RMSE) est indiqué sur les graphiques.

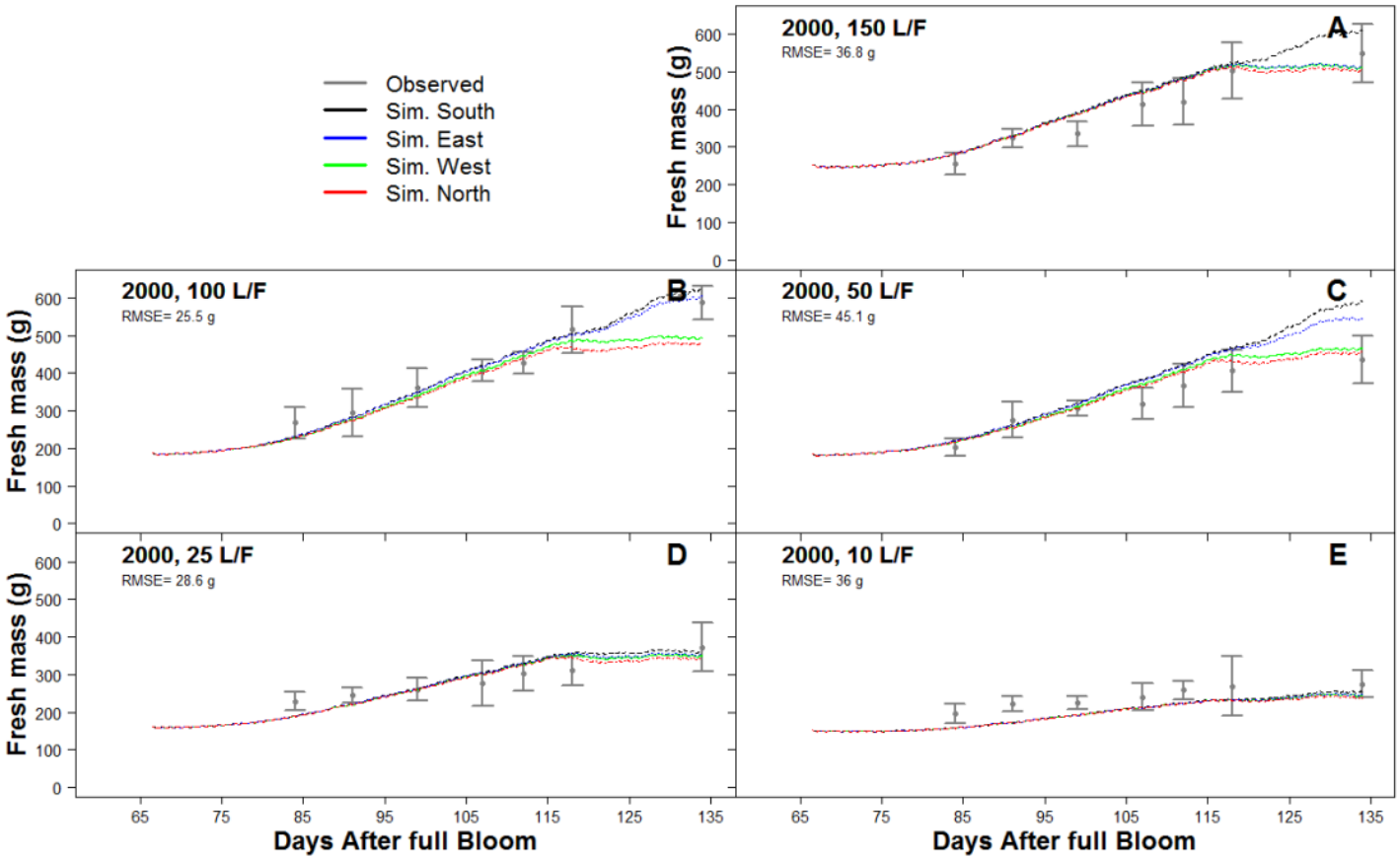

Figure 40: Les variations saisonnières simulées (ligne) et observées (points) de la matière fraiche des fruits, en fonction du nombre de feuilles par fruit (L:F), i.e. 10, 25, 50, 100 et 150 L:F, et de la position du fruit dans l'arbre, i.e. au nord, au sud, à l'est et à l'ouest, pour la saison de croissance 2000-2001. Le nombre de feuilles par fruit, la position du fruit dans l'arbre, le root mean square error (RMSE) est indiqué sur les graphiques.

Les simulations du modèle et les mesures de croissance des mangues en matière sèche et en matière fraiche ont été comparées (Figure 39 et Figure 40). Les résultats indiquent que le modèle permet de simuler correctement la croissance en matière sèche (Figure 39) et en matière fraiche (Figure 40) des mangues, quelle que soit la charge en fruits. Il a toutefois été noté que pour le traitement de forte charge en fruits, i.e., 10 L/F, le modèle a tendance à sous-estimer la croissance en matière sèche du fruit (Figure 39E). Les différences d'accumulation de matière fraiche et de matière sèche mesurées entre les différents traitements de charge en fruits sont correctement simulées par le modèle. Contrairement à l'accumulation de matière fraiche, l'accumulation de matière sèche simulée ne varie pas entre les fruits positionnés au nord, au sud, à l'est et l'ouest de la canopée. Les simulations

du modèle indiquent qu'en l'absence de contrainte carbonée, i.e. 100 et 150 L/F, les fruits les plus exposés, i.e. au nord, s'arrêtent de grandir après 115 DAB à cause de l'embolisation des vaisseaux conducteurs de sève (Figure 41) contrairement aux fruits moins exposés, i.e. au sud.

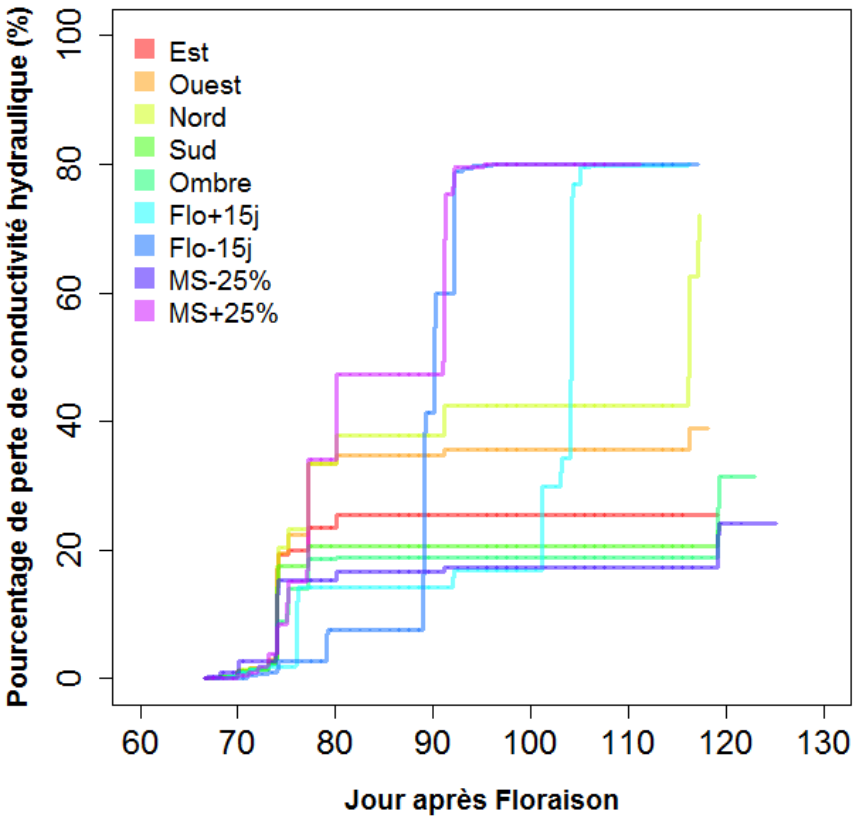

Figure 41 : Les variations saisonnières de perte de conductivité hydraulique des vaisseaux conducteurs de sève simulées par le modèle due à la formation d'embolie pour différentes positions dans l'arbre, i.e., au sud, au nord, à l'est, à l'ouest et à l'ombre, pour différentes dates de floraison, i.e., ± 15 jours, et différentes masse sèche du fruit à la fin de la division cellulaire, i.e., ± 25%, pour le traitement 100 feuilles par fruit. Les positions dans l'arbre, les dates de floraison et les masses sèches des fruits à la fin de la division cellulaire sont indiquées sur le graphique.

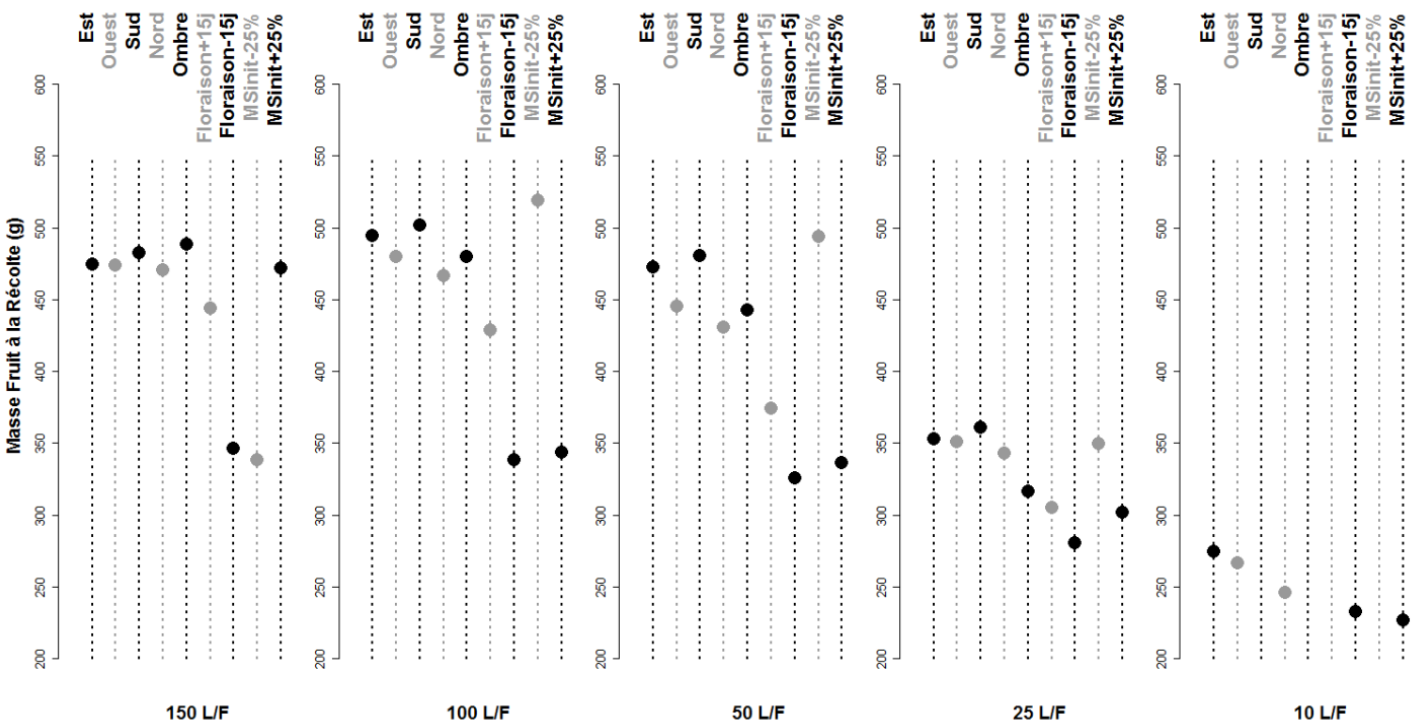

Figure 42: Masses du fruit à la récolte simulées par le modèle pour différentes positions dans l'arbre, i.e. au sud, au nord, à l'est, à l'ouest et à l'ombre, différentes dates de floraison, i.e., ± 15 jours, différentes masses sèches du fruit à la fin de la division cellulaire, i.e. ± 25%, et différentes charges en fruits (L/F), i.e. 10, 25, 50, 100 et 150 L/F. Les charges en fruits, les positions des fruits dans l'arbre, les dates de floraison et les masses sèches des mangues à la fin de la division cellulaire sont indiquées sur le graphique.

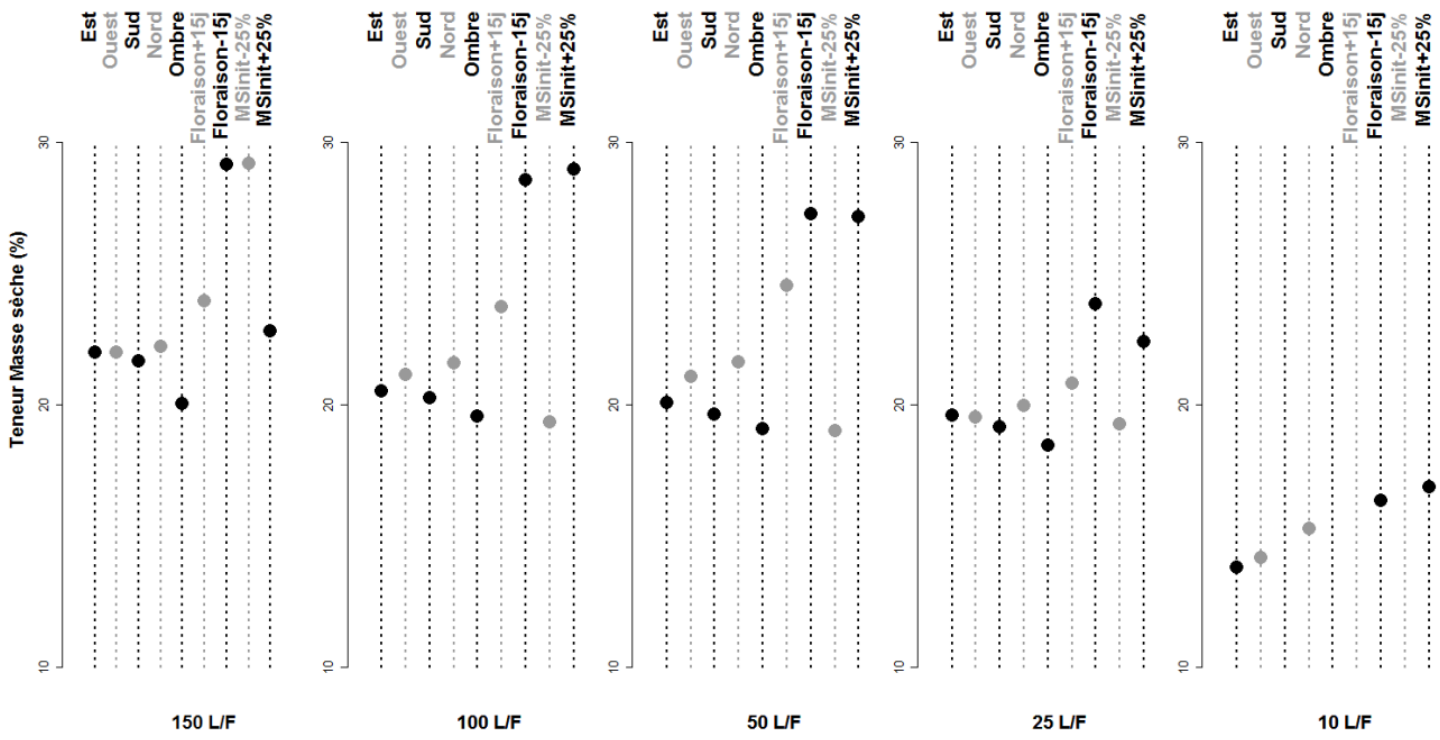

Figure 43: Teneurs en matière sèche du fruit à la récolte simulées par le modèle pour différentes positions dans l'arbre, i.e. au sud, au nord, à l'est, à l'ouest et à l'ombre, différentes dates de floraison, i.e., ± 15 jours, différentes masses sèches du fruit à la fin de la division cellulaire, i.e. ± 25%, et différentes charges en fruits (L/F), i.e. 10, 25, 50, 100 et 150 L/F. Les charges en fruits, les positions des fruits dans l'arbre, les dates de floraison et les masses sèches des fruits à la fin de la division cellulaire sont indiquées sur le graphique.

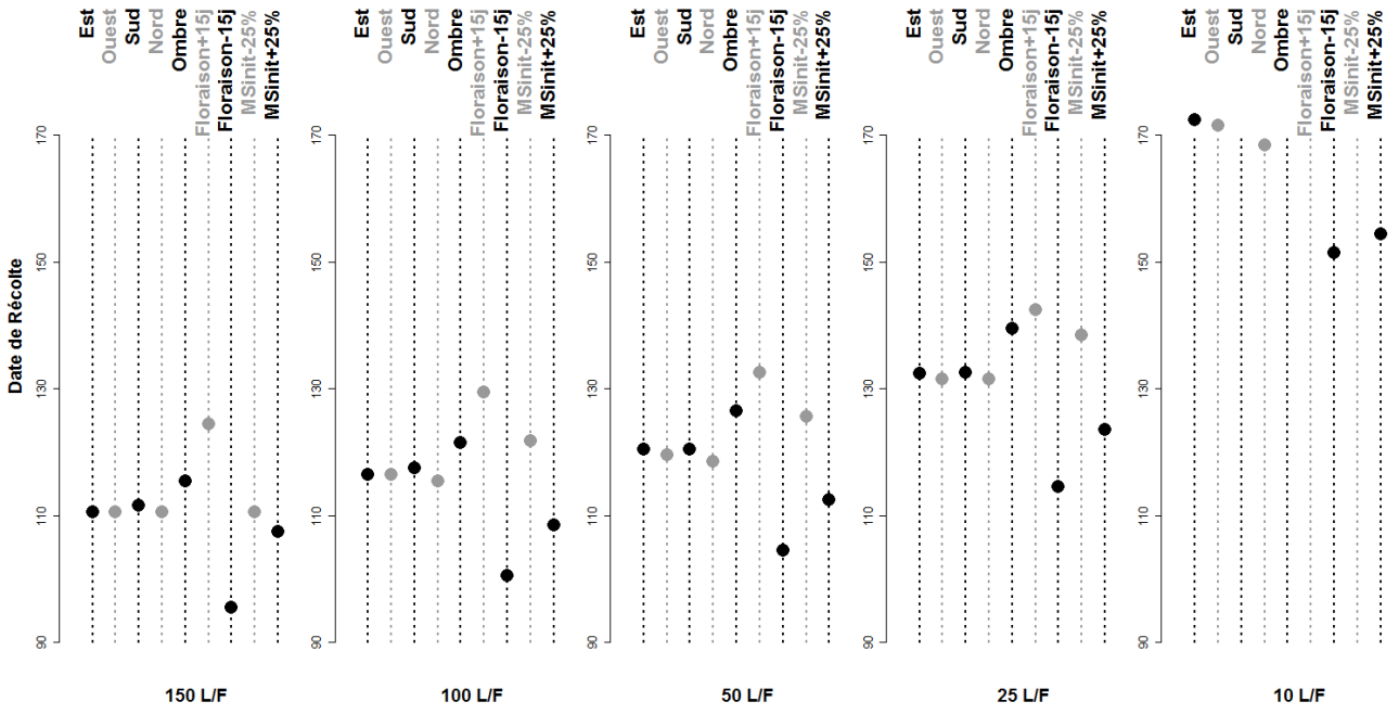

Figure 44: Dates de récolte des mangues simulées par le modèle pour différentes positions dans l'arbre, i.e. au sud, au nord, à l'est, à l'ouest et à l'ombre, différentes dates de floraison, i.e., ± 15 jours, différentes masses sèches du fruit à la fin de la division cellulaire, i.e. ± 25%, et différentes charges en fruits (L/F), i.e. 10, 25, 50, 100 et 150 L/F. Les charges en fruits, les positions des fruits dans l'arbre, les dates de floraison et les masses sèches des fruits à la fin de la division cellulaire sont indiquées sur le graphique.

2) **Simulation de l'impact des conditions de croissance de la mangue sur sa masse fraiche, sa teneur en matière sèche et sa date de récolte.**

Le modèle a été utilisé pour simuler l'impact des conditions de croissance de la mangue sur sa date de récolte, sa masse fraiche et sa teneur en matière sèche (Figure 42, Figure 43 et Figure 44). Certaines simulations du traitement 10 L/F, i.e. -25% MS, Flo-15 et Sud, n'ont pas pu être présentées faute de données météorologiques. En lien avec les résultats précédents, d'importantes variations de calibre, de teneur en matière sèche et de date de récolte ont été simulées entre les charges en fruits. Les simulations du modèle ont indiqué que les fruits avec une alimentation carbonée limitante, i.e. 10, 25 et 50 L/F, sont récoltés plus tard et ont un calibre et une teneur en matière sèche inférieurs. Le calibre et la teneur en matière sèche simulés pour des mangues à l'ombre et au soleil sont similaires, bien que des dates de récolte différentes aient été simulées. Il a été simulé que les fruits issus d'une floraison plus précoce sont récoltés plus tôt, ont un calibre inférieur et une teneur en matière sèche plus élevée. Ceci s'explique par les résultats présentés dans la Figure 41 qui montrent qu'une embolisation plus précoce des vaisseaux conducteurs de la sève a été simulée pour ces fruits.

Le modèle indique que les fruits avec une masse sèche plus importante à la fin de la division cellulaire sont récoltés plus tôt, quelle que soit la charge en fruits. Il a été simulé que ces fruits ont un calibre inférieur et une teneur en matière sèche plus élevée, pour tous les traitements de charge en fruits sauf celui de 150 L/F. Cette différence s'explique également par une embolisation plus précoce des vaisseaux conducteurs de la sève (Figure 41).

D - Discussion

Ce travail de modélisation vise à comprendre quels sont les facteurs impliqués dans les différences de qualité et de maturité observées entre les mangues à la récolte. Plusieurs modèles développés précédemment sur la mangue ont été couplés afin de simuler simultanément la croissance en matière fraiche, la croissance en matière sèche et la synthèse d'éthylène dans le fruit. Le modèle proposé permet de simuler correctement la croissance en matière sèche et en matière fraiche des mangues, quelle que soit la charge en fruits (Figure 39 et Figure 40).

L'utilisation du modèle a mis en évidence que la charge en fruits est impliquée à plusieurs niveaux dans l'élaboration de la qualité du fruit et dans sa maturité. En accord avec les études précédentes (Léchaudel and Joas, 2006, Joas et al., 2012), il a été simulé que les mangues qui se développent avec une forte charge en fruits sont récoltées plus tardivement et ont un calibre et une teneur en matière sèche inférieurs (Figure 42, Figure 43 et Figure 44). Les simulations indiquent qu'une charge en fruits de 100 L/F est un bon compromis entre le rendement et la qualité des fruits, en accord avec les résultats de Léchaudel and Joas (2006). Il a en effet été simulé et observé que le calibre et la teneur en matière sèche des mangues augmentent jusqu'à 100 feuilles par fruit mais pas au-delà. Les différences de croissance en matière sèche simulées entre les différents traitements de charge en fruits s'expliquent à la fois par les différences de disponibilité carbonée et par les différences de masse sèche des fruits à la fin de la division cellulaire. Dans le formalisme proposé par Léchaudel et al. (2005a), la croissance potentielle de la mangue en matière sèche est estimée en fonction de sa masse sèche à la fin de la division cellulaire (Equation 58). C'est pourquoi des différences de teneur en matière sèche ont été simulées quand la masse sèche du fruit à la fin de la division cellulaire a été augmentée ou diminuée.

Les différences de calibre simulées et mesurées entre les traitements de charge en fruits confirment la relation que nous avions mise en évidence dans notre étude précédente (Partie II chapitre IV) entre l'accumulation de matière fraiche et de matière sèche dans la mangue. Il avait été montré que les flux d'eau entrant dans le fruit dépendent du potentiel hydrique du fruit qui varie en fonction de sa composition en matière sèche. En conséquent, une forte charge en fruit restreint à la fois la croissance en matière sèche et en matière fraiche de la mangue.

Le modèle a par ailleurs indiqué que la charge en fruits impactait la vitesse de mûrissement de la mangue. Dans le modèle proposé il est considéré que la production d'éthylène du fruit régule son mûrissement. En lien avec le formalisme proposé par Génard and Gouble (2005), il a été estimé que la production d'éthylène du fruit dépend de sa concentration en ATP qui augmente avec sa respiration de croissance en matière sèche. C'est pourquoi les simulations du modèle indiquent que les mangues avec une faible charge en fruits, qui ont une croissance en matière sèche plus rapide, murissent plus vite.

Des différences de croissance et de vitesse de mûrissement ont également été simulées entre les mangues selon leur position dans l'arbre. Ces résultats confirment les études réalisées sur la mangue (Hofman et al., 1995, Uthaibutra et al., 1998). Les simulations indiquent que les fruits à l'ombre, murissent plus tard que les fruits au soleil mais ont un calibre et une teneur en matière sèche à la récolte similaires, en accord avec l'étude de Joas et al. (2012). L'absence de différence de calibre et de teneur en matière sèche entre les fruits à l'ombre et au soleil repose en partie sur le fait qu'il a été estimé que la masse sèche des mangues à la fin de la division cellulaire ne varie qu'en fonction de la charge en fruits. Hors, comme suggéré par Léchaudel and Joas (2007) les différences de climat au sein de la l'arbre sont susceptibles d'induire des variations de masse sèche entre mangues à la fin de la division cellulaire. Il serait donc intéressant de vérifier dans de prochaines études si la masse sèche des mangues à la fin de la division cellulaire ne varie pas au sein de l'arbre.

Les simulations ont indiquées que l'asynchronisme de la floraison du manguier participe à la différence de qualité et de maturité entre les mangues. Des différences de calibre et de teneur en matière sèche ont été effectivement simulées entres les mangues issues de floraisons différentes du fait qu'elles n'aient pas subit les même conditions climatiques pendant leur développement. La maitrise de la floraison permettrait de produire des mangues de qualité homogène aux périodes où le marché est le plus favorable. Cependant la floraison du manguier est un processus physiologique complexe qui dépend de multiples facteurs comme l'âge des pousses végétatives (Dambreville et al., 2013), les conditions climatiques et la disponibilité hydrique (Davenport, 2007, Litz, 2009).

L'analyse du modèle indique que les différences de calibre et de teneur en matière sèche simulées sont liées en partie aux différences d'embolisation des vaisseaux conducteurs de sève. Il peut être observé sur la Figure 41 que la perte de conductivité hydraulique due à la présence d'embolie est un processus très sensible car il augmente de manière très brutale. Ceci s'explique par la relation utilisée dans le modèle entre le potentiel hydrique du fruit et la perte de conductivité hydraulique. Cette relation implique qu'une diminution du potentiel hydrique du fruit de -0.7 à -0.8 MPa fait augmenter la perte de conductivité hydraulique de 30% à 70%. Etant donné l'importance de ce processus dans le modèle, de prochains travaux devraient affiner cette relation.

Conclusions et perspectives.

I - Bilan des connaissances acquises

Des approches expérimentale et de modélisation ont été employées dans ce travail de thèse pour identifier les causes de l'hétérogénéité de la qualité et de la maturité au sein de la mangue et entre les mangues dans l'arbre.

A - Les variations spatiales et temporelles de la qualité la mangue sont liées à son mûrissement.

En lien avec les études précédentes (Joas et al., 2012, Litz, 2009) il a été montré que les attributs de la qualité de la mangue, i.e., la couleur de la peau et de la pulpe, la teneur en composés solubles et l'acidité, évoluent considérablement au cours de son mûrissement. Ces résultats confirment que la gestion de la qualité du fruit est indissociable du contrôle de son mûrissement. Dans la partie II chapitre II il a été montré que la vitesse de mûrissement des mangues varie en fonction des conditions de croissance, de la date de récolte et des conditions de stockage. Ces résultats soulignent l'importance d'appréhender la qualité de la mangue de manière intégrée (Joas and Lechaudel, 2008). Ceci va dans la sens des études précédentes sur la mangue (Lechaudel et al., 2010, Léchaudel and Joas, 2006, Joas et al., 2012) qui ont souligné l'importance de contrôler le stade de maturité de la mangue à la récolte pour maitriser sa qualité et son mûrissement.

Nos études expérimentales ont montré que les changements de couleur de la peau apparaissent après les changements de la composition interne de la mangue. Ces résultats indiquent que les critères visuels comme la couleur de la peau du fruit ne sont pas des indicateurs fiables du stade de maturité de la mangue. Ils confirment l'étude de Lechaudel et al. (2010) sur la nécessité d'utiliser des méthodes de mesures non destructives pour estimer le stade de maturité du fruit. Jha et al. (2012) et Saranwong et al. (2004) ont rapporté l'intérêt des mesures de spectroscopie proche infrarouge (SPIR) pour prédire de manière non destructive la maturité du fruit en mesurant plusieurs attributs de la qualité de la mangue, comme la teneur en matière sèche, la teneur en composés solubles et l'acidité titrable. Cependant ces mesures requièrent un matériel couteux et une calibration conséquente. McGlone et al. (2002) rapportent que les mesures de la densité du fruit à la récolte et de SPIR permettent de prédire avec une finesse similaire les teneurs en matière sèche et en composés solubles du kiwi. C'est pourquoi une étude a été menée en parallèle

de la thèse pour déterminer si la densité de la mangue à la récolte est un bon indicateur de sa teneur en composés solubles (Annexe II).

En plus des variations temporelles des différences de qualité ont été mesurées au sein de la mangue (Partie I chapitre III). Celles-ci ont été attribuées à des variations de concentration en composés primaires (sucres, acides) et secondaires (pigments). Il a été montré dans la partie I chapitre I que l'hétérogénéité spatiale de la couleur de la mangue est liée aux variations de teneur en pigments, i.e. chlorophylles, caroténoïdes et anthocyanes, de la peau. Ces résultats confirment les études sur le melon (Biais et al., 2010, Moing et al., 2011) qui mettent en évidence les différences de métabolisme au sein du fruit.

Les résultats présentés dans la partie I chapitre III indiquent que les variations de qualité au sein de la mangue sont en partie liées au gradient de maturité dans le fruit. Des concentrations en éthylène plus importantes ont en effet été mesurées à proximité du noyau. Ces mesures soutiennent les conclusions de Hershkovitz et al. (2011) sur l'avocat et de Zhang et al. (2009) sur la tomate concernant le rôle déterminant du noyau et des graines dans le mûrissement du fruit. Les changements de composition de la mangue ont été mesurés en amont de l'augmentation de sa concentration en éthylène. Ces résultats soutiennent l'étude de Zaharah et al. (2013) indiquant que l'éthylène n'est pas impliquée dans les premiers processus du mûrissement de la mangue. Pech et al. (2008) rapportent par ailleurs que certains processus liés au mûrissement du melon comme la dégradation des acides organiques et l'accumulation des sucres ne sont pas régulées par l'éthylène. Ces résultats soutiennent les conclusions de McAtee et al. (2013) soulignant que le mûrissement des fruits climactériques est régulé conjointement par l'acide abscissique et l'éthylène. Ceci expliquerait pourquoi des différences de mûrissement ont été observées dans la partie II chapitre I entre les fruits récoltés précocement et tardivement alors que tous ont synthétisé d'importantes quantités d'éthylène.

B - Facteurs impliqués dans la qualité et la maturité des fruits.

Pour étudier l'impact des nombreux facteurs impliqués dans la qualité et la maturité de la mangue, une approche de modélisation a été employée. Celle-ci s'appuie sur les modèles développés précédemment sur la mangue (Léchaudel et al., 2007, Léchaudel et al., 2005a) et sur la pêche (Génard and Gouble, 2005) ainsi que sur les nouveaux modèles développés et sur les nouvelles connaissances acquises au cours de cette thèse. Une des originalités de

l'approche de modélisation proposée est d'avoir couplé différents modèles éco-physiologiques à un modèle thermodynamique afin de simuler l'impact du climat sur la qualité et le mûrissement du fruit.

1) **Les différences de température ne sont pas à l'origine des variations de qualité et de maturité**

Il a été fait l'hypothèse que les différences de climat au sein de l'arbre (Léchaudel et al., 2012) sont impliquées dans les variations de qualité et de maturité entre les fruits. Un modèle thermodynamique a été développé (Partie I chapitre II) afin de simuler les variations spatiales et temporelles de la température des fruits au travers de l'arbre. En lien avec les mesures, d'importants gradients de température ont été simulés au sein de la mangue.

De manière surprenante, les différences de qualité et de maturité mesurées à l'intérieur du fruit ne sont pas liées aux gradients de température simulés dans la mangue (chapitre I.III -). Seule l'hétérogénéité de la couleur de la mangue est liée aux gradients de température simulés. Cette relation s'explique par le fait que l'exposition lumineuse fait varier à la fois la teneur en pigments de la peau de la mangue et sa température (Partie I chapitres I et II).

Il a été montré que les gradients de température varient selon la position du fruit dans l'arbre (Partie I chapitre II). Malgré ces différences, les simulations ont indiqué que la température moyenne des fruits à l'échelle de la saison varie peu entre les mangues. Ces résultats confirment ceux obtenus par Saudreau et al. (2009) sur la pomme. Le couplage des modèles présenté dans la partie II chapitre V a permis de montrer que les faibles différences de température moyenne entre les fruits selon leur position dans l'arbre ne sont pas à l'origine des variations de croissance et de mûrissement entre les mangues. Cependant, il a été montré que la température à travers son effet sur la transpiration a un effet indirect sur la croissance en matière fraiche de la mangue.

Ce travail de thèse ne s'est pas intéressé à l'effet de la température sur les métabolites secondaires, mis à part les pigments. Hors, Léchaudel et al. (2012) ont mesuré des concentrations en acide ascorbique suppérieures dans les faces ensoillées des mangues. Ces résultats sont cohérents avec ceux de Gautier et al. (2008) qui montrent que la température n'affecte pas considérablement les concentrations de la tomate en métabolites primaires (sucres et acides) mais d'avantage celles en métabolites secondaires (acide ascorbique, caroténoïdes). En conséquent de prochaines études devraient s'intéresser à l'effet de la température sur la concentration de la mangue en métabolites secondaires.

2) **La charge en fruits fait varier le calibre, la teneur en matière sèche et la vitesse de mûrissement du fruit.**

Les résultats présentés dans la partie II chapitre V mettent en avant l'impact de la disponibilité carbonée des fruits sur leur calibre, leur teneur en matière sèche, et leur vitesse de mûrissement. En accord avec les études précédentes (Léchaudel et al., 2005b, Léchaudel and Joas, 2006), il a été montré qu'une mangue se développant avec une forte charge en fruits était récoltée plus tardivement et avait un calibre et une teneur en matière sèche inférieurs. Les résultats présentés dans ce chapitre indiquent également que les différences de date de récolte observées entre les mangues à l'ombre et au soleil sont en majeure partie causées par les différences de croissance en matière sèche. Aussi les résultats obtenus dans cette thèse confirment l'importance de maitriser la charge en fruits pour homogénéiser la qualité et la maturité des mangues.

3) **Les variations de calibre entre les mangues sont liées en partie aux différences de transpiration et de conductivité hydraulique.**

Les simulations présentées dans la partie II chapitres IV et V indiquent que la croissance en matière fraiche des fruits varie selon leur position dans l'arbre à cause des différences de transpiration. Il a ainsi été simulé que les mangues les plus exposées au soleil, i.e. au nord, perdent d'avantage d'eau et ont un plus petit calibre. Ces résultats sont en accord avec les mesures de Hofman et al. (1995) et de Simmons et al. (1998) sur la mangue. Les différences de croissance en matière fraiche simulées entres les fruits sont en partie liées à la variation d'embolisation des vaisseaux conducteurs de sève. Cette hypothèse originale dans le cas du fruit, est cohérente avec les mesures d'embolie réalisées pour d'autres organes de la plante comme les racines, les branches, et les feuilles (Damour, 2008, Meinzer and McCulloh, 2013, Sperry and Ikeda, 1997).

II - Perspectives de recherche

Ce travail de thèse fournit des réponses sur les sources de variation de la qualité et de la maturité de la mangue. L'approche de modélisation proposée dans ce travail permet de mieux prendre en compte l'effet des pratiques culturales et des conditions climatiques sur la qualité et la maturité des mangues. Cependant les résultats de ce travail soulèvent de nouveaux questionnements sur les processus impliqués dans l'élaboration de la qualité du fruit dans son mûrissement.

A - Limites et perspectives d'amélioration du modèle

1) **Estimation des flux de xylème et de phloème**

Dans l'approche de modélisation proposée les flux de xylème et de phloème ne sont pas dissociés par soucis de simplification. Il est ainsi estimé que ces flux sont tous les deux passifs et dépendent du gradient de potentiel hydrique entre le fruit et la tige. Hors, il est connu que le flux de phloème peut aller contre des gradients de potentiel hydrique. Il serait intéressant de simuler indépendamment les flux de phloème et de xylème afin de mieux représenter le bilan hydrique du fruit. La dissociation de ces flux permettrait en outre de mieux estimer l'effet de l'embolie sur la croissance du fruit. Dans le modèle proposé il est estimé que l'embolie affecte la conductivité hydraulique du xylème et du phloème, alors que seul le xylème est sensible à la cavitation. Des études expérimentales plus approfondies devraient être menées afin de mieux comprendre ce processus et de mieux le simuler. Dans le modèle, le niveau d'embolie des vaisseaux est estimé en fonction du potentiel hydrique du fruit. Cette relation a été obtenue en exprimant les pertes de conductivité hydraulique mesurée dans le pédoncule en fonction du potentiel hydrique du fruit. Il serait donc intéressant de valider cette relation en la comparant à une courbe de cavitation obtenue par centrifugation, comme proposé par Cochard et al. (2005). L'utilisation de cette relation dans le modèle induit qu'une diminution du potentiel hydrique du fruit cause directement une augmentation irréversible de l'embolisation des vaisseaux conducteurs de sève. Ce formalisme est vraisemblablement la cause de l'augmentation brutale du niveau d'embolie simulée par le modèle. Il serait intéressant de vérifier si l'embolie se forme effectivement instantanément lorsque le potentiel hydrique de l'organe diminue. L'hypothèse que

l'embolie est irréversible est également à vérifier car il a été suggéré que les vaisseaux embolisés du xylème pouvaient être remplis à nouveau (Tyree and Sperry, 1988).

2) **Lien entre la croissance du fruit et son murissement**

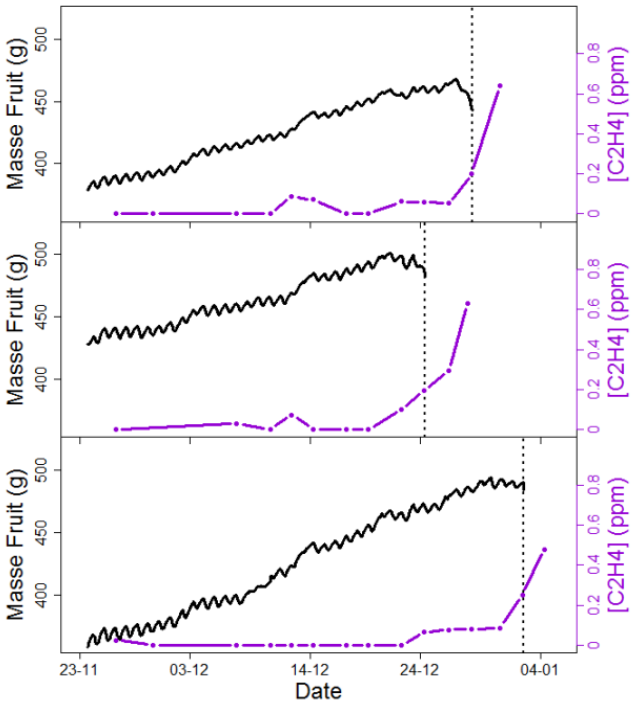

Figure 45: Variations saisonnières de la masse fraiche et de la concentration en éthylène de trois mangues avec une charge en fruits de 100 feuilles par fruit.

Les résultats obtenus montrent que la croissance de la mangue est ralentie à cause de l'augmentation de sa transpiration et de la diminution des flux d'eau entrant dans le fruit. Ces derniers diminuent à cause de l'apparition d'embolie dans les vaisseaux conducteurs de sève suite à la diminution du potentiel hydrique du fruit due aux changements de sa composition et à l'augmentation de sa transpiration. Du fait de l'effet du murissement sur la composition du fruit, ces résultats suggèrent qu'il existe une relation entre la croissance de la mangue et son murissement. Cette hypothèse est soutenue par les résultats présentés dans la Figure 45 qui montrent que la synthèse autocatalytique de l'éthylène est concomitante avec l'arrêt de croissance du fruit. Le lien entre le mûrissement et l'arrêt de croissance du fruit est d'autant plus plausible que plusieurs études indiquent que l'éthylène est impliqué dans l'abscission du fruit (Nunez-Elisea and Davenport, 1986, Cin et al., 2005). Cette relation pourrait être à double sens étant donné que nos résultats ont indiqué que le murissement de la mangue est impacté par les pertes en eau du fruit qui augmentent au

cours de sa croissance. Ces résultats confirment les précédentes études sur l'avocat (Adato and Gazit, 1974), la banane (Finger et al., 1995), et le kaki (Nakano et al., 2003), indiquant que la production d'éthylène est modulée par les pertes en eau du fruit. Il apparait dans ce système présenté en Figure 46 que la croissance du fruit et son mûrissement sont interdépendants.

Dans le modèle proposé, il est estimé que la composition de la mangue change en fonction des degrés jours et de la masse sèche du fruit. En conséquent, le modèle en l'état actuel ne permet pas d'estimer l'effet du murissement sur la composition du fruit. De prochaines études devraient donc s'intéresser à simuler l'impact des processus physiologiques liés au murissement sur la composition du fruit dans le but de mieux comprendre la relation entre la croissance du fruit et son murissement.

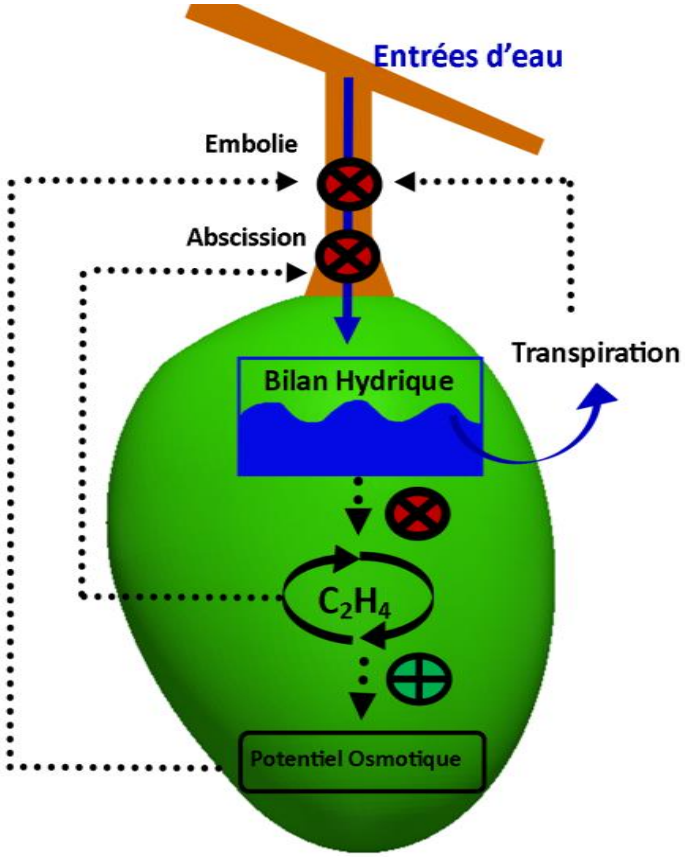

Figure 46: Représentation schématique de la relation entre le bilan hydrique du fruit, son potentiel osmotique, et la synthèse d'éthylène. Les flèches représentent les relations, soit positives (rond vert) soit négatives (rond rouge), entre les entrées d'eau dans le fruit, son bilan hydrique, sa transpiration, son potentiel osmotique et sa synthèse d'éthylène.

B - Le rôle potentiel des gradients de gaz sur l'hétérogénéité de la qualité et de la maturité des mangues

Dans la partie I chapitre III, des gradients de concentration en éthylène ont été mesurés dans le fruit. Il a été montré que ces gradients expliquent en partie les différences de qualité mesurées dans la mangue. Il a été suggéré que d'autres gradients et notamment ceux en oxygène et dioxyde de carbone pouvaient également être impliqués dans l'hétérogénéité de la qualité du fruit. Grâce à des approches de modélisation il a été possible de représenter les gradients de dioxyde de carbone et d'oxygène au sein de la pomme (Ho et al., 2010b) et de la poire (Lammertyn et al., 2003b, Ho et al., 2008). Il serait donc intéressant de modéliser les gradients d'oxygène et de dioxyde de carbone au sein de la mangue afin de déterminer s'ils sont liés à l'hétérogénéité de la qualité mesurée au sein du fruit. L'étude de la diffusion des gaz au sein des mangues permettrait en outre de déterminer si les gradients d'éthylène mesurés dans la partie I chapitre III s'expliquent par une synthèse d'éthylène plus importante dans le noyau. Ceci permettrait de confirmer le rôle du noyau dans le mûrissement du fruit. La modélisation des transferts de gaz à l'intérieur du fruit permettrait également d'étudier l'effet des gradients de température et des changements de résistance de la peau à la diffusion des gaz sur les gradients d'éthylène, d'oxygène, et de dioxyde de carbone au sein du fruit. Cette approche a été initiée dans ce travail de thèse (Annexe III)

Annexes

Annexe I: Détails des calculs utilisés pour déterminer la résistance de peau à la diffusion du dioxyde de carbone, de l'oxygène et de l'éthylène.

Diffusions of C_2H_4, O_2 and CO_2 from fruits inside to gas sample apparatus sealed at their surfaces were measured to determine skin resistance of attached fruit to gas diffusion.

According to first Fick law, diffusion of "x" gas (D_x, mol s^{-1}) in a gas sample apparatus sealed on the fruit surface depends on, difference in gas concentration between fruit inside ($[X]_{Fruit}$, mol m^{-3}) and gas sample apparatus ($[X]_{Apparatus}$, mol m^{-3}), skin resistance to gas diffusion (R_x, in s m^{-1}) and exchange surface between fruit and gas apparatus (A, in m^2):

$$D_x = \frac{A}{R_x}\left([X]_{Fruit} - [X]_{Apparatus}\right) \qquad \textit{Equation 63}$$

Internal gas concentration of attached fruits to the tree is assumed to change owing to daily fruit temperature variations (Nordey et al., 2014c, Ravindra and Goswami, 2008). The effect of temperature change, from T_0 (in °C) to T (°C), on fruit respiratory rate, RR (either in mmol CO_2 h^{-1} or in mmol O_2 h^{-1}), is commonly estimated using the Q_{10} concept (Léchaudel et al., 2005a, Ravindra and Goswami, 2008) as :

$$RR = RR_0\, Q_{10}^{\frac{T-T0}{10}} \qquad \textit{Equation 64}$$

where RR is the respiratory rate at the T temperature and RR_0 is the reference respiratory rate at the T_0 temperature. Q_{10} values of 1.61 and 1.67 were used for O_2 and CO_2, respectively, in lines with measurements of Ravindra and Goswami (2008).

According to the first Fick's law the respiration rate of CO_2 (RR_{CO2}, mmol CO_2 h^{-1}) can be expressed as:

$$RR_{CO_2} = \frac{A}{R_x}([CO_2]_{fruit} - [CO_2]_{Air}) \qquad \textit{Equation 65}$$

where $[CO_2]_{fruit}$ (mol m^{-3}) and $[CO_2]_{Air}$ (mol m^{-3}) are the carbon dioxide concentrations in the fruit and in the air, respectively. Since $[CO_2]_{Air}$ is negligible in comparison to$[CO_2]_{fruit}$, it was assumed for the sake of simplicity that $[CO_2]_{Air}$ was nil, consequently RR_{CO_2} can be expressed as:

$$RR_{CO_2} = \frac{A}{R_x}([CO_2]_{fruit}) \qquad \textit{Equation 66}$$

Combining Equation 64 with Equation 66, $[CO_2]_{fruit}$ at the temperature T (°C) can be deduced from the reference carbon dioxide content in the fruit ($[CO_2]^0_{fruit}$, mol m^{-3}) at T_0 temperature (°C):

$$\frac{A}{R_x}[CO_2]_{fruit} = \frac{A}{R_x}\,[CO_2]^0_{fruit}\,Q_{10}{}^{\frac{T-T0}{10}} \qquad \textit{Equation 67}$$

Assuming that fruit surface and skin resistance to gas diffusion are not affected by temperature, Equation 67 can be developed as:

$$[CO_2]_{fruit} = \,[CO_2]^0_{fruit}\,Q_{10}{}^{\frac{T-T0}{10}} \qquad \textit{Equation 68}$$

Combining Equation 63 and Equation 68, carbon dioxide diffusion in gas sample apparatus ($D_{(CO2)}$, in mol s^{-1}) can be expressed as:

$$D_{(CO_2)} = \,\frac{A}{R_{CO_2}} \times \left(\,[CO_2]_{Fruit}\,Q_{10}{}^{\frac{T1-T0}{10}} - \,[CO_2]_{Apparatus}\right) \qquad \textit{Equation 69}$$

The respiration rate expressed in moles of oxygen (RR_{O2}, mmol CO_2 h^{-1}) can also be expressed using first Fick's law. Since the oxygen content in the fruit is smaller than in the air, RR_{O2} is expressed as:

$$RR_{O_2} = \frac{A}{R_x}([O_2]_{Air} - [O_2]_{fruit}) \qquad \textit{Equation 70}$$

Combining Equation 64 with Equation 70, fruit concentration in oxygen ($[O_2]_{fruit}$, mol m^{-3}) at the T temperature (°C) is calculated from the reference fruit concentration in oxygen ($[O_2]^0_{fruit}$, mol m^{-3}) at the T_0 temperature (°C):

$$\frac{A}{R_x}\left([O_2]_{Air} - [O_2]_{fruit}\right) = \frac{A}{R_x}\left([O_2]^0_{Air} - [O_2]^0_{fruit}\right)Q_{10}{}^{\frac{T-T0}{10}} \qquad \textit{Equation 71}$$

For the sake of simplicity, it has been assumed that temperature does not affect fruit surface, skin resistance, and O_2 content in air. Consequently Equation 71 can be developed as:

$$[O_2]_{Air} - [O_2]_{fruit} = \left([O_2]_{Air} - [O_2]^0_{fruit}\right) Q_{10}^{\frac{T-T0}{10}} \qquad \textit{Equation 72}$$

$$[O_2]_{fruit} = [O_2]_{Air} - \left([O_2]_{Air} - [O_2]^0_{fruit}\right) Q_{10}^{\frac{T-T0}{10}}$$

$$[O_2]_{fruit} = [O_2]_{Air}\left(1 - Q_{10}^{\frac{T-T0}{10}}\right) + [O_2]^0_{fruit} Q_{10}^{\frac{T-T0}{10}}$$

Combining Equation 72 and Equation 63, the oxygen diffusion in the gas sample apparatus ($D_{(O_2)}$, in mol s^{-1}) can be expressed as:

$$D_{(O_2)} = \frac{A}{R_{O_2}} \times \left([O_2]_{Air}(1 - Q_{10}^{\frac{T-T0}{10}}) + [O_2]^0_{fruit}\, Q_{10}^{\frac{T-T0}{10}} - [O_2]_{Apparatus}\right) \qquad \textit{Equation 73}$$

Annexe II : Utilisation de la densité des mangues à la récolte comme indicateur de leur teneur en composés solubles pendant leur conservation.

Introduction

L'hétérogénéité de la qualité des mangues à la récolte, nécessite de trier les fruits afin de former des lots homogènes et diminuer ainsi les pertes en post récolte. Afin de mesurer de manière précise et répétable la qualité des fruits il est nécessaire de recourir à des méthodes de mesures non destructives (Abbott, 1999). Il a été proposé d'utiliser la spectroscopie proche infrarouge (SPIR) (Jha et al., 2012, Saranwong et al., 2004) pour estimer les teneurs en matière sèche et en composé solubles de la mangue. Ces mesures sont coûteuses et nécessitent une calibration importante. McGlone et al. (2002) rapportent que les mesures de densité et de SPIR permettent de prédire avec une précision comparable les teneurs en matière sèche et en composés solubles du kiwi. La mesure de la densité présente l'avantage d'être facile, rapide et de nécessiter qu'une une simple balance. La relation entre la densité du fruit et sa teneur en matière sèche repose sur le fait que les composés solubles de la mangue, i.e. les sucres et les acides organiques, ont une masse volumique suppérieure à celle de l'eau. En conséquent, comme l'indique les résultats de Léchaudel and Joas (2006), la densité de la mangue augmente au cours de sa croissance du fait de l'augmentation de sa teneur en matière sèche. Etant donné que la qualité du fruit mur dépend de sa concentration en matière sèche à la récolte (Léchaudel and Joas, 2006, Joas et al., 2012), la densité de la mangue à la récolte semble être un critère de tri interessant. Une étude a donc été entreprise pour déterminer l'intérêt d'utiliser la densité de la mangue à la récolte comme indicateur de la teneur en composés solubles du fruit.

Matériels et méthodes

Matériel végétal

Cette étude a été réalisée sur des mangues de la variété Cogshall. Les fruits se sont développés pendant les saisons de croissance, 2002-2003, 2004-2005, 2005-2006 et 2007-2008 dans le verger du CIRAD à l'île de la Réunion (20°52' 48'' S, 55°31' 48" E) composé de manguiers âgés de 18 ans en 2008, greffés sur la variété 'Maison rouge'. Les arbres espacés de 5 x 6 m ont été correctement irrigués et mesuraient approximativement 3 m de haut. Deux traitements de charge en fruits ont été considérés, 25 et 100 feuilles par fruit (L/F). En lien avec l'étude précédente de Léchaudel and Joas (2006) le traitement de 100 L/F a été considéré comme non restrictif pour la croissance en matière sèche du fruit contrairement au traitement de 25 L/F. Ces traitements ont été réalisés en annelant les rameaux portant les fruits et les défoliant si nécessaire. Pour le traitement 25 L/F, 61, 12 et 13 fruits ont été récoltés et analysés pendant les saisons de croissance de 2002-2003, 2004-2005 et 2005-2006, respectivement. Pour le traitement 100 L/F, 63, 77, et 59 fruits ont été récoltés et analysés pendant les saisons de croissance de 2002-2003, 2004-2005, et 2007-2008, , respectivement.

Mesures de la densité et de la qualité des fruits.

La densité des mangues a été mesurée juste après la récolte grâce au principe d'Archimède en mesurant avec une balance la masse du fruit dans l'air puis la force qu'il exerce vers le haut lorsqu'il est immergé dans de l'eau. La densité de la mangue (D_{Fruit}) est déduit de :

$$D_{Fruit} = \frac{m}{|m - r|} \qquad \textit{Equation 74}$$

Où m est la masse du fruit (Kg) et r (Kg) est la force exercée vers le haut par le fruit lorsqu'il est immergé.

Les fruits ont été conservés à 20°C et à 90% d'humidité relative pendant 1 à 22 jours et détruits à différentes dates afin de mesurer leur teneur en composés solubles grâce à un réfractomètre ATC-1E (Atago, Tokyo, Japan).

Etablissement et validation du modèle.

La teneur en composés solubles de la mangue (TSS_j, °Brix) au jour *j* de conservation a été estimée en fonction de sa densité initiale (ρ_{ini}) grâce à l'Equation 75, où JC est le nombre de jours de conservation et b_1, b_2, a_1, et a_2 sont des paramètres.

$$TSS_j = b_1 \, \rho_{ini}{}^{b_2} + a_1 \, (1 - e^{a_2 \, JC}) \qquad \textit{Equation 75}$$

Les mesures réalisées sur les fruits du traitement 100 L/F ont été scindées en deux, 80% a été utilisé pour calibrer le modèle et 20% pour le valider. Les mesures réalisées sur les fruits du traitement 25 L/F ont été utilisées pour tester en validation croisée la robustesse du modèle pour des conditions de croissance contrastées. Les paramètres b_1, b_2, a_1 et a_2 ont été estimés avec les données de calibration grâce à une régression non linéaire.

Résultats et discussion

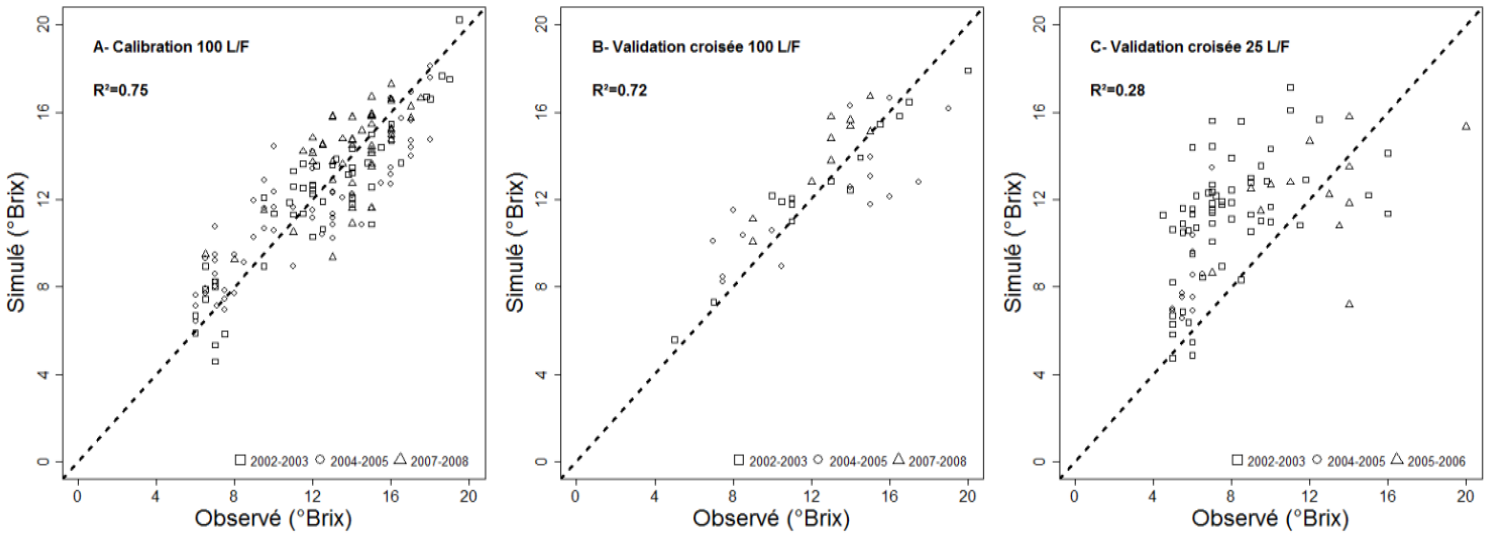

Figure 47: Comparaisons des teneurs en composés solubles simulées à celles observées issues des données de calibration (A), et de validation du traitement 100 feuilles par fruit (L/F) (B) et 25 L/F (C).

L'ajustement du modèle aux données de calibration et de validation est présenté dans la Figure 47. Les résultats indiquent que le modèle permet de prédire correctement les teneurs en composés solubles des mangues du traitement 100 L/F pendant leur conservation (Figure 47A et Figure 47B). Le fait que l'ajustement du modèle soit comparable avec les données de calibration et de validation indique sa robustesse pour prédire les teneurs en composés solubles des mangues issues du traitement 100 L/F. Cependant, la Figure 47 indique que le modèle surestime la teneur en composés solubles des mangues issues du traitement 25 L/F. Ceci indique que la relation établie entre la densité de la mangue à la récolte et sa teneur en composés solubles pendant sa conservation dépend des conditions de croissance. Cela peut s'expliquer par les différences de composition entre les mangues issues de charge en fruits différentes (Léchaudel and Joas, 2006, Joas et al., 2012). Il est en effet rapporté dans ces études que les concentrations en matière sèche et en saccharose des mangues du traitement 25 L/F sont inférieures à celles des mangues du traitement 100 L/F, contrairement à leur acidité titrable qui elle est supérieure. La charge en fruits impacte également le calibre des mangues. Le poids moyen des mangues du traitement 100 L/F était de 378 g ± 74.9g contre 198 g ± 65.2g pour les mangues du

traitement 25 L/F. En conséquent, l'utilisation de la masse des mangues à la récolte comme donnée d'entrée du modèle permettrait peut-être de mieux prendre en compte l'effet des conditions de croissance et d'améliorer ainsi les prédictions du modèle.

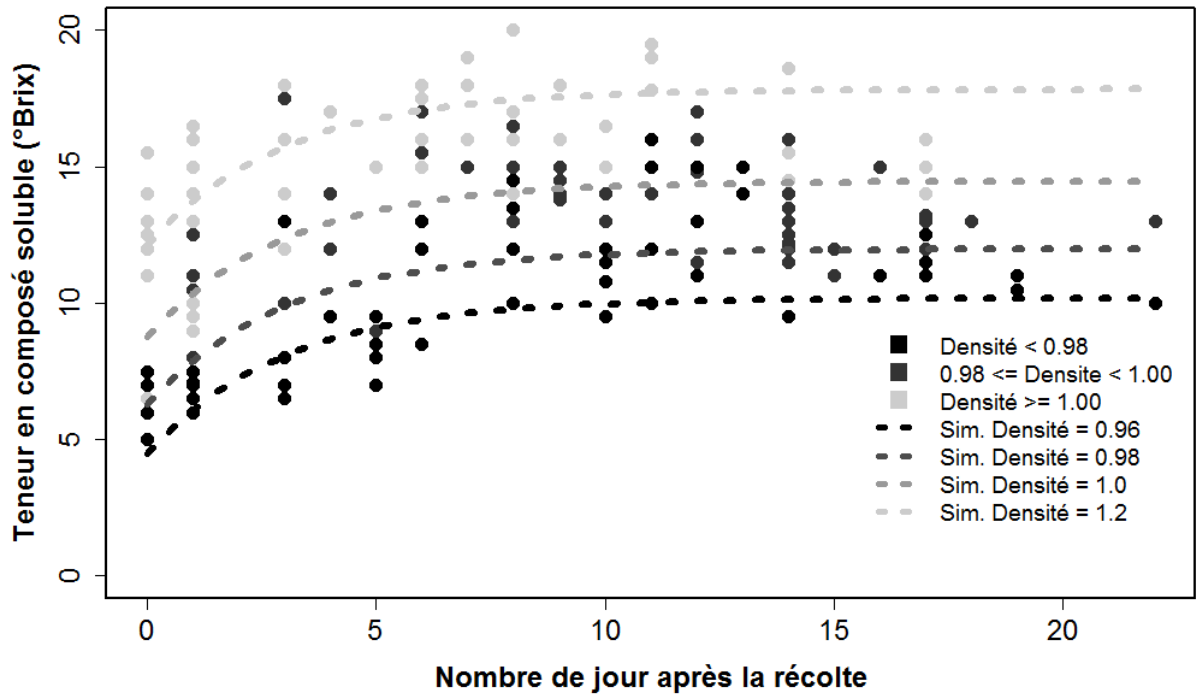

Figure 48: Les évolutions simulées (lignes) et observées (points) de la teneur en composés solubles des mangues du traitement 100 feuilles par fruit au cours de leur conservation en fonction de leur densité à la récolte. Les points sont représentés selon la densité initiale des mangues en trois catégories. L'évolution de la teneur en composés solubles des mangues au cours de leur conservation a été simulée pour quatre densités à la récolte. Les catégories de densité et les densités utilisées pour les simulations sont indiquées sur le graphique.

La Figure 48 présente les changements mesurés et simulés de la teneur en composés solubles des mangues du traitement 100 L/F après la récolte. Il a été simulé que la teneur maximale en composés solubles atteint par la mangue au cours de sa conservation dépend de sa densité à la récolte. Ce résultats confirment les conclusions de Joas et al. (2012) et Léchaudel and Joas (2006) qui indiquent que la qualité du fruit mûr dépend de sa composition à la récolte. Ceci confirme la nécessité de développer des techniques de mesure non destructive pour estimer la qualité des mangues à la récolte.

Annexe III: Modélisation des gradients de gaz, i.e., oxygène et dioxyde de carbone, au sein de la mangue.

Introduction

La consommation d'oxygène et la production de dioxyde de carbone lors de la respiration d'un organe de la plante induisent des échanges gazeux entre cet organe et l'environnement extérieur. Ces échanges causent des gradients de dioxyde de carbone et d'oxygène au sein des organes volumineux comme que les fruits ou les racines (Ho et al., 2010a). Des études ont montré que l'augmentation de la concentration interne en dioxyde de carbone dans la mangue acidifie le fruit (Baldwin et al., 1999, Carrillo-Lopez et al., 2000). C'est pourquoi nous avions suggéré dans une étude précédente que les différences d'acidité mesurées au sein de la mangue pouvaient être liées à des gradients de concentration en dioxyde de carbone (Nordey et al., 2014b). Grâce à des approches de modélisation il a été possible de représenter les gradients de dioxyde de carbone et d'oxygène au sein de la pomme (Ho et al., 2010b) et de la poire (Lammertyn et al., 2003b, Ho et al., 2008). Il est donc proposé dans cette étude de d'adapter ces approches de modélisation à la mangue pour simuler les gradients de gaz au sein du fruit.

Matériels et méthodes

Présentation du modèle de diffusion des gaz.

Pour déterminer les transferts de gaz au sein de la mangue, le volume du fruit a été découpé en une infinité de sous unités comme proposé dans notre étude précédente (Nordey et al., 2014c) pour calculer les transferts d'énergie dans la mangue.

Les variations de concentration en oxygène (ΔO_2, %) et en dioxyde de carbone (ΔCO_2, %) dans chaque sous unité du fruit pendant un pas de temps Δt (s) sont calculées en fonction (i) de la production de dioxyde de carbone (RCO_2, $m^3\ s^{-1}$) et de la consommation d'oxygène (RO_2, $m^3\ s^{-1}$) liées à la respiration de maintenance, (ii) de la diffusion du dioxyde de carbone ($CO_{2\ émission}$, $m^3\ s^{-1}$) et de l'oxygène ($O_{2\ émission}$, $m^3\ s^{-1}$) vers le milieu extérieur et (iii) des transferts de dioxyde de carbone ($CO_{2diffusion}$, $m^3\ s^{-1}$) et d'oxygène ($O_{2diffusion}$, $m^3\ s^{-1}$) entre les sous unités :

$$\Delta[CO_2] = (RCO_2 + CO_{2_{Emission}} + CO_{2_{Diffusion}})\,\Delta t\,\frac{\rho}{M}\,100 \qquad \textit{Equation 76}$$

$$\Delta[O_2] = \left(RO_2 + O_{2_{Emission}} + O_{2_{Diffusion}}\right)\Delta t\,\frac{\rho}{M}\,100$$

Où M représente la masse du fruit (Kg) et ρ sa masse volumique (Kg m^{-3}). En accord avec les études précédentes sur la mangue (Nordey et al., 2014c, Léchaudel and Joas, 2006), il a été estimé que ρ est égal à 1000 Kg. m^{-3}.

RCO_2 et RO_2 ont été estimés grâce une équation de Michaelis-Menten avec une inhibition non compétitive comme proposé par Ho et al. (2010a) pour prendre en compte l'effet des concentrations en oxygène et en dioxyde de carbone sur la respiration :

$$R_{O2} = \frac{V_{mo} \times [O_2]}{(K_{mO} + [O_2]) \times (1 + \frac{[CO_2]}{Kic})} \times M \qquad \textit{Equation 77}$$

$$R_{CO2} = -r_q \times R_{O2}$$

Où, $[CO_2]$ (%) et $[O_2]$ (%) sont les concentrations des sous unités en CO_2 et O_2, respectivement, K_{ic} (%) est la constantes d'inhibition du CO_2 sur la consommation de d'O_2, K_{mo} (%) est la constante de Michaelis-Menten de la consommation d'oxygène (en %), V_{mo} est la consommation maximale d'O_2 (en $m^3\ s^{-1}\ Kg^{-1}$) et M représente la masse de la sous unité (en Kg). Il a été estimé que le quotient de respiration (r_q) est égale à 1, en accord avec Ho et al. (2010a). Il est donc estimé que la consommation d'une mole d'oxygène produit une mole de dioxyde de carbone. Par soucis de simplification, la production de dioxyde de carbone par le processus de fermentation n'est pas considérée, contrairement aux modèles développés sur la poire (Lammertyn et al., 2003b, Ho et al., 2008) et la pomme (Ho et al., 2010b).

La respiration du fruit dépend de la température (Ravindra and Goswami, 2008). Les variations des paramètres V_{mo} et K_{mO} de l'équation de Michaelis-Menten (Equation 77) avec la température sont estimées en utilisant l'équation d'Arrhénius (Ravindra and Goswami, 2008) :

$$R_x = R_p \exp(\frac{-E_a}{RT}) \qquad \textit{Equation 78}$$

$$\ln(R_x) = \ln(A) + \frac{-Ea}{R}\ \frac{1}{T}$$

où, R_x représente le paramètre de l'équation de Michaelis-Menten (soit V_{mo} ou K_{mO}), R_p est le facteur pré-exponentiel, E_a est l'énergie d'activation (Kj g^{-1} mol^{-1}), T est la température (K), et R est la constante universelle des gaz parfaits (R= 8.314 Kj Kg^{-1} mol^{-1} K^{-1}).

La diffusion du CO_2 et d'O_2 entre les sous unités a été estimée grâce à Equation 79, avec $DiCO_2$ (m^2 s^{-1}) et DiO_2 (m^2 s^{-1}) qui sont les coefficients de diffusion du CO_2 et de l'O_2 à travers la pulpe du fruit, respectivement, A qui est la surface d'échange entre les sous unités (m^2), L (en m) qui est la distance entre les sous unités, et $\Delta[CO_2]$ (%) et $\Delta[O_2]$ (%) qui sont les différences de concentration entre les sous unités en CO_2 et en O_2, respectivement.

$$CO_{2_{Diffusion}} = \frac{DiCO_2\ A\ \Delta[CO_2]\ 10^{-2}}{L} \qquad \textit{Equation 79}$$

$$O_{2_{Diffusion}} = \frac{DiO_2\ A\ \Delta[O_2]\ 10^{-2}}{L}$$

Les échanges de CO_2 et d'O_2 entre les sous unités de surface du fruit et l'environnement extérieur ont été calculés grâce à Equation 80 :

$$CO_{2_{Emission}} = \frac{A_{ext}}{RES_{CO_2}} \left([CO_2] - [CO_2]_{air} \right) 10^2 \qquad \textit{Equation 80}$$

$$O_{2_{Emission}} = \frac{A_{ext}}{RES_{O_2}} \left([O_2]_{Fruit} - [O_2]_{air} \right) 10^2$$

où $[CO_2]$ (%) et $[CO_2]_{air}$ (%) sont les concentrations en CO_2 de la sous unité et de l'air, respectivement, A_{ext} (en m^2) est la surface d'échange entre la sous unité et l'extérieur, et RES_{CO2} (s m^{-1}) et RES_{O2} (s m^{-1}) sont les résistances de la peau à la diffusion du CO_2 et de l' O_2.

Paramétrisation du modèle

Pour résoudre l'Equation 76, il est nécessaire de déterminer les valeurs de $DiCO_2$, DiO_2, V_{mo}, K_{ic} et K_{mo}. Ces paramètres ont été déterminés en calibrant le modèle à partir de mesures de respiration de fruits détachés, comme proposé par Lammertyn et al. (2003a). L'étude de Ravindra and Goswami (2008) a été utilisée pour simuler l'émission de dioxyde de carbone et la consommation d'oxygène de mangues détachées au stade vert mature. Les résultats de cette étude ont permis de simuler les respirations théoriques d'une mangue de 280 grammes placée dans un bocal de 0.31 litre, à différentes températures, i.e. 10, 15, 20, 25 et

30°C. Ces données théoriques ont été utilisées pour calibrer les valeurs des paramètres $DiCO_2$, DiO_2, V_{mo}, K_{ic}, K_{mo} à différentes températures.

Résultats et discussion

Ajustement des données simulées aux données observées

La calibration du modèle a permis de déterminer les valeurs des paramètres $DiCO_2$, DiO_2, K_{ic}, V_{mo} et K_{mo} à différentes températures. Les comparaisons des respirations théoriques du fruit et celles simulées par le modèle à différentes température sont présentées dans la Figure 49.

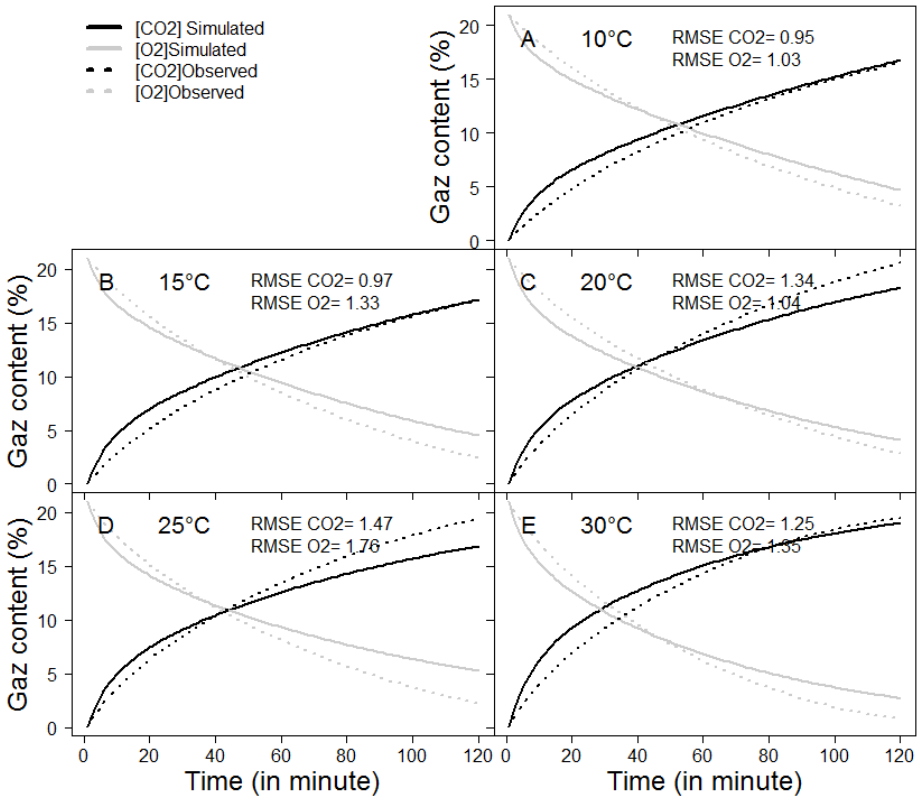

Figure 49 : Changements simulés (lignes continues) et déduits d'après l'étude de Ravindra and Goswami (2008)(lignes pointillées) de la concentration en CO_2 et en O_2 d'un bocal clos de 0.31 litre contenant une mangue de 280g.

Quelle que soit la température, le modèle simule correctement les variations de concentration en oxygène et en dioxyde de carbone dans le bocal. Il a été noté que le modèle a tendance à surestimer la respiration du fruit. Les valeurs des paramètres de la respiration Km et Vm ont montré d'importantes variations avec la température. L'effet de la température sur ces paramètres a été estimé en utilisant l'équation d'Arrhenius. Pour déterminer les valeurs des coefficients des équations d'Arrhenius, i.e. E_a et R_p, les valeurs des paramètres Km et Vm estimées avec le modèle ont été représentées en fonction de la température (Figure 50).

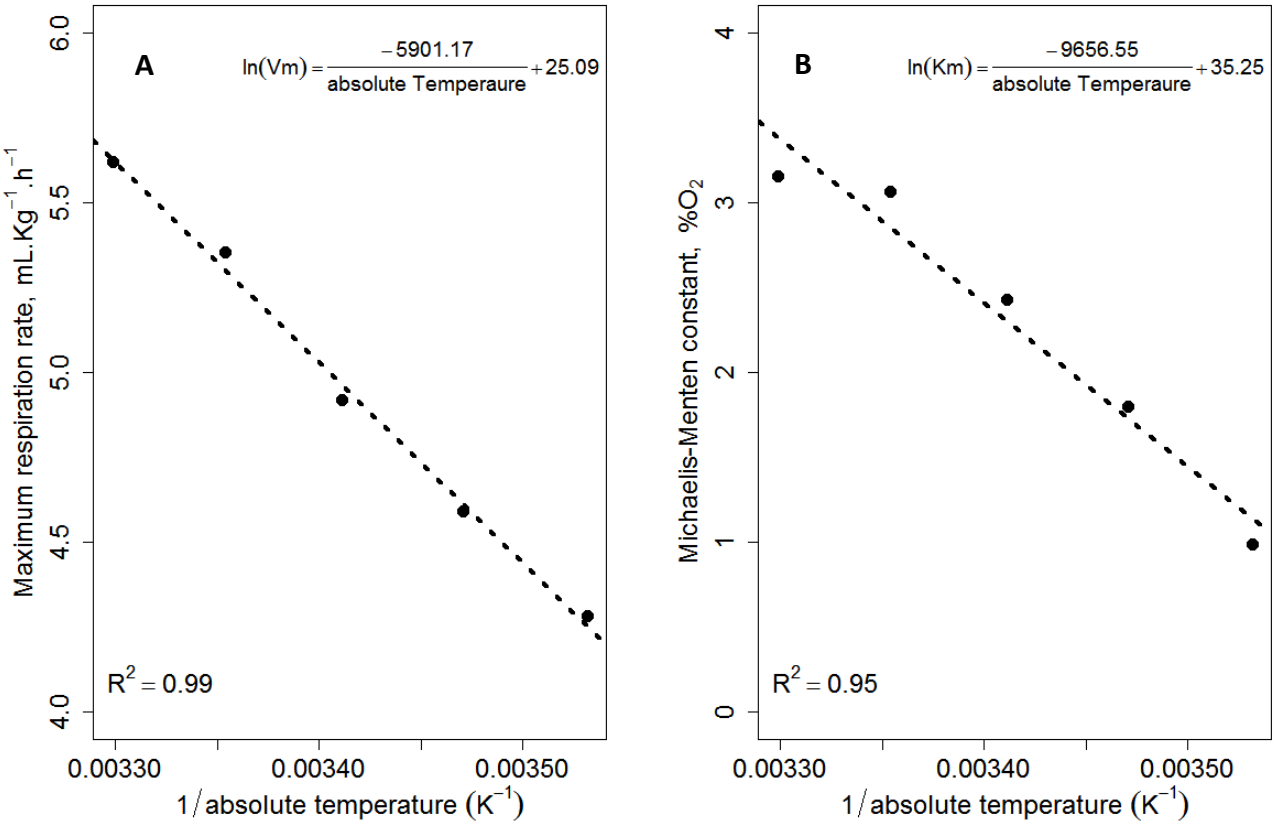

Figure 50: Relations entre les valeurs estimées de Vm (A) et Km_o (B) et la température.

Modélisation des gradients de CO_2 et O_2 au sein du fruit

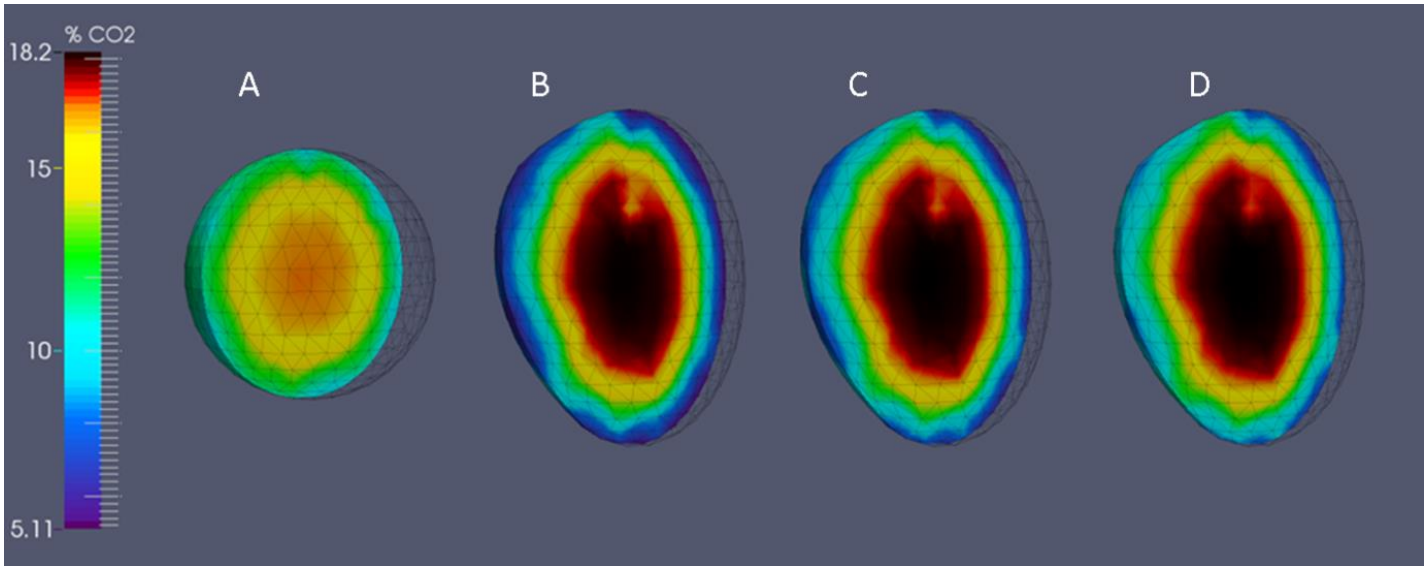

Figure 51 : Gradients de CO_2 simulés dans une mangue de forme ronde (A), dans une mangue dont la résistance de la peau à la diffusion des gaz a été réduite de 25% (B), dans une mangue normale (C) et dans une mangue dont la résistance de la peau à la diffusion des gaz a été augmentée de 25% (D).

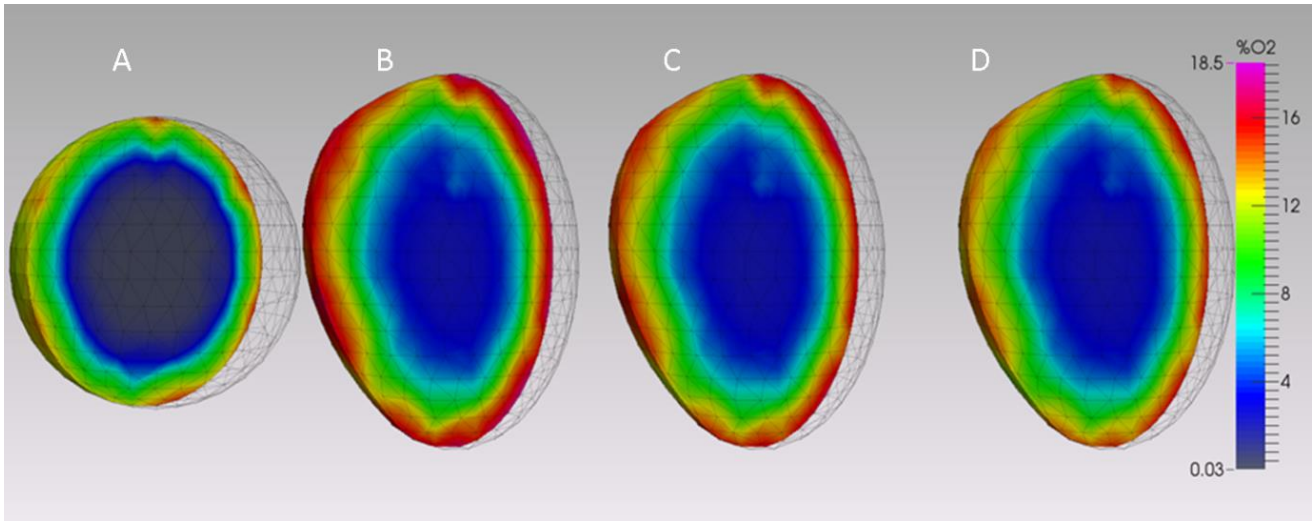

Figure 52 : Gradients d'O_2 simulés dans une mangue avec une forme ronde (A), dans une mangue dont la résistance de la peau à la diffusion des gaz a été réduite de 25% (B), dans une mangue normale (C) et dans une mangue dont la résistance de la peau à la diffusion des gaz a été augmentée de 25% (D).

La Figure 51 et la Figure 52 présentent les concentrations de gaz simulées par le modèle pour des fruits détachés en faisant varier la forme et les résistances de la peau à la diffusion des gaz. Les concentrations de CO_2 simulées à la surface du fruit témoin sont de l'ordre de 6 à 8% et atteignent 18% au centre du fruit. Pour l'O_2 les concentrations simulées varient de 1.85% à 17.9% entre la surface et le centre du fruit, respectivement. Les études précédentes sur la pomme et la poire ont également simulé des concentrations en O_2 au centre du fruit proche de 0% (Lammertyn et al., 2003b, Ho et al., 2010b). Dans une étude précédente il a été mesuré que les concentrations de CO_2 et d'O_2 à la surface des mangues attachés à l'arbre varient entre 3% et 18% et entre 5% et 20%, respectivement, selon le stade de maturité du fruit (Partie II chapitre I). Les simulations étant réalisées sur des mangues à un stade vert mature, ces résultats indiquent que le modèle à tendance à surestimer la concentration CO_2 et à sous-estimer celle en O_2. Ceci s'explique par les résultats précédents indiquant que la calibration des paramètres, $DiCO_2$, DiO_2, V_{mo}, K_{ic} et $K_{mo,}$ à tendance à surestimer la respiration du fruit. Pour valider l'ajustement du modèle des mesures de concentrations en CO_2 et O_2 à différents endroits du fruit, i.e. à la surface et à l'intérieur du fruit, sont nécessaires.

Les gradients de CO_2 simulés sont cohérents avec l'acidité titrable plus importante mesurée au centre de la mangue dans notre étude précédente (Nordey et al., 2014b). Etant donné la faible concentration en oxygène simulée au centre du fruit, de prochaines études devraient déterminer s'il n'y a pas de métabolites liés à la fermentation au centre du fruit, tel que l'éthanol, comme reporté par Biais et al. (2010) sur le melon.

Les simulations indiquent que la forme du fruit influence considérablement les gradients de gaz. Les gradients sont moins importants dans un fruit avec une forme sphérique que dans un fruit, de même masse, de forme ellipsoïdale comme la mangue. Cela s'explique par le fait que la distance entre le centre et la surface du fruit est constante dans le cas d'une forme sphérique contrairement à une forme ellipsoïdale. Les simulations ont également indiqué que les gradients de gaz varient en fonction de la résistance de la peau à la diffusion des gaz. Ces résultats indiquent qu'il serait intéressant d'utiliser ce type de modèle pour estimer l'effet de l'enrobage sur la concentration interne du fruit en gaz.

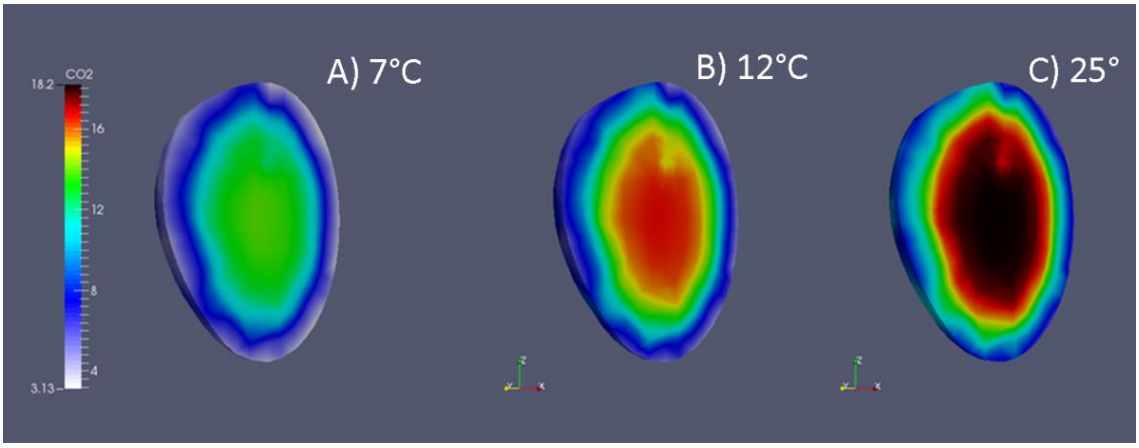

Figure 53: Effet de la température sur les gradients de concentration en CO_2 dans la mangue

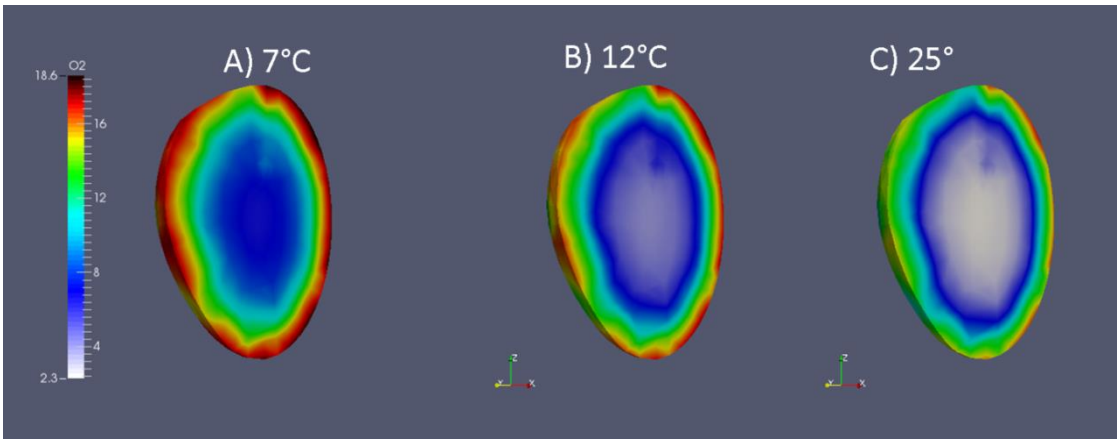

Figure 54: Effet de la température sur les gradients de concentration en O_2 dans la mangue

L'effet de la température sur les gradients de concentration en CO_2 et en O_2 dans la mangue a été simulé (Figure 53 et Figure 54). En accord avec les précédentes études sur la pomme et sur la poire (Lammertyn et al., 2003b, Ho et al., 2010b) il a été montré que l'augmentation de la température diminue la concentration en oxygène du fruit et augmente celle en dioxyde de carbone. Etant donné l'effet de la température sur les gradients de gaz il serait intéressant dans de prochaines études d'étudier l'effet des gradients de température au sein du fruit (Nordey et al., 2014c) sur les gradients d'O_2 et de CO_2.

Les travaux présentés nécessitent d'être approfondit. Il est notamment nécessaire de confronter les gradients de gaz simulés dans le fruit à des mesures réalisées à différents endroits du fruit. Il serait également intéressant de mesurer les coefficients de diffusion de l'O_2 et du CO_2 dans la pulpe pour les confronter à ceux estimés par le modèle.

Annexe IV: Photographies

Figure 55: Rameau de manguier annelé

Figure 56: Rameau de manguier annelé.

Bibliographie

Abbott JA. 1999. Quality measurement of fruits and vegetables. *Postharvest Biology and Technology,* **15**: 207-225.

Adams DO, Yang SF. 1977. Methionine Metabolism in Apple Tissue Implication of S-Adenosylmethionine as an Intermediate in the Conversion of Methionine to Ethylene. *Plant Physiology,* **60**: 892-896.

Adams SR, Cockshull KE, Cave CRJ. 2001. Effect of Temperature on the Growth and Development of Tomato Fruits. *Annals of Botany,* **88**: 869-877.

Adato I, Gazit S. 1974. Water-deficit Stress, Ethylene Production, and Ripening in Avocado Fruits. *Plant Physiology,* **53**: 45-46.

Agar IT, Biasi WV, Mitcham EJ. 1999. Exogenous ethylene accelerates ripening responses in Bartlett pears regardless of maturity or growing region. *Postharvest Biology and Technology,* **17**: 67-78.

Ahrens J, Geveci B, Law C. 2005. Paraview: An end-user tool for large data visualization. *The Visualization Handbook,* **717**: 731.

Ajila CM, Bhat SG, Prasada Rao UJS. 2007a. Valuable components of raw and ripe peels from two Indian mango varieties. *Food Chemistry,* **102**: 1006-1011.

Ajila CM, Naidu KA, Bhat SG, Rao UJSP. 2007b. Bioactive compounds and antioxidant potential of mango peel extract. *Food Chemistry,* **105**: 982-988.

Ajila CM, Rao LJ, Rao UJ. 2010. Characterization of bioactive compounds from raw and ripe Mangifera indica L. peel extracts. *Food and chemical toxicology : an international journal published for the British Industrial Biological Research Association,* **48**: 3406-3411.

Almeida AM, Navet R, Jarmuszkiewicz W, Vercesi AE, Sluse-Goffart CM, Sluse FE. 2002. The energy-conserving and energy-dissipating processes in mitochondria isolated from wild type and nonripening tomato fruits during development on the plant. *Journal of bioenergetics and biomembranes,* **34**: 487-498.

Andersen CM, Bro R. 2010. Variable selection in regression—a tutorial. *Journal of Chemometrics,* **24**: 728-737.

Andrews J. 1995. The climacteric respiration rise in attached and detached tomato fruit. *Postharvest Biology and Technology,* **6**: 287-292.

Arshad M, Frankenberger Jr WT. 2002. Ethylene in plant physiology. *Ethylene*: Springer.

Ayala-Silva T, J.Schenell R, W.Merrow A, Winterstein M, Cervantes C, Brown S. 2005. Determination of color and Fruit traits of half-sib families of Mango (Mangifera Indica L.). *Proc. Fla. State Hort Soc.,* **118**: 253-257.

Baldwin EA, Burns JK, Kazokas W, Brecht JK, Hagenmaier RD, Bender RJ, Pesis E. 1999. Effect of two edible coatings with different permeability characteristics on mango (Mangifera indica L.) ripening during storage. *Postharvest Biology and Technology,* **17**: 215-226.

Bally ISE. 1999. Changes in the cuticular surface during the development of mango (Mangifera indica L.) cv. Kensington Pride. *Scientia Horticulturae,* **79**: 13-22.

Banks NH. 1985. Responses of banana fruit to pro-long coating at different times relative to the initiation of ripening. *Scientia Horticulturae,* **26**: 149-157.

Bapat VA, Trivedi PK, Ghosh A, Sane VA, Ganapathi TR, Nath P. 2010. Ripening of fleshy fruit: Molecular insight and the role of ethylene. *Biotechnology Advances,* **28**: 94-107.

Barry CS, Giovannoni JJ. 2007. Ethylene and fruit ripening. *Journal of Plant Growth Regulation,* **26**: 143-159.

Bengtsson H, Riedy J. 2011. R.matlab: Read and write of MAT files together with R-to-Matlab.

Berardini N, Fezer R, Conrad J, Beifuss U, Carle R, Schieber A. 2005. Screening of Mango (Mangifera indica L.) Cultivars for Their Contents of Flavonol O- and Xanthone C-Glycosides, Anthocyanins, and Pectin. *Journal of Agricultural and Food Chemistry,* **53**: 1563-1570.

Biais B, Beauvoit B, William Allwood J, Deborde C, Maucourt M, Goodacre R, Rolin D, Moing A. 2010. Metabolic acclimation to hypoxia revealed by metabolite gradients in melon fruit. *Journal of Plant Physiology,* **167**: 242-245.

Biale JB. 1964. Growth, Maturation, and Senescence in Fruits Recent knowledge on growth regulation and on biological oxidations has been applied to studies with fruits. *Science,* **146**: 880-888.

Bondada BR, Matthews MA, Shackel KA. 2005. Functional xylem in the post-veraison grape berry. *Journal of Experimental Botany,* **56**: 2949-2957.

Bonhomme R. 2000. Bases and limits to using 'degree.day' units. *European Journal of Agronomy,* **13**: 1-10.

Bonora E, Noferini M, Vidoni S, Costa G. 2013. Modeling fruit ripening for improving peach homogeneity< i> in planta</i>. *Scientia Horticulturae,* **159**: 166-171.

Bower J, Holford P, Latché A, Pech J-C. 2002. Culture conditions and detachment of the fruit influence the effect of ethylene on the climacteric respiration of melon. *Postharvest Biology and Technology,* **26**: 135-146.

Buck AL. 1981. New equations for computing vapor pressure and enhancement factor. *Journal of Applied Meteorology,* **20**: 1527-1532.

Burdon JN, Moore KG, Wainwright H. 1991. Mineral distribution in mango fruit susceptible to the physiological disorder soft-nose. *Scientia Horticulturae,* **48**: 329-336.

Burg SP, Burg EA. 1962. Role of ethylene in fruit ripening. *Plant Physiology,* **37**: 179.

Cannell M, Thornley J. 2000. Modelling the components of plant respiration: some guiding principles. *Annals of Botany,* **85**: 45-54.

Carrara S, Pardossi A, Soldatini G, Tognoni F, Guidi L. 2001. Photosynthetic activity of ripening tomato fruit. *Photosynthetica,* **39**: 75-78.

Carrillo-Lopez A, Ramirez-Bustamante F, Valdez-Torres JB, Rojas-Villegas R, Yahia EM. 2000. Ripening and quality changes in mango fruit as affected by coating with an edible film. *Journal of Food Quality,* **23**: 479-486.

Castañeda-Ovando A, Pacheco-Hernández MdL, Páez-Hernández ME, Rodríguez JA, Galán-Vidal CA. 2009. Chemical studies of anthocyanins: A review. *Food Chemistry,* **113**: 859-871.

Castellarin S, Matthews M, Gaspero G, Gambetta G. 2007. Water deficits accelerate ripening and induce changes in gene expression regulating flavonoid biosynthesis in grape berries. *Planta,* **227**: 101-112.

Cellier P, Ruget F, Chartier M, Bonhomme R. 1993. Estimating the temperature of a maize apex during early growth stages. *Agricultural and Forest Meteorology,* **63**: 35-54.

Chatelet DS, Rost TL, Shackel KA, Matthews MA. 2008. The peripheral xylem of grapevine (Vitis vinifera). 1. Structural integrity in post-veraison berries. *Journal of Experimental Botany,* **59**: 1987-1996.

Choat B, Gambetta GA, Shackel KA, Matthews MA. 2009. Vascular Function in Grape Berries across Development and Its Relevance to Apparent Hydraulic Isolation. *Plant Physiology,* **151**: 1677-1687.

Chonhenchob V, Kamhangwong D, Kruenate J, Khongrat K, Tangchantra N, Wichai U, Singh SP. 2011. Preharvest bagging with wavelength-selective materials enhances development and quality of mango (Mangifera indica L.) cv. Nam Dok Mai #4. *Journal of the Science of Food and Agriculture,* **91**: 664-671.

Cieslak M, Génard M, Boudon F, Baldazzi V, Godin C, Bertin N. 2013. Integrating architecture and physiological perspective in fruit development. *7th International Conference on Functional-Structural Plant Models*. Saariselkä, Finland.

Cin VD, Danesin M, Boschetti A, Dorigoni A, Ramina A. 2005. Ethylene biosynthesis and perception in apple fruitlet abscission (Malus domestica L. Borck). *Journal of Experimental Botany,* **56**: 2995-3005.

Clearwater MJ, Luo Z, Mazzeo M, Dichio B. 2009. An external heat pulse method for measurement of sap flow through fruit pedicels, leaf petioles and other small-diameter stems. *Plant, Cell & Environment,* **32**: 1652-1663.

Clearwater MJ, Luo Z, Ong SEC, Blattmann P, Thorp TG. 2012. Vascular functioning and the water balance of ripening kiwifruit (Actinidia chinensis) berries. *Journal of Experimental Botany,* **63**: 1835-1847.

Cochard H, Damour G, Bodet C, Tharwat I, Poirier M, Améglio T. 2005. Evaluation of a new centrifuge technique for rapid generation of xylem vulnerability curves. *Physiologia Plantarum,* **124**: 410-418.

Colorimetry C. 2004. Colorimetry. *CIE Pub*.

Considine MJ, Daley DO, Whelan J. 2001. The expression of alternative oxidase and uncoupling protein during fruit ripening in mango. *Plant Physiology,* **126**: 1619-1629.

Cornillon PA. 2010. *Statistiques avec R: 2e édition augmentée*: Presses universitaires de Rennes.

Courant R, Friedrichs K, Lewy H. 1928. Über die partiellen Differenzengleichungen der mathematischen Physik. *Mathematische Annalen,* **100**: 32-74.

Cracknell Torres A, Cid Ballarín M, Socorro Monzón A, Fernández Galván D, Rosell García P, Galán Saúco V. 2002. EFFECTS OF NITROGEN AND CALCIUM SUPPLY ON THE INCIDENCE OF INTERNAL FRUIT BREAKDOWN IN¿ TOMMY ATKINS¿ MANGOES (MANGIFERA INDICA L.) GROWN IN A SOILLESS SYSTEM. *VII International Mango Symposium 645*.

Dambreville A, Lauri P-É, Trottier C, Guédon Y, Normand F. 2013. Deciphering structural and temporal interplays during the architectural development of mango trees. *Journal of Experimental Botany,* **64**: 2467-2480.

Damour G. 2008. *Bases théoriques et approches expérimentales de la modélisation des effets de la contrainte hydrique sur les échanges gazeux foliaires du manguier et du litchi*, Université de la Réunion.

Davenport TL. 2007. Reproductive physiology of mango. *Brazilian Journal of Plant Physiology,* **19**: 363-376.

De Mendiburu F. 2012. agricolae: Statistical Procedures for Agricultural Research.

Dichio B, Remorini D, Lang S. 2002. Developmental changes in xylem functionality in kiwifruit fruit: implications for fruit calcium accumulation. *V International Symposium on Kiwifruit 610*.

Dorta E, Lobo MG, González M. 2012. Using drying treatments to stabilise mango peel and seed: Effect on antioxidant activity. *LWT - Food Science and Technology,* **45**: 261-268.

Dražeta L, Lang A, Hall AJ, Volz RK, Jameson PE. 2004. Causes and Effects of Changes in Xylem Functionality in Apple Fruit. *Annals of Botany,* **93**: 275-282.

Duchêne E, Dumas V, Jaegli N, Merdinoglu D. 2012. Deciphering the ability of different grapevine genotypes to accumulate sugar in berries. *Australian Journal of Grape and Wine Research,* **18**: 319-328.

Duque P, Arrabaça JD. 1999. Respiratory metabolism during cold storage of apple fruit. II. Alternative oxidase is induced at the climacteric. *Physiologia Plantarum,* **107**: 24-31.

Eaks IL. 1978. Ripening, respiration, and ethylene production of 'Hass' avocado fruits at 20 to 40 C. *J. Amer. Soc. Hort. Sci,* **103**: 576-578.

Etienne C, Moing A, Dirlewanger E, Raymond P, Monet R, Rothan C. 2002. Isolation and characterization of six peach cDNAs encoding key proteins in organic acid metabolism and solute accumulation: involvement in regulating peach fruit acidity. *Physiologia Plantarum,* **114**: 259-270.

Fanta SW, Abera MK, Ho QT, Verboven P, Carmeliet J, Nicolai BM. 2013. Microscale modeling of water transport in fruit tissue. *Journal of Food Engineering,* **118**: 229-237.

FAO. 2011a. CURRENT SITUATION AND SHORT-TERM OUTLOOK. *COMMITTEE ON COMMODITY PROBLEMS INTERGOVERNMENTAL GROUP ON BANANAS AND TROPICAL FRUITS* Yaoundé, Cameroon, 3 – 5 May 2011

FAO. 2011b. TROPICAL FRUITS COMPENDIUM. *COMMITTEE ON COMMODITY PROBLEMS INTERGOVERNMENTAL GROUP ON BANANAS AND TROPICAL FRUITS*. Yaoundé, Cameroon, 3 – 5 May 2011.

Fernández-Otero C, Matilla AJ, Rasori A, Ramina A, Bonghi C. 2006. Regulation of ethylene biosynthesis in reproductive organs of damson plum (Prunus domestica L. subsp. Syriaca). *Plant Science,* **171**: 74-83.

Findlay N, Oliver KJ, Nil N, Coombe BG. 1987. Solute Accumulation by Grape Pericarp Cells: IV. PERFUSION OF PERICARP APOPLAST VIA THE PEDICEL AND EVIDENCE FOR XYLEM MALFUNCTION IN RIPENING BERRIES. *Journal of Experimental Botany,* **38**: 668-679.

Finger FL, Puschmann R, Barros RS. 1995. Effects of water loss on respiration, ethylene production and ripening of banana fruit. *Revista Brasileira de Fisiologia Vegetal,* **7**: 115-118.

Fishman S, Génard M. 1998. A biophysical model of fruit growth: simulation of seasonal and diurnal dynamics of mass. *Plant, Cell & Environment,* **21**: 739-752.

Fishman S, Génard M, Huguet J-G. 2001. Theoretical Analysis of Systematic Errors Introduced by a Pedicel-Girdling Technique used to Estimate Separately the Xylem and Phloem Flows. *Journal of Theoretical Biology,* **213**: 435-446.

Fonseca SC, Oliveira FAR, Brecht JK. 2002. Modelling respiration rate of fresh fruits and vegetables for modified atmosphere packages: a review. *Journal of Food Engineering,* **52**: 99-119.

Frensch J, Hsiao TC. 1995. Rapid Response of the Yield Threshold and Turgor Regulation during Adjustment of Root Growth to Water Stress in Zea mays. *Plant Physiology,* **108**: 303-312.

Gautier H, Diakou-Verdin V, Bénard C, Reich M, Buret M, Bourgaud F, Poëssel JL, Caris-Veyrat C, Génard M. 2008. How Does Tomato Quality (Sugar, Acid, and Nutritional

Quality) Vary with Ripening Stage, Temperature, and Irradiance? *Journal of Agricultural and Food Chemistry,* **56**: 1241-1250.

Génard M, Baldazzi V, Gibon Y. 2014. Metabolic studies in plant organs: don't forget dilution by growth. *Frontiers in plant science,* **5**.

Génard M, Bertin N, Borel C, Bussières P, Gautier H, Habib R, Léchaudel M, Lecomte A, Lescourret F, Lobit P, Quilot B. 2007. Towards a virtual fruit focusing on quality: modelling features and potential uses. *Journal of Experimental Botany,* **58**: 917-928.

Génard M, Bruchou C. 1992. Multivariate analysis of within-tree factors accounting for the variation of peach fruit quality. *Scientia Horticulturae,* **52**: 37-51.

Génard M, Gouble B. 2005. ETHY. A Theory of Fruit Climacteric Ethylene Emission. *Plant Physiology,* **139**: 531-545.

Génard M, Souty M. 1996. Modeling the Peach Sugar Contents in Relation to Fruit Growth. *Journal of the American Society for Horticultural Science,* **121**: 1122-1131.

Gibert C, Génard M, Vercambre G, Lescourret F. 2010. Quantification and modelling of the stomatal, cuticular and crack components of peach fruit surface conductance. *Functional Plant Biology,* **37**: 264-274.

Gibert C, Lescourret F, Génard M, Vercambre G, Pérez pastor A. 2005. Modelling the Effect of Fruit Growth on Surface Conductance to Water Vapour Diffusion. *Annals of Botany,* **95**: 673-683.

Gitelson AA, Merzlyak MN, Chivkunova OB. 2001. Optical Properties and Nondestructive Estimation of Anthocyanin Content in Plant Leaves¶. *Photochemistry and Photobiology,* **74**: 38-45.

Gitelson AA, Zur Y, Chivkunova OB, Merzlyak MN. 2002. Assessing Carotenoid Content in Plant Leaves with Reflectance Spectroscopy¶. *Photochemistry and Photobiology,* **75**: 272-281.

Godoy H, Rodriguez-Amaya D. 1989. Carotenoid composition of commercial mangoes from Brazil. *Lebensmittel-Wissenschaft+ Technologie,* **22**: 100-103.

Green P, Erickson R, Buggy J. 1971. Metabolic and physical control of cell elongation rate In vivo studies in Nitella. *Plant Physiology,* **47**: 423-430.

Greenspan MD, Shackel KA, Matthews MA. 1994. Developmental changes in the diurnal water budget of the grape berry exposed to water deficits. *Plant, Cell & Environment,* **17**: 811-820.

Grossman YL, DeJong TM. 1994. PEACH: A simulation model of reproductive and vegetative growth in peach trees. *Tree Physiology,* **14**: 329-345.

Guichard S, Gary C, Leonardi C, Bertin N. 2005. Analysis of Growth and Water Relations of Tomato Fruits in Relation to Air Vapor Pressure Deficit and Plant Fruit Load. *Journal of Plant Growth Regulation,* **24**: 201-213.

Guilioni L, Lhomme JP. 2006. Modelling the daily course of capitulum temperature in a sunflower canopy. *Agricultural and Forest Meteorology,* **138**: 258-272.

Hadfield KA, Rose JKC, Bennett AB. 1995. The respiratory climacteric is present in Charentais (Cucumis melo cv. Reticulatus F1 Alpha) melons ripened on or off the plant. *Journal of Experimental Botany,* **46**: 1923-1925.

Hamby D. 1994. A review of techniques for parameter sensitivity analysis of environmental models. *Environmental Monitoring and Assessment,* **32**: 135-154.

Hershkovitz V, Friedman H, Goldschmidt EE, Feygenberg O, Pesis E. 2011. Effect of seed on ripening control components during avocado fruit development. *Journal of Plant Physiology,* **168**: 2177-2183.

Hershkovitz V, Friedman H, Goldschmidt EE, Pesis E. 2009. The role of the embryo and ethylene in avocado fruit mesocarp discoloration. *Journal of Experimental Botany,* **60**: 791-799.

Hershkovitz V, Friedman H, Goldschmidt EE, Pesis E. 2010. Ethylene regulation of avocado ripening differs between seeded and seedless fruit. *Postharvest Biology and Technology,* **56**: 138-146.

Hetherington S. 1997. Profiling photosynthetic competence in mango fruit. *Journal of Horticultural Science,* **72**: 755-763.

Hewett EW. 2006. An overview of preharvest factors influencing postharvest quality of horticultural products. *International Journal of Postharvest Technology and Innovation,* **1**: 4-15.

Higuchi H, Sakuratani T. 2006. Water dynamics in mango (Mangifera indica L.) fruit during the young and mature fruit seasons as measured by the stem heat balance method. *Journal of the Japanese Society for Horticultural Science,* **75**.

Ho LC, Grange RI, Picken AJ. 1987. An analysis of the accumulation of water and dry matter in tomato fruit. *Plant, Cell & Environment,* **10**: 157-162.

Ho QT, Verboven P, Verlinden BE, Lammertyn J, Vandewalle S, Nicolaï BM. 2008. A continuum model for metabolic gas exchange in pear fruit. *PLoS computational biology,* **4**: e1000023.

Ho QT, Verboven P, Verlinden BE, Nicolaï BM. 2010a. A model for gas transport in pear fruit at multiple scales. *Journal of Experimental Botany,* **61**: 2071-2081.

Ho QT, Verboven P, Verlinden BE, Schenk A, Delele MA, Rolletschek H, Vercammen J, Nicolaï BM. 2010b. Genotype effects on internal gas gradients in apple fruit. *Journal of Experimental Botany,* **61**: 2745-2755.

Hofman P, Smith L, Holmes R, Campbell T, Meiburg G. 1995. Mango fruit quality at harvest is affected by production conditions.

Honda C, Kotoda N, Wada M, Kondo S, Kobayashi S, Soejima J, Zhang Z, Tsuda T, Moriguchi T. 2002. Anthocyanin biosynthetic genes are coordinately expressed during red coloration in apple skin. *Plant Physiology and Biochemistry,* **40**: 955-962.

Hossain MM, Nonami H. 2010. Effects of water flow from the xylem on the growth-induced water potential and the growth-effective turgor associated with enlarging tomato fruit. *Environment control in biology,* **48**: 101-116.

Hubbard RM, Bond BJ, Ryan MG. 1999. Evidence that hydraulic conductance limits photosynthesis in old Pinus ponderosa trees. *Tree Physiology,* **19**: 165-172.

Huguet J, Génard M, Laurent R, Besset J, Bussi C, Girard T. 1997. Xylemic, phloemic and transpiration flows to and from a peach. *IV International Peach Symposium 465*.

Iglesias I, Echeverría G, Lopez ML. 2012. Fruit color development, anthocyanin content, standard quality, volatile compound emissions and consumer acceptability of several 'Fuji' apple strains. *Scientia Horticulturae,* **137**: 138-147.

Iglesias I, Echeverría G, Soria Y. 2008. Differences in fruit colour development, anthocyanin content, fruit quality and consumer acceptability of eight 'Gala' apple strains. *Scientia Horticulturae,* **119**: 32-40.

Ihaka R, Murrell P, Hornik K, Zeileis A. 2008. colorspace: Color Space Manipulation. *R package version*: 1.0-0.

Jaeger SR, Harker R, Triggs CM, Gunson A, Campbell RL, Jackman R, Requejo-Jackman C. 2011. Determining Consumer Purchase Intentions: The Importance of Dry Matter, Size, and Price of Kiwifruit. *Journal of Food Science,* **76**: S177-S184.

Jeffery D, Smith C, Goodenough P, Prosser I, Grierson D. 1984. Ethylene-Independent and Ethylene-Dependent Biochemical Changes in Ripening Tomatoes. *Plant Physiology,* **74**: 32-38.

Jha SN, Chopra S, Kingsly ARP. 2007. Modeling of color values for nondestructive evaluation of maturity of mango. *Journal of Food Engineering,* **78**: 22-26.

Jha SN, Jaiswal P, Narsaiah K, Gupta M, Bhardwaj R, Singh AK. 2012. Non-destructive prediction of sweetness of intact mango using near infrared spectroscopy. *Scientia Horticulturae,* **138**: 171-175.

Jing P, Giusti MM. 2007. Effects of Extraction Conditions on Improving the Yield and Quality of an Anthocyanin-Rich Purple Corn (Zea mays L.) Color Extract. *Journal of Food Science,* **72**: C363-C368.

Joas J, Lechaudel M. 2008. A comprehensive integrated approach for more effective control of tropical fruit quality. *Stewart Postharvest Review,* **4**: 1-14.

Joas J, Léchaudel M. 2009. La récolte et la conservation. In: CIRAD, ed. *Guide de production intégrée de mangues à la Réunion*. Montpellier.

Joas J, Vulcain E, Desvignes C, Morales E, Léchaudel M. 2012. Physiological age at harvest regulates the variability in postharvest ripening, sensory and nutritional characteristics of mango (Mangifera indica L.) cv. Coghshall due to growing conditions. *Journal of the Science of Food and Agriculture,* **92**: 1282-1290.

Jordan RB, Walton EF, Klages KU, Seelye RJ. 2000. Postharvest fruit density as an indicator of dry matter and ripened soluble solids of kiwifruit. *Postharvest Biology and Technology,* **20**: 163-173.

Kang SP, East AR, Trujillo FJ. 2008. Colour vision system evaluation of bicolour fruit: A case study with 'B74' mango. *Postharvest Biology and Technology,* **49**: 77-85.

Keller M, Smith JP, Bondada BR. 2006. Ripening grape berries remain hydraulically connected to the shoot. *Journal of Experimental Botany,* **57**: 2577-2587.

Ketsa S, Phakawatmongkol W, Subhadrabhandhu S. 1999. Peel Enzymatic Activity and Colour Changes in Ripening Mango Fruit. *Journal of Plant Physiology,* **154**: 363-366.

Khabba S, Ledent JF, Lahrouni A. 2001. Maize ear temperature. *European Journal of Agronomy,* **14**: 197-208.

Kitinoja L, AlHassan H, Saran S, Roy S. 2010. Identification of appropriate postharvest technologies for improving market access and incomes for small horticultural farmers in Sub-Saharan Africa and South Asia. Part.

Lammertyn J, Scheerlinck N, Jancsók P, Verlinden BE, Nicolaï BM. 2003a. A respiration–diffusion model for 'Conference' pears I: model development and validation. *Postharvest Biology and Technology,* **30**: 29-42.

Lammertyn J, Scheerlinck N, Jancsók P, Verlinden BE, Nicolaï BM. 2003b. A respiration–diffusion model for 'Conference' pears: II. Simulations and relation to core breakdown. *Postharvest Biology and Technology,* **30**: 43-55.

Lancaster JE, Lister CE, Reay PF, Triggs CM. 1997. Influence of Pigment Composition on Skin Color in a Wide Range of Fruit and Vegetables. *Journal of the American Society for Horticultural Science,* **122**: 594-598.

Lang A. 1990. Xylem, Phloem and Transpiration Flows in Developing Apple Fruits. *Journal of Experimental Botany,* **41**: 645-651.

Lang A, Ryan KG. 1994. Vascular Development and Sap Flow in Apple Pedicels. *Annals of Botany,* **74**: 381-388.

Lang A, Thorpe M. 1989. Xylem, phloem and transpiration flows in a grape: application of a technique for measuring the volume of attached fruits to high resolution using Archimedes' principle. *Journal of Experimental Botany,* **40**: 1069-1078.

Lebrun M, Plotto A, Goodner K, Ducamp M-N, Baldwin E. 2008. Discrimination of mango fruit maturity by volatiles using the electronic nose and gas chromatography. *Postharvest Biology and Technology,* **48**: 122-131.

Lechaudel M, Genard M, Lescourret F, Urban L, Jannoyer M. 2002. Leaf-to-fruit ratio affects water and dry-matter content of mango fruit. *Journal of Horticultural Science and Biotechnology,* **77**: 773-777.

Léchaudel M, Génard M, Lescourret F, Urban L, Jannoyer M. 2005a. Modeling effects of weather and source–sink relationships on mango fruit growth. *Tree Physiology,* **25**: 583-597.

Léchaudel M, Joas J. 2006. Quality and maturation of mango fruits of cv. Cogshall in relation to harvest date and carbon supply. *Australian Journal of Agricultural Research,* **57**: 419-426.

Léchaudel M, Joas J. 2007. An overview of preharvest factors influencing mango fruit growth, quality and postharvest behaviour. *Brazilian Journal of Plant Physiology,* **19**: 287-298.

Léchaudel M, Joas J, Caro Y, Génard M, Jannoyer M. 2005b. Leaf:fruit ratio and irrigation supply affect seasonal changes in minerals, organic acids and sugars of mango fruit. *Journal of the Science of Food and Agriculture,* **85**: 251-260.

Léchaudel M, Lopez-Lauri F, Vidal V, Sallanon H, Joas J. 2012. Response of the physiological parameters of mango fruit (transpiration, water relations and antioxidant system) to its light and temperature environment. *Journal of plant physiology*.

Lechaudel M, Urban L, Joas J. 2010. Chlorophyll Fluorescence, a Nondestructive Method To Assess Maturity of Mango Fruits (Cv. 'Cogshall') without Growth Conditions Bias. *Journal of Agricultural and Food Chemistry,* **58**: 7532-7538.

Léchaudel M, Vercambre G, Lescourret F, Normand F, Génard M. 2007. An analysis of elastic and plastic fruit growth of mango in response to various assimilate supplies. *Tree Physiology,* **27**: 219-230.

Lee J, Durst RW, Wrolstad RE. 2005. Determination of Total Monomeric Anthocyanin Pigment Content of Fruit Juices, Beverages, Natural Colorants, and Wines by the pH Differential Method: Collaborative Study. *Journal of AOAC International,* **88**: 1269-1278.

Lelièvre JM, Latche A, Jones B, Bouzayen M, Pech JC. 1997. Ethylene and fruit ripening. *Physiologia plantarum,* **101**: 727-739.

León AP, Viña SZ, Frezza D, Chaves A, Chiesa A. 2007. Estimation of Chlorophyll Contents by Correlations between SPAD-502 Meter and Chroma Meter in Butterhead Lettuce. *Communications in Soil Science and Plant Analysis,* **38**: 2877-2885.

Leonardi C, Baille A, Guichard S. 2000a. Predicting transpiration of shaded and non-shaded tomato fruits under greenhouse environments. *Scientia Horticulturae,* **84**: 297-307.

Leonardi C, Guichard S, Bertin N. 2000b. High vapour pressure deficit influences growth, transpiration and quality of tomato fruits. *Scientia Horticulturae,* **84**: 285-296.

Lescourret F, Génard M, Habib R, Fishman S. 2001. Variation in surface conductance to water vapor diffusion in peach fruit and its effects on fruit growth assessed by a simulation model. *Tree Physiology,* **21**: 735-741.

Lester GE. 2008. Antioxidant, Sugar, Mineral, and Phytonutrient Concentrations across Edible Fruit Tissues of Orange-Fleshed Honeydew Melon (Cucumis melo L.). *Journal of Agricultural and Food Chemistry,* **56**: 3694-3698.

Lewicki PP. 2004. Water as the determinant of food engineering properties. A review. *Journal of Food Engineering,* **61**: 483-495.

Li S-H, Huguet J-G, Bussi C. 1989. Irrigation scheduling in a mature peach orchard using tensiometers and dendrometers. *Irrigation and Drainage Systems,* **3**: 1-12.

Lin S-f, Walsh CS. 2008. Studies of the "tree factor" and its role in the maturation and ripening of 'Gala' and 'Fuji' apples. *Postharvest Biology and Technology,* **48**: 99-106.

Litz RE. 2009. *The Mango, 2nd Edition: Botany, Production and Uses*: Wiley Online Library.

Lobit P, Génard M, Wu BH, Soing P, Habib R. 2003. Modelling citrate metabolism in fruits: responses to growth and temperature. *Journal of Experimental Botany,* **54**: 2489-2501.

Loeillet D. 1994. The European mango market: A promising tropical fruit. *Fruits,* **49**: 434-435.

Luchsinger L, Ortin P, Reginato G, Infante R. 2001. INFLUENCE OF CANOPY FRUIT POSITION ON THE MATURITY AND QUALITY OF¿ ANGELUS¿ PEACHES. *V International Peach Symposium 592*.

Lytovchenko A, Eickmeier I, Pons C, Osorio S, Szecowka M, Lehmberg K, Arrivault S, Tohge T, Pineda B, Anton MT, Hedtke B, Lu Y, Fisahn J, Bock R, Stitt M, Grimm B, Granell A, Fernie AR. 2011. Tomato Fruit Photosynthesis Is Seemingly Unimportant in Primary Metabolism and Ripening But Plays a Considerable Role in Seed Development. *Plant Physiology,* **157**: 1650-1663.

Maguire KM, Banks NH, Lang A. 1999. Sources of variation in water vapour permeance of apple fruit. *Postharvest Biology and Technology,* **17**: 11-17.

Mangaraj S, Goswami TK. 2011. Modeling of Respiration Rate of Litchi Fruit under Aerobic Conditions. *Food and Bioprocess Technology,* **4**: 272-281.

Marschner H. 1995. *Mineral Nutrition of Higher Plants*: Acad. Press.

Maxwell E.L. 1987. A quasi-physical model for converting hourly global horizontal to direct normal insolation. *Report SERI/TR-215-3087, Solar Energy Research Institute, Golden, CO (1987)*.

Mazzeo M, Dichio B, Clearwater MJ, Montanaro G, Xiloyannis C. 2013. Hydraulic resistance of developing Actinidia fruit. *Annals of Botany,* **112**: 197-205.

McAtee P, Karim S, Schaffer R, David K. 2013. A dynamic interplay between phytohormones is required for fruit development, maturation, and ripening. *Front Plant Sci,* **4**: 79.

McDonald RE, Nordby HE, McCollum TG. 1993. Epicuticular Wax Morphology and Composition are Related to Grapefruit Chilling Injury. *HortScience,* **28**: 311-312.

McGlone VA, Jordan RB, Seelye R, Martinsen PJ. 2002. Comparing density and NIR methods for measurement of Kiwifruit dry matter and soluble solids content. *Postharvest Biology and Technology,* **26**: 191-198.

Measham PF, Wilson SJ, Gracie AJ, Bound SA. 2014. Tree water relations: Flow and fruit. *Agricultural Water Management,* **137**: 59-67.

Medlicott AP, Bhogal M, Reynolds SB. 1986. Changes in peel pigmentation during ripening of mango fruit (Mangifera indica var. Tommy Atkins). *Annals of Applied Biology,* **109**: 651-656.

Meinzer FC, McCulloh KA. 2013. Xylem recovery from drought-induced embolism: where is the hydraulic point of no return? *Tree Physiology,* **33**: 331-334.

Mendoza D, Wills RBH. 1984. *Mango: fruit development, postharvest physiology and marketing in ASEAN*: ASEAN Food Handling Bureau.

Mercado-Silva E, Benito-Bautista P, de los Angeles García-Velasco M. 1998. Fruit development, harvest index and ripening changes of guavas produced in central Mexico. *Postharvest Biology and Technology,* **13**: 143-150.

Merzlyak MN, Gitelson AA, Chivkunova OB, Solovchenko AE, Pogosyan SI. 2003a. Application of Reflectance Spectroscopy for Analysis of Higher Plant Pigments. *Russian Journal of Plant Physiology,* **50**: 704-710.

Merzlyak MN, Solovchenko AE. 2002. Photostability of pigments in ripening apple fruit: a possible photoprotective role of carotenoids during plant senescence. *Plant Science,* **163**: 881-888.

Merzlyak MN, Solovchenko AE, Chivkunova OB. 2002. Patterns of pigment changes in apple fruits during adaptation to high sunlight and sunscald development. *Plant Physiology and Biochemistry,* **40**: 679-684.

Merzlyak MN, Solovchenko AE, Gitelson AA. 2003b. Reflectance spectral features and non-destructive estimation of chlorophyll, carotenoid and anthocyanin content in apple fruit. *Postharvest Biology and Technology,* **27**: 197-211.

Mevik B-H, Wehrens R. 2007. The pls package: principal component and partial least squares regression in R. *Journal of Statistical Software,* **18**: 1-24.

Mielke MS, Schaffer B, Schilling AC. 2012. Evaluation of reflectance spectroscopy indices for estimation of chlorophyll content in leaves of a tropical tree species. *Photosynthetica,* **50**: 343-352.

Milad RE, Shackel KA. 1992. Water Relations of Fruit End Cracking in French Prune (Prunus domestica L. cv. French). *Journal of the American Society for Horticultural Science,* **117**: 824-828.

Mills TM, Behboudian MH, Clothier BE. 1996. Water Relations, Growth, and the Composition of `Braeburn' Apple Fruit under Deficit Irrigation. *Journal of the American Society for Horticultural Science,* **121**: 286-291.

Mita S, Kawamura S, Yamawaki K, Nakamura K, Hyodo H. 1998. Differential Expression of Genes Involved in the Biosynthesis and Perception of Ethylene during Ripening of Passion Fruit (Passiflora edulis Sims). *Plant and Cell Physiology,* **39**: 1209-1217.

Mitcham EJ, McDonald RE. 1992. Cell Wall Modification during Ripening of `Keitt' and `Tommy Atkins' Mango Fruit. *Journal of the American Society for Horticultural Science,* **117**: 919-924.

Moing A, Aharoni A, Biais B, Rogachev I, Meir S, Brodsky L, Allwood JW, Erban A, Dunn WB, Kay L, de Koning S, de Vos RCH, Jonker H, Mumm R, Deborde C, Maucourt M,

Bernillon S, Gibon Y, Hansen TH, Husted S, Goodacre R, Kopka J, Schjoerring JK, Rolin D, Hall RD. 2011. Extensive metabolic cross-talk in melon fruit revealed by spatial and developmental combinatorial metabolomics. *New Phytologist,* **190**: 683-696.

Montanaro G, Dichio B, Xiloyannis C. 2010. Significance of fruit transpiration on calcium nutrition in developing apricot fruit. *Journal of Plant Nutrition and Soil Science,* **173**: 618-622.

Montanaro G, Dichio B, Xiloyannis C, Celano G. 2006. Light influences transpiration and calcium accumulation in fruit of kiwifruit plants (Actinidia deliciosa var. deliciosa). *Plant Science,* **170**: 520-527.

Montanaro G, Dichio B, Xiloyannis C, Lang A. 2012. Fruit transpiration in kiwifruit: environmental drivers and predictive model. *AoB plants,* **2012**.

Monteith J, Unsworth ME. 1990. Principles of Environmental Physics. Edward Arnold, London. London.

Morandi B, Manfrini L, Losciale P, Zibordi M, Corelli Grappadelli L. 2010. Changes in vascular and transpiration flows affect the seasonal and daily growth of kiwifruit (Actinidia deliciosa) berry. *Annals of Botany,* **105**: 913-923.

Morandi B, Rieger M, Grappadelli LC. 2007. Vascular flows and transpiration affect peach (Prunus persica Batsch.) fruit daily growth. *Journal of Experimental Botany,* **58**: 3941-3947.

Morandi B, Zibordi M, Losciale P, Manfrini L, Pierpaoli E, Grappadelli LC. 2011. Shading decreases the growth rate of young apple fruit by reducing their phloem import. *Scientia Horticulturae,* **127**: 347-352.

Morgan PW, Drew MC. 1997. Ethylene and plant responses to stress. *Physiologia Plantarum,* **100**: 620-630.

Nakano R, Ogura E, Kubo Y, Inaba A. 2003. Ethylene biosynthesis in detached young persimmon fruit is initiated in calyx and modulated by water loss from the fruit. *Plant Physiology,* **131**: 276-286.

Nguyen H., Hofman P., Holmes R., Bally I., Stubbings B., R. M. 2004. Effect of nitrogen on the skin colour and other quality attributes of ripe 'Kensington Pride' mango (Mangifera indica L.) fruit. *Ashford, ROYAUME-UNI,* **79**: 204-210.

Nicolaï BM, Beullens K, Bobelyn E, Peirs A, Saeys W, Theron KI, Lammertyn J. 2007. Nondestructive measurement of fruit and vegetable quality by means of NIR spectroscopy: A review. *Postharvest Biology and Technology,* **46**: 99-118.

Njoroge CK, Kerbel EL, Briskin DP. 1998. Effect of calcium and calmodulin antagonists on ethylene biosynthesis in tomato fruits. *Journal of the Science of Food and Agriculture,* **76**: 209-214.

Nordby HE, McDonald RE. 1995. Variations in Chilling Injury and Epicuticular Wax Composition of White Grapefruit with Canopy Position and Fruit Development during the Season. *Journal of Agricultural and Food Chemistry,* **43**: 1828-1833.

Nordey T, Joas J, Davrieux F, Génard M, Léchaudel M. 2014a. Non-destructive prediction of color and pigment contents in mango peel. *Scientia Horticulturae,* **171**: 37-44.

Nordey T, Lechaudel M, Génard M, Joas J. 2014b. Spatial and temporal variations of mango colour, acidity and sweetness in relation to temperature and ethylene gradients within the fruit. *Journal of Plant Physiology*.

Nordey T, Léchaudel M, Saudreau M, Joas J, Génard M. 2014c. Model-Assisted Analysis of Spatial and Temporal Variations in Fruit Temperature and Transpiration Highlighting the Role of Fruit Development. *PloS one,* **9**: e92532.

Normand F, Habib R. 2001. Phenology of strawberry guava (Psidium cattleianum) in Réunion Island. *Journal of Horticultural Science and Biotechnology,* **76**: 541-545.

Nunez-Elisea R, Davenport TL. 1986. Abscission of Mango Fruitlets as Influenced by Enhanced Ethylene Biosynthesis. *Plant Physiology,* **82**: 991-994.

Olano CT, Schnell RJ, Quintanilla WE, Campbell RJ. 2005. Pedigree analysis of Florida mango cultivars. *Proc. Fla. State Hort. Soc*.

Ornelas-Paz JdJ, Yahia EM, Gardea AA. 2008. Changes in external and internal color during postharvest ripening of 'Manila' and 'Ataulfo' mango fruit and relationship with carotenoid content determined by liquid chromatography–APcI+-time-of-flight mass spectrometry. *Postharvest Biology and Technology,* **50**: 145-152.

Park S, Cheng NH, Pittman JK, Yoo KS, Park J, Smith RH, Hirschi KD. 2005. Increased Calcium Levels and Prolonged Shelf Life in Tomatoes Expressing Arabidopsis H+/Ca2+ Transporters. *Plant Physiology,* **139**: 1194-1206.

Paul V, Malik S, Srivastava G. 2007. Intervarietal differences in the surface morphology and anatomy of mango (Mangifera indica L.) fruit. *Phytomorphology,* **57**: 211-220.

Paul V, Pandey R, Srivastava G. 2012. The fading distinctions between classical patterns of ripening in climacteric and non-climacteric fruit and the ubiquity of ethylene—An overview. *Journal of Food Science and Technology,* **49**: 1-21.

Paull R. 1999. Effect of temperature and relative humidity on fresh commodity quality. *Postharvest Biology and Technology,* **15**: 263-277.

Paull RE, Jung Chen N. 2000. Heat treatment and fruit ripening. *Postharvest Biology and Technology,* **21**: 21-37.

Pech JC, Bouzayen M, Latché A. 2008. Climacteric fruit ripening: Ethylene-dependent and independent regulation of ripening pathways in melon fruit. *Plant Science,* **175**: 114-120.

Pedreschi R, Franck C, Lammertyn J, Erban A, Kopka J, Hertog M, Verlinden B, Nicolaï B. 2009. Metabolic profiling of 'Conference' pears under low oxygen stress. *Postharvest Biology and Technology,* **51**: 123-130.

Perotti VE, Moreno AS, Podestá FE. 2014. Physiological aspects of fruit ripening: The mitochondrial connection. *Mitochondrion,* **17**: 1-6.

Picard A, Davis RS, Gläser M, Fujii K. 2008. Revised formula for the density of moist air (CIPM-2007). *Metrologia,* **45**: 149.

Proctor J, Creasy L. 1969. The anthocyanin of the mango fruit. *Phytochemistry,* **8**: 2108.

Raimondo F, Trifilò P, Gullo MAL, Buffa R, Nardini A, Salleo S. 2009. Effects of reduced irradiance on hydraulic architecture and water relations of two olive clones with different growth potentials. *Environmental and Experimental Botany,* **66**: 249-256.

Ravindra MR, Goswami TK. 2008. Modelling the respiration rate of green mature mango under aerobic conditions. *Biosystems Engineering,* **99**: 239-248.

RDC Team. 2012. R: A Language and Environment for Statistical Computing.

Reda I, Andreas A. 2004. Solar position algorithm for solar radiation applications. *Solar Energy,* **76**: 577-589.

Ribeiro da Luz B. 2006. Attenuated total reflectance spectroscopy of plant leaves: a tool for ecological and botanical studies. *New Phytologist,* **172**: 305-318.

Richter A, Nikrityuk PA. 2012. Drag forces and heat transfer coefficients for spherical, cuboidal and ellipsoidal particles in cross flow at sub-critical Reynolds numbers. *International Journal of Heat and Mass Transfer,* **55**: 1343-1354.

Ross Ihaka, Paul Murrell, Kurt Hornik, Zeileis A. 2012. colorspace: Color Space Manipulation.

Saltveit ME. 1993. Internal carbon dioxide and ethylene levels in ripening tomato fruit attached to or detached from the plant. *Physiologia Plantarum,* **89**: 204-210.

Saltveit ME. 1999. Effect of ethylene on quality of fresh fruits and vegetables. *Postharvest Biology and Technology,* **15**: 279-292.

Sánchez T, Chávez AL, Ceballos H, Rodriguez-Amaya DB, Nestel P, Ishitani M. 2006. Reduction or delay of post-harvest physiological deterioration in cassava roots with higher carotenoid content. *Journal of the Science of Food and Agriculture,* **86**: 634-639.

Sangsing K, Kasemsap P, Thanisawanyangkura S, Sangkhasila K, Gohet E, Thaler P, Cochard H. 2004. Xylem embolism and stomatal regulation in two rubber clones (Hevea brasiliensis Muell. Arg.). *Trees,* **18**: 109-114.

Saranwong S, Sornsrivichai J, Kawano S. 2004. Prediction of ripe-stage eating quality of mango fruit from its harvest quality measured nondestructively by near infrared spectroscopy. *Postharvest Biology and Technology,* **31**: 137-145.

Saudreau M, Marquier A, Adam B, Monney P, Sinoquet H. 2009. Experimental study of fruit temperature dynamics within apple tree crowns. *Agricultural and Forest Meteorology,* **149**: 362-372.

Saudreau M, Marquier A, Adam B, Sinoquet H. 2011. Modelling fruit-temperature dynamics within apple tree crowns using virtual plants. *Annals of Botany,* **108**: 1111-1120.

Saudreau M, Sinoquet H, Santin O, Marquier A, Adam B, Longuenesse J-J, Guilioni L, Chelle M. 2007. A 3D model for simulating the spatial and temporal distribution of temperature within ellipsoidal fruit. *Agricultural and Forest Meteorology,* **147**: 1-15.

Schreiner M, Korn M, Stenger M, Holzgreve L, Altmann M. 2013. Current understanding and use of quality characteristics of horticulture products. *Scientia Horticulturae,* **163**: 63-69.

Shellie KC, Saltveit ME. 1993. The Lack of a Respiratory Rise in Muskmelon Fruit Ripening on the Plant Challenges the Definition of Climacteric Behaviour. *Journal of Experimental Botany,* **44**: 1403-1406.

Shiomi S, Wamocho LS, Agong SG. 1996. Ripening characteristics of purple passion fruit on and off the vine. *Postharvest Biology and Technology,* **7**: 161-170.

Siebel E. 1982. Specific heat of various products. *Ice and Refrigeration,* **2**: 256-257.

Simmons S, Hofman P, Whiley A, Hetherington S. 1998. Effects of preharvest calcium sprays and fertilizers, leaf: fruit ratios, and water stress on mango fruit quality. *ACIAR PROCEEDINGS*: Australian Centre for International Agricultural Research.

Sims DA, Gamon JA. 2002. Relationships between leaf pigment content and spectral reflectance across a wide range of species, leaf structures and developmental stages. *Remote Sensing of Environment,* **81**: 337-354.

Singh Z, Malik AU, Davenport TL. 2010. Fruit Drop in Mango. *Horticultural Reviews,* **31**: 111.

Sivakumar D, Jiang Y, Yahia EM. 2011. Maintaining mango (Mangifera indica L.) fruit quality during the export chain. *Food Research International,* **44**: 1254-1263.

Smith GS, Gravett IM, Edwards CM, Curtis JP, Buwalda JG. 1994. Spatial Analysis of the Canopy of Kiwifruit Vines as it Relates to the Physical, Chemical and Postharvest Attributes of the Fruit. *Annals of Botany,* **73**: 99-111.

Solovchenko AE, Chivkunova OB, Merzlyak MN, Gudkovsky VA. 2005. Relationships between chlorophyll and carotenoid pigments during on- and off-tree ripening of apple fruit as revealed non-destructively with reflectance spectroscopy. *Postharvest Biology and Technology,* **38**: 9-17.

Song J, Bangerth F. 1996. The effect of harvest date on aroma compound production from 'Golden Delicious' apple fruit and relationship to respiration and ethylene production. *Postharvest Biology and Technology,* **8**: 259-269.

Song J, Deng W, Beaudry RM, Armstrong PR. 1997. Changes in Chlorophyll Fluorescence of Apple Fruit during Maturation, Ripening, and Senescence. *HortScience,* **32**: 891-896.

Souty M, Génard M, Reich M, Albagnac G. 1999. Effect of assimilate supply on peach fruit maturation and quality. *Canadian Journal of Plant Science,* **79**: 259-268.

Sperry JS, Ikeda T. 1997. Xylem cavitation in roots and stems of Douglas-fir and white fir. *Tree Physiology,* **17**: 275-280.

Steyn WJ, Holcroft DM, Wand SJE, Jacobs G. 2004. Anthocyanin Degradation in Detached Pome Fruit with Reference to Preharvest Red Color Loss and Pigmentation Patterns of Blushed and Fully Red Pears. *Journal of the American Society for Horticultural Science,* **129**: 13-19.

Steyn WJ, Wand SJE, Holcroft DM, Jacobs G. 2002. Anthocyanins in vegetative tissues: a proposed unified function in photoprotection. *New Phytologist,* **155**: 349-361.

Steyn WJ, Wand SJE, Jacobs G, Rosecrance RC, Roberts SC. 2009. Evidence for a photoprotective function of low-temperature-induced anthocyanin accumulation in apple and pear peel. *Physiologia Plantarum,* **136**: 461-472.

Sugiyama J. 1999. Visualization of Sugar Content in the Flesh of a Melon by Near-Infrared Imaging. *Journal of Agricultural and Food Chemistry,* **47**: 2715-2718.

Tharanathan RN, Yashoda HM, Prabha TN. 2006. Mango (Mangifera indica L.), "The King of Fruits"—An Overview. *Food Reviews International,* **22**: 95-123.

Tingwa P, Young R. 1974. The effect of calcium on the ripening of avocado (Persea americana Mill.) fruits. *J. Amer. Soc. Hort. Sci,* **99**: 540-542.

Tovar Bz, García HS, Mata M. 2001. Physiology of pre-cut mango. I. ACC and ACC oxidase activity of slices subjected to osmotic dehydration. *Food research international,* **34**: 207-215.

Trifilò P, Raimondo F, Lo Gullo MA, Nardini A, Salleo S. 2010. Hydraulic connections of leaves and fruit to the parent plant in Capsicum frutescens (hot pepper) during fruit ripening. *Annals of Botany,* **106**: 333-341.

Turner N. 1981. Techniques and experimental approaches for the measurement of plant water status. *Plant and Soil,* **58**: 339-366.

Tyerman SD, Tilbrook J, Pardo C, Kotula L, Sullivan W, Steudle E. 2004. Direct measurement of hydraulic properties in developing berries of Vitis vinifera L. cv Shiraz and Chardonnay. *Australian Journal of Grape and Wine Research,* **10**: 170-181.

Tyree MT, Sperry JS. 1988. Do Woody Plants Operate Near the Point of Catastrophic Xylem Dysfunction Caused by Dynamic Water Stress?: Answers from a Model. *Plant Physiology,* **88**: 574-580.

Urbano Bron I, Vasconcelos Ribeiro R, Azzolini M, Pedro Jacomino A, Caruso Machado E. 2004. Chlorophyll fluorescence as a tool to evaluate the ripening of 'Golden' papaya fruit. *Postharvest Biology and Technology,* **33**: 163-173.

Uthaibutra J, Saegnil K, Sornsrivichai J, Kumpoun W, Sardsud V. 1998. Effects of Fruit Position and Preharvest Calcium Dips on'Nam Doc Mai'Mango Fruit Quality. *ACIAR PROCEEDINGS*: Australian Centre for International Agricultural Research.

Valente M, Nicolas J. 1990. Thermal conductivity of avocado pulp. *Engineering and Food,* **1**: 432-440.

Van Ieperen W, Volkov VS, Van Meeteren U. 2003. Distribution of xylem hydraulic resistance in fruiting truss of tomato influenced by water stress. *Journal of Experimental Botany,* **54**: 317-324.

Vásquez-Caicedo AL, Neidhart S, Carle R. 2002. Postharvest ripening behavior of nine Thai mango cultivars and their suitability for industrial applications. *VII International Mango Symposium 645*.

Vasquez-Caicedo AL, Sruamsiri P, Carle R, Neidhart S. 2005. Accumulation of All-trans-β-carotene and Its 9-cis and 13-cis Stereoisomers during Postharvest Ripening of Nine Thai Mango Cultivars. *Journal of Agricultural and Food Chemistry,* **53**: 4827-4835.

Veraverbeke EA, Lammertyn J, Saevels S, Nicolaï BM. 2001. Changes in chemical wax composition of three different apple (Malus domestica Borkh.) cultivars during storage. *Postharvest Biology and Technology,* **23**: 197-208.

Verboven P, Kerckhofs G, Mebatsion HK, Ho QT, Temst K, Wevers M, Cloetens P, Nicolaï BM. 2008. Three-Dimensional Gas Exchange Pathways in Pome Fruit Characterized by Synchrotron X-Ray Computed Tomography. *Plant Physiology,* **147**: 518-527.

Vogg G, Fischer S, Leide J, Emmanuel E, Jetter R, Levy AA, Riederer M. 2004. Tomato fruit cuticular waxes and their effects on transpiration barrier properties: functional characterization of a mutant deficient in a very-long-chain fatty acid β-ketoacyl-CoA synthase. *Journal of Experimental Botany,* **55**: 1401-1410.

Vos J. 1978. Colorimetric and photometric properties of a 2 fundamental observer. *Color Research & Application,* **3**: 125-128.

Wagner AM, Krab K, Wagner MJ, Moore AL. 2008. Regulation of thermogenesis in flowering Araceae: The role of the alternative oxidase. *Biochimica et Biophysica Acta (BBA) - Bioenergetics,* **1777**: 993-1000.

Walter WM, Randall-Schadel B, Schadel WE. 1990. Wound Healing in Cucumber Fruit. *Journal of the American Society for Horticultural Science,* **115**: 444-452.

Wang B, Wang J, Feng X, Lin L, Zhao Y, Jiang W. 2009. Effects of 1-MCP and exogenous ethylene on fruit ripening and antioxidants in stored mango. *Plant Growth Regulation,* **57**: 185-192.

Wang B, Wang J, Liang H, Yi J, Zhang J, Lin L, Wu Y, Feng X, Cao J, Jiang W. 2008. Reduced chilling injury in mango fruit by 2,4-dichlorophenoxyacetic acid and the antioxidant response. *Postharvest Biology and Technology,* **48**: 172-181.

Wang SY, Camp MJ. 2000. Temperatures after bloom affect plant growth and fruit quality of strawberry. *Scientia Horticulturae,* **85**: 183-199.

Wellburn A.R. 1994. The Spectral Determination of Chlorophylls a and b, as well Total Carotenoids, Using Various Solvents with Spectrophotometers of Differents Resolution. *Journal Plant Physiologie,* **144**: 307-313.

Whitaker S. 1972. Forced convection heat transfer correlations for flow in pipes, past flat plates, single cylinders, single spheres, and for flow in packed beds and tube bundles. *AIChE Journal,* **18**: 361-371.

Wold S, Sjöström M, Eriksson L. 2001. PLS-regression: a basic tool of chemometrics. *Chemometrics and Intelligent Laboratory Systems,* **58**: 109-130.

Wolfe K, Wu X, Liu RH. 2003. Antioxidant Activity of Apple Peels. *Journal of Agricultural and Food Chemistry,* **51**: 609-614.

Woolf AB, Bowen JH, Ferguson IB. 1999. Preharvest exposure to the sun influences postharvest responses of 'Hass' avocado fruit. *Postharvest Biology and Technology,* **15**: 143-153.

Yamada H, Ohmura H, Arai C, Terui M. 1994. Effect of Preharvest Fruit Temperature on Ripening, Sugars, and Watercore Occurrence in Apples. *Journal of the American Society for Horticultural Science,* **119**: 1208-1214.

Young T, Koo RC, Miner JT. 1965. Fertilizer trials with Kent mangos. *Proc. Fla. State Hortic. Soc*.

Zaharah SS, Singh Z, Symons GM, Reid JB. 2013. Mode of action of abscisic acid in triggering ethylene biosynthesis and softening during ripening in mango fruit. *Postharvest Biology and Technology,* **75**: 37-44.

Zhang M, Yuan B, Leng P. 2009. The role of ABA in triggering ethylene biosynthesis and ripening of tomato fruit. *Journal of Experimental Botany,* **60**: 1579-1588.

Zude-Sasse M, Truppel I, Herold B. 2002. An approach to non-destructive apple fruit chlorophyll determination. *Postharvest Biology and Technology,* **25**: 123-133.

Zude M. 2003. Comparison of indices and multivariate models to non-destructively predict the fruit chlorophyll by means of visible spectrometry in apple fruit. *Analytica Chimica Acta,* **481**: 119-126.

Abstract

One of the major difficulties involved in marketing fresh mango is to manage its quality. Mango quality includes several attributes such as size, total soluble solids content, acidity and color, all of which vary with growing conditions and during ripening. The aim of this thesis is to determine the impact of growing conditions on fruit quality and ripening through experimental and modeling approaches.

Experimental studies have revealed that size, dry mass and maturity vary considerably between mangoes according to their position in the tree and fruit load. Measurements suggest that fruit growth is affected by the embolization of sap-conducting vessels. In addition to differences measured between mangoes, our results showed that quality attributes vary within fruits in relation to the maturity gradient.

A physical model showed that climatic variations within the tree caused substantial temperature gradients within mangoes that change with the fruit position in the tree. These simulations revealed that quality differences within mangoes are not related to the temperature gradient, except for fruit color. Use of a model that simulates the biosynthetic pathway of ethylene indicated that maturity differences between mangoes are explained by differences in carbon supply and, to a much lesser extent, to differences in temperature. The integration of experimental results into a growth model revealed that the embolization of sap-conducting vessels caused the slowdown of fruit enlargement. Lastly, when all of these models were coupled to a model that simulates fruit growth in dry mass, it was demonstrated that variations in size, dry matter content and maturity between mangoes were caused by differences in fruit load, flowering time, fruit dry mass at the end of cell division and transpiration, rather than by differences in temperature.

The multidisciplinary approach developed made it possible to better understand the processes involved in fruit quality and ripening and to open new areas of research.

Résumé

La qualité du fruit regroupe un ensemble d'attributs, comme le calibre, la teneur en composés solubles, l'acidité et la couleur, qui varient en fonction des conditions de croissance rencontrées par le fruit pendant son développement et au cours de son murissement. Ce travail de thèse vise à déterminer, par des approches expérimentales et de modélisation, l'impact des conditions de croissance de la mangue sur les processus impliqués dans l'élaboration de sa qualité et de son murissement.

Les approches expérimentales ont révélé d'importantes variations de calibre, masse sèche, et maturité entre les mangues selon leur position dans l'arbre et la charge en fruits. Nos mesures ont suggéré que la croissance des mangues est impactée par la diminution des flux de xylème causé par l'embolisation des vaisseaux conducteurs de sève. En plus des différences mesurées entre les fruits, nos résultats ont indiqué des variations de couleur de peau et de pulpe, d'acidité et de teneur en composés solubles au sein même des mangues qui s'expliquent en partie par les gradients de maturité.

L'établissement d'un modèle thermodynamique a permis de montrer que les microclimats au sein de l'arbre génèrent un gradient de température au sein de la mangue qui varie en fonction de la position dans l'arbre. Il a été montré que ce gradient de température n'explique pas les variations d'acidité, de couleur de pulpe et de teneur en composés solubles au sein de la mangue. L'utilisation d'un modèle simulant la synthèse de l'éthylène dans la mangue a mis en évidence que les différences de maturité entre les mangues dans l'arbre s'expliquent davantage par les différences de disponibilité carbonée que par les différences de température. L'intégration des résultats expérimentaux dans un modèle de croissance en matière fraiche a permis de confirmer que l'embolisation des vaisseaux conducteurs de sève est à l'origine du ralentissement de croissance de la mangue. Enfin, le couplage de tous ces modèles à un modèle de croissance en matière sèche a montré que les variations de calibre, teneur en matière sèche et maturité entre les mangues ne sont pas causées par les différences de température, mais par les différences de charge en fruits, de période de floraison, de masse sèche des fruits à la fin de la division cellulaire, et de transpiration.

L'approche pluridisciplinaire, i.e., physique, écophysiologique et biochimique, utilisée dans ce travail de thèse a permis d'acquérir de nouvelles connaissances sur l'élaboration de la qualité du fruit et son murissement et ouvre de nouvelles perspectives de recherche.